

Chemical-Scale Studies of Ligand-Gated Ion Channels

Thesis by

Kathryn Anna McMenimen

In Partial Fulfillment of the

Requirements for the Degree of

Doctor of Philosophy



California Institute of Technology
Pasadena, CA

2010

(Defended October 30, 2009)

© 2010

Kathryn Anna McMenimen

All Rights Reserved

Dedicated to my parents:

Dennis and Jean McMenimen

And in memory of Fae Eloise Miller

Acknowledgements

Chemistry is all about getting lucky.

-Robert Curl

After working towards the completion of this Ph.D. for more than six years, I have many people to thank. The path was not always clear and for that I thank everyone who contributed to helping me along the way.

My first set of thanks goes to my advisor, Dennis Dougherty. Before my first trip to Caltech for a visit, I was told by some of my chemistry friends to meet with Dennis because he gave such inspiring lectures about his group's work, and happened to be one of the "normal" people at Caltech. Well, I quickly learned that both are true. I am always and will continue to be inspired by the scientific questions that he chooses to tackle and his amazing ability to tell a story. I also greatly appreciate the guidance he has provided over the years, especially for allowing me to pursue many different scientific interests and for allowing me to pursue a somewhat non-standard career path. I am truly grateful for all of his support and guidance over the years.

I would also like to thank Professor Henry Lester and his lab for providing an incredible amount of insight and thought about different aspects of my projects over the years. Henry's insights and questioning always lead to intriguing new ideas and approaches to solving problems. Without him, our "Unnaturals" meetings just wouldn't have been the same. In addition, members of his lab, particularly Fraser Moss, helped me with many molecular biology questions I had along the way, and I appreciate all of their helpful suggestions.

I would also like to thank my committee members, Professors John Bercaw, Peter Dervan, and Dave Tirrell. I am grateful for their advice and guidance over the years.

They have all been very supportive of my future career goals and interested in discussing how I can achieve them.

When I arrived at Caltech and was trying to determine which lab I would join, the ultimate deal breaker were the people in the Dougherty group. They are some of the most amazing and inspiring people I have ever met. Although we didn't overlap for long, Darren Beene, Sarah Monahan May, David Dahan, and Don Elmore all provided helpful advice when I first arrived. I also greatly appreciate all of the help Steve Spronk provided for all things computer related, especially for teaching me how to use the command line. Tingwei Mu and Lori Lee both provided me with advice, particularly about future career plans, and I appreciate their insight and advice. James Petersson was one of my early mentors and collaborator on the NMDA receptor cation- π study. I'll never forget when I first told him I was interested in studying the NMDA receptors. He told me to just start working on the project and then let Dennis know, that way he wouldn't be able to say no. It definitely worked and I'm incredibly grateful for our countless discussions, scientific and otherwise. I wouldn't have been able to get started so quickly in the lab if it hadn't been for Amanda Cashin. She helped me get my feet wet in the Dougherty lab and has continued to be a great friend over the years. I will always appreciate her continued friendship over the years and her enjoyment of all things dog related.

I would also like to thank Joanne Xu, Erik Rodriguez, Amy Eastwood, Jinti Wang, Jai Shanata, Angela Blum, Kay Limapichat, and Kristin Gleitsman for all of the help over the years and contributing to the general enjoyment of being a member of the Dougherty group. I would also like to thank the newer lab members, Sean Kedrowski, Noah Duffy, Maggie Thompson, Kristina McCleary, Ethan Van Arnam, and Ximena Da Silva Tavares Bongoll, for continuing the pursuits of the Dougherty lab. I would also like to thank Mike Torrice, Nyssa Puskar, Ariele Hanek, and Kiowa Bower for not only providing valuable scientific advice, but also for listening to my general discussions and ramblings over the years while in the middle bay.

There are of course many people outside of the lab who contributed to the completion of this thesis. I want to thank all of the friends and students I met while teaching at Pomona College. They convinced me that I love teaching and definitely wanted to pursue my teaching interests. Especially to Matt Sazinsky and Lisa Sharpe Elles, I look forward to our future discussions about teaching at small colleges. I don't think I would have ended up at Caltech if it hadn't been for some great mentors along the way. I want to thank Donnie Cotter, Darren Hamilton, and Jeremy Sanders, and my friends from Mount Holyoke College, who encouraged me to pursue my interests in chemistry. Of course there are many more people who have contributed to this thesis, and I know this doesn't even scratch the surface, but to everyone else that supported me along the way, thank you!

Last, but not least, I want to thank my family. My parents have always supported my endeavors and provided guidance along the way. It hasn't always been the smoothest road, but they were always there to help me find the way. My parents have always encouraged me to pursue my dreams and I couldn't have done this without them. I would also like to thank Amy, Sean, and "Little John" Bailey. They have always supported my scientific interests and remind me of the many non-science related things in the world that I enjoy. This last summer in California wouldn't have been complete without my brother James, who I am secretly turning into a chemist! Thanks for not letting me remain the lone scientist in the family. Finally, to the two best dogs in the world, Hunter and Watson, who have made my life that much more interesting.

Abstract

The studies discussed in this dissertation are aimed at the chemical-scale interactions involved in neuroreceptor structure and function. Unnatural amino acids were incorporated into several ligand-gated ion channels. Two different ionotropic glutamate receptors (iGluRs), the N-methyl-D-aspartate (NMDA) receptor and the α -amino-3-hydroxy-5-methyl-4-isoxazolepropionic acid (AMPA) receptor were studied, along with an acetylcholine receptor - the nicotinic acetylcholine receptor (nAChR), and all were analyzed with electrophysiology—an assay of receptor function.

In Chapter 2, a highly conserved tryptophan (Trp607) in the ion channel pore of the NMDA receptor was investigated for its role during extracellular Mg^{2+} block. Previous studies hypothesized that a cation- π interaction between NR2BW607 and Mg^{2+} contributed to the receptor blockade. However, our studies suggest that Trp607 is not involved in a cation- π interaction with Mg^{2+} , instead it is a structural component of the pore. NR2B Trp607 acts as a steric “plug,” preventing Mg^{2+} permeation through the ion channel. These studies were the first to incorporate unnatural amino acids into a glutamate receptor, extending the scope of nonsense suppression methodology to a new class of neuroreceptors.

Chapter 3 describes the incorporation of unnatural amino acids into the ligand binding domain (LBD) of NMDA and AMPA receptors. Previous structural studies of AMPA receptors established the overall topology of the LBD to be a clamshell, two domains clamp down around a central cleft. Further studies utilizing agonists that induce full receptor activation and partial receptor activation demonstrate a relationship between cleft closure and agonist efficacy, which is the ability to activate a receptor. Full agonists correlate with more cleft closure than partial agonists, which induce less cleft closure. To examine this relationship, we used unnatural amino acid mutagenesis to convert an NR2-conserved tyrosine to homotyrosine and an NR1 glutamine to homoglutamine, residues designed to disrupt clamshell closure by expanding the side chain without altering its functionality. The development of our functional probe demonstrates that the clamshell closure mechanism, previously shown for AMPA receptors, likely also applies to NMDA receptors, but to different degrees in the NR1 and NR2 subunits.

Finally, in Chapter 4 we use unnatural amino acids, mutagenesis, and computational simulations to probe the binding interactions that are involved in agonist selectivity at the muscle-type nicotinic acetylcholine receptor. Acetylcholine (ACh) and nicotine, both agonists for nAChRs, have a high potency for neuronal receptors. However, nicotine is a weak agonist for the muscle-type nAChRs, yet the amino acids that contribute to the binding site remain the same between both types of receptors. These studies use mutagenesis and unnatural amino acids to introduce changes in the muscle-type receptor to increase nicotine potency. Although some of the mutations increase nicotine potency, none of the mutations result in a muscle-type receptor with nicotine potency as great as the neuronal receptors. A second set of studies generated a mouse muscle homology model and used molecular dynamics to simulate movements in the receptor with and without agonist bound. These structures demonstrate the importance of a hydrogen-bonding network that contributes to the pre-organization of the aromatic box.

Table of Contents

Acknowledgements	iv
Abstract	vii
List of Figures	xiv
List of Tables	xviii

Chapter 1: Chemical-Scale Neuroscience 1

1.1 Introduction to Neurochemistry	1
1.1.1 <i>Chemical Signal Transduction</i>	1
1.1.2 <i>Ion Channel Functional Studies</i>	4
1.2 Introduction to Unnatural Amino Acid Mutagenesis	7
1.2.1 <i>Unnatural Amino Acid Mutagenesis</i>	7
1.2.2 <i>Nonsense Suppression</i>	9
1.3 Dissertation Work	14
1.4 Conclusion	16
1.5 Cited References	17

Chapter 2: Exploring the Chemical Nature of the N-methyl-D-aspartate (NMDA) Receptor Pore Blockade 20

2.1 Introduction to Learning and Memory	20
2.1.1 <i>Long-term potentiation and Long-term Depression</i>	20
2.1.2 <i>Synaptic Plasticity and iGluRs</i>	22
2.1.3 <i>The LTP Switch: NMDA Receptor Mg^{2+} Block</i>	27
2.1.4 <i>Glutamate Receptor Structure and Diversity</i>	29
2.1.5 <i>AMPA Receptor Diversity</i>	30
2.1.6 <i>NMDA Receptor Diversity</i>	31
2.1.7 <i>iGluR Subunit Topology</i>	32
2.1.8 <i>NMDA Receptor Mg^{2+} Block</i>	34

2.2 Results	36
2.2.1 <i>Previous Studies of the NMDAR Mg^{2+} Binding Site</i>	36
2.2.2 <i>Wild type NMDA Receptor Expression</i>	40
2.2.3 <i>Control Experiments</i>	42
2.2.4 <i>Incorporation of F_n-Tryptophans at NR2BW607</i>	45
2.2.5 <i>Calculated Magnesium Binding Energies</i>	48
2.2.6 <i>Mutagenesis studies of Inter-Subunit Contacts in the NMDAR Pore</i>	49
2.2.7 <i>Current-Voltage (I-V) Relationships</i>	50
2.2.8 <i>Similarities of the P-Loop of Glutamate Receptors and Potassium Channels</i>	52
2.2.9 <i>Asparagine Residues and NMDA Receptor Block by Extracellular Cations</i>	55
2.2.10 <i>Additional Studies of NMDA Receptor Blockade</i>	61
2.3 Discussion and Conclusions	64
2.4 Materials and Methods	67
2.4.1 <i>Molecular Biology</i>	67
2.4.2 <i>Electrophysiology</i>	69
2.4.3 <i>Immunolocalization of Wild type and Mutant NMDA Receptors</i>	70
2.4.4 <i>Computational Modeling</i>	71
2.5 Cited References	72

Chapter 3: Studies of Partial Agonist Interactions in the Binding Site of Glutamate Receptors Using Unnatural Amino Acid Mutagenesis

79

3.1 Introduction	79
3.1.1 <i>The Mechanism of Partial Agonist Action on Glutamate Receptors</i>	81

3.1.2 <i>Previous Studies of Partial Agonism and Structural Evidence for the Clamshell Model of Partial Agonism in AMPA-Selective Receptors</i>	88
3.1.3 <i>Structural Studies of NMDA-Selective Receptors</i>	94
3.1.4 <i>Previous Studies of Partial Agonism and the Clamshell Model of Partial Agonism in NMDA Receptors: The NR1 Glycine-Binding Site</i>	97
3.1.5 <i>Previous Studies of Partial Agonism and the Clamshell Model of Partial Agonism in NMDA Receptors: The NR2 Glutamate-Binding Subunit</i>	99
3.2 NMDA Receptor Ligand-Binding Domain Studies	101
3.2.1 <i>Project Overview</i>	101
3.2.2 <i>Studies of an Ion-Pair Interaction at the NR2B D1-D2 Interface</i>	101
3.2.3 <i>Homo-tyrosine Incorporation at Y705</i>	105
3.2.4 <i>Inter-domain Contacts and Mutations in the Glycine-Binding NR1 Subunit</i>	109
3.2.5 <i>Homo-glutamine Incorporation at NR1 Q403</i>	112
3.2.6 <i>GluR2 Structural Study Correlation</i>	114
3.2.7 <i>Implications for the Functional Study of the Clamshell Mechanism of Agonist Action</i>	115
3.3 AMPA Receptor Ligand-Binding Domain Studies	118
3.3.1 <i>Mutational Probe of the GluR2 Clamshell</i>	119
3.3.2 <i>Studies of Ligand Binding Domain Hinge Residues Involved in Receptor Activation</i>	124
3.4 Conclusions and Future Work	126
3.5 Methods	127
3.5.1 <i>Electrophysiology</i>	127
3.5.2 <i>Mutagenesis and preparation of cRNA and Unnatural Amino Acid Suppression</i>	128

3.5.3 <i>Immunolocalization of Wild type and Mutant NMDA Receptors</i>	129
3.6 Cited References	130
 Chapter 4: Studies of the Binding Site of the Mouse Muscle Nicotinic Acetylcholine Receptor	 134
4.1 Introduction	134
4.1.1 <i>The Nicotinic Acetylcholine Receptor</i>	134
4.1.2 <i>Acetylcholine Binding to the nAChR</i>	137
4.1.3 <i>Nicotine Binding to the nAChR and Ligand Discrimination</i>	140
4.1.4 <i>Computational Modeling of nAChRs</i>	143
4.1.5 <i>Project Goals</i>	143
4.2 Results	145
4.2.1 <i>Conventional Mutations of the Outer Shell of the Mouse Muscle nAChR Binding Box</i>	145
4.2.2 <i>Chimera Experiments Between Mouse Muscle and Neuronal nAChRs</i>	151
4.2.3 <i>Unnatural Amino Acid Mutagenesis of Outer Shell Amino Acids</i>	152
4.2.4 <i>Computational Model of Extracellular Domain of Mouse Muscle nAChR</i>	156
4.2.5 <i>Computational Studies of the Mouse Muscle nAChR Binding Site</i>	160
4.3 Discussion and Conclusions	164
4.4 Materials and Methods	166
4.4.1 <i>Mutagenesis and Unnatural Amino Acid Suppression</i>	166
4.4.2 <i>Electrophysiology</i>	167

4.4.3 <i>Mouse Muscle Homology Model of D89N Mutant Structures</i>	167
4.5 Cited References	169

Appendix A: Studies of Ionotropic Glutamate Receptors in Mammalian Cells	174
A.1 Introduction	174
A.2 Results and Discussion	176
A.3 Methods	181
A.4 Cited References	184

List of Figures

Chapter 1

Figure 1.1 Synaptic transmission	2
Figure 1.2 Ligand-gated ion channels	3
Figure 1.3 Two-electrode voltage clamp	5
Figure 1.4 Electrophysiological traces	6
Figure 1.5 The power of unnatural amino acid mutagenesis	9
Figure 1.6 Nonsense suppression	10
Figure 1.7 Semi-synthesis of aminoacyl tRNA	11
Figure 1.8 <i>In vivo</i> nonsense suppression methodology	12
Figure 1.9 Unnatural amino acid side chains	13

Chapter 2

Figure 2.1 LTP and LTD	20
Figure 2.2 Synaptic changes after LTP induction	21
Figure 2.3 iGluR agonists	23
Figure 2.4 Schematic of iGluR classes	24
Figure 2.5 Overview of LTP	26
Figure 2.6 The postsynaptic density	29
Figure 2.7 Topology of iGluR subunits	33
Figure 2.8 NMDA receptor activation	35
Figure 2.9 NMDA P-loop structure	37
Figure 2.10 Cation- π binding	39
Figure 2.11 NMDA receptor Mg^{2+} Block	41
Figure 2.12 Misincorporation currents	44
Figure 2.13 Wild type recovery IC_{50}	45
Figure 2.14 Electrophysiology traces	46
Figure 2.15 NR2BW607F ₂ -Trp Trace	47
Figure 2.16 Electrostatic potential surfaces of tryptophan derivatives	47
Figure 2.17 Calculated Mg^{2+} binding energies	48

Figure 2.18 I-V Curves	51
Figure 2.19 Schematic of NMDA receptor pore	53
Figure 2.20 Immunolocalization of NMDA receptors	54
Figure 2.21 Asparagine analogs	56
Figure 2.22 Asparagine site IC ₅₀ curves	59
Figure 2.23 Asparagine site IC ₅₀ curves with memantine	60
Figure 2.24 Percent block for Mg ²⁺ and memantine	61
Figure 2.25 NMDA receptor blockers	62
Figure 2.26 Electrophysiology traces from MK-801	63
Figure 2.27 IC ₅₀ curves for PCP	64
Figure 2.28 NMDA receptor cloning	68
 Chapter 3	
Figure 3.1 iGluR families	80
Figure 3.2 iGluR Topology	82
Figure 3.3 GluR2 Ligand binding domain	83
Figure 3.4 iGluR Domain Organization	84
Figure 3.5 iGluR agonists	85
Figure 3.6 iGluR domain closure	87
Figure 3.7 AMPAR antagonists	89
Figure 3.8 Willardiine structures	91
Figure 3.9 AMPAR agonist induced domain closure	92
Figure 3.10 iGluR domain closure and channel activation	94
Figure 3.11 NMDA heterodimer structure	95
Figure 3.12 NMDAR agonist binding site	96
Figure 3.13 NR1 partial agonists	97
Figure 3.14 NR1 domain closure	98
Figure 3.15 NR2 Ligand binding domain	100
Figure 3.16 Tyrosine analogs	102
Figure 3.17 NR2 agonists and amino acid analogs	104
Figure 3.18 Homotyrosine traces and EC ₅₀ curve	106

Figure 3.19 NR2 relationship between activity and efficacy	108
Figure 3.20 TIRF images of wild type and mutant NMDARs	109
Figure 3.21 NR1 ligand binding domain amino acid analogs	110
Figure 3.22 NMDA receptor shifts for mutations in the LBD	113
Figure 3.23 Functional probe of the clamshell	114
Figure 3.24 GluR2 domain closure distances	115
Figure 3.25 Side chain geometries for Tyr and hTyr	117
Figure 3.26 Wild type GluR2 dose-response relationship	119
Figure 3.27 GluR2 EC ₅₀ shifts for LBD mutations	123
Figure 3.28 GluR2 Y483 4-MeO-Phe dose response curve	125

Chapter 4

Figure 4.1 Muscle nAChR Structure	135
Figure 4.2 nAChR subunit topology	136
Figure 4.3 nAChR agonist binding site	137
Figure 4.4 EC ₅₀ shifts for F _n -Trps at α 149 in muscle nAChR	138
Figure 4.5 AChBP structure	139
Figure 4.6 ACh and Nicotine binding to α Trp149 muscle nAChR	141
Figure 4.7 Cation- π interactions at α Trp149	142
Figure 4.8 nAChR sequence alignment	145
Figure 4.9 Electrophysiology traces of α T196 mutation	147
Figure 4.10 Ratio of EC ₅₀ shifts for nAChR outer shell mutations	149
Figure 4.11 AChBP binding site with nicotine bound	150
Figure 4.12 nAChR β 9- β 10 loop surrounding the conserved aromatic box	151
Figure 4.13 α W86 and α D89 hydrogen bonding	153
Figure 4.14 α 86 EC ₅₀ shifts for wild type and mutant receptor	154
Figure 4.15 <i>Torpedo</i> α subunit alignment with α 1 from mouse muscle	157
Figure 4.16 Charges generated for CCh and Nicotine	159
Figure 4.17 α D89 and Loop B interactions	161
Figure 4.18 Mouse muscle binding site, CCh bound and agonist free structures	162
Figure 4.19 Hydrogen bonding between α D89 and loop B	163

Appendix A

A.1 Wild type NMDAR expression on Flexstation	178
A.2 Wild type 5-HT ₃ A Receptors on the Flexstation	179
A.3 5HT ₃ A S183TAG Lah-THG-73 mutant responses	180
A.4 Untransfected HEK293 cels on the Flexstation	181
A.5 HEK cells transfected with Lah-THG-73 only	181

List of Tables

Table 2.1 IC ₅₀ data for Wild type and Mutant NMDA Receptors	50
Table 2.2 IC ₅₀ values for N and N+1 site mutations	58
Table 3.1 NR2B D1-D2 interface mutations with glutamate and NMDA	103
Table 3.2 NR2B D1-D2 interface mutations with HQA and QA	107
Table 3.3 NR1a D1-D2 interface mutations with glycine and ACPC	111
Table 3.4 NR1a D1-D2 interface mutations with ACBC and D-CS	111
Table 3.5 Data for GluR2 receptors with glutamate	120
Table 3.6 Data for GluR2 receptors with the willardiines	122
Table 3.7 EC ₅₀ values of glutamate for GluR2Y483 mutations	125
Table 4.1 EC ₅₀ values of ACh, Nicotine, and Epibatidine at wild type nAChRs	144
Table 4.2 Outer shell mutation EC ₅₀ values	148
Table 4.3 α 151 and α 21 muscle nAChR data	155
Table 4.4 Hydrogen bonding distances calculated from MD simulations	164

Chapter 1: *Chemical-Scale Neuroscience*

1.1 Introduction to Neurochemistry

1.1.1 Chemical Signal Transduction

The entire human experience is derived from four pounds of Nature's most intriguing and complex creation, the brain. The human brain (Figure 1.1a) is comprised of more than 100 billion ($>10^{11}$) neurons, and each one can connect with 1,000-10,000 (10^3 - 10^4) other neurons through specialized connections, and synapses (*I*) (Figure 1.1b). In four pounds of tissue, an unimaginable network of a quadrillion (10^{15}) connections regulates communication and unconscious activities and structures our imagination. Yet this complex communication can be traced back to synapses, or chemical junctions, between neurons. In fact, Nature has cleverly devised a way to utilize chemicals, or neurotransmitters, to facilitate communication along this complex pathway of neurons. One of the most fascinating questions we can ask is how does the brain use these chemicals to create and regulate the human experience? Is it possible to learn how the human brain functions by understanding the chemical-scale communication between neurons?

To study the chemical-scale communication of the brain, we turn to synapses. Synapses are the junctures between neurons where synaptic transmission, or chemical communication occurs (Figure 1.1c). Synaptic transmission is initiated by an electrical signal, an action potential, which travels down a neuron to its axon terminal. This axon terminal must form a synapse with the dendrite from a neighboring neuron (Figure 1.1c) in order to generate communication between neurons. Once the action potential reaches the pre-synaptic terminal, vesicles containing neurotransmitters, such as glutamate or acetylcholine (ACh), are released into the synaptic cleft. The neurotransmitters diffuse across the cleft and bind to neurotransmitter receptors on the post-synaptic dendrite (Figure 1.1c). Neurotransmitter receptors then regenerate, either directly or indirectly, the electrical signal, which can activate or inhibit the generation of another action potential. The overall flow of communication begins with an electrical signal in the pre-

synaptic cell, which turns into a chemical signal in between neurons. The electrical signal is regenerated in the following neuron, and the cascade continues throughout thousands of cells and occurs very quickly, on the millisecond timescale (2).

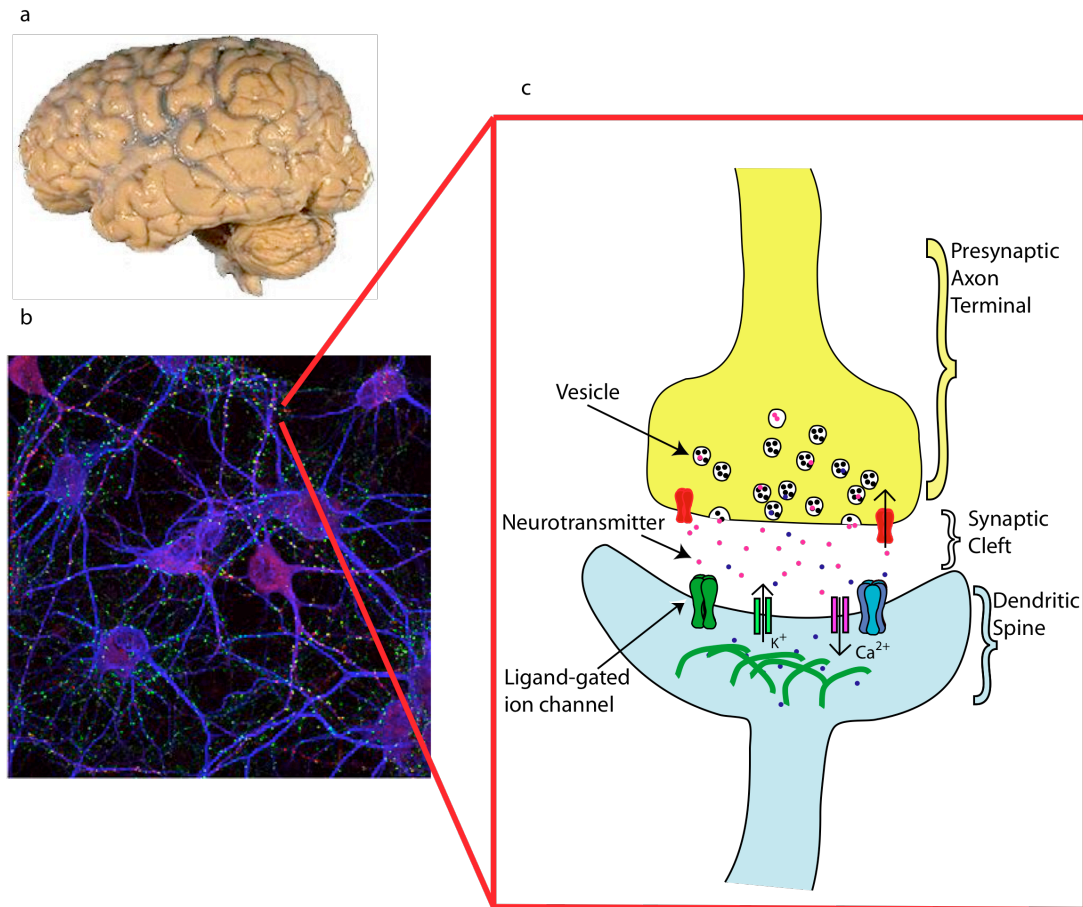


Figure 1.1 Synaptic Transmission. a) The human brain.

(<http://www.healcentral.org/healapp/showMetadata?metadataId=40566> (John A Beal, PhD. Dept. of Cellular Biology & Anatomy, Louisiana State University Health Sciences Center Shreveport))

b) Stained neurons and receptors. Yellow dots correspond to active synapses, adapted from (3).

c) Representation of the synapse where the pre-synaptic axon terminal meets with the post-synaptic dendritic spine. An electrical signal in the pre-synaptic cell releases neurotransmitters from vesicles into the synaptic cleft. Neurotransmitters flow across the synaptic cleft and bind to neuroreceptors in the dendritic membrane where an electrical signal is regenerated.

There are many types of neurotransmitters and neuroreceptors that intertwine to produce a plethora of signals. Neurotransmitters come in many flavors, from small molecules to fatty acids and peptides (4). There are two main types of neuroreceptors. The first is the ligand-gated ion channel (LGICs), which directly binds a neurotransmitter. Ligand binding triggers a conformational change in the protein, opening the ion channel and allowing ion flux across the dendritic membrane (Figure 1.2). Ion flux across a membrane changes the voltage across the membrane, which can result in the generation of an electrical signal if a sufficiently large change occurs. The second type of neuroreceptor is a G-protein coupled receptor (GPCR), which causes alterations that are indirectly related to neurotransmitter-receptor interactions. Upon neurotransmitter binding, a cascade of second messengers are activated triggering downstream changes in the neuron such as activation of other ion channels, signaling pathways, and regulation of gene transcription (5).

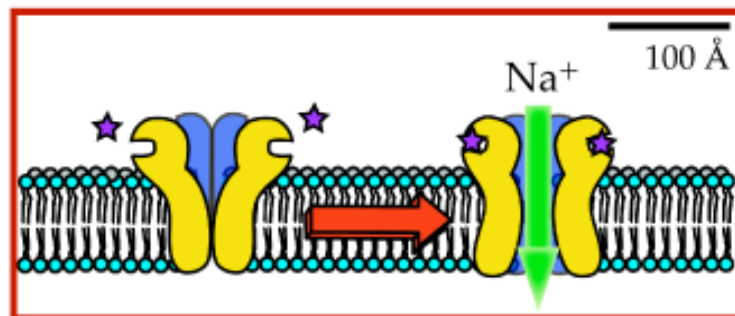


Figure 1.2 Ligand-gated ion channels are closed prior to neurotransmitter binding. Once a neurotransmitter binds, the ion channel opens and allows ion flux across the cell membrane.

The essential goal of chemical-scale neuroscience is to study these neurotransmitter/ neuroreceptor systems. To understand these systems, one must examine at a molecular level how different neurotransmitters are recognized by different neuroreceptors. In addition, one must analyze the structures of these complex, multi-subunit proteins through their gating and activation mechanisms to determine how the structure contributes to the specific cellular functions.

1.1.2 Ion Channel Functional Studies

The first ion channel characterization began in the early 1970's by Hille (6). Since the early studies, the development of molecular biology techniques, cloning, and manipulation of DNA has evolved a typical method for analyzing ion channels. This method generally involves a structure/function study where mutagenesis of amino acids at the DNA level is followed by the production of the ion channel in a heterologous expression system, typically a *Xenopus laevis* oocyte. Then using electrophysiological techniques, primarily the two-electrode voltage clamp (TEVC), the functional channels are analyzed. The principles behind TEVC electrophysiology utilize one electrode as a voltage “clamp” of the cell membrane to maintain a constant potential, which is achieved by injecting current into the membrane (Figure 1.3a). The second electrode measures the voltage difference across the membrane in response to the opening of ion channels and ion flux across the membrane (relative to a ground electrode). Typically a neurotransmitter is applied to the oocyte to generate a current and the “clamp” electrode must then inject more voltage into the membrane in order to maintain a constant voltage (Figure 1.3b). Thus, a direct measurement of the ion flow through the channel is recorded and provides information about the ion channel gating mechanism (7, 8).

The *Xenopus* expression system is used to express either DNA or RNA of mammalian ion channels. After an appropriate amount of time, the ion channels are produced and trafficked to the oocyte membrane. A solution resembling the fluid at the synapse is perfused around the oocyte followed by the application of varying neurotransmitter concentrations. Many types of ligands are studied, such as, agonists (molecules that activate the ion channel, e.g., ACh), antagonists (inactivate), blockers, and potentiators. Electrophysiological recordings measure the response of the ion channel to varying concentrations of ligand and dose-response curves are generated to analyze the functional channels.

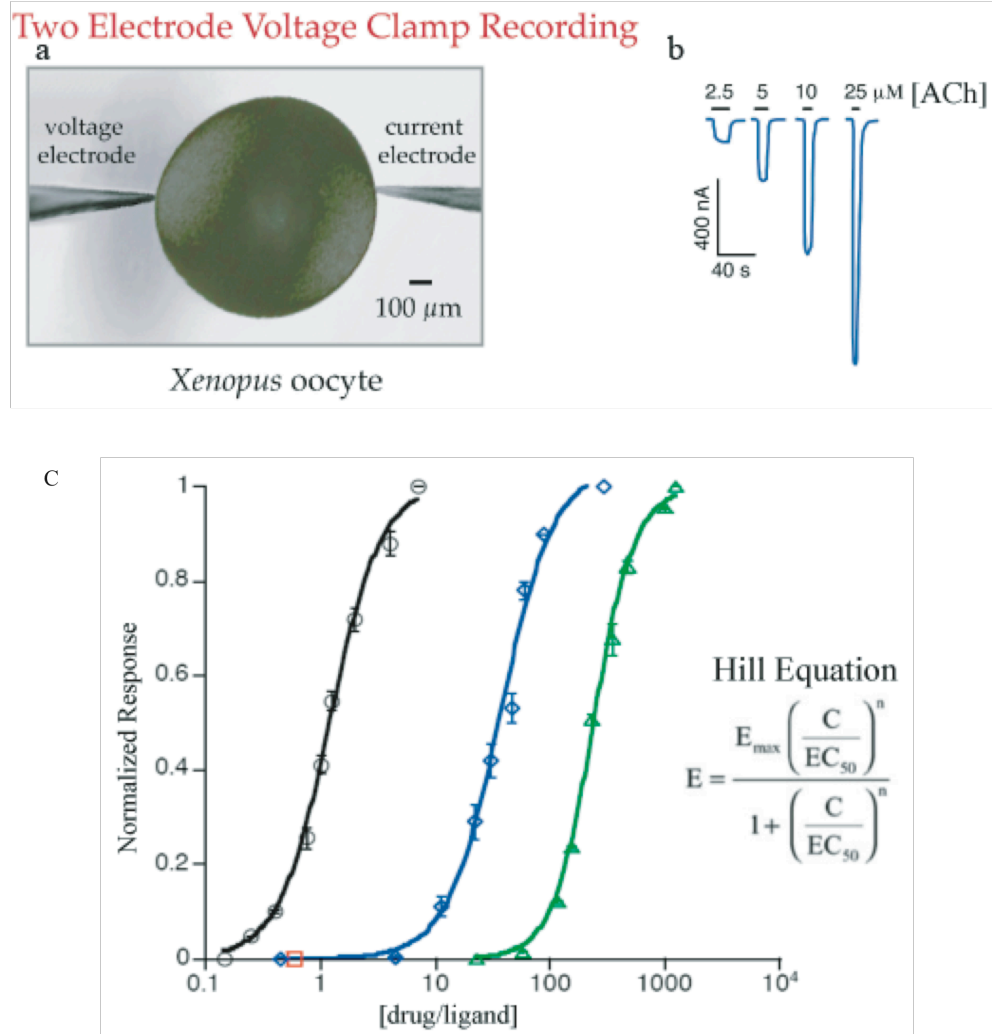


Figure 1.3 Two-electrode voltage clamp. a) The *Xenopus laevis* oocyte with two electrodes, a voltage “clamp” electrode and a second electrode that measures the current across the oocyte membrane. b) An example of an electrophysiological trace. Application of a neurotransmitter (ACh) produces a downward current, measured in nanoamperes (nA). Larger concentrations of neurotransmitters produce larger currents. c) The Hill equation is used to fit dose-response relationships producing EC_{50} , a measure of the concentration of ligand required to produce half-maximal current responses.

The Hill equation (9) is used to fit dose-response data. The equation produces a value for EC_{50} , which is defined as the amount of ligand required to produce a half-maximal response from the neuroreceptors (Figure 1.3c) and is a quantitative measure of the potency of a ligand. Potency (EC_{50}) describes the combined effects of the

neuroreceptor's ability to bind a drug or ligand (affinity) and the ability of the ligand to activate the channel (efficacy). Comparing shifts in EC_{50} values is a convenient method for analyzing different ligands as well as mutations to the neuroreceptors. For example, a rightward shift in EC_{50} demonstrates the decreased potency of a ligand whereas a leftward shift would indicate an increase in ligand potency (Figure 1.3c). General assumptions are made when interpreting EC_{50} data. For example, mutations made to a receptor's binding site that shift EC_{50} are believed to mostly affect affinity while mutations outside of the direct binding site that shift EC_{50} are treated as gating mutations affecting efficacy. These assumptions are generally useful, although there are always exceptions to the rule.

Measuring ligand potency is a useful way to characterize the interaction between drugs and receptors. However, different drugs do not activate receptors equally. Many drugs only partially activate or gate a receptor and are termed partial agonists. One can think of partial agonists as binding with full affinity to a receptor, but not fully gating the receptor, resulting in lower efficacy. The most common method to determine the efficacy of an agonist is to compare the amount of current generated by the receptor in response to a saturating dose of each agonist. Full agonists will produce larger amounts of current compared to partial agonists (Figure 1.4). Efficacy measurements are usually reported as a fraction of one (1) determined from the ratio of the current from the partial agonist divided by that generated by the full agonist.

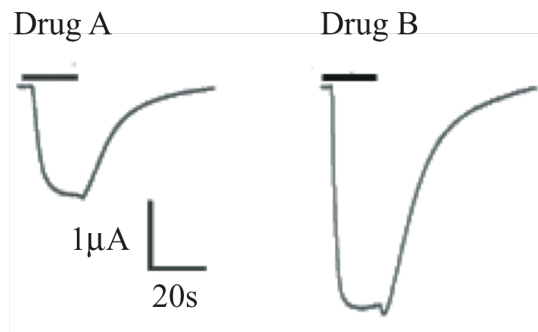


Figure 1.4 Electrophysiological traces representing differences in agonist efficacy. Saturating doses of both Drug A and Drug B generate different levels of current from a receptor. Drug A demonstrates a partial agonist and Drug B demonstrates the response of a full agonist.

Utilizing different agonists, partial agonists, and blockers is very helpful when analyzing these complex receptors. However, generating full pictures to describe the structure and function of these receptors and their interactions with different ligands is difficult. In fact, the atomic-scale details of ion channels, which are large, multi-subunit proteins, is essential to understanding the biological function of these neuroreceptors and their interactions with drugs. For example, agonists for several different ion channels have binding sites that are more than 50 Å away from the ion channel pore where gating occurs. As chemists, we seek to study the atomic-scale interactions that underlie ion channel function. However, there is limited atomic-scale structural data about these receptors due to their complexity. Luckily, we can take advantage of molecular biology tricks such as site-directed mutagenesis to probe chemical-scale interactions by altering specific amino acids in the protein. However, from a chemist's point of view, the 20 natural amino acids are severely limiting when trying to understand how specific bonds and interactions influence the function of an ion channel. Therefore, standard mutagenesis is not always sufficient. As a result, we combine molecular biology with chemistry to utilize unnatural amino acid mutagenesis. Unnatural amino acid mutagenesis allows us to study specific hydrogen bonds, hydrophobic interactions, etc., that influence LGICs. It provides a very clever and precise tool to probe the interactions that underlie LGIC structure and function.

1.2 Introduction to Unnatural Amino Acid Mutagenesis

1.2.1 Unnatural Amino Acid Mutagenesis

Since the late 1980's, site-specific incorporation of unnatural amino acids into proteins *in vivo* has been possible using the nonsense suppression methodology (10). This tool provides many opportunities for the chemical biologist to explore. Using chemistry to design unnatural amino acids facilitates the exploration of seemingly endless chemical interactions that structure ion channels, which greatly surpasses conventional mutagenesis techniques. For example, in order to study a phenylalanine residue in protein structure and function our options using conventional site-directed mutagenesis would allow us to incorporate alanine, tryptophan, and tyrosine. Alanine completely

obliterates the side-chain, which is not subtle by any means as it destroys hydrophobic, aromatic, and steric interactions. Tryptophan on the other hand maintains aromaticity, but is sterically bulky and tyrosine is similar, in size and aromaticity, yet introduces a hydrogen-bonding component (Figure 1.5). Each of these options has significant limitations from a chemical perspective.

The use of unnatural amino acid mutagenesis enhances the ability to study precise chemical aspects of an amino acid. In the case of phenylalanine, amino acids like cyclohexylalanine (Cha) can be incorporated to test the aromatic character of Phe without perturbing steric interactions. The importance of the cation- π binding ability of Phe also can be tested using fluorinated phenylalanine derivatives. Organic and inorganic cations can be stabilized through a favorable electrostatic interaction with the π surface of aromatic rings (11-15). The π surface of aromatic rings, like those of Phe, Tyr, and Trp, have a build up of negative electrostatic potential due to the quadrupole moment of the ring. The ideal way to study the cation- π interaction in proteins is to sequentially fluorinate the aromatic side chain. Adding fluorines to an aromatic ring decreases the negative charge density of the ring and makes it a weaker cation binder. Unnatural amino acid mutagenesis provides a “series” of fluorinated derivatives that can be used to probe these subtle interactions. Although these mutations are subtle, the chemical interactions they probe are energetically non-trivial. In proteins, it is believed that for approximately every 77 amino acids in the protein data bank there is a cation- π interaction (13).

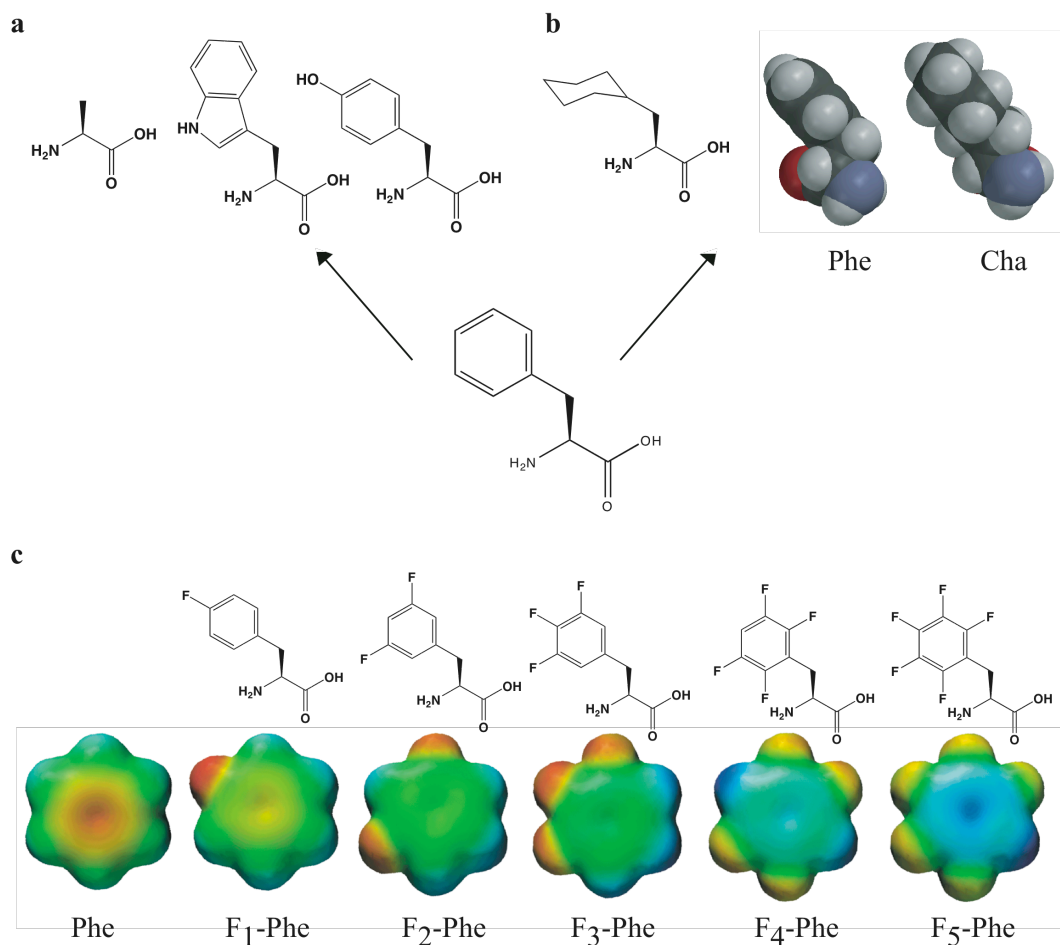


Figure 1.5. The power of unnatural amino acid mutagenesis. a) Conventional mutagenesis allows for alanine, tryptophan, and tyrosine mutations. b) The importance of side chain aromaticity can be explored with the cyclohexylalanine (Cha) mutation without altering side chain sterics. c) The cation- π interaction can be tested with a series of fluorinated Phe derivatives.

1.2.2 Nonsense Suppression

Unnatural amino acids provide a powerful tool for chemical biologists to study proteins. There are several different methodologies for incorporating unnatural amino acids site-specifically into proteins. We utilize the nonsense suppression methodology (16-21). The basic procedure is outlined below in Figure 1.6, and makes use of one of the cell's stop codons, UAG (Amber stop codon), as the codon for the unnatural amino acid. The UAG stop codon is incorporated into the ion channel mRNA at the site of interest using mutagenesis. Additionally, a suppressor tRNA_{CUA} (containing a CUA anticodon) that

recognizes the amber stop codon, is chemically prepared and appended with the unnatural amino acid of choice (22, 23). During translation, the ribosome “reads” the UAG stop codon and instead of terminating protein translation, it is suppressed by the tRNA_{CUA}, and the unnatural amino acid is inserted into the protein in the same manner as any naturally occurring amino acid. Protein translation continues and produces a full-length protein with the unnatural amino acid inserted at a specified site.

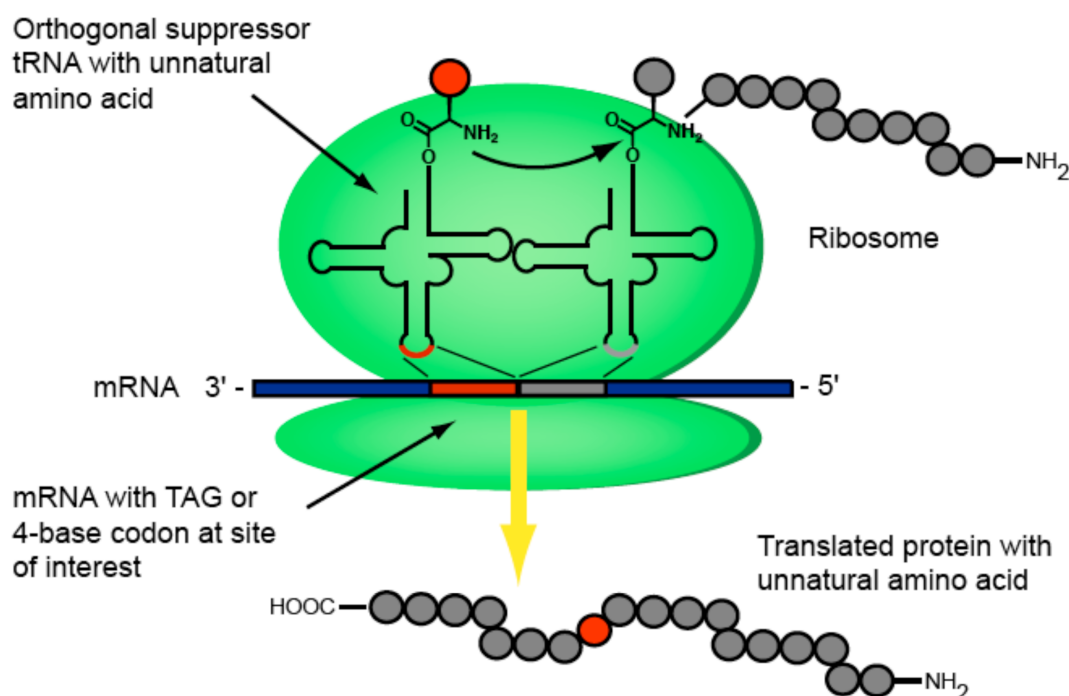


Figure 1.6 Outline of the nonsense suppression methodology. The ribosome of the expression system incorporates an unnatural amino acid at the site of interest (red dot).

A similar approach utilizes a four-base codon instead of the UAG stop codon. This methodology, called frameshift suppression (24), uses the four-base GGGU codon. The four-base codon normally would shift the ribosome out of the proper reading frame, resulting in the production of mistranslated proteins. However, a specialized tRNA containing the appropriate anticodon, ACCC, suppresses the mistranslation by inserting an unnatural amino acid (chemically appended to the tRNA_{ACCC}) at the site of the frameshift mutation. This methodology has also been extended to another stop codon,

the opal suppressor (UGA), which has allowed for the incorporation of multiple unnatural amino acids into a single protein (25).

Nonsense suppression blends together tools of molecular biology and chemistry. Simple molecular biology allows for mutagenesis of the codon of interest. However, the limiting step is chemical production of the aminoacylated tRNA. In the late 1970's, Hecht and coworkers were able to synthesize misacylated, chemically derived tRNAs (23). Since then, several different groups have expanded the methodology to include a large variety of unnatural amino acids and several different protein systems (26-28).

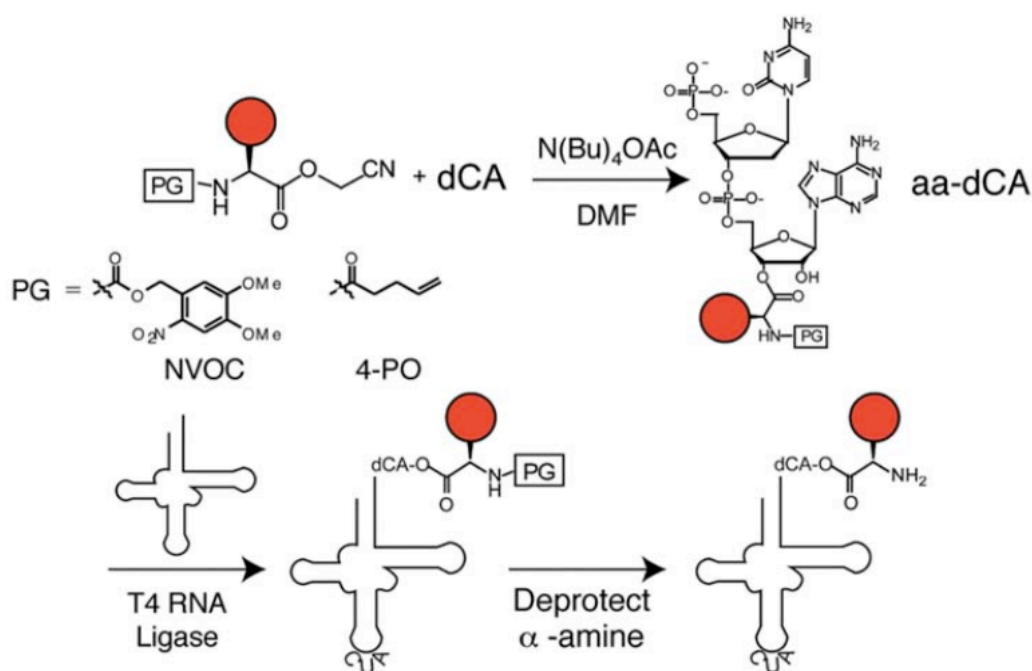


Figure 1.7 The steps involved in the semisynthesis of suppressor aminoacylated tRNA. The unnatural amino acid is protected by either NVOC or 4-PO and coupled to dCA in DMF. Aminoacylated-dCA (aa-dCA) is ligated to a truncated 74-mer tRNA_{CUA}. The final step involves deprotection of the α -amine.

The nonsense suppression method begins with the transcription of a truncated 74-mer suppressor tRNA lacking the final two nucleotides, C and A. A separate step requires the chemical synthesis of the final two nucleotides, deoxy-C-A (dCA) (Figure 1.7). The unnatural amino acid is also chemically synthesized and it contains an α -N-protecting group that is either photolabile, 6-nitroveratryloxycarbonyl (NVOC) or I₂-

labile, 4-pentenoyl (4-PO) groups, chemistry that is orthogonal to tRNA functional groups (29). The carboxyl group is synthesized with an activating group, a cyanomethyl ester, for coupling to dCA, aminoacyl tRNA (aa-tRNA). The dCA is used as a handle for acylation of the suppressor tRNA. Then, aa-dCA is enzymatically ligated with T4 RNA ligase to the 74-mer tRNA_{CUA} to produce a full-length 76-mer tRNA_{CUA} (Figure 1.7) (18, 21, 22, 30-32). Additionally, the α -N-protecting group remains on the amino acid through all of the coupling and ligation reactions to stabilize the bond between the terminal adenosine and the amino acid.

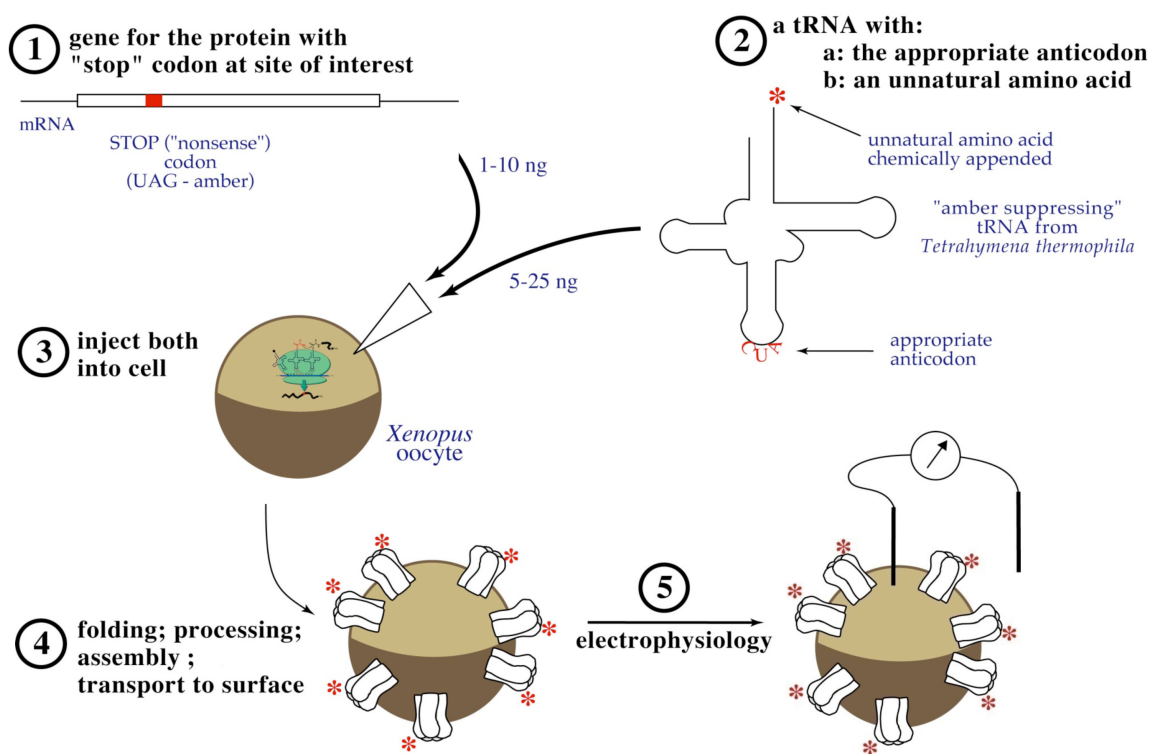


Figure 1.8 *In vivo* nonsense suppression methodology. It begins with mRNA containing a UAG (or 4-base) codon and aa-tRNA that are injected into an oocyte, where the endogenous ribosome synthesizes the protein and traffics it to the surface. Then functional electrophysiological studies are performed on the ion channels.

The deprotected amino-acylated tRNA and the mRNA containing the UAG codon (or four-base codon) are manually injected into a *Xenopus laevis* oocyte (18-20, 22, 26, 31, 33). The mRNA and aa-tRNA are incubated in the cell, typically for 1-3 days to

allow for protein synthesis, folding, and trafficking to the surface (Figure 1.8). This methodology allows for an almost limitless incorporation of amino acids into proteins. Over 100 different amino acids have been incorporated into proteins (Figure 1.9) both *in vivo* and *in vitro* (21). The method is very versatile as this approach allows the incorporation of alpha hydroxy acids, hydrazides, and N-hydroxylamines (20, 34), along with many other fluorescent and protonated amino acids, etc. However, this technique has limits, as D-amino acids and β -amino acids are not incorporated (35).

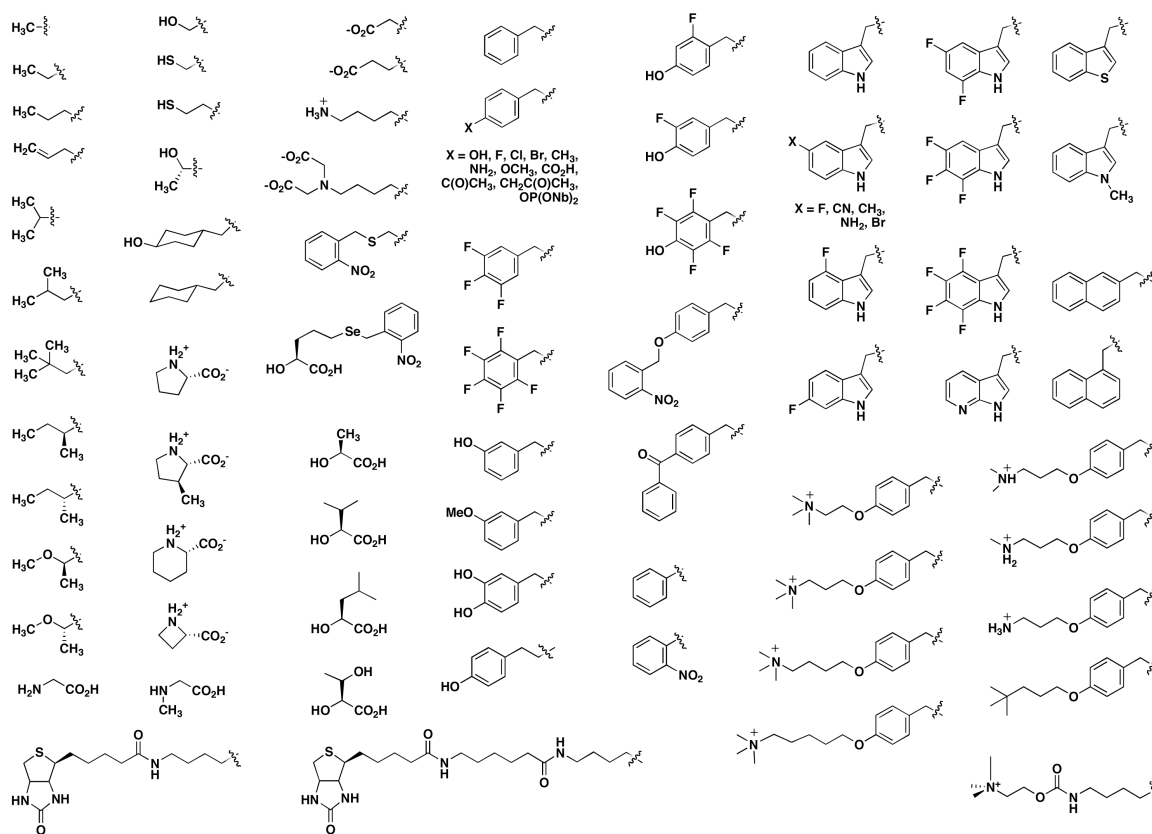


Figure 1.9 Examples of some of the unnatural amino acid side chains that have been incorporated into proteins.

In order to increase the integrity of the nonsense suppression technique, we utilize two controls, both involving the suppressor tRNA_{CUA}. The first control experiment tests for “readthrough” of the stop or 4-base codon by endogenous tRNAs. The mutated mRNA containing the UAG or 4-base codon alone is injected; no ion channel production should result, since translation should be blocked in the absence of suppressor tRNA. In

the second control experiment, a full-length suppressor tRNA without an amino acid appended to it is co-injected with the mutated mRNA into an oocyte to control for misacylation. The “orthogonality” of the tRNA_{CUA} (its ability to be unrecognized) by the cell’s endogenous tRNA synthetases is extremely important. tRNA synthetases are enzymes that charge tRNAs with the appropriate amino acid during protein synthesis. However, the tRNA_{CUA} must remain orthogonal, otherwise, after it incorporates the desired unnatural amino acid into the protein, it could be “misacylated” with a natural amino acid, producing mixtures of proteins, some with the unnatural amino acid and some without. This would be problematic for our studies since we are unable to separate the proteins. To gain orthogonality, Schultz and co-workers originally used a yeast phenylalanine tRNA_{CUA}^{Phe} with the modified anticodon in an *in vitro* *Escherichia coli* expression system (10). In the *in vivo* *Xenopus* expression system, we utilized a tRNA_{CUA}^{Phe} from *Tetrahymena thermophila*, which is not recognized by the endogenous *Xenopus* synthetases. This modified tRNA is often called THG73 and is also viable in an *in vitro* *E. coli* system (22).

Since the suppressor tRNA_{CUA} is orthogonal to the expression system, it cannot be reamino-acylated with the unnatural amino acid in the cell, and therefore is a stoichiometric reagent. Theoretically, only one ion channel can be synthesized per aa-tRNA using this methodology. In practice, even fewer ion channels are produced due to complications such as amino acid hydrolysis from the tRNA. Luckily, we can take advantage of a very sensitive assay for studying ion channels, TEVC electrophysiology. Limited amounts of ion channels can be detected on the whole cell level, as low as 10 attomols (10⁻¹⁸) (21). In fact, electrophysiology is sensitive enough to detect single ion channels as well.

1.3 Dissertation Work

The work described here can be divided into three sections, which combine the tools of unnatural amino acid mutagenesis and electrophysiology to study several neuroreceptors. The first studies, Chapters 2 and 3 will focus on a type of LGIC that is a member of a large, superfamily of ionotropic glutamate receptors (glutamate-gated receptors), iGluRs. Chapter 4 describes work performed to study a different LGIC, the muscle nicotinic

acetylcholine receptor (nAChR), which is a member of a different superfamily, the Cys-Loop superfamily of LGICs, and is gated instead by the neurotransmitter acetylcholine (ACh).

The first study described will focus on the N-methyl-D-aspartate (NMDA) receptors, which are members of the iGluR superfamily of neuroreceptors. Prior to the work described, the unnatural amino acid methodology had not been used to study any of the iGluR neuroreceptors. Our initial studies incorporating unnatural amino acids into an NMDA receptor were to study a potential cation- π interaction between an external Mg^{2+} ion and a conserved tryptophan in the pore of NMDA receptors and are described in Chapter 2. Since these were the first studies to incorporate unnatural amino acids into any iGluR, we developed optimal conditions necessary for expression of these ion channels and describe their characterization.

In Chapter 3 we continued to use unnatural amino acid mutagenesis to study the NMDA receptors. In these experiments we used conventional and unnatural amino acids to probe the interactions involved in agonist binding to the ligand-binding domain (LBD) of an NMDA receptor. We also used unnatural amino acids to create a functional probe of the mechanism that different agonists use to activate the NMDA receptor. We developed a novel method for determining how a NMDA receptor responds to different partial agonists.

Chapter 4 describes a series of studies designed to understand the mechanism by which the muscle nAChR discriminates between several ligands, including ACh and nicotine. Nicotine is a more potent agonist for neuronal nAChRs than it is for muscle nAChRs, and we are interested in identifying the structural components involved in ligand discrimination. These studies encompass a series of experimental work involving unnatural amino acid mutagenesis, conventional mutagenesis, and computational modeling.

1.4 Conclusion

Every year, millions of people are affected by neurological disease and disorders. Although great strides are being made towards understanding complications of the nervous system, there is still a great deal to be determined. Neuroreceptors lie at the nexus of regulating learning and memory, basic cellular homeostasis, and neurological disorders and diseases, such as Alzheimer's Disease, Parkinson's Disease, and Huntington's Disease, and are implicated in drug addictions and non-degenerative disorders as well. Ion channels in particular are the perfect targets for chemical biologists to study due to their complicated structures that correspond to regulation of very specific functions. Many current drugs target LGICs and their neurotransmitters, such as Namenda[®] (AD), Xanax[®] (anxiety disorders), and Aricept[®] (AD). One overarching goal of our research is to use the chemical-scale structural information we obtain to enable more precise drug design to target and regulate these neuroreceptors.

Our understanding and characterization of ion channels has come a long way since the 1970's however, much is still unknown about their structure. These are trans-membrane proteins that are often composed of multiple, different subunits. As such, ion channels remain elusive targets of the crystallographer. As a result, direct structural information available is very limited. That is why our functional studies to probe the chemical interactions necessary to maintain ion channel structure and influence agonist binding are optimal for determining how these essential receptors function.

1.5 Cited References

1. Williams, R. W., and Herrup, K. (1988) The control of neuron number, *Annu Rev Neurosci* 11, 423-453.
2. Clements, J. D. (1996) Transmitter timecourse in the synaptic cleft: its role in central synaptic function, *Trends Neurosci* 19, 163-171.
3. Valor, L. M., Charlesworth, P., Humphreys, L., Anderson, C. N., and Grant, S. G. (2007) Network activity-independent coordinated gene expression program for synapse assembly, *Proc Natl Acad Sci U S A* 104, 4658-4663.
4. Triggle, D. J., and Triggle, C. R. (1976) *Chemical pharmacology of the synapse*, Academic Press, London ; New York.
5. Gilman, A. G. (1987) G proteins: transducers of receptor-generated signals, *Annu Rev Biochem* 56, 615-649.
6. Hille, B. (1971) The permeability of the sodium channel to organic cations in myelinated nerve, *J Gen Physiol* 58, 599-619.
7. Kandel, E. R., Schwartz, J. H., and Jessell, T. M. (2000) *Principles of neural science*, 4th ed., McGraw-Hill, Health Professions Division, New York.
8. Hille, B. (2001) *Ion channels of excitable membranes*, 3rd ed., Sinauer, Sunderland, Mass.
9. Hill, A. V. (1910) A new mathematical treatment of changes of ionic concentration in muscle and nerve under the action of electric currents, with a theory as to their mode of excitation, *J Physiol* 40, 190-224.
10. Noren, C. J., Anthony-Cahill, S. J., Griffith, M. C., and Schultz, P. G. (1989) A general method for site-specific incorporation of unnatural amino acids into proteins, *Science* 244, 182-188.
11. Dougherty, D. A. (1996) Cation-pi interactions in chemistry and biology: a new view of benzene, Phe, Tyr, and Trp, *Science* 271, 163-168.
12. Dougherty, D. A. (2007) Cation-pi interactions involving aromatic amino acids, *J Nutr* 137, 1504S-1508S; discussion 1516S-1517S.
13. Gallivan, J. P., and Dougherty, D. A. (1999) Cation-pi interactions in structural biology, *Proc Natl Acad Sci U S A* 96, 9459-9464.
14. Ma, J. C., and Dougherty, D. A. (1997) The Cationminus signpi Interaction, *Chem Rev* 97, 1303-1324.
15. Zacharias, N., and Dougherty, D. A. (2002) Cation-pi interactions in ligand recognition and catalysis, *Trends Pharmacol Sci* 23, 281-287.
16. Ellman, J. A., Mendel, D., and Schultz, P. G. (1992) Site-specific incorporation of novel backbone structures into proteins, *Science* 255, 197-200.
17. Judice, J. K., Gamble, T. R., Murphy, E. C., de Vos, A. M., and Schultz, P. G. (1993) Probing the mechanism of staphylococcal nuclease with unnatural amino acids: kinetic and structural studies, *Science* 261, 1578-1581.
18. Nowak, M. W., Kearney, P. C., Sampson, J. R., Saks, M. E., Labarca, C. G., Silverman, S. K., Zhong, W., Thorson, J., Abelson, J. N., Davidson, N., and et al. (1995) Nicotinic receptor binding site probed with unnatural amino acid incorporation in intact cells, *Science* 268, 439-442.
19. Kearney, P. C., Zhang, H., Zhong, W., Dougherty, D. A., and Lester, H. A. (1996) Determinants of nicotinic receptor gating in natural and unnatural side chain structures at the M2 9' position, *Neuron* 17, 1221-1229.

20. Koh, J. T., Cornish, V. W., and Schultz, P. G. (1997) An experimental approach to evaluating the role of backbone interactions in proteins using unnatural amino acid mutagenesis, *Biochemistry* 36, 11314-11322.
21. Dougherty, D. A. (2000) Unnatural amino acids as probes of protein structure and function, *Curr Opin Chem Biol* 4, 645-652.
22. Saks, M. E., Sampson, J. R., Nowak, M. W., Kearney, P. C., Du, F., Abelson, J. N., Lester, H. A., and Dougherty, D. A. (1996) An engineered Tetrahymena tRNA^{Gln} for in vivo incorporation of unnatural amino acids into proteins by nonsense suppression, *J Biol Chem* 271, 23169-23175.
23. Hecht, S. M., Alford, B. L., Kuroda, Y., and Kitano, S. (1978) "Chemical aminoacylation" of tRNA's, *J Biol Chem* 253, 4517-4520.
24. Rodriguez, E. A., Lester, H. A., and Dougherty, D. A. (2006) In vivo incorporation of multiple unnatural amino acids through nonsense and frameshift suppression, *Proc Natl Acad Sci U S A* 103, 8650-8655.
25. Rodriguez, E. A., Lester, H. A., and Dougherty, D. A. (2007) Improved amber and opal suppressor tRNAs for incorporation of unnatural amino acids in vivo. Part 2: evaluating suppression efficiency, *RNA* 13, 1715-1722.
26. England, P. M., Lester, H. A., Davidson, N., and Dougherty, D. A. (1997) Site-specific, photochemical proteolysis applied to ion channels in vivo, *Proc Natl Acad Sci U S A* 94, 11025-11030.
27. Hohsaka, T., Ashizuka, Y., and Sisido, M. (1999) Incorporation of two nonnatural amino acids into proteins through extension of the genetic code, *Nucleic Acids Symp Ser*, 79-80.
28. Sakamoto, K., Hayashi, A., Sakamoto, A., Kiga, D., Nakayama, H., Soma, A., Kobayashi, T., Kitabatake, M., Takio, K., Saito, K., Shirouzu, M., Hirao, I., and Yokoyama, S. (2002) Site-specific incorporation of an unnatural amino acid into proteins in mammalian cells, *Nucleic Acids Res* 30, 4692-4699.
29. Petersson, E. J., Brandt, G. S., Zacharias, N. M., Dougherty, D. A., and Lester, H. A. (2003) Caging proteins through unnatural amino acid mutagenesis, *Methods Enzymol* 360, 258-273.
30. Kearney, P. C., Nowak, M. W., Zhong, W., Silverman, S. K., Lester, H. A., and Dougherty, D. A. (1996) Dose-response relations for unnatural amino acids at the agonist binding site of the nicotinic acetylcholine receptor: tests with novel side chains and with several agonists, *Mol Pharmacol* 50, 1401-1412.
31. Nowak, M. W., Gallivan, J. P., Silverman, S. K., Labarca, C. G., Dougherty, D. A., and Lester, H. A. (1998) In vivo incorporation of unnatural amino acids into ion channels in *Xenopus* oocyte expression system, *Methods Enzymol* 293, 504-529.
32. Beene, D. L., Dougherty, D. A., and Lester, H. A. (2003) Unnatural amino acid mutagenesis in mapping ion channel function, *Curr Opin Neurobiol* 13, 264-270.
33. England, P. M., Zhang, Y., Dougherty, D. A., and Lester, H. A. (1999) Backbone mutations in transmembrane domains of a ligand-gated ion channel: implications for the mechanism of gating, *Cell* 96, 89-98.
34. England, P. M., Lester, H. A., and Dougherty, D. A. (1999) Mapping disulfide connectivity using backbone ester hydrolysis, *Biochemistry* 38, 14409-14415.

35. Tan, Z., Forster, A. C., Blacklow, S. C., and Cornish, V. W. (2004) Amino acid backbone specificity of the Escherichia coli translation machinery, *J Am Chem Soc* 126, 12752-12753.

Chapter 2: Exploring the Chemical Nature of the *N*-methyl-D-aspartate (NMDA) Receptor Pore Blockade^{*}

2.1 Introduction to Learning and Memory

2.1.1 Long-term Potentiation and Long-term Depression

In Chapter 1 we described and recognized the importance of neuroreceptors and neurotransmitters in neurobiological functions. These proteins and chemicals are implicated in both normal and abnormal or diseased biological function. The exploration of these proteins and chemicals leads to more specific questions concerning the role of these biological structures in learning and memory function. At a biological and chemical level, how does the human brain learn? What biological processes contribute to learning and the formation and function of a memory? These are complicated questions to resolve. However, at the chemical-scale, we know that many of the neuroreceptors and neurotransmitters mentioned in Chapter 1 play a vital role in these processes.

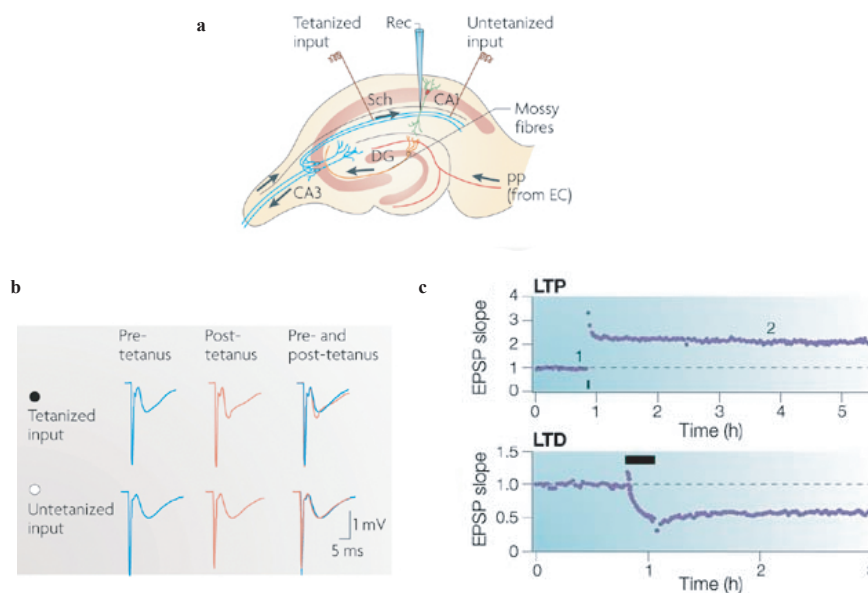


Figure 2.1 LTP and LTD. a) Hippocampal slice depicting the major excitatory neural pathways in the rat brain. b) Schematic outlining the stimulus (tetanus) applied to the hippocampal slice to induce LTP. c) LTP shown as an increase in the excitatory post-synaptic potential (EPSP) over

^{*}Reproduced in part with permission from McMenimen, K.A., Petersson, E.J., Lesater, H.A., Dougherty, D.A. *ACS Chemical Biology* **2006**, 1, 227–234. Copyright 2006 American Chemical Society

the baseline. LTD is demonstrated by a decrease in EPSP and is maintained for hours. Figure is adapted from (1, 2).

One approach to exploring learning and memory is to examine the manner in which neurons communicate with one another. It has been established that the central form of communication between neurons involves an electrical signal, the change to a chemical signal, and then back to an electrical signal in the next neuron. Prior study also established that for learning and memory to occur, the electrical to chemical to electrical change between neurons must take place. This process of change in the signals is referred to as synaptic plasticity. One form of synaptic plasticity occurs with the strengthening of this signal over a period of time, referred to as long-term potentiation (LTP). Its counterpart, long-term depression (LTD) is a reduction in the signal over time (Figure 2.1). LTP was discovered in the mid 1960's and has become the basis for determining how learning and memory are achieved on the molecular level (3-5).

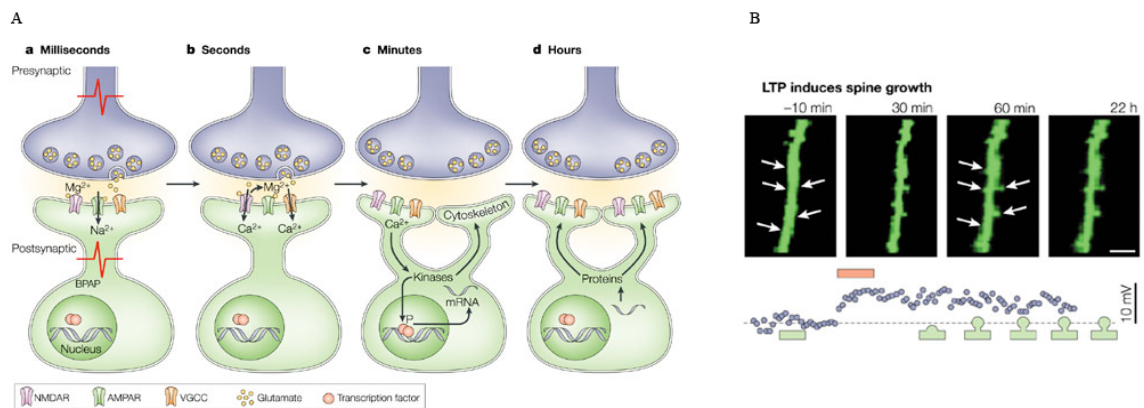


Figure 2.2 Synaptic changes after LTP induction. A) iGluRs are inserted into the synapse of cells that undergo LTP induction. Over several hours, not only is the composition of the synapse altered as more receptors are inserted into the membrane, but new synapses are formed and associated with new protein synthesis. B) LTP induces cell morphology changes as well, and over several hours new dendritic spines are created. Adapted from reference (6).

Electrophysiology performed on slices of the hippocampus show LTP induced by tetanus or large stimulus followed by recordings that remain above the baseline level recorded prior to the tetanus (Figure 2.1). In the absence of a large enough tetanus, no

LTP is recorded. The LTP counterpart, LTD results in a weakening of the synapse between cells triggered by a less intense tetanus of a longer duration (Figure 2.1c) (1, 3, 7-10). Directly extrapolating these molecular events to learning and memory formation is not possible, as many other events must take place for those large changes to occur, such as new synapse formation (Figure 2.2 A-B). However, identifying a basis for how cell-cell communication is altered over periods of time provides a starting point for determining the factors that contribute to learning and memory. Using LTP and LTD as a molecular framework will allow an exploration of the effect of changes in synaptic strength on the processes of learning and memory.

2.1.2 Synaptic Plasticity and iGluRs

On a smaller molecular scale, the molecules that contribute to some forms of LTP and LTD are LGICs(2). Although many different types of LGICs are important for communication in the central nervous system (CNS), glutamate-gated receptors (GluRs) and GABA (γ -aminobutyric acid) receptors, both ionotropic and metabotropic types, are essential for triggering synaptic transmission in learning and memory pathways (2, 11-14). The iGluRs have been a focus of our study due to their essential contribution to these intriguing and fundamental neuro-pathways and their role in diseases. The goal of our study has been to expand the nonsense suppression methodology to a new family of LGICs.

iGluRs are a superfamily of LGICs all activated by the endogenous neurotransmitter, glutamate (Glu). There are three main classes of iGluRs- the AMPA (α -amino-3-hydroxy-5-methyl-4-isoxazole-propionic acid), NMDA (N-methyl-D-aspartate), and kainate (KA) receptors- each named for their selective, synthetic agonists (Figure 2.3) (15). All of the iGluRs are tetrameric, cation-selective channels (Figure 2.4). NMDA receptors (NMDARs) are permeable to Ca^{2+} , K^{+} , and Na^{+} and AMPA and KA receptors are generally only permeable to Na^{+} and K^{+} . AMPA and NMDA receptors are directly implicated in LTP and LTD while KA receptors are indirectly associated with LTP (6, 16, 17).

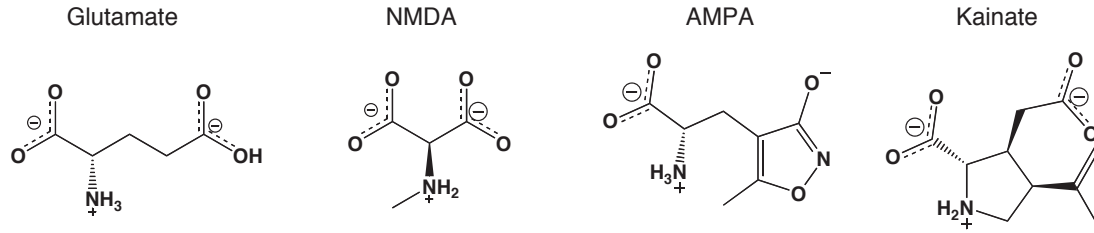


Figure 2.3 iGluR endogenous and selective agonists.

There are two general forms of synaptic plasticity, both of which rely on an alteration in AMPAR (AMPA receptor) and NMDAR in response to a stimulus (*18, 19*). The first form involves altering AMPARs already present at the synapse. Typically, AMPAR function is altered through a modification of an amino acid in the receptor, such as protein phosphorylation (*18*). Phosphorylation of serine (Ser), threonine (Thr), and tyrosine (Tyr) residues is a posttranslational modification used in many signaling pathways and other processes as a reversible method to change protein function. In the context of AMPAR and NMDARs, it is used repeatedly for targeting, trafficking, and altering protein function (*20*). Phosphorylation of AMPARs changes levels of postsynaptic currents contributing to LTP and LTD, but these changes in AMPAR phosphorylation are triggered by ion flow (Ca^{2+}) through NMDARs (*18, 20-22*).

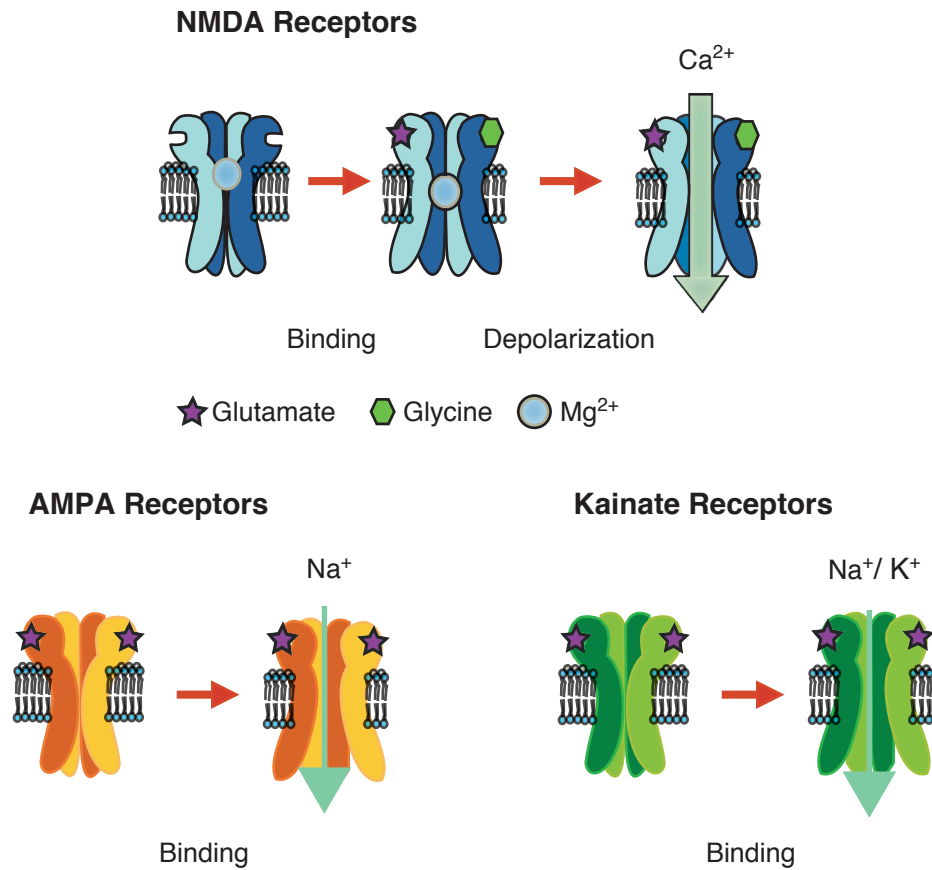


Figure 2.4 Schematic view of iGluR classes. The NMDA receptors are shown binding both glutamate and glycine. AMPA and Kainate receptors bind only glutamate. All of the iGluRs are tetrameric receptors.

The second mode of synaptic plasticity arises from alterations in protein levels, either by up or down-regulating protein production that corresponds to changes in the numbers of receptors at the synapse. Phosphorylation of AMPARs changes levels of postsynaptic currents that directly contribute to LTP and LTD. The second form of synaptic plasticity stems from changes in protein expression resulting from changes in gene regulation. These are changes in protein expression within the cell, and occur over longer time periods. Transcription of new proteins results in the formation of new synaptic connections and new proteins (may be other iGluRs or other proteins) trafficked to the membrane (23).

LTP is a complicated and very dynamic process. However, a simplified version is described to impart the importance of AMPAR and NMDARs in the process. Although both AMPARs and NMDARs are mobile and trafficked in and out of the synaptic membrane during LTP and LDP, the simplified outline begins with a few AMPARs in the synaptic membrane followed by LTP induction via newly trafficked NMDARs. AMPAR trafficking has been associated with many different proteins that associate with the synaptic membrane, such as Stargazin, a transmembrane AMPA receptor associated protein (TARP), PSD-95 (post-synaptic density protein-95), cytoskeletal proteins like actin and myosin, and several different kinases (2, 12). In general, receptors are synthesized within the cell, mobilized to the plasma membrane by exocytosis, and removed from the membrane for degradation by endocytosis. Once the receptors are at the cell surface in the membrane, they can diffuse laterally into and around the synapse (2, 12).

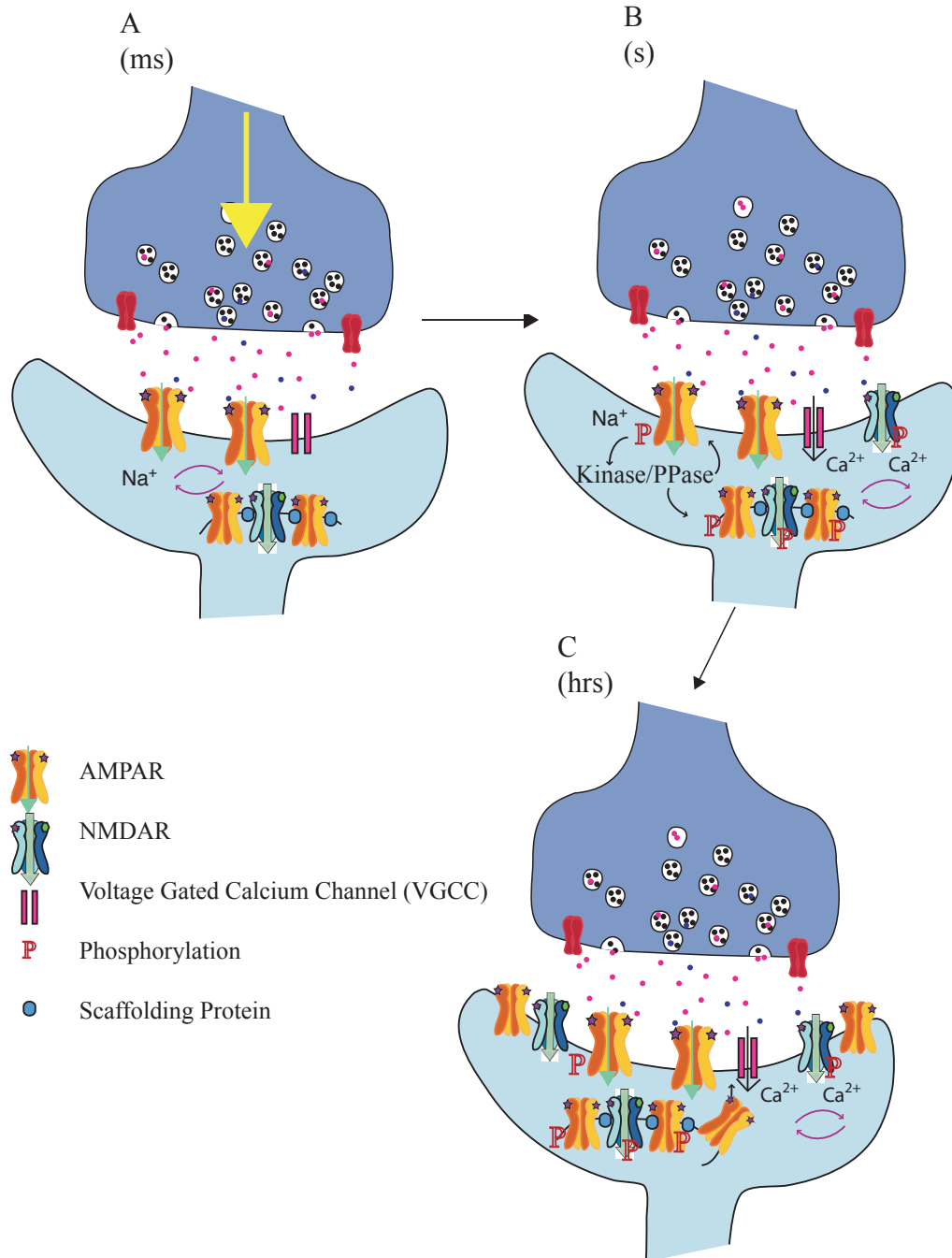


Figure 2.5 Overview of LTP. A) Basal level of control at glutamatergic synapses relies on AMPAR in the synapse. B) Sufficient membrane depolarization triggers VGCC and NMDAR activation, producing significant Ca²⁺ current into the post-synaptic cell activating kinase cascades and inducing receptor phosphorylation. C) Over longer periods of time, new receptors are trafficked into the synaptic membrane, strengthening the signal and inducing LTP.

Over short time-scales (ms) and in the absence of LTP, the release of glutamate at the synapse triggers response from AMPARs that are dynamically trafficked in and out of the synapse (13, 24). When a sufficient number of AMPARs have been activated, they cause the post-synaptic membrane to depolarize enough to open voltage-gated calcium channels (VGCCs) and NMDARs present in the membrane. The membrane depolarization is necessary to trigger NMDAR activation, but is not always sufficiently strong enough to trigger their activation (9). VGCC and NMDAR activation triggers a large flux of Ca^{2+} into the post-synaptic membrane causing activation of several kinases, such as the calcium/calmodulin-dependent protein kinase II (CaMKII) (2). These kinases can phosphorylate NMDARs, AMPARs, and other surrounding scaffolding proteins, altering the function of iGluRs (amount and type of current passing through the channel), channel trafficking and composition of the synapse (2). A change in synaptic composition is associated with an increase in AMPARs and NMDARs for LTP and a decrease in channels for LTD. These channels are typically located directly underneath the cell surface in vesicles or immediately outside of the synapse, awaiting a “signal” to send them to the synapse, which will increase the strength of the synapse by increasing the amount of current that is passed into the post-synaptic cell, inducing LTP. On a larger timescale, over hours and days, other kinases become activated (i.e., MAPK - mitogen-activated protein kinase pathway), which up-regulate gene transcription leading to new protein production (Figure 2.5). These new proteins contribute to the formation of new synapses and physically altering synapses (6).

2.1.3 The LTP Switch: NMDA Receptor Mg^{2+} Block

Although the details will be presented later in the chapter, it is important to mention one difference between AMPARs and NMDARs - the NMDAR Mg^{2+} block. It is important to remember that large Ca^{2+} currents traveling through NMDARs trigger LTP, since the currents from VGCCs are not sufficient on their own. The process of NMDAR regulation is extremely important, and one mechanism that prevents random LTP induction by NMDAR-evoked current involves a NMDAR blockade. At resting membrane potentials (no AMPAR-induced membrane depolarization) NMDARs in the cell membrane are blocked by an external Mg^{2+} ion, preventing Ca^{2+} flux into the cell

(even in the presence of Glu and Gly). Sufficient membrane depolarization (making the cell more positive, less negative relative to the outside) ejects the Mg^{2+} from the NMDAR pore, allowing Ca^{2+} flux. Overall, Glu activates AMPARs, which can depolarize the membrane enough to release NMDAR Mg^{2+} block followed by an influx of Ca^{2+} that triggers downstream signaling pathways. The function of this crucial trigger is the first target of our NMDAR studies.

LTP and LTD induction is controlled through the trafficking and physical movement of iGluRs and related proteins in and out of the synapse. These processes are controlled through a variety of very dynamic protein-protein interactions that occur between the receptors, kinases, scaffolding, and regulatory proteins (25). On a larger scale, these proteins are imaged by electron microscopy and are shown to associate in very concentrated groups (Figure 2.6A), yet are active and constantly moving depending on the signals present at the synapse. In particular, iGluRs directly associate with proteins that link to the cytoskeleton, which are involved in endo and exocytosis (Figure 2.6 B, C) (25, 26).

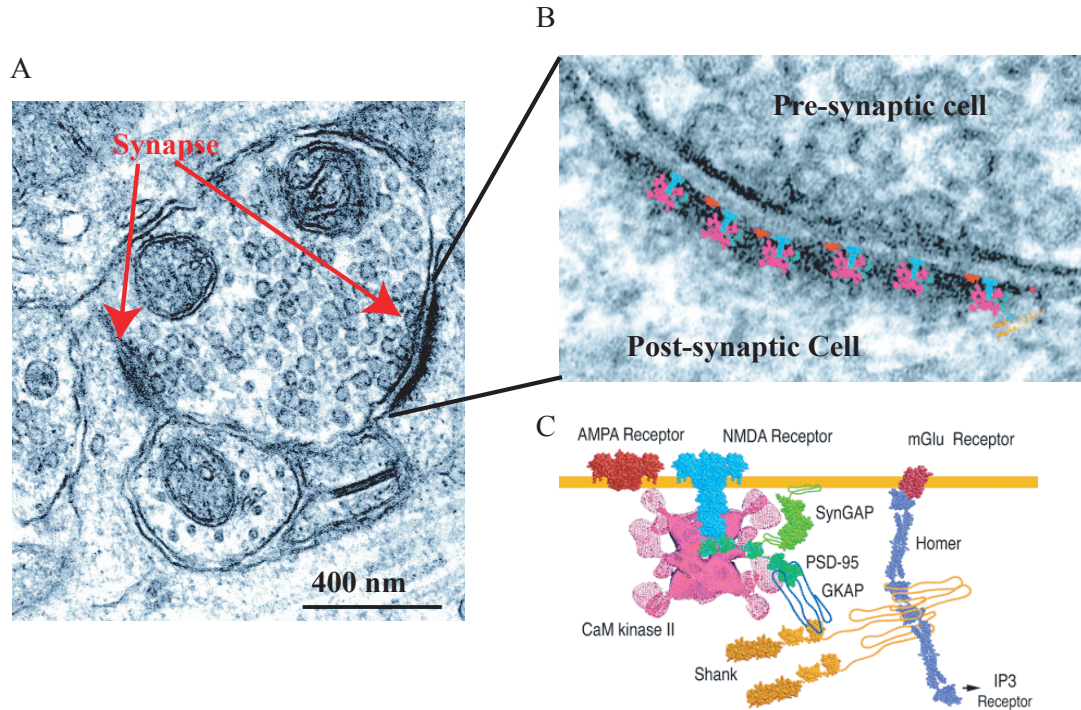


Figure 2.6 The Postsynaptic Density. A) A pre-synaptic cell associating with two dendrites forming two glutamatergic synapses. B) The synaptic interface from electron microscopy demonstrates iGluRs in the post-synaptic membrane and electron density of the surrounding associated proteins. C) Diagram representing some of the proteins that are found in electron microscopy images of the post-synaptic density. Image adapted from Kennedy, M.B.(27).

The above overview demonstrates the importance of iGluRs in synaptic plasticity and large biological processes such as learning and memory. The depicted processes generate signals between cells and explain how the signals are strengthened or weakened over time. Again, not only are the glutamate receptors important for maintaining cell-cell communication, but their dysfunction is associated with many neurodegenerative diseases. This exploration of glutamate receptors now will focus on the molecular-scale representation of these receptors.

2.1.4 Glutamate Receptor Structure and Diversity

There are several structural aspects that are conserved among all ionotropic glutamate receptors. Glutamate receptors are tetrameric, trans-membrane channels. Additionally, the tetramers are thought to associate as a dimer of dimers. Many structural aspects of

the iGluRs are different between the three families. For example, each family has a different set of subunits that can form the ion channel. There are also pre-transcriptional modifications that occur to impart diversity among the subunits, such as alternative gene splicing, and pre-translational modifications such as RNA editing. All of these modifications impart a lot of diversity among the iGluRs and create many mechanisms that allow for the regulation of functional aspects of these neuroreceptors.

AMPA receptors can be either homomeric or heteromeric channels comprised of GluR1, 2, 3, or 4 subunits, each containing approximately 850 amino acids. Typically, AMPARs are heterotetrameric channels containing GluR2 and GluR1, GluR3, or GluR4 in a symmetric “dimer of dimers” assembly (28-30). All AMPARs are activated by the binding of L-glutamate (Glu), which can bind to one site on each subunit (30). NMDARs are heterotetrameric channels composed of combinations of NR1, NR2A, 2B, 2C, and 2D subunits, each approximately 1,500 amino acids, and pass both Na^+ and Ca^{2+} . More recently, a third related gene family was discovered that codes for the NR3A and 3B subunits, which possess an inhibitory effect on receptor function (31). Kainate receptors are composed of GluR5, GluR6, GluR7, KA1, and KA2 subunits. Homotetramers form from GluR5-7 subunits while KA1 and KA2 subunits must be combined with one type of the GluR5-7 subunits (15).

All of the iGluRs gate in response to the endogenous neurotransmitter, Glu, but NMDARs also require another co-agonist for activation, which can be glycine (Gly) or D-serine (D-Ser) (15). Both of these endogenous co-agonists bind to the NR1 and NR3 (if present) subunits (Gly-binding subunits), and are present in the cytoplasm (in the CNS) at saturating concentrations required for NMDAR activation (32). Essentially, the co-agonist is always present and NMDA receptors (NR2 subunits) are activated by glutamate binding, after it is released at the synapse.

2.1.5 AMPA Receptor Diversity

Each of the GluR subunits is coded for by a separate gene and is susceptible to several post-translational modifications and RNA editing, which contributes to defining the properties of each subunit. It was established that AMPARs are always able to conduct Na^+ current. However, this is complicated by the presence or absence of the

GluR2 subunit (present in most AMPAR channels) in the composition of the particular ion channel. AMPARs lacking the GluR2 subunit will be permeable to Na^+ , Ca^{2+} and K^+ while most GluR2-containing receptors are Ca^{2+} impermeable. The GluR2 subunit contains a neutral glutamine (residue 586) in the gene transcript, which is edited to a positively charged arginine residue in the mRNA called the Q/R site (33, 34). This is believed to prevent excitotoxicity induced by excessive Ca^{2+} flow into the cell. There is another site of RNA editing, the R/G site (arginine becomes glycine), which is only edited approximately 50% of the time in the adult brain. One additional site of editing is the flip/flop exon that is alternatively spliced. This is a 38-amino acid sequence adjacent to the final trans-membrane domain that alters the desensitization kinetics of the receptor, as a receptor containing the flip form does not desensitize (35, 36). Although there are only four GluR subunits, modifications to these subunits impart a lot of diversity that can impact the function of the ion channel. These modifications are regulated and as new receptors are transcribed, these different functionalities can be introduced into the glutamate synapse, impacting LTP and LTD.

2.1.6 NMDA Receptor Diversity

Similar to the AMPARs, the NMDARs contain great diversity as well. A single gene codes for the glycine-binding NR1 subunit. Nature cleverly uses exon splicing to produce eight variants of the NR1 subunit, which interact with different intracellular proteins, and are expressed at various developmental stages to regulate NMDAR function (37, 38). In our discussion of NMDARs we study the most common CNS splice variant, NR1a (39), which we will reference as “NR1.” The glutamate-binding subunit of the NMDAR comes in four flavors, 2A, 2B, 2C, and 2D, each one a separate gene. These subunits are expressed during different developmental periods (NR2B is up-regulated prenatally and NR2A is up-regulated postnatally) and localize in specific areas of the synapse or extra-synaptic areas of the CNS. This diversity contributes to the role iGluRs play in LTP and synaptic transmission. As will be explained, assumptions about one specific receptor will not always apply to a related receptor.

2.1.7 iGluR Subunit Topology

Relative to other neuroreceptors, a lot of structural information is known about the agonist binding domain of iGluRs (discussed in more depth in Chapter 3), however much less is known about the overall receptor structure. Limited structural data exists about the subunit topology, however, many years of biochemical experiments and data suggest that each of the iGluR subunits (independent of receptor type) contain: a large extracellular amino terminal domain (ATD), followed by an extracellular ligand-binding domain, three trans-membrane domains, and an intracellular C-terminal domain (Figure 2.7A). The size of the C-terminal domain (CTD) varies widely within the family as well as between the receptor subtypes (40). The CTD is important for maintaining interactions with scaffolding proteins in the PSD and with proteins involved in signal transduction pathways. In the EM images from Sheng and co-workers, it appears that extra density in the C-terminal region (Figure 2.7C) belongs to an AMPAR-associated protein, Stargazin (41).

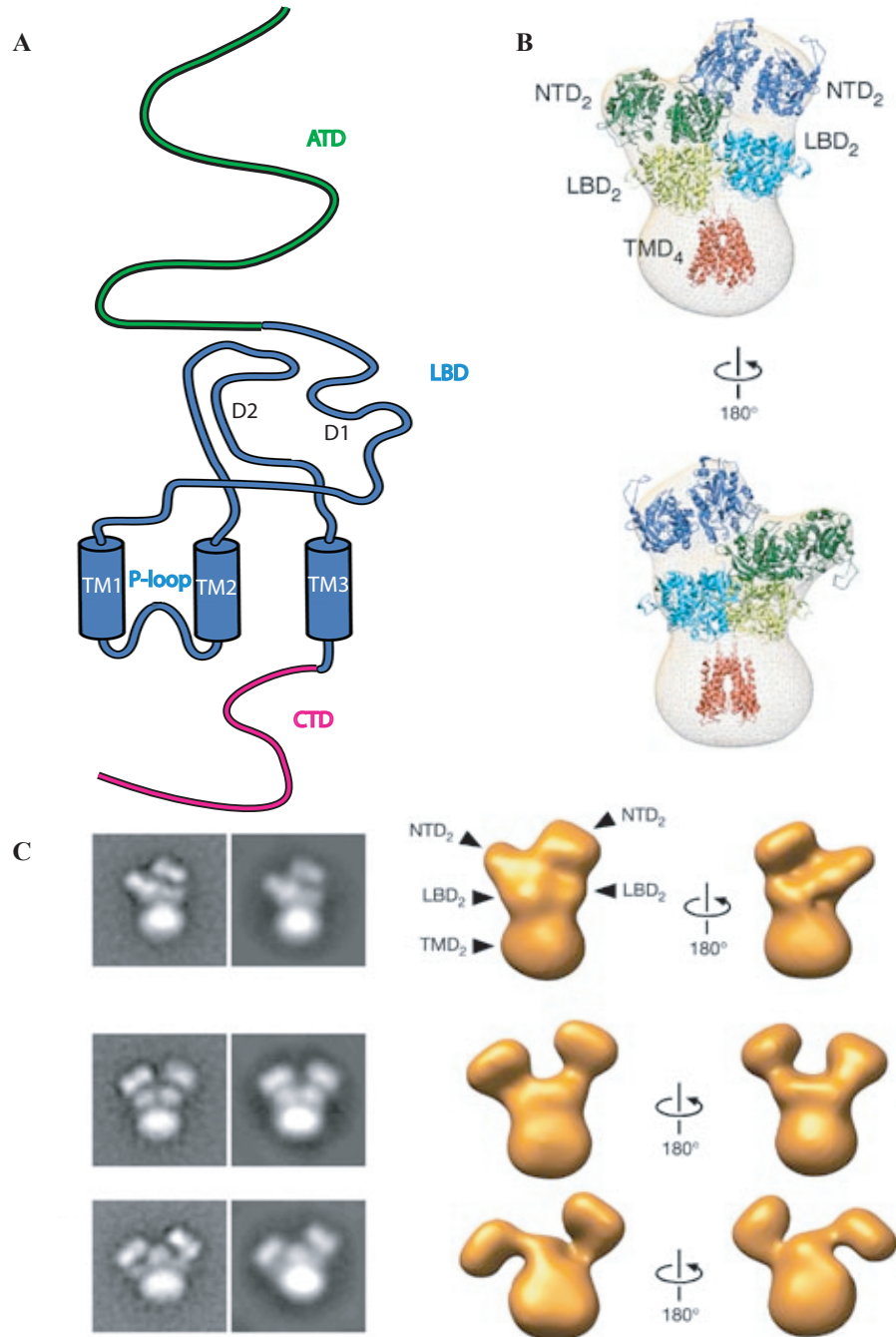


Figure 2.7 A) Topology of an individual iGluR subunit. A large cytoplasmic N-terminal domain (ATD or NTD) followed by the ligand-binding domain (LBD) composed of the D1 and D2 pieces, and three transmembrane domains with a re-entrant P-loop between TM1 and TM2. There is also an intracellular C-terminal domain (CTD) of varying length. B) Image of known crystal structures mapped onto the density map from electron microscopy of AMPARs. The crystal structures used are: extracellular domain of mGluR1 (Protein Data Bank 1EWV; dark blue

and dark green); ligand-binding domain of GluR2 (Protein Data Bank 1LBC; light blue and light green); and transmembrane segment of KcsA (Protein Data Bank 1BL8; red). Adapted from Nakagawa, T., et al. (41) C) Electron microscopy electron density maps of AMPARs showing two types of receptor structures, adapted from (41).

Much more direct structural information is available on the iGluR glutamate and glycine LBDs due to the work by Gouaux and coworkers (42-48), which we will describe in subsequent chapters. Briefly, a soluble protein containing the D1 and D2 domains (Figure 2.7A) of a NR1 or a related glutamate receptor subunit are linked together and expressed, with crystallography providing detailed structural insights into this domain of the protein. All of this work provides insight into our understanding of the function of iGluRs, particularly the LBDs. However, the trans-membrane domains in particular remain elusive.

The very limited direct structural information about the iGluRs is due to the immense difficulty in crystallizing large trans-membrane receptors. The available information suggests that the receptors are tetramers with unique subunit topology, due to a re-entrant P-loop that is reminiscent of the P-loop of the distantly related K^+ channels (49-51). The large ATD (Figure 2.7B), still un-crystallized (52), is structurally related to bacterial periplasmic binding proteins (LIV binding proteins) and the ligand-binding domain of the G-protein coupled receptor (GPCR), metabotropic glutamate receptors (mGluRs) (42, 53). Crystal structures of the bacterial amino acid-binding proteins and the ligand-binding domain of the mGluRs are modeled into electron density maps of the GluRs along with the trans-membrane domains from the K^+ channels to create a full picture of these receptors, since crystallizing the entirety of the receptors remains elusive (Figure 2.7B). This prompted our first studies of the trans-membrane region of the NMDARs and a site implicated in binding of a magnesium ion that blocks the NMDAR channel pore.

2.1.8 NMDA Receptor Mg^{2+} Block

As mentioned above, glutamate and glycine bind to the extracellular portion of the NMDAR receptor (Gly to NR1 and Glu to NR2), which initiates a conformational change

that opens the pore of the ion channel. In order for the channel to function, the Mg^{2+} ion that blocks the pore of the channel must be removed first, before Ca^{2+} can flow across the membrane (Figure 2.8). Mg^{2+} block is only alleviated by membrane depolarization (by convention, the outside of the cell has a potential of 0 mV and the inside of the cell is negative, usually -50mV to -100mV). Membrane depolarization moves the resting membrane potential toward a more positive value (towards zero). The biological implication is to make it more probable to fire an action potential. The Mg^{2+} block is one of nature's ways of preventing too much Ca^{2+} from flowing into a cell, which is directly correlated to excitotoxicity and cell death. These processes seem to be an underlying factor in the onset of some neurodegenerative diseases - just another reason why we are interested in understanding the molecular mechanisms of the Mg^{2+} block. Unfortunately, there is little structural evidence related to the Mg^{2+} binding site, which is deep within the pore of NMDARs. These initial research studies focused on the NMDA receptor and the Mg^{2+} blockade site.

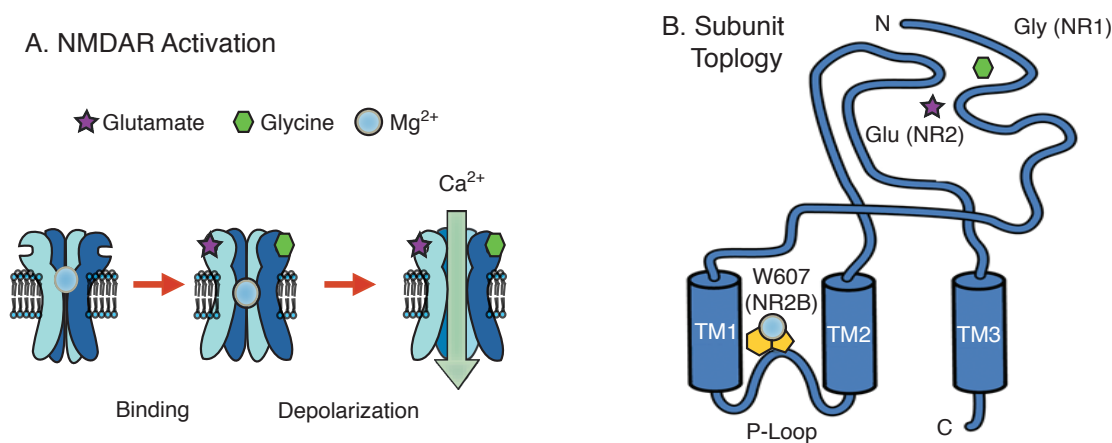


Figure 2.8 A) Schematic overview of NMDAR Mg^{2+} activation. Binding of Glu and Gly does not alleviate block, only the combination of Glu, Gly, and membrane depolarization allow Ca^{2+} flux through the receptor. B) Individual subunit topology of the NMDAR. Mg^{2+} is proposed to bind in the trans-membrane region of the pore at a site on the P-loop.

This chapter will outline several experiments aimed at understanding chemical-scale interactions involved in the pore of the NMDA receptor. The first studies will examine a proposed cation- π interaction between the Mg^{2+} ion during receptor blockade

and a conserved tryptophan (Trp607) located in the NR2 subunits. We will also examine a possible inter-subunit interaction between this Trp and an arginine (Arg630) in the NR1 subunits. The second group of experiments will explore the role of the N/Q site that is located at the narrowest constriction of the ion channel pore. We will use mutagenesis to analyze the importance of several conserved asparagines (Asn615 and Asn 616) during Mg^{2+} block and block attributed to small, synthetic organic molecules (i.e., Memantine).

2.2 Results

2.2.1 Previous Studies of the NMDAR Mg^{2+} Binding Site

Early electrophysiological studies of the NMDA receptor were able to localize the site of Mg^{2+} block and provide insights into the interaction between the ion and receptor.

Studying the voltage dependence of the block led to the proposal that blockage occurs deep within the pore of the ion channel (47, 54-57). At large hyperpolarized potentials (the inside of the cell is highly negative), Mg^{2+} can be driven through the membrane. It is likely that in order for Mg^{2+} to permeate the channel it must be dehydrated. Additional evidence for this comes from the fact that divalent metal ion permeabilities correlate inversely with dehydration energies (58). Hydrated Mg^{2+} has a diameter of 0.64 nm, which is larger than the NMDAR pore (<0.6 nm) (58-60). These studies suggest that in order for Mg^{2+} to permeate the pore, it must be stripped of its solvation shell (61).

Several studies of K^+ channels demonstrate that ion conduction through a pore can “rehydrate” or solvate dehydrated ions via ion-protein interactions as the ion travels through the pore (49, 62, 63).

Based on these early studies, mutagenesis of different residues within the NMDAR pore pointed to two different types of interactions important for Mg^{2+} binding, arising from amino acids located on the P-loop. The first interaction occurs at a hydrophobic site, a conserved tryptophan (NR2 W607) in the NR2 subunit (Figure 2.9A, B, and C). Many mutagenesis studies were performed at sites within the P-loop of the NR1 and NR2 subunits (Figure 2.9B). Williams *et al.* performed mutagenesis at the conserved Trp site in the NR1 and NR2 subunits and demonstrated the importance of the NR2 tryptophan in Mg^{2+} block, suggesting that the aromatic Trp side chain interacts via a cation- π interaction with the Mg^{2+} ion (64). Mutagenesis experiments substituting non-aromatic residues at the NR2B W607 resulted in a large increase in Mg^{2+} IC_{50} (the concentration producing half-maximal inhibition, similar to EC_{50}) values from 19 μM to greater than 300 μM (at -70 mV) (Figure 2.9B). Additionally, mutations at analogous Trp residues in the NR1 subunit did not have any effect on Mg^{2+} IC_{50} values, indicating

that only NR2B W607 was implicated in Mg^{2+} block. A significant disparity was observed with mutations replacing the Trp with the other aromatic residues, Tyr and Phe. As seen in Figure 2.9B, IC_{50} values for Mg^{2+} increased only slightly (64) when the other aromatic amino acids replaced Trp. Receptors containing aromatic amino acid mutations in the P-loop all demonstrate wild type like responses to glutamate, glycine, and pH, implying that they are otherwise unchanged. One important caveat is that receptors containing the NR2B W607Tyr or W607Phe mutations are more permeable to Mg^{2+} than the wild-type receptors, which could be due to the size differences among the amino acids or the relative cation- π binding abilities of the side chains.

The second interaction implicated in contributing to Mg^{2+} block occurs between several highly conserved asparagine residues (NR1 N616 and NR2 N615 and N616) that appear on both NR1 and NR2 subunits (thought to lie at the apex of the turn) (Figure 2.9A,C) and the metal ion. Mutagenesis of the asparagines in NR1 and NR2 to Gly, Gln, Ser, and Asp establish that they interact with the cation through an electrostatic interaction instead of just through a steric occlusion of the pore (65-67). Wollmuth *et al.* found that block was slightly attenuated, but not abolished, when Gln was mutated to Gly or Ser and did not substantially increase upon mutation to Asp (a fully charged sidechain). Additionally, their results demonstrate that residues along the P-loop are asymmetrically involved in Mg^{2+} block. Wollmuth *et al.* propose that Mg^{2+} becomes at least partially dehydrated during block and compensates for the reduced hydration shell by obtaining a six-coordinate geometry (preferred) via interactions with the NR2A asparagines (65). The asparagines replace the hydration shell around Mg^{2+} .

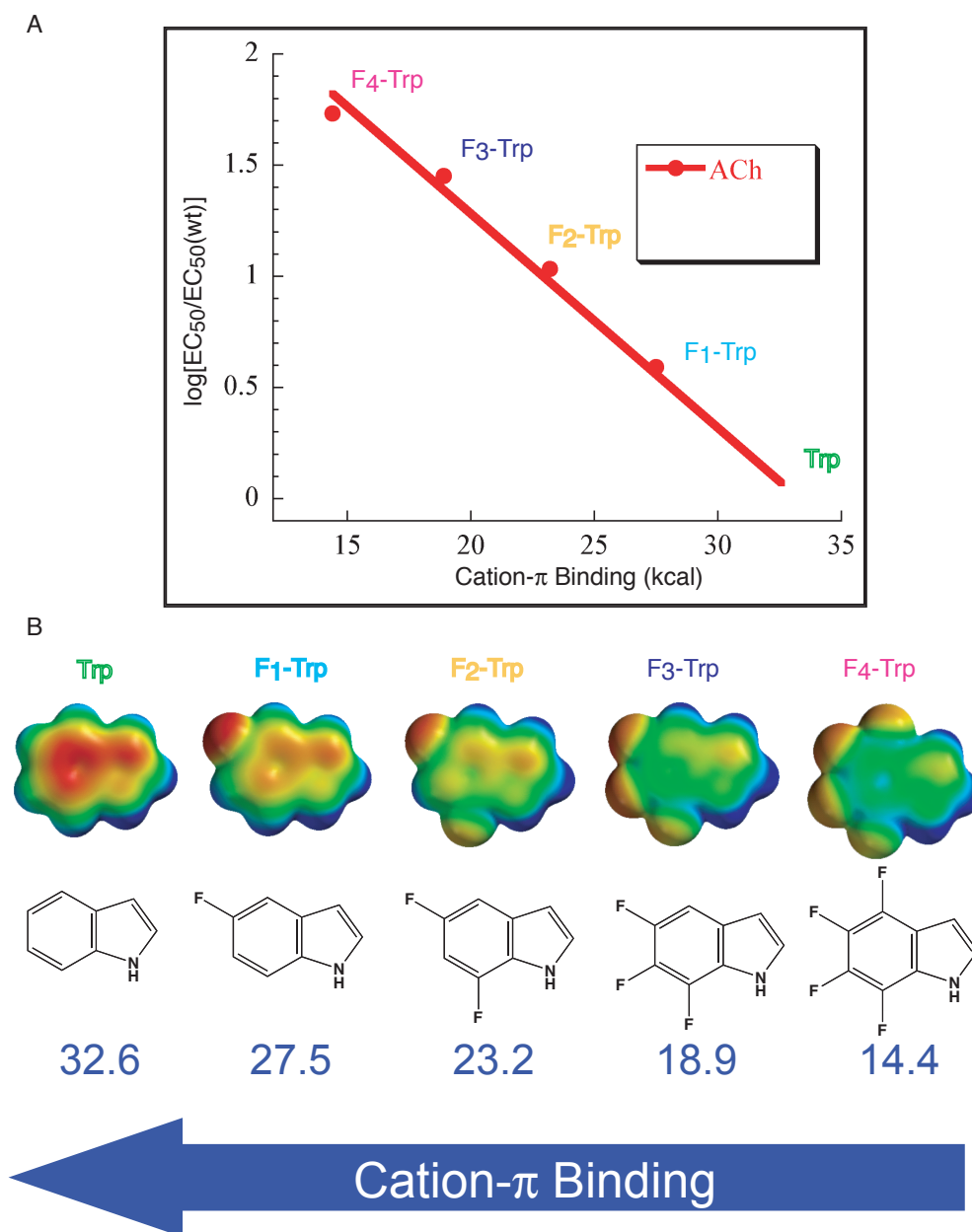


Figure 2.10 A) Cation- π plot demonstrating a linear relationship between the cation- π binding ability of the side chain aromatic amino acid and the shift in ACh EC_{50} with each mutation. B) Electrostatic potential surfaces representing each of the fluorinated Trp side chains and the calculated cation- π binding energies

The above work established a starting point for our analysis of the NMDAR Mg^{2+} binding site. We began by focusing on the hypothesis postulated by Williams' that Mg^{2+} binds to NR2 W607 *via* a cation- π interaction. Our group had successful prior experience

incorporating fluorinated Trp residues into the ACh receptor to establish the existence of a cation- π interaction with a cationic agonist; therefore, we wanted to harness this same technique for this study (68-73). Using the fluorinated Trp series we would observe a step-wise decrease in Mg^{2+} block if a cation- π interaction contributed to blockade. This exact experiment was performed and identified a cation- π interaction between a conserved Trp (residue 149) of the muscle nicotinic acetylcholine receptor and the endogenous neurotransmitter, acetylcholine (68). The unnatural amino acid methodology is perfectly aligned for these experiments, as fluorinated Trp analogs are a precise chemical perturbation of this interaction. Fluorinated Trp is a much weaker cation- π binder than Trp, yet is almost completely isosteric, free from inflicting steric perturbations. In order to study the cation- π interaction, we sequentially replace Trp with monofluoro-, difluoro-, trifluoro-, and tetrafluoro-Trp and compared the calculated (innate) cation- π binding ability of the aromatic side chain (kcal/mol) to the EC_{50} of the agonist when the mutation is present ($\log EC_{50}$ is plotted to maintain a similar energy scale) (Figure 2.10). A similar scale was used for measuring IC_{50} as well. Initially, in the case of ACh, an exceptional correlation was observed that was later extended to explain the binding of additional agonists (68, 72).

Since we had developed a protocol for analyzing the importance of cation- π interactions, we began our investigation at the NR2B W607 site. This site was implicated in previous studies and believed to be the most important aromatic residue involved in Mg^{2+} block. It was first explored with the fluorinated Trp series. It was expected that upon incorporation of the fluorinated tryptophan residues a step-wise decrease in Mg^{2+} block would be observed if the cation- π interaction was implicated in the blockade. A linear relationship would be observed between the calculated cation- π binding energies of the fluorinated Trp side chains and the log of the measured IC_{50} from each mutation compared to wild type. These initial studies were performed in collaboration with another graduate student, E. James Petersson.

2.2.2 Wild Type NMDA Receptor Expression

Prior to unnatural amino acid mutagenesis in the NMDA receptor, a robust and reproducible expression system needed to be established for the wild type receptors.

Precedents reported in prior literature from the Williams laboratory for NMDA receptor expression in oocytes were used and constructs for NR1a and NR2B (NMDARs most sensitive to Mg^{2+} block) were obtained. These constructs were originally cloned into the pBluescript vector. However, more recent studies demonstrate that using a *Xenopus laevis* expression vector for oocytes will increase the resulting receptor yields. Therefore, both the NR1a and NR2B genes were subcloned into a vector designed for expression in oocytes, pAMV vector. pAMV is derived from pBluescript but contains an additional 5' untranslated region from the alfalfa mosaic virus that aids in binding to the ribosome (74).

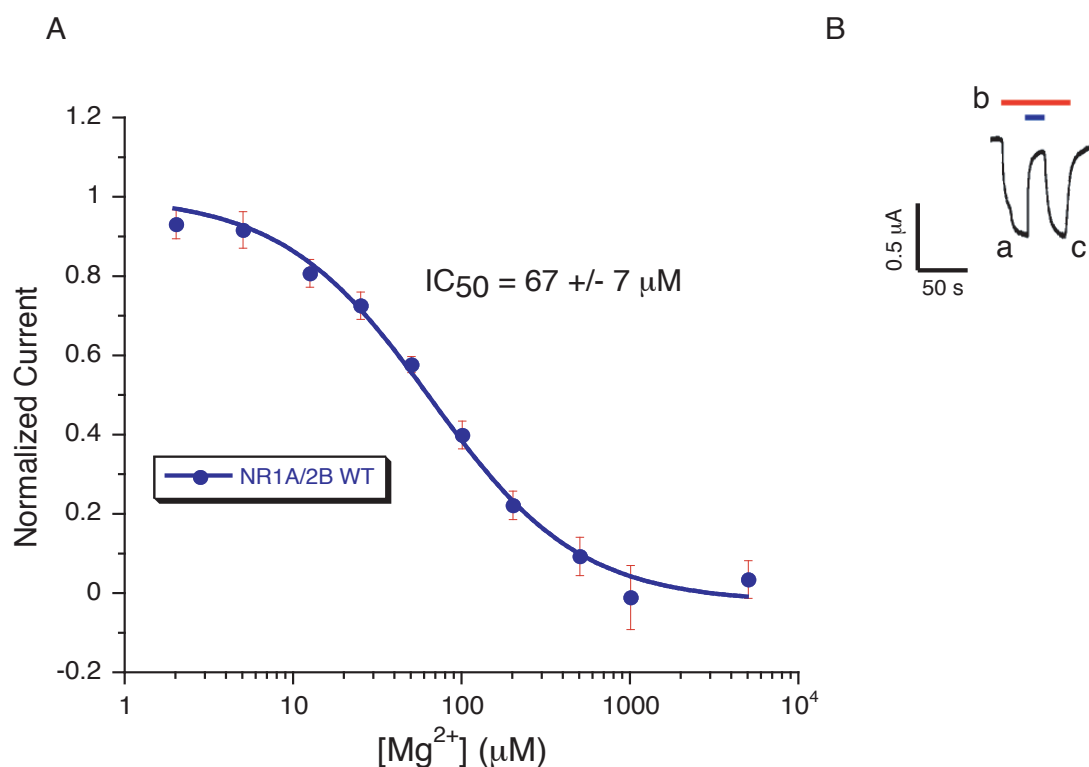


Figure 2.11 NMDA receptor Mg^{2+} block. A) Dose-response curve generated for Mg^{2+} block. B) Electrophysiology trace of wild type NR1a/NR2B receptors. Red bar = 100 μM Glu + 10 μM Gly. Blue bar = 500 μM Mg^{2+} .

Wild type NR1a/NR2B mRNA subunits were injected into *Xenopus* oocytes in a 1:1 ratio. Oocytes were incubated for a standard 2 days. A dose-response curve for Mg^{2+} block obtained of the wild type receptors (Figure 2.11A) to confirm expression.

Protocols previously described by Williams and coworkers (64) were followed. Briefly, a series of saturating doses of each agonist, 100 μM Glu and 10 μM Gly, were applied to each oocyte for a given duration of time (Figure 2.11B). EC_{50} values for Glu and Gly were determined as 1.4 μM and 0.14 μM , respectively. When obtaining EC_{50} values for Glu and Gly, a saturating dose of Gly (10 μM) or Glu (100 μM) was always applied, respectively. Concentrations much larger than the EC_{50} values are used during the experiments to ensure that full receptor activation is achieved, which is important in determining the effects of mutations on Mg^{2+} block. After the initial application of Glu and Gly (Figure 2.11B (a)), a dose of Mg^{2+} that also contains the agonists was applied (Figure 2.11B (b)), followed by a washout solution with just the agonists (Figure 2.11B (c)). This procedure reveals the receptor activation, Mg^{2+} block, and the reversibility of the blockade.

In order to generate the IC_{50} graph (Figure 2.11A), the ratio of the response (signal) in the presence and absence of Mg^{2+} versus the concentration (doses) of Mg^{2+} used to generate the IC_{50} was plotted. Previous studies have recorded the Mg^{2+} IC_{50} value at 19 μM for the wild type NR1a/2B receptor (64). Using the OpusXpress™ and the cloned constructs, the wild type NR1a/2B receptor Mg^{2+} block was recorded at 66.7 ± 7 μM (Figure 2.11A). Although this number is different from that of the Williams' lab, it is not surprising, as previously obtained EC_{50} s from acetylcholine and GABA receptors recorded on the OpusXpress™ were larger than those recorded on traditional electrophysiological rigs.

2.2.3 Control Experiments

One set of control experiments was performed due to reports of homomeric NR1a subunits forming functional channels in *Xenopus* oocytes (75, 76). In order to confirm that the responses analyzed were from properly formed heteromeric NR1a/2B receptors, the NR1a subunit mRNA was injected into oocytes without NR2 mRNA. Doses of 100 μM glutamate and 10 μM glycine were applied to the oocyte (protocol shown above). However, no current was recorded from these oocytes. This indicated that the previous experiments that produced responses to 100 μM glutamate and 10 μM glycine were in fact recording heteromeric NR1a/2B receptors.

Based on previous studies with the nicotinic acetylcholine receptor, which normally incubates for 1-2 days post mRNA injection, this incubation time was used initially. However, in order to optimize the NMDAR expression, the incubation time was altered by allowing the oocytes to incubate at 16°C for 2-4 days post mRNA injection. After 4 days of incubation post wild type NR1a/2B mRNA injection, the oocytes were unhealthy and useful data was not obtained or recorded. As a result, the optimal incubation time for wild type NR1a/2B receptors was determined to be two days. One reason why the oocytes may become unhealthy is due to the activation of Ca^{2+} activated Cl^- channels, which would disrupt the membrane potential of the oocyte.

After successful expression of the appropriate wild type receptors and generating reproducible results, the next step was to demonstrate the recovery of the wild type receptor phenotype using nonsense suppression to incorporate Trp at position 607 in the NR2B subunit (a “wild type recovery” experiment). Several experiments were performed to optimize unnatural amino acid incorporation into functional NMDA receptors. The experiments first began by making a TAG (stop codon) mutation at residue 607 in the NR2B gene. Wild type recovery experiments were performed by co-injecting NR1a/NR2BW607TAG mRNA (1:5 ratio) and $\text{tRNA}_{\text{CUA}}\text{-Trp}$. After optimizing incubation conditions again, it was concluded that 2 days produced optimal results. In order to increase expression, a “booster” injection was given to each oocyte after 24 hours of $\text{tRNA}_{\text{CUA}}\text{-Trp}$. The booster injection only contained $\text{tRNA}_{\text{CUA}}\text{-Trp}$ because the limiting factor in nonsense suppression is the amount of aminoacyl tRNA that is injected into the oocyte.

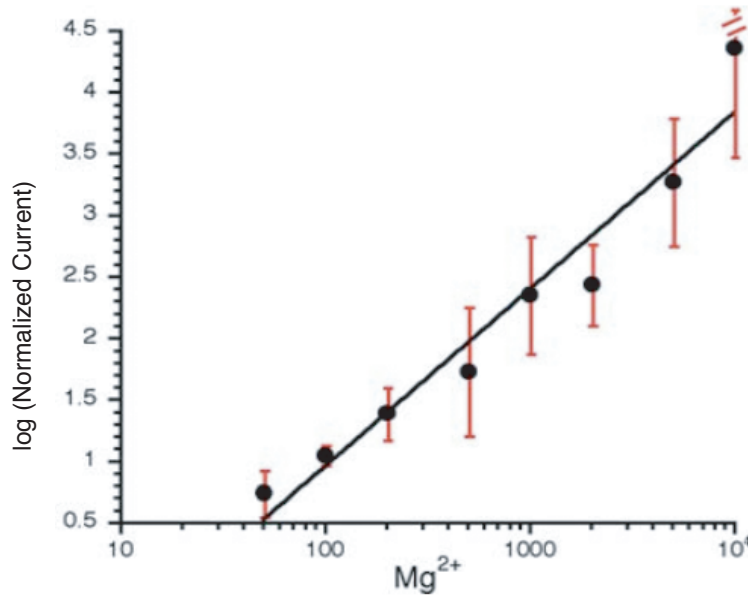


Figure 2.12 Misincorporation phenotype generated by receptors expressed from NR1a/2B607TAG mRNA co-injected with tRNA_{CUA}.

One possible complication due to the nonsense suppression method is the re-acylation of tRNA by the oocytes' endogenous aminoacyl tRNA synthetases after the unnatural amino acid is incorporated into the protein. If this occurs, it will lead to “misincorporation” of an undesired amino acid at the site of interest. In order to test the amount of misincorporation current generated, NR1a/2B607TAG mRNA was injected into oocytes without injecting the corresponding aminoacyl-tRNA. Glutamate and glycine were co-applied to these oocytes and no current was recorded. To determine if the synthetic tRNA could be used by the oocyte, as a control NR1a/2B607TAG mRNA was co-injected with an unaminoacylated tRNA_{CUA} (76 mer, biologically relevant unaminoacylated tRNA). The results produced substantial background currents. However, Mg²⁺ could not block these receptors. Instead, they were permeable to Mg²⁺ at concentrations larger than ~1000 μM. In Figure 12, the currents produced at Mg²⁺ concentrations less than 1000 μM are typical Na²⁺ currents, and the amount of current then increases as Mg²⁺ concentration increases (>1000 μM), indicative of more ion flow across the membrane. A logarithmic relationship was observed between the magnesium concentration and the NMDAR currents recorded, signifying that Mg²⁺ does not block the receptor but functions as a charge carrier (Figure 2.12) (77).

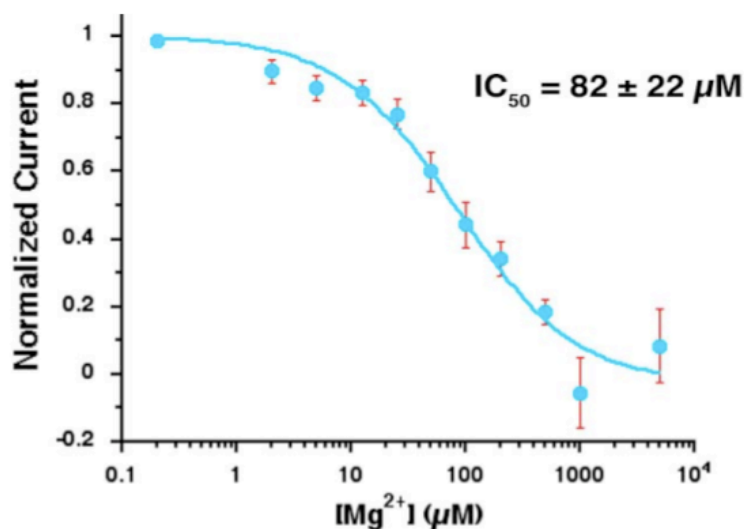


Figure 2.13 Wild type recovery experiment producing an Mg^{2+} IC_{50} of $82 \pm 22 \mu\text{M}$. NR1a/2B607TAG mRNA was co-injected with $\text{tRNA}_{\text{CUA}}\text{-Trp}$.

Williams and co-workers also found that Mg^{2+} permeates the pore for some poorly blocking mutant receptors, such as the NR2B 607Leu mutant (64). Optimization experiments conducted as part of this study demonstrated that misincorporation currents are greatly reduced when nonsense suppression experiments are performed 2 days after the initial oocyte injection. With these conditions, it was concluded that the background was sufficiently low to produce reasonable data for the unnatural amino acid experiments of this study. The first wild type recovery experiments were performed and generated a dose-response curve for Mg^{2+} block by incorporating Trp via suppression at NR2B607. The results were within error of the wild type IC_{50} value indicating successful nonsense suppression of NMDARs (Figure 2.13).

2.2.4 Incorporation of F_n -Tryptophans at NR2BW607

The above protocol was followed for expression of receptors containing F_n -Trps. NR1a/2B607TAG mRNA was co-injected with $\text{tRNA}_{\text{CUA}}\text{-F-Trp}$ to determine the importance of a cation- π interaction in Mg^{2+} block. First, it was noticed that F-Trp incorporation resulted in currents that were approximately 20% smaller than those from Trp incorporation as well as more sporadic expression levels overall, yet dose-response relationships were still generated without difficulty. As with most electrophysiological

experiments, it is important to look at traces, which are shown below for wt (wild type), Trp, and F-Trp (Figure 2.14).

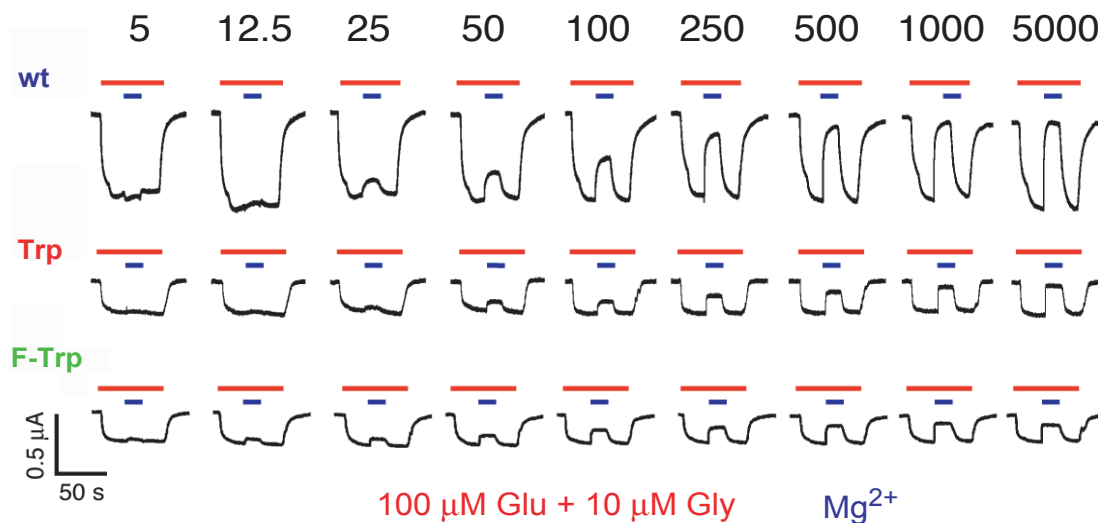


Figure 2.14 Electrophysiological traces for wt, Trp, and F-Trp incorporation in the NR1a/NR2B607 receptors. Expression levels decrease and full Mg^{2+} block is not achieved with suppressed receptors. Mg^{2+} concentrations are shown at the top in (μM).

The only observable difference between Trp and F-Trp incorporation is that full Mg^{2+} block is not observed with F-Trp incorporation. Even at high Mg^{2+} concentrations, full receptor block was not reached (Figure 2.13 and 2.14). It is likely that the small amount of “misincorporation” currents skewed the results. However, despite this data, reasonable IC_{50} values were obtained and resulted in the dose-response data comparable to wild type data.

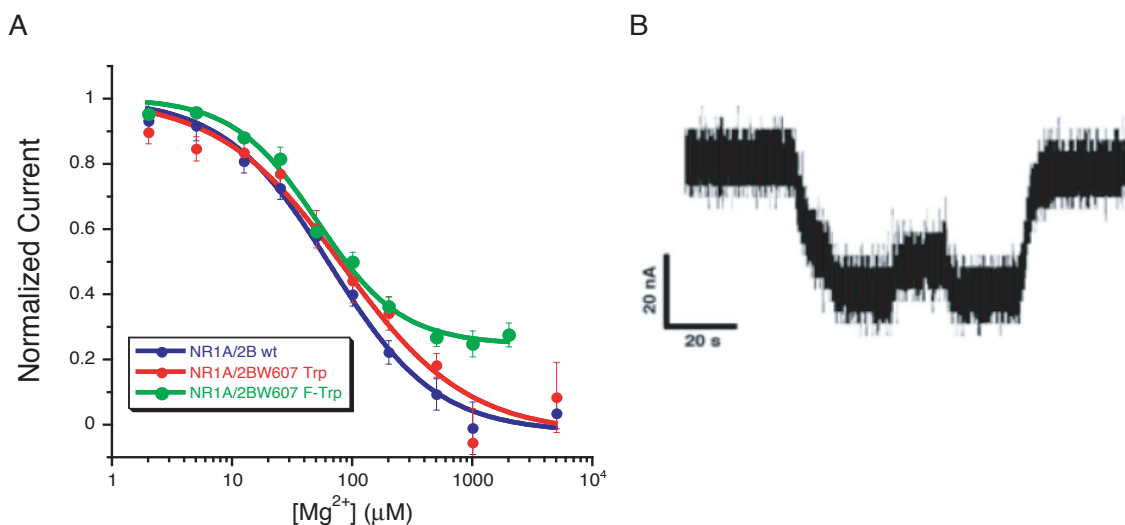


Figure 2.15 NR2B607F Trp Data. A) IC_{50} values for Mg^{2+} block at wt, Trp, and F-Trp NMDARs. B) F_2 -Trp Electrophysiology data.

As seen above (Figure 2.15A) incorporation of F-Trp at NR2B607 did not result in a rightward (or any) shift in Mg^{2+} IC_{50} with a value of 52 μM . Since no significant rightward shift was observed with NR2B607F-Trp, it appears that a cation- π interaction is not likely to occur between W607 and the metal ion. To rule out the possibility of a cation- π interaction, F_2 -Trp was incorporated at NR2B607. Initially, small currents were recorded (Figure 2.15B), but with double injections of $tRNA_{CUA}$ - F_2 Trp increased expression was sufficient enough to determine an IC_{50} for Mg^{2+} of $52 \pm 10 \mu M$.

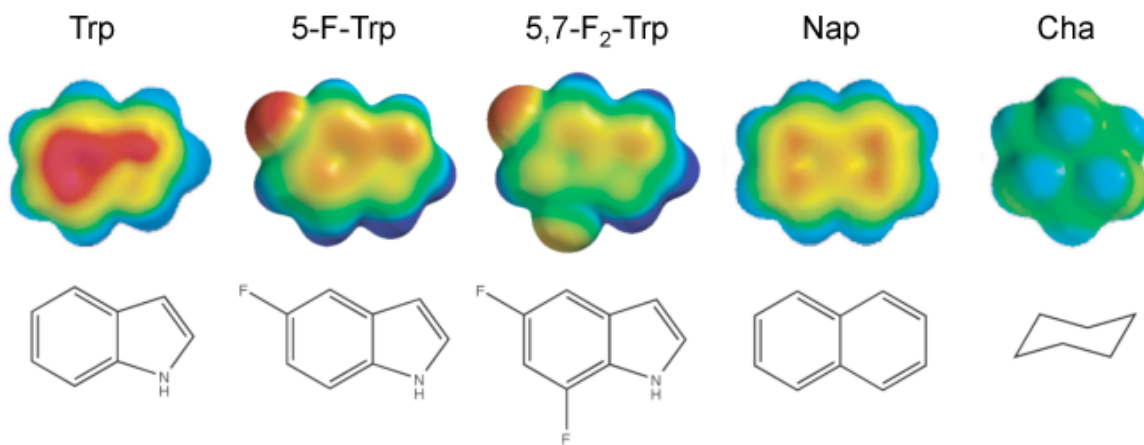
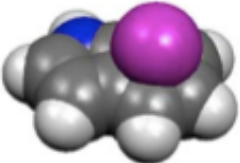


Figure 2.16 Electrostatic potential surfaces for Trp analogs used in the NR2B607 Mg^{2+} binding studies. Stick representations of the side chains are below.

2.2.5 Calculated Magnesium Binding Energies

In previous studies, the calculated *ab initio* binding energy of a Na^+ ion to an aromatic ring was used as a measure of the ring's cation- π binding ability (68, 70) (Figure 2.16). Fluorination of the aromatic ring reduces the cation- π binding ability by reducing the negative electrostatic potential at the center of the ring. In order to verify that nothing unusual occurred with Mg^{2+} , high level *ab initio* calculations were performed using indole and fluorinated derivatives with Mg^{2+} . In the gas phase, the binding of Mg^{2+} to indole gives a ΔE of -142.3 kcal/mol (vs. -32.6 kcal/mol for Na^+). With 5-fluoroindole the affinity is decreased by 11.3 kcal/mol (vs. 5.1 kcal/mol when Na^+ is the probe cation). The cation- π interaction is much stronger for Mg^{2+} than for Na^+ due to the larger charge density on the divalent ion, an anticipated result for an interaction with a large electrostatic component. Fluorination of the side chain also has a greater effect. Similar calculations were performed using implicit solvation models for water, ethanol, and THF (Figure 2.17). The calculations clearly establish that a substantial change would be seen in the results if a direct cation- π interaction were important. For reference, in both the serotonin and γ -aminobutyric acid receptors, the ligands for each receptor (of the type RNH_3^+), resulted in decreased ligand affinity values ranging from 30-fold to 180-fold, respectively (73, 78) to difluorination of a binding site aromatic amino acid.



	Mg^{2+} Binding Energy (kcal/mol)		
	Trp	5-F-Trp	5-F-Trp - Trp
Gas	-142.3	-131.0	11.3
THF	-24.2	-14.8	9.4
EtOH	4.0	11.3	7.3
H₂O	6.7	15.1	8.4

Figure 2.17 Mg^{2+} cation- π binding energies calculated with Trp side chains. Counter-poise corrections were used and all calculations performed at B3LYP/6-31⁺⁺G (d,p) level of theory and basis set.

2.2.6 Mutagenesis studies of Inter-Subunit Contacts in the NMDAR Pore

Previous work demonstrated that only aromatic residues functioned in the pore at NR2B607 (64). However, the results of this study rule out any interaction containing a significant electrostatic component, i.e., the cation- π interaction and π - π interactions. Moreover, a simple hydrophobic side chain such as Leu is not sufficient since the W607L mutation demonstrates no Mg^{2+} block. The W607L mutation also rules out the possibility of the cation- π interaction “jumping” to the NR1 subunit (NR1 W608) when fluorinated derivatives are placed in NR2B. Another explanation is sterics - that a relatively large, flat, hydrophobic side chain is required to “plug” the pore. In order to probe this possibility, several additional Trp analogs were incorporated at NR2B607, 2-Naphthylalanine (2-Nap), Tyr, and cyclohexylalanine (Cha). These Trp analogs are residues used to test steric interactions of the side chain. 2-Nap is structurally similar to Trp but does not contain an indole moiety. Cha is the non-aromatic side chain corresponding to Phe, structurally similar in size and shape to Phe. Incorporation of 2-Nap results in wildtype Mg^{2+} block. Incorporation of Tyr and Cha resulted in an approximate 4-fold shift in Mg^{2+} IC₅₀, but still maintained some receptor block and were essentially identical (Table 2.1). It thus appears that a rigid, relatively flat, hydrophobic residue is required at position 607 for potent Mg^{2+} block.

Table 2.1 IC₅₀ Data for Wild type and Mutant NMDA Receptors. The numbers in parenthesis are the number of oocytes measured to obtain each value. IC₅₀ values, δ values, and K_{0.5} values are shown as mean \pm s.e.m Cation- π binding values are computed as in (64, 70).

Subunit/Amino Acid	Mg ²⁺ IC ₅₀ (μ M) -60 mV	Cation- π Binding (Na ⁺) kcal/mol	n	I Max Avg. (nA)	δ	K _{0.5} (0 mV) (mM)
Wild-type NR1a/2B	76 (\pm 5.5)	32.6	7	850	0.74 (\pm 0.11)	3.7 (\pm 2.9)
NR1a/2B607TAG W	82 (\pm 22)	32.6	6	102	0.77 (\pm 0.07)	11 (\pm 3.2)
NR1a/2B607TAG 2-Nap	37 (\pm 4)	28.9	5	102	0.54 (\pm 0.15)	0.5 (\pm 0.3)
NR1a/2B607TAG 5-F-Trp	52 (\pm 5)	27.5	8	170	0.36 (\pm 0.11)	1.6 (\pm 1.1)
NR1a/2B607TAG 5,7-F2-Trp	52 (\pm 10)	23.3	5	35	0.73 (\pm 0.03)	2.9 (\pm 0.6)
NR1a/2B607TAG Cha	190 (\pm 11)	8.4	4	160	0.39 (\pm 0.06)	1.1 (\pm 0.3)
NR1a/2B607L	No Block		4	510		
NR1a/2B607TAG Y	170 (\pm 28)	26.9	4	1100		
NR1a/NR2BW607R	No Block		4	100		
NR1aR630W/2B	NF					
NR1aR630W/2BW607R	NF					
NR1a/2B607TAG 76mer	No Block		5	25		

2.2.7 Current-Voltage (I-V) Relationships

Since the Mg²⁺ block is voltage-dependent, the agonist-induced current-voltage (I-V) relationships were examined in the presence and absence of Mg²⁺. One way to analyze I-V relationships is by comparing a set of parameters discussed by Woodhull (63). The Woodhull parameters were obtained by plotting the logarithm of the IC₅₀ (LogIC₅₀) over a range of voltage potentials versus the holding potentials. Then a straight line was fit to the data to determine δ and K_{0.5} (Table 2.1). The parameter δ represents the portion of the electric field sensed by the site and K_{0.5} is the half-maximal block at 0 mV. This study determined that wild type NR1a/NR2B receptors demonstrate the expected concentration and voltage dependent Mg²⁺ block (Table 2.1) (79). A mutation that has similar size and cation- π binding ability to Trp, W607 2-Nap, was strongly concentration and voltage dependent. Interestingly, the W607Y mutant does not reach full Mg²⁺ block even though the cation- π binding ability of Tyr is very similar to Trp and 2-Nap (Figure 2.16). This suggests that the voltage-dependent Mg²⁺ block is not correlated to the cation- π binding ability at NR2BW607.

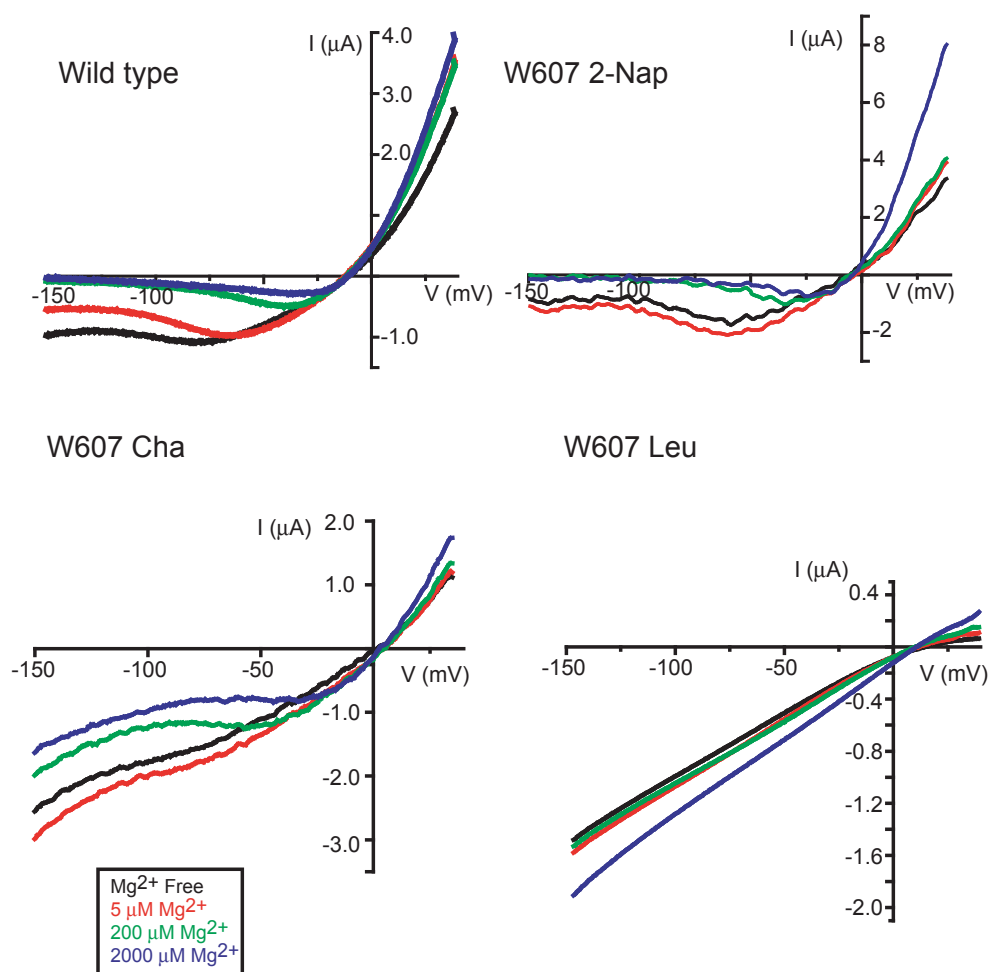


Figure 2.18 Current-voltage (I-V) relations generated by voltage ramps; see methods. NR1a/NR2B, NR1a/NR2BW607 2-Nap, NR1a/NR2BW607 Cha, and NR1a/NR2BW607L.

The voltage-dependence of Mg^{2+} block for the NR2BW607 Cha mutant (Figure 2.18) also was determined. Although the I-V relationship demonstrates some concentration and voltage-dependent Mg^{2+} block of the receptor, the block is incomplete at even the highest Mg^{2+} concentration (2 mM). Additionally, the block is relieved at high negative potentials. This suggests that Mg^{2+} can permeate the pore and block the pore with this mutation. On the other hand, the W607L mutation, also shown in previous studies, displays no relevant Mg^{2+} block at any concentration or voltage tested. From a chemical perspective both Cha and Leu are hydrophobic residues with no significant cation- π ability, yet there are noticeable differences between the Mg^{2+} block of Cha and

Leu. The Cha-containing receptor partially blocks Mg^{2+} , whereas the Leu-containing receptor does not. The experiments conducted in this study suggest that the size and shape of the side chain at NR2B607 influences Mg^{2+} block more than aromaticity.

2.2.8 Similarities of the P-Loop of Glutamate Receptors and Potassium Channels

Since we determined that a cation- π interaction between NR2BW607 and Mg^{2+} doesn't exist, we were interested in investigating other roles for this conserved Trp in channel function. Previous studies and sequence alignments suggest the structural similarity between the pores of potassium channels and glutamate receptors (49) and are often used for modeling purposes when creating images of glutamate receptor overall topology. Sequence comparisons demonstrate a high homology between the pore-forming regions of K^+ channels and the P-loop of glutamate receptors (49, 80), including conservation of the residue that corresponds to NR2BW607. The KcsA K^+ channel corresponding residue, W67 (NR2BW607 equivalent), was identified as being involved in an inter-subunit cation- π interaction with KcsA R49 (Figure 2.19).

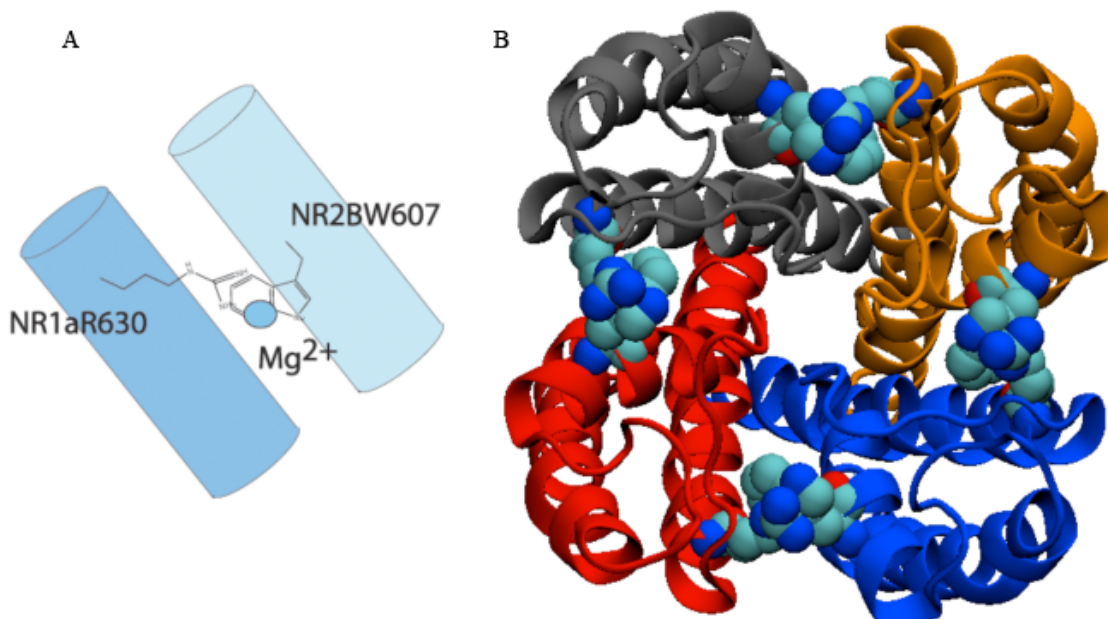


Figure 2.19 Schematic of NMDA receptor pore. A) Schematic demonstrating a possible inter-subunit cation- π interaction between NR1R630 and NR2BW607. B) Crystal structure of KcsA showing the four inter-subunit cation- π interactions between W67 and R49, structure adapted from (81). PDB file: 1BL8.

During the comparison of the receptors, it was noticed that the glutamate receptor residue corresponding to KcsA R49 is either an Arg or Lys, which would be amenable to a cation- π interaction. In order to determine if this inter-subunit interaction translated to the glutamate receptors and to further probe the interaction, “residue swapping” experiments were performed to evaluate NR2BW607R and NR1aR630W mutations and the double mutation. The NR2BW607R mutant activated upon agonist application, but, as expected, the block by extracellular Mg²⁺ was abolished. The NR1aR630W single mutant and NR1aR630W/NR2BW607R double mutant did not produce any current in response to agonist application.

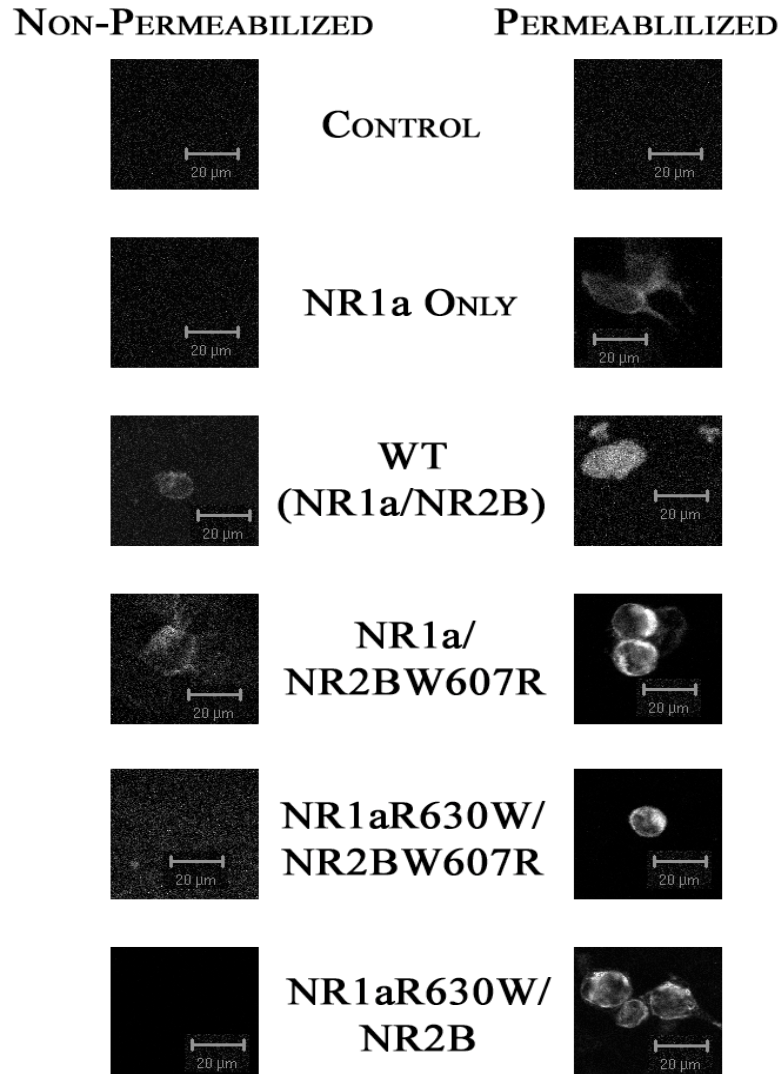


Figure 2.20 Immunolocalization of wild type, functional, and nonfunctional mutant NMDA receptors expressed in HEK293T cells. Permeabilized and non-permeabilized membrane images are labeled.

To determine whether the apparently non-functional mutant receptors were expressing at the plasma membrane, the localization of these mutants was studied using an NR1-specific antibody. HEK293T cells expressing the wild type or the functional mutant (NR1a/NR2BW607R) showed clear labeling of the membrane in non-permeabilized cells. In contrast, no such labeling was seen for the nonfunctional receptor mutants (NR1aR630W/NR2B and NR1aR630W/NR2BW607R) (Figure 2.20). Permeabilization of the membranes allowed labeling of intracellular NR1a subunits in all

cases. While it is possible that expression patterns would be different in HEK293T cells than in *Xenopus* oocytes, we feel the more reasonable explanation is that the receptors that were “nonfunctional” in fact failed to fold and/or transport properly to the cell surface. Although we hypothesized that the double mutant (NR1aR630W/NR2BW607R) might rescue the receptor by re-establishing a cation- π interaction, the results suggest that the Arg at position 630 in NR1a is necessary for receptor assembly and/or transport.

2.2.9 Asparagine Residues and NMDA Receptor Block by Extracellular Cations

After our characterization of the conserved Trp site involved in Mg^{2+} block, this study turned to an investigation of the conserved asparagines in both NMDAR subunits. There are two conserved asparagines in NR2B at positions Asn 615 and Asn 616. Only one exists in the NR1a subunit, Asn 616. By convention, the NR2 subunit N615 is labeled the N site or N(0) site and, N616 is the N+1 site. Previous studies have implicated the asparagine residues in Mg^{2+} block. In addition, these Asn residues are also associated with NMDA receptor block caused by extracellular cations, such as the synthetic small molecules, phencyclidine (PCP), a common drug of abuse, MK-801, an NMDAR antagonist, and memantine (Namenda®), which is a pharmaceutical currently on the market for treatment of moderate to severe Alzheimer’s Disease (82). Using conventional mutagenesis, several studies demonstrated that the Asn residues did not contribute equally to block by external Mg^{2+} (65, 67). As demonstrated in Figure 9, the asparagines are thought to lie at the narrowest constriction of the channel pore and at the top of the P-loop (60), suggesting that one of the side chains can interact more favorably with an extracellular cation compared to the other. Mutagenesis studies in the NR1 and NR2A subunit have demonstrated that the N+1 site contributes to Mg^{2+} block more than the N site (65, 67) of NR2A, while the NR1 subunit Asn contributes very little to Mg^{2+} block.

Keeping in mind the previous studies, this exploration of the N and N+1 sites first focused on the NR2B subunit. Mutagenesis of the Asn residues to Gln, Asp, Ser, and Gly produced evidence that the N+1 site in NR2 provided an energy barrier to ion flux through the channel, establishing a block. Wollmuth *et. al* postulated that the asparagines

could act as a steric block since the size of hydrated Mg^{2+} (> 0.7 nm) would be larger than the pore (0.55 nm). On the other hand, the asparagines could act as a binding site for Mg^{2+} through ion-dipole coordination due to the polarity of the Asn side chain (65). However, one would expect that if the latter were important for Mg^{2+} block, then mutation of the side chain to Asp (full negative charge) would enhance Mg^{2+} block, which was never observed (83, 84). The novel chemical approach used in this study to probe chemical-scale interactions involved incorporation of a series of fluorinated Asns to decrease the side chain polarity. This essentially mirrored the fluorinated Trp experiment, but with a different amino acid side chain.

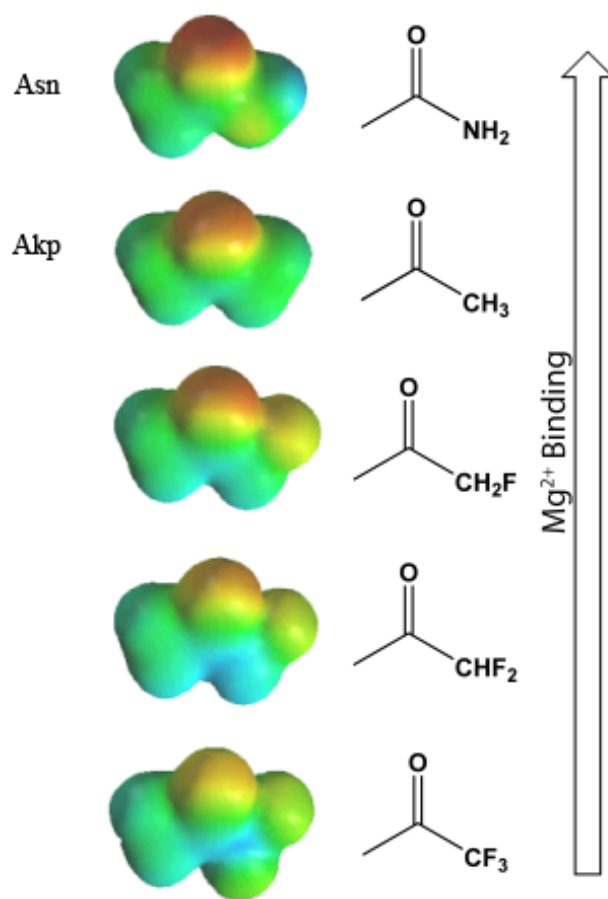


Figure 2.21 Analogs of asparagine that decrease the negative charge density on the amide carbonyl. Electrostatic potential surfaces demonstrate the weaker (less red) amide carbonyl as fluorination of the ketone increases.

The chemistry of Asn would allow the amide carbonyl to chelate Mg^{2+} during NMDAR blockade. The negative electron density would coordinate to Mg^{2+} through an ion-dipole interaction forming an energy barrier to Mg^{2+} release from the pore. This is an ideal interaction to probe chemically. Analogs of Asn that would reduce the negative charge density of the amide carbonyl were sought for incorporation. These analogs would weaken the Mg^{2+} -carbonyl interaction, and it was hoped this would result in a shift in Mg^{2+} IC_{50} . In previous studies of the muscle type nAChR, the neutral Asn analog, 2-amino-4-ketopentanoic acid (Akp, Figure 2.21), was used to delineate the effects of a carbonyl side chain in stabilizing different agonists in the binding site (85-87).

To study the NR2B N and N+1 site residues the N615D, N615TAG, N616Q, N616D, and N616TAG mutations were created. Conventional mutagenesis studies were conducted and resulted in shifts in IC_{50} (Table 2.2). The experiments conducted demonstrated that both the N and N+1 site influenced Mg^{2+} block. Amino acid substitutions at NR2B N615 resulted in no Mg^{2+} block whereas mutations at NR2B N616 resulted in greatly attenuated block. One noticeable shift was the N616D mutation, which slightly decreased IC_{50} . This shift supports previous suggestions that an ion-dipole interaction stabilizes Mg^{2+} block (Table 2.2, Figure 2.22). Following the analysis with conventional mutations, Akp was incorporated at the N and N+1 sites (Table 2.2). The N615Akp mutation resulted in ablation of Mg^{2+} block, whereas the N616Akp mutation produced wild type like Mg^{2+} block. Although these results reinforce the unsymmetrical contribution of the N and N+1 site Asns to Mg^{2+} block, the results of this study suggest that the amide carbonyl of the N site contributes more to Mg^{2+} binding than the N+1 site.

Table 2.2 IC₅₀ values for Mg²⁺ block at the N and N+1 site in NR1a/NR2B NMDA receptors.

*The number of oocytes contributing to each IC₅₀ value is in parenthesis.

Mutation	Mg²⁺ (μM)*	Hill
wild type	76.3 ± 5.46 (7)	1.22 ± 0.086
2BN615D	No Block (6)	
2BN615Akp	No Block	
2BN616D	46.3 ± 5.43 (8)	1.06 ± 0.122
2BN616Q	>2000 (5)	
2BN616Akp	~90.0 ± 5 (6)	
1aN616D	607 ± 168 (2)	1.07 ± 0.22
1aN616Q	>3000 (4)	

Following the analysis of Mg²⁺ block for the Asn mutations, an investigation was conducted of the chemical mechanisms of NMDA receptor block by other extracellular cations. Due to the importance of NMDARs in learning and memory and the implications for these receptors in stroke and neurodegenerative diseases, much time and effort already has been spent in an attempt to specifically target and regulate these receptors with small molecules. Memantine (Namenda©) is a cationic NMDAR blocker that reversibly blocks the channel (88, 89). Memantine is often referred to as a “better magnesium ion,” in that it has a higher affinity for the receptor, a slower unblocking rate, and moderate voltage dependence (90-92). Several mutagenesis studies demonstrate that there are two sites of memantine interaction with the NMDARs. The primary binding site occurs at N site Asns, the narrowest constriction of the pore. The secondary binding site is more controversial, but appears to be located in a shallow extracellular vestibule and/or a more extracellular region of the pore (92-97).

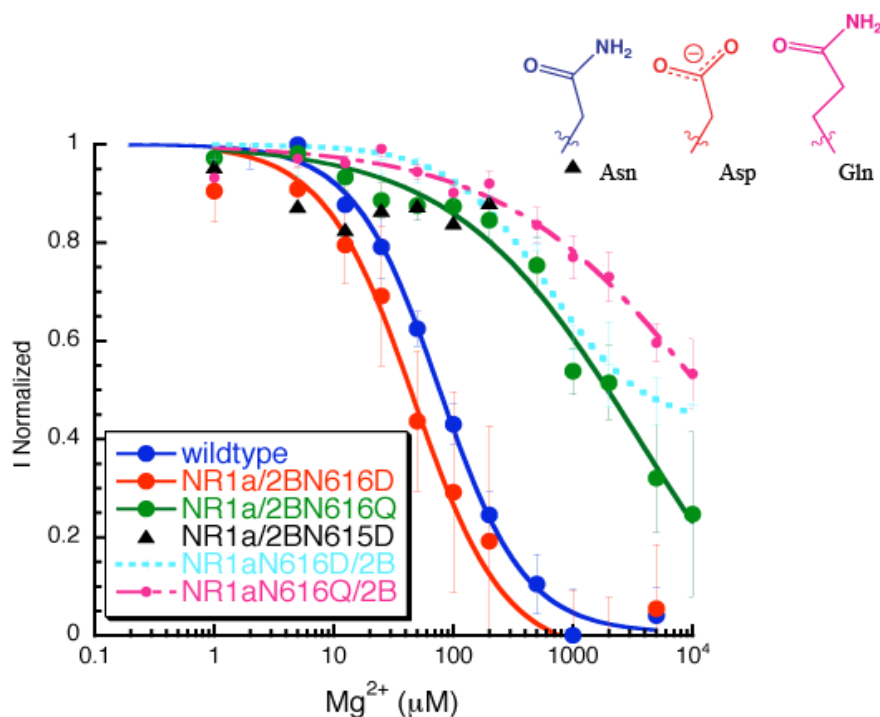


Figure 2.22 Asparagine site IC_{50} curves. IC_{50} dose-response data for NR1a/NR2B receptors with mutations at the N and N+1 sites. Stick representations of the different conventional side chain mutations for the Asp and Gln mutations compared to wild type Asn.

Similar to the Mg^{2+} block, an electrostatic interaction was suspected in the block by memantine. Therefore, parallel experiments were conducted with Asn site mutations to record memantine IC_{50} data. Based on these experiments, memantine is a more potent NMDAR channel blocker with a wild type IC_{50} of 2.4 μM (Figure 2.23). As in previous studies, the NR1a N616Q mutation results in the largest shift in IC_{50} (~10-fold shift) and the NR2 Asn site mutations produce no shift.

After obtaining several IC_{50} values for different N site mutations with both Mg^{2+} and memantine, it was observed that not all of the mutations resulted in full receptor block. This was a concern because the method used for comparing IC_{50} values for the mutations was suspected to not provide an accurate account of the effects these mutations were having on the receptor. For example, several of the mutations do not shift IC_{50} (NR2B N616Q mutation) significantly, but they do greatly attenuate block. Therefore, this study then compared the total amount of receptor block at both the wild type receptor

IC₅₀ value for each blocker and at maximal blocker concentration. Using this method it was expected that large differences in how the mutation affects receptor blockade would be detected.

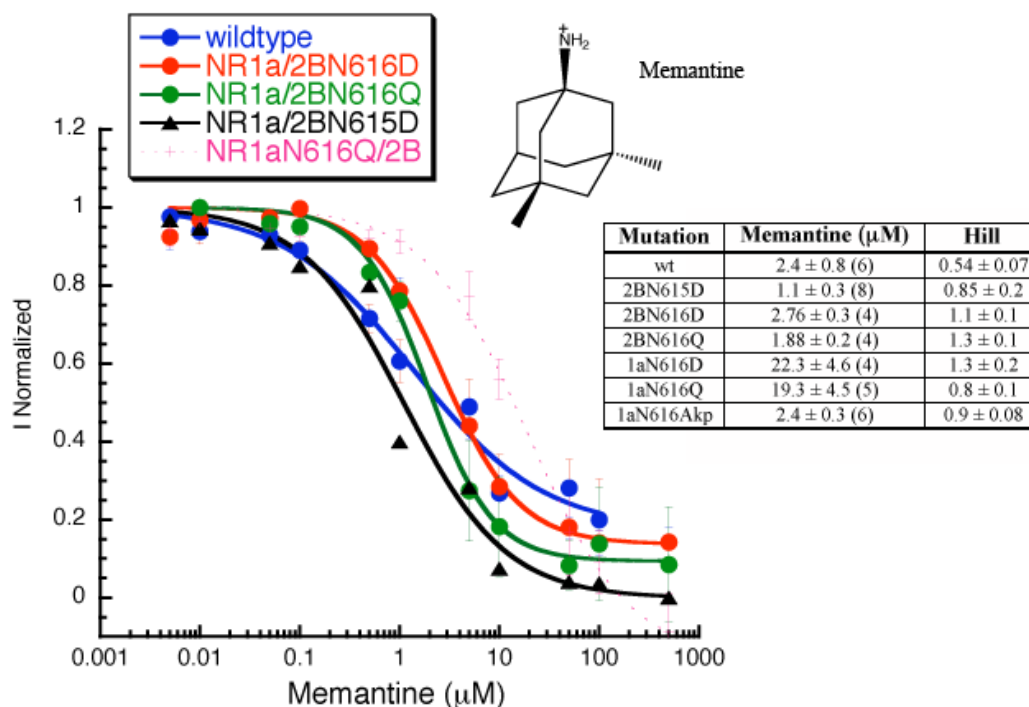


Figure 2.23 Asparagine IC₅₀ curves with memantine. IC₅₀ data for memantine block of wild type (wt) and Asn site mutations in NR1a/NR2B receptors.

This analysis was performed for both Mg²⁺ and memantine block. The overall results suggest that, for Mg²⁺ block, the amide carbonyl of NR2BN615 contributes to Mg²⁺ binding and block. However, altering the sterics of the NR2B N616 side chain with the N616Q mutation resulted in ablation of Mg²⁺ block (Figure 2.24). These results suggest that the size and sterics of the N+1 site contribute to Mg²⁺ block, and that the amide carbonyl of the N site coordinates to the magnesium ion during block. The results with memantine demonstrate that, on the whole, neither the NR2B N or N+1 site contributes to block. In fact, although the block at IC₅₀ levels of memantine varies slightly with the mutations, a large shift is never observed and full receptor block is maintained. These results, combined with those of prior studies using NR1a mutations,

suggest that the N site in the NR1 subunit is involved with memantine block and the NR2B mutations contribute very little to block. Interestingly, these results suggest that these blockers utilize different electrostatic and steric interactions on binding to NMDARs.

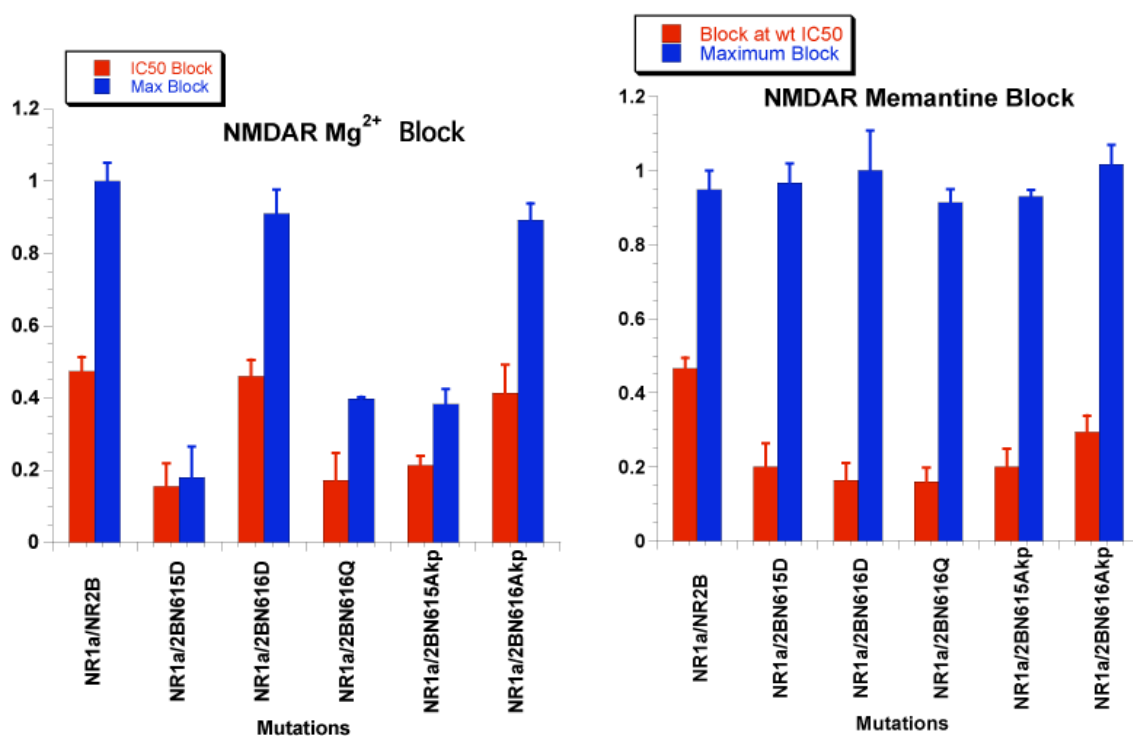


Figure 2.24 Percent block for Mg^{2+} and memantine. Studies of NR1a/NR2B receptor block at N and N+1 site mutations. Receptor block was characterized at wild type IC₅₀ values (red) and at maximal concentrations for Mg^{2+} and memantine (blue).

2.2.10 Additional Studies of NMDA Receptor Blockade

There are many additional molecules that block the NMDA receptors. Investigations of a couple of these were started. MK-801, which is a very potent open channel blocker that binds in the pore of NMDARs, and phencyclidine (PCP), which also binds to and blocks the NMDAR pore, were examined. Both of these molecules are cationic blockers and bind within the pore of NMDARs (Figure 2.25).

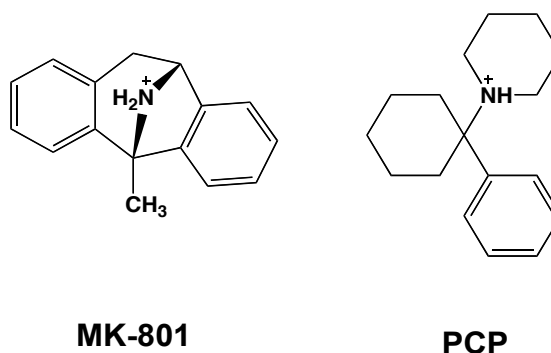


Figure 2.25 NMDA receptor blockers. Structures of the NMDAR blockers MK-801 and PCP.

It quickly became clear that electrophysiology experiments using the OpusXpress would be difficult with MK-801, which is a very potent blocker of the NMDAR and binds at nanomolar concentrations. One issue with MK-801, which also makes it a less than ideal pharmaceutical, is its inability to be “washed off” of the channel. In other words, once it binds to the pore it sticks with such high affinity that it is not removed easily. This can be observed by looking at electrophysiological recordings (Figure 22.26). This feature makes data acquisition very difficult, because in order to generate a dose-response curve, the channel must be reactivated before each dose of blocker is applied. Active channels cannot be reactivated with MK-801 because it remains in the channel. The resulting responses to drug and blocker are not accurate and skew the dose-response relationship, impeding experimentation. Although efforts were made to explore MK-801 further, ultimately these experiments were put aside in place of other experiments.

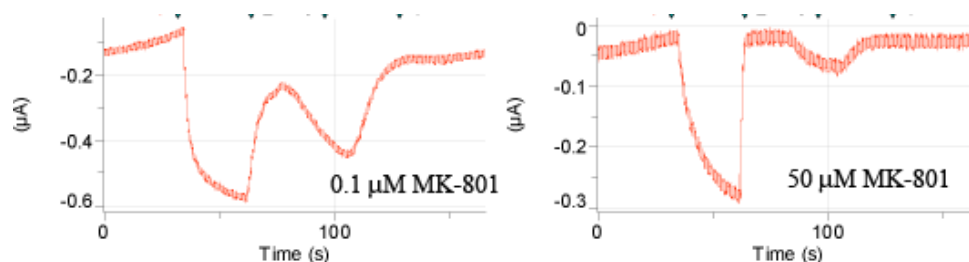


Figure 2.26 Electrophysiology traces from two doses of MK-801. As the concentration of MK-801 increases, more channels remained blocked and channels do not reactivate.

Following the examination of MK-801, the study turned to the blocker PCP. The studies of NR1a/NR2B wild type receptor demonstrated that PCP also is a very potent blocker. The IC_{50} value obtained for wild type receptor block was 204 nM. Two subsequent mutations, NR1a N616Q/NR2B and NR1a/NR2B N615A_{kp}, both shifted PCP IC_{50} by ~ 4 and 7-fold, respectively (Figure 2.27). Although these studies did not conclusively characterize the N and N+1 site Asns in PCP block, the initial results suggest that PCP binds differently than either Mg^{2+} or memantine. Since the N site of both the NR1a and NR2B subunits influences PCP block, it appears that PCP contacts more of the pore. The studies conducted were unable to determine if the PCP block is mostly steric or electrostatic in character. Future studies may be able to clarify this interaction.

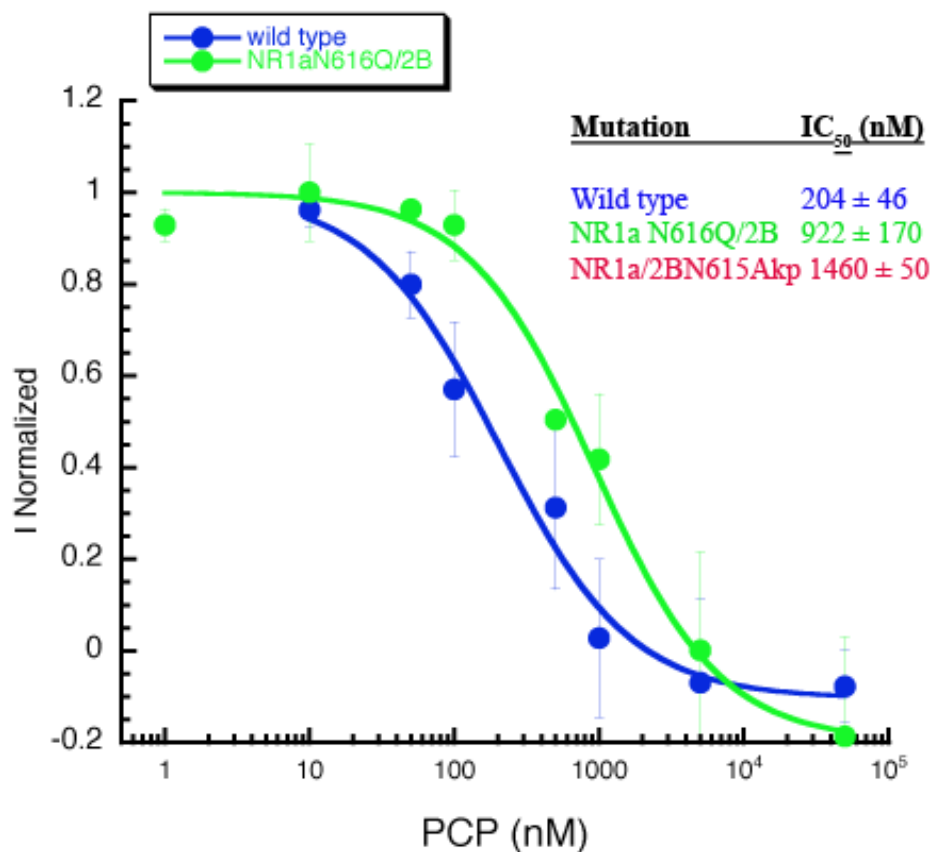


Figure 2.27 PCP IC₅₀ curves. IC₅₀ values for the wild type NR1a/NR2B receptor and two mutations, NR1a N616Q and NR2B N615Akp.

2.3 Discussion and Conclusions

The studies conducted support the conclusion that Mg^{2+} does not interact with the NR2B Trp607 through a cation- π interaction. All previous studies using conventional mutagenesis led to the conclusion that the aromaticity of Trp 607 was crucial for Mg^{2+} blockade. However, the results obtained from employing unnatural amino acid mutagenesis via nonsense suppression have definitively demonstrated that the interaction is not electrostatic in nature. The subtle results of this approach reveal that the more likely interaction that Trp607 is involved in is steric. Simply put, a large, flat residue is required at NR2B 607 (98).

Our studies with several different side chains support the idea that structural requirements at W607 are necessary to maintain Mg^{2+} block. For example, large, flat

side chains such as Trp, 2-Nap, F₂-Trp, and Cha all maintain levels of Mg²⁺ block similar to the wild type receptors. At the same time, we also noticed subtler effects on Mg²⁺ block such as the incorporation of Tyr and Cha, which seem to distort the receptor pore enough for incomplete Mg²⁺ block (although it can be relieved at high negative potentials). This implies that the size and/or shape of the Tyr or Cha side chains at position 607 does subtly distort the pore, so that Mg²⁺ can permeate more easily. Additionally, the W607Cha data would suggest that an aromatic residue is not absolutely necessary for receptor function, since partial block is observed in these channels. It is reasonable to suggest that the important features of the Trp residue are its size, shape, and hydrophobicity, which allow it to fit into the channel architecture to create the desired Mg²⁺ block during NMDA receptor function (98).

In studies conducted of the Mg²⁺ block we have demonstrated that the conserved N and N+1 site Asn residues in both NR1a and NR2B are important during Mg²⁺ block. Prior studies suggested that the two NR2 sites do not contribute equally to Mg²⁺ block. Conventional mutagenesis studies concluded that the NR2 N+1 site contributed to Mg²⁺ block more than the N site of either subunit. By using the unnatural amino acid mutagenesis technique, the importance of the amide carbonyl of Asn could be tested in an electrostatic interaction with the metal cation. The experiments conducted, incorporating the unnatural amino acid Akp, suggest that the amide carbonyl of NR2B N615 (N site) is more important for Mg²⁺ block than the amide carbonyl of the N+1 site. At the same time, the conventional mutagenesis experiments also demonstrated the importance of the N+1 site in Mg²⁺ block. Combining these studies it is suggested that although the N+1 site Asn may provide a steric component to Mg²⁺ block (it is thought to lie at the narrowest constriction of the pore), the N site may coordinate to Mg²⁺ through an ion-dipole interaction.

The studies of the pore Asns also provided interesting suggestions about the mechanism of memantine block of the NR1a/NR2B receptor. Memantine block is complicated since there is a proposed primary and secondary binding site (90, 92). Instead of the NR2 subunit Asns contributing to memantine block via electrostatic interactions, the mutation with the most dramatic influence on memantine block was NR1a N616Q. None of the other mutations at either site in NR2B resulted in a

substantial shift in receptor blockade, likely suggesting that these are not the only chemical interactions at play between the receptor and memantine during block. Previous studies by the Lipton group have postulated that several binding sites for memantine exist in and around the NMDAR pore (92). This can complicate mutagenesis studies because as one set of NMDAR-memantine interactions is altered, other important interactions between the receptor and blocker can (and likely do) compensate for the mutations. However, the more subtle mutations, inherent in the technique used here, provide precise evidence of the molecular nature of the interactions involved in memantine block. These distinguish memantine block from Mg^{2+} block. It is likely that Mg^{2+} interacts with the amide carbonyl via an electrostatic interaction of the NR2B N site while memantine seems not to be influenced by the NR2B subunit at all during receptor block. The use of unnatural amino acid mutagenesis has revealed that Mg^{2+} and memantine, although both cationic blockers, interact with the NMDAR pore via different mechanisms.

The results of this study and prior studies demonstrate the limits of current understanding of the action of cations in blocking the pore of NMDA receptors. Additionally, recent evidence suggests that the pore region may not be the only area of the protein involved in receptor blockade. Contributions from the LBD also may influence the structure of the pore and how different cations interact in the pore domain (99). This area of research is ongoing and provides a prime example for how biophysical chemistry on the molecular scale contributes unique insights and understanding of these complex biological processes. Several lab members, including Walrati Limapichat and Wesley Yu, will continue future studies of the mechanism of block by memantine.

These experiments demonstrate that a new family of neuroreceptors (iGluRs), the NMDA receptor in particular, is amenable to study using unnatural amino acid mutagenesis. Now that a protocol has been established for use of the nonsense suppression methodology to incorporate unnatural amino acids into these highly important receptors, the role of many chemical interactions involved in their structure and function can be explored.

Chapter 3 will examine how this methodology has been used to focus on a different domain of the NMDAR, the ligand-binding domain. Also, the efforts to expand the methodology into another iGluR subfamily, the AMPA receptors, will be described. Because glutamate receptors in general and, specifically, NMDA receptors, play such an integral role in many neuronal functions and diseases due mostly to their high Ca^{2+} permeability, they are an incredibly interesting set of neuroreceptors for exploration. The long-term goal of these efforts is to study these receptors in a mammalian cell system and explore how their structure and function interplay with different neuronal signaling cascades within the cell.

2.4 Materials and Methods

2.4.1 Molecular Biology

The NR1a and NR2B subunits were subcloned from pBluescript into pAMV (100) for increased expression in *Xenopus laevis* oocytes. For the NR1a subcloning, primers complimentary to the 5' and 3' ends of the gene were synthesized (Integrated DNA Technologies), the gene was amplified using PCR, and then subcloned into the pAMV vector using the *NcoI* and *BamHI* restriction enzymes and DNA ligase. The NR2B subcloning was more involved. Initially, the first 1.5 kb of the NR2B subunit (from the 5' end) was amplified using PCR and subcloned into pAMV utilizing overlapping primers and PCR. The overlapping primers were constructed using 12 amino acids from the AMV sequence that directly preceded the start codon of the plasmid and the first 12 amino acids from the NR2B gene (72 bp/primer). The second 3.0 kb of NR2B were subcloned into the modified pAMV containing 1.5 kb from NR2B by restriction digestion between the plasmid and the fragment (3.0 kb) using *BamHI* and *AflIII* and ligating with T4 DNA Ligase (Figure 2.28).

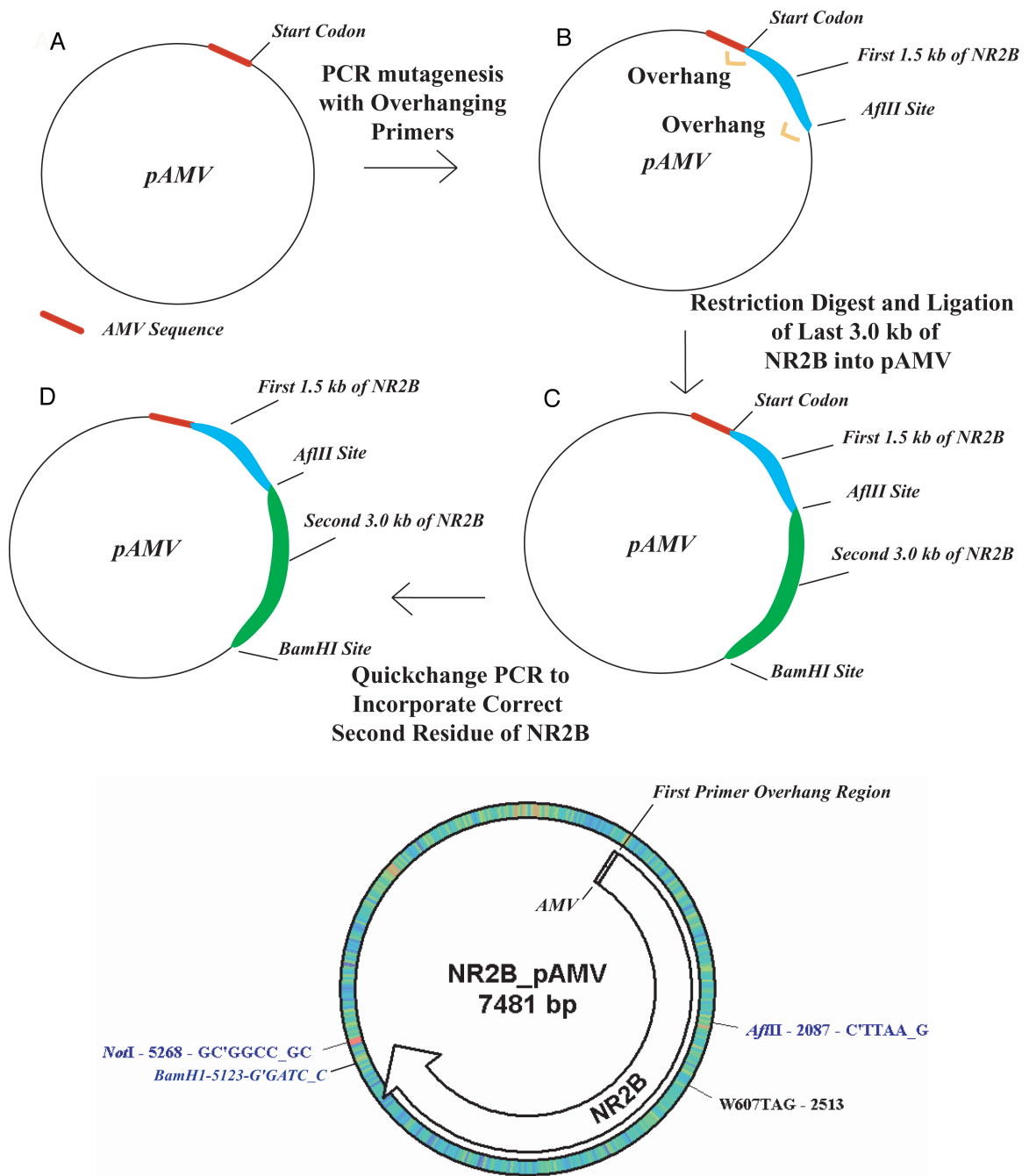


Figure 2.28 NMDA receptor cloning. Cloning schematic for NR2B insertion into pAMV from pBluescript. Final vector map of NR2B in pAMV with the TAG (stop) codon inserted at site 607.

Mutant NR1a and NR2B subunits were prepared by site-directed mutagenesis. All mutant and wild type cDNA was linearized with *NotI* and mRNA was synthesized by

in vitro runoff transcription using the T7 mMESSAGE mMACHINE kit (Ambion). Conventional mutants and wild type mRNA were injected in a NR1a:NR2B (1:5) ratio. Synthetic amino acids were ligated to truncated 74 nt tRNA as described previously (100). The aminoacyl tRNA was deprotected by photolysis immediately prior to co-injection with mRNA. Typically, 5 ng mRNA and 25 ng tRNA-aa were injected into oocytes in a total volume of 50 nL. To increase expression of suppressed receptors, 1 day after the first injection a “booster” of 25 ng tRNA-aa was given and the cells incubated one additional day before electrophysiological measurements were made (48 hours total).

2.4.2 Electrophysiology

Stage V-VI *Xenopus laevis* oocytes were injected with 50nL/cell of mRNA/tRNA mixtures. Oocytes were evaluated in a Mg^{2+} and Ca^{2+} free saline solution (96 mM NaCl, 5 mM HEPES, 2 mM KCl, 1 mM $BaCl_2$). The receptors were activated in a Mg^{2+} and Ca^{2+} free solution containing 100mM glutamate (Aldrich), 10 mM glycine (Aldrich), and 100 mM niflumic acid (to reduce activity of Ca^{2+} activated Cl^- channels, Sigma). All oocyte recordings were made 48 hours after initial injection in two-electrode voltage clamp mode using the OpusXpress 6000A (Molecular Devices). Solutions were superfused at flow rates of 1 and 4 mL/min during Mg^{2+} application and 3 mL/min during wash. Eight oocytes were simultaneously voltage clamped at -60 mV and dose-response relationships were obtained by delivery of various concentrations of Mg^{2+} in 1 mL aliquots. The data were analyzed using the Clampfit 9.0 software (Axon).

The Hill equation was used to fit data: $I/I_{max}=1/(1+(IC_{50}/[A]^{n_H}))$, where I is peak current at drug concentration (A), IC_{50} is the concentration of drug that inhibits 50% of the maximal response, and n_H is the Hill coefficient. Voltage ramps (-150 mV to $+40$ mV during 4 s) were used to construct I–V curves for (glutamate and glycine)-evoked conductance in the presence and absence of Mg^{2+} . Leak currents measured in the absence of glutamate, glycine, niflumic acid, and Mg^{2+} were subtracted. The voltage dependence of block (δ , fraction of the electric field that the blocker experiences) and the affinity of Mg^{2+} at 0 mV ($K_{0.5}$) were calculated by determining the IC_{50} at varying potentials (-40 to -100 mV). The logarithm of IC_{50} was plotted against the holding potentials and a straight line was fitted to the data to determine δ and $K_{0.5}$. The δ and $K_{0.5}$ were calculated

according to Woodhull (63): $K_{0.5}(V) = K_{0.5} \times \exp(zdVF/RT)$, V is membrane potential, z is valence, R , T , and F have their traditional meaning. For the Mg^{2+} and memantine block experiments, we measured % block at wild type IC_{50} levels by measuring the amount of whole-cell current generated for each mutation (induced by glutamate and glycine application) and the amount of current that was blocked by a dose of Mg^{2+} or memantine at the IC_{50} value (determined for wild type receptor) of each blocker. We determined the amount of current that was blocked vs. the amount of current generated by agonist application. This was done for many oocytes and the amount of block was averaged. Before plotting, we determined % block by subtracting the amount of block from 1. To determine the % maximal block we used the largest concentration of either Mg^{2+} or memantine and used the same analysis previously described.

2.4.3 Immunolocalization of Wild type and Mutant NMDA Receptors.

These experiments were performed by adapting previously reported procedures (101, 102). HEK293T cells were calcium phosphate transfected with 10 ng of cDNA. Cells were incubated at 37°C for 2 days. Transfected cells were washed with Tris-buffered saline (3x) and fixed using ice-cold 4% paraformaldehyde in phosphate buffer. The receptors were labeled with anti-NMDAR1 clone 54.1 (Zymed) at a 1:100 dilution in phosphate-buffered saline. Inclusion of 0.3% Triton X-100 permeabilized the membranes for detection of intracellular receptor expression. The cells were incubated with primary antibody for 1 hour at room temperature. Cells were washed (3x) with phosphate-buffered saline. Biotinylated anti-mouse IgG (Vector) was added to the cells and incubated for 1 hour and then rinsed (3x) with phosphate-buffered saline. Fluorescein isothiocyanate avidin D (Vector) was then added to the cells and incubated for 1 hour. Coverslips were mounted in Vectashield mounting medium (Vector) and immunofluorescence was observed using a confocal microscope.

2.4.4. Computational Modeling

The indole-Mg²⁺ complex in Figure 16 and the analogous 5-F-indole complex were optimized at B3LYP/6-31⁺⁺G (d,p) level of theory. The geometries were optimized and fully characterized as minima by analysis of frequency. Energies were calculated at the B3LYP/6-31⁺⁺G (d,p) level. Additionally, basis set superposition error (BSSE) corrections were determined in the gas phase at the B3LYP/6-31⁺⁺G (d,p) level using the counterpoise correction method from Boys and Bernardi (103). All calculations were performed with the Gaussian 98 program (104).

2.5 Cited References

1. Neves, G., Cooke, S. F., and Bliss, T. V. (2008) Synaptic plasticity, memory and the hippocampus: a neural network approach to causality, *Nat Rev Neurosci* 9, 65-75.
2. Collingridge, G. L., Isaac, J. T., and Wang, Y. T. (2004) Receptor trafficking and synaptic plasticity, *Nat Rev Neurosci* 5, 952-962.
3. Lomo, T. (2003) The discovery of long-term potentiation, *Philos Trans R Soc Lond B Biol Sci* 358, 617-620.
4. Andersen, P., Andersson, S. A., and Lomo, T. (1966) Patterns of spontaneous rhythmic activity within various thalamic nuclei, *Nature* 211, 888-889.
5. Douglas, R. M., and Goddard, G. V. (1975) Long-term potentiation of the perforant path-granule cell synapse in the rat hippocampus, *Brain Res* 86, 205-215.
6. Lamprecht, R., and LeDoux, J. (2004) Structural plasticity and memory, *Nat Rev Neurosci* 5, 45-54.
7. Yasuda, H., Barth, A. L., Stellwagen, D., and Malenka, R. C. (2003) A developmental switch in the signaling cascades for LTP induction, *Nat Neurosci* 6, 15-16.
8. Malenka, R. C., and Bear, M. F. (2004) LTP and LTD: an embarrassment of riches, *Neuron* 44, 5-21.
9. Malenka, R. C. (2003) The long-term potential of LTP, *Nat Rev Neurosci* 4, 923-926.
10. Frey, U., and Morris, R. G. (1997) Synaptic tagging and long-term potentiation, *Nature* 385, 533-536.
11. Shi, S. H., Hayashi, Y., Petralia, R. S., Zaman, S. H., Wenthold, R. J., Svoboda, K., and Malinow, R. (1999) Rapid spine delivery and redistribution of AMPA receptors after synaptic NMDA receptor activation, *Science* 284, 1811-1816.
12. Malinow, R., and Malenka, R. C. (2002) AMPA receptor trafficking and synaptic plasticity, *Annu Rev Neurosci* 25, 103-126.
13. Liu, S. Q., and Cull-Candy, S. G. (2000) Synaptic activity at calcium-permeable AMPA receptors induces a switch in receptor subtype, *Nature* 405, 454-458.
14. Brecht, D. S., and Nicoll, R. A. (2003) AMPA receptor trafficking at excitatory synapses, *Neuron* 40, 361-379.
15. Dingledine, R., Borges, K., Bowie, D., and Traynelis, S. F. (1999) The glutamate receptor ion channels, *Pharmacol Rev* 51, 7-61.
16. Schmitz, D., Mellor, J., Breustedt, J., and Nicoll, R. A. (2003) Presynaptic kainate receptors impart an associative property to hippocampal mossy fiber long-term potentiation, *Nat Neurosci* 6, 1058-1063.
17. Bortolotto, Z. A., Lauri, S., Isaac, J. T., and Collingridge, G. L. (2003) Kainate receptors and the induction of mossy fibre long-term potentiation, *Philos Trans R Soc Lond B Biol Sci* 358, 657-666.
18. Song, I., and Huganir, R. L. (2002) Regulation of AMPA receptors during synaptic plasticity, *Trends Neurosci* 25, 578-588.
19. Malenka, R. C. (2003) Synaptic plasticity and AMPA receptor trafficking, *Ann N Y Acad Sci* 1003, 1-11.

20. Santos, S. D., Carvalho, A. L., Caldeira, M. V., and Duarte, C. B. (2009) Regulation of AMPA receptors and synaptic plasticity, *Neuroscience* 158, 105-125.
21. Lisman, J., and Raghavachari, S. (2006) A unified model of the presynaptic and postsynaptic changes during LTP at CA1 synapses, *Sci STKE* 2006, re11.
22. Malinow, R., Mainen, Z. F., and Hayashi, Y. (2000) LTP mechanisms: from silence to four-lane traffic, *Curr Opin Neurobiol* 10, 352-357.
23. Sweatt, J. D. (1999) Toward a molecular explanation for long-term potentiation, *Learn Mem* 6, 399-416.
24. Benke, T. A., Luthi, A., Isaac, J. T., and Collingridge, G. L. (1998) Modulation of AMPA receptor unitary conductance by synaptic activity, *Nature* 393, 793-797.
25. Kennedy, M. B., Beale, H. C., Carlisle, H. J., and Washburn, L. R. (2005) Integration of biochemical signalling in spines, *Nat Rev Neurosci* 6, 423-434.
26. Barry, M. F., and Ziff, E. B. (2002) Receptor trafficking and the plasticity of excitatory synapses, *Curr Opin Neurobiol* 12, 279-286.
27. Kennedy, M. B. (2000) Signal-processing machines at the postsynaptic density, *Science* 290, 750-754.
28. Greger, I. H., Ziff, E. B., and Penn, A. C. (2007) Molecular determinants of AMPA receptor subunit assembly, *Trends Neurosci* 30, 407-416.
29. Greger, I. H., and Esteban, J. A. (2007) AMPA receptor biogenesis and trafficking, *Curr Opin Neurobiol* 17, 289-297.
30. Mayer, M. L. (2005) Glutamate receptor ion channels, *Curr Opin Neurobiol* 15, 282-288.
31. Eriksson, M., Nilsson, A., Samuelsson, H., Samuelsson, E. B., Mo, L., Akesson, E., Benedikz, E., and Sundstrom, E. (2007) On the role of NR3A in human NMDA receptors, *Physiol Behav* 92, 54-59.
32. Wood, P. L. (1995) The co-agonist concept: is the NMDA-associated glycine receptor saturated in vivo?, *Life Sci* 57, 301-310.
33. Sommer, B., Kohler, M., Sprengel, R., and Seeburg, P. H. (1991) RNA editing in brain controls a determinant of ion flow in glutamate-gated channels, *Cell* 67, 11-19.
34. Egebjerg, J., Kukekov, V., and Heinemann, S. F. (1994) Intron sequence directs RNA editing of the glutamate receptor subunit GluR2 coding sequence, *Proc Natl Acad Sci U S A* 91, 10270-10274.
35. Sommer, B., Keinänen, K., Verdoorn, T. A., Wisden, W., Burnashev, N., Herb, A., Kohler, M., Takagi, T., Sakmann, B., and Seeburg, P. H. (1990) Flip and flop: a cell-specific functional switch in glutamate-operated channels of the CNS, *Science* 249, 1580-1585.
36. Mosbacher, J., Schoepfer, R., Monyer, H., Burnashev, N., Seeburg, P. H., and Ruppersberg, J. P. (1994) A molecular determinant for submillisecond desensitization in glutamate receptors, *Science* 266, 1059-1062.
37. Sheng, M., Cummings, J., Roldan, L. A., Jan, Y. N., and Jan, L. Y. (1994) Changing subunit composition of heteromeric NMDA receptors during development of rat cortex, *Nature* 368, 144-147.

38. Monyer, H., Burnashev, N., Laurie, D. J., Sakmann, B., and Seeburg, P. H. (1994) Developmental and regional expression in the rat brain and functional properties of four NMDA receptors, *Neuron* 12, 529-540.
39. Buller, A. L., and Monaghan, D. T. (1997) Pharmacological heterogeneity of NMDA receptors: characterization of NR1a/NR2D heteromers expressed in *Xenopus* oocytes, *Eur J Pharmacol* 320, 87-94.
40. Hollmann, M., and Heinemann, S. (1994) Cloned glutamate receptors, *Annu Rev Neurosci* 17, 31-108.
41. Nakagawa, T., Cheng, Y., Ramm, E., Sheng, M., and Walz, T. (2005) Structure and different conformational states of native AMPA receptor complexes, *Nature* 433, 545-549.
42. Kunishima, N., Shimada, Y., Tsuji, Y., Sato, T., Yamamoto, M., Kumasaka, T., Nakanishi, S., Jingami, H., and Morikawa, K. (2000) Structural basis of glutamate recognition by a dimeric metabotropic glutamate receptor, *Nature* 407, 971-977.
43. Jin, R., Singh, S. K., Gu, S., Furukawa, H., Sobolevsky, A. I., Zhou, J., Jin, Y., and Gouaux, E. (2009) Crystal structure and association behaviour of the GluR2 amino-terminal domain, *EMBO J* 28, 1812-1823.
44. Jin, R., Banke, T. G., Mayer, M. L., Traynelis, S. F., and Gouaux, E. (2003) Structural basis for partial agonist action at ionotropic glutamate receptors, *Nat Neurosci* 6, 803-810.
45. Gouaux, E. (2004) Structure and function of AMPA receptors, *J Physiol* 554, 249-253.
46. Furukawa, H., Singh, S. K., Mancusso, R., and Gouaux, E. (2005) Subunit arrangement and function in NMDA receptors, *Nature* 438, 185-192.
47. Furukawa, H., and Gouaux, E. (2003) Mechanisms of activation, inhibition and specificity: crystal structures of the NMDA receptor NR1 ligand-binding core, *EMBO J* 22, 2873-2885.
48. Armstrong, N., Sun, Y., Chen, G. Q., and Gouaux, E. (1998) Structure of a glutamate-receptor ligand-binding core in complex with kainate, *Nature* 395, 913-917.
49. Wood, M. W., VanDongen, H. M., and VanDongen, A. M. (1995) Structural conservation of ion conduction pathways in K channels and glutamate receptors, *Proc Natl Acad Sci U S A* 92, 4882-4886.
50. Rosenmund, C., Stern-Bach, Y., and Stevens, C. F. (1998) The tetrameric structure of a glutamate receptor channel, *Science* 280, 1596-1599.
51. Bennett, J. A., and Dingledine, R. (1995) Topology profile for a glutamate receptor: three transmembrane domains and a channel-lining reentrant membrane loop, *Neuron* 14, 373-384.
52. Kumar, J., Schuck, P., Jin, R., and Mayer, M. L. (2009) The N-terminal domain of GluR6-subtype glutamate receptor ion channels, *Nat Struct Mol Biol*.
53. O'Hara, P. J., Sheppard, P. O., Thogersen, H., Venezia, D., Haldeman, B. A., McGrane, V., Houamed, K. M., Thomsen, C., Gilbert, T. L., and Mulvihill, E. R. (1993) The ligand-binding domain in metabotropic glutamate receptors is related to bacterial periplasmic binding proteins, *Neuron* 11, 41-52.

54. Nowak, L., Bregestovski, P., Ascher, P., Herbet, A., and Prochiantz, A. (1984) Magnesium gates glutamate-activated channels in mouse central neurones, *Nature* 307, 462-465.
55. Mayer, M. L., Westbrook, G. L., and Guthrie, P. B. (1984) Voltage-dependent block by Mg^{2+} of NMDA responses in spinal cord neurones, *Nature* 309, 261-263.
56. Li-Smerin, Y., and Johnson, J. W. (1996) Effects of intracellular Mg^{2+} on channel gating and steady-state responses of the NMDA receptor in cultured rat neurons, *J Physiol* 491 (Pt 1), 137-150.
57. Mori, H., Masaki, H., Yamakura, T., and Mishina, M. (1992) Identification by mutagenesis of a $Mg(2+)$ -block site of the NMDA receptor channel, *Nature* 358, 673-675.
58. Ascher, P., and Nowak, L. (1988) The role of divalent cations in the N-methyl-D-aspartate responses of mouse central neurones in culture, *J Physiol* 399, 247-266.
59. Antonov, S. M., and Johnson, J. W. (1999) Permeant ion regulation of N-methyl-D-aspartate receptor channel block by $Mg(2+)$, *Proc Natl Acad Sci U S A* 96, 14571-14576.
60. Wollmuth, L. P., Kuner, T., Seeburg, P. H., and Sakmann, B. (1996) Differential contribution of the NR1- and NR2A-subunits to the selectivity filter of recombinant NMDA receptor channels, *J Physiol* 491 (Pt 3), 779-797.
61. Villarroel, A., Burnashev, N., and Sakmann, B. (1995) Dimensions of the narrow portion of a recombinant NMDA receptor channel, *Biophys J* 68, 866-875.
62. Zhou, Y., Morais-Cabral, J. H., Kaufman, A., and MacKinnon, R. (2001) Chemistry of ion coordination and hydration revealed by a K^{+} channel-Fab complex at 2.0 Å resolution, *Nature* 414, 43-48.
63. Woodhull, A. M. (1973) Ionic blockage of sodium channels in nerve, *J Gen Physiol* 61, 687-708.
64. Williams, K., Pahk, A. J., Kashiwagi, K., Masuko, T., Nguyen, N. D., and Igarashi, K. (1998) The selectivity filter of the N-methyl-D-aspartate receptor: a tryptophan residue controls block and permeation of Mg^{2+} , *Mol Pharmacol* 53, 933-941.
65. Wollmuth, L. P., Kuner, T., and Sakmann, B. (1998) Adjacent asparagines in the NR2-subunit of the NMDA receptor channel control the voltage-dependent block by extracellular Mg^{2+} , *J Physiol* 506 (Pt 1), 13-32.
66. Kupper, J., Ascher, P., and Neyton, J. (1998) Internal Mg^{2+} block of recombinant NMDA channels mutated within the selectivity filter and expressed in *Xenopus* oocytes, *J Physiol* 507 (Pt 1), 1-12.
67. Burnashev, N., Schoepfer, R., Monyer, H., Ruppersberg, J. P., Gunther, W., Seeburg, P. H., and Sakmann, B. (1992) Control by asparagine residues of calcium permeability and magnesium blockade in the NMDA receptor, *Science* 257, 1415-1419.
68. Zhong, W., Gallivan, J. P., Zhang, Y., Li, L., Lester, H. A., and Dougherty, D. A. (1998) From ab initio quantum mechanics to molecular neurobiology: a cation- π binding site in the nicotinic receptor, *Proc Natl Acad Sci U S A* 95, 12088-12093.

69. Mu, T. W., Lester, H. A., and Dougherty, D. A. (2003) Different binding orientations for the same agonist at homologous receptors: a lock and key or a simple wedge?, *J Am Chem Soc* 125, 6850-6851.
70. Mecozzi, S., West, A. P., Jr., and Dougherty, D. A. (1996) Cation-pi interactions in aromatics of biological and medicinal interest: electrostatic potential surfaces as a useful qualitative guide, *Proc Natl Acad Sci U S A* 93, 10566-10571.
71. Dougherty, D. A. (1996) Cation-pi interactions in chemistry and biology: a new view of benzene, Phe, Tyr, and Trp, *Science* 271, 163-168.
72. Cashin, A. L., Petersson, E. J., Lester, H. A., and Dougherty, D. A. (2005) Using physical chemistry to differentiate nicotinic from cholinergic agonists at the nicotinic acetylcholine receptor, *J Am Chem Soc* 127, 350-356.
73. Beene, D. L., Brandt, G. S., Zhong, W., Zacharias, N. M., Lester, H. A., and Dougherty, D. A. (2002) Cation-pi interactions in ligand recognition by serotonergic (5-HT_{3A}) and nicotinic acetylcholine receptors: the anomalous binding properties of nicotine, *Biochemistry* 41, 10262-10269.
74. Petersson, E. J., Brandt, G. S., Zacharias, N. M., Dougherty, D. A., and Lester, H. A. (2003) Caging proteins through unnatural amino acid mutagenesis, *Methods Enzymol* 360, 258-273.
75. Williams, K., Russell, S. L., Shen, Y. M., and Molinoff, P. B. (1993) Developmental switch in the expression of NMDA receptors occurs in vivo and in vitro, *Neuron* 10, 267-278.
76. Green, T., Rogers, C. A., Contractor, A., and Heinemann, S. F. (2002) NMDA receptors formed by NR1 in *Xenopus laevis* oocytes do not contain the endogenous subunit XenU1, *Mol Pharmacol* 61, 326-333.
77. Hille, B. (2001) *Ion channels of excitable membranes*, 3rd ed., Sinauer, Sunderland, Mass.
78. Lummis, S. C., D, L. B., Harrison, N. J., Lester, H. A., and Dougherty, D. A. (2005) A cation-pi binding interaction with a tyrosine in the binding site of the GABAC receptor, *Chem Biol* 12, 993-997.
79. Wollmuth, L. P., Kuner, T., and Sakmann, B. (1998) Intracellular Mg²⁺ interacts with structural determinants of the narrow constriction contributed by the NR1-subunit in the NMDA receptor channel, *J Physiol* 506 (Pt 1), 33-52.
80. Kuner, T., Seeburg, P. H., and Guy, H. R. (2003) A common architecture for K⁺ channels and ionotropic glutamate receptors?, *Trends Neurosci* 26, 27-32.
81. Doyle, D. A., Morais Cabral, J., Pfuetzner, R. A., Kuo, A., Gulbis, J. M., Cohen, S. L., Chait, B. T., and MacKinnon, R. (1998) The structure of the potassium channel: molecular basis of K⁺ conduction and selectivity, *Science* 280, 69-77.
82. Hargreaves, R. J., Hill, R. G., and Iversen, L. L. (1994) Neuroprotective NMDA antagonists: the controversy over their potential for adverse effects on cortical neuronal morphology, *Acta Neurochir Suppl (Wien)* 60, 15-19.
83. Frausto da Silva, J. J. R. a. W., R.J.P. (1991) *The Biological Chemistry of the Elements* Vol. 1, Clarendon Press, Oxford.
84. Falke, J. J., Drake, S. K., Hazard, A. L., and Peersen, O. B. (1994) Molecular tuning of ion binding to calcium signaling proteins, *Q Rev Biophys* 27, 219-290.

85. Torrice, M. M. (2008) Chemical-scale studies of the nicotinic and muscarinic acetylcholine receptors, in *Chemistry and Chemical Engineering*, California Institute of Technology, Pasadena.
86. Cashin, A. L., Torrice, M. M., McMenimen, K. A., Lester, H. A., and Dougherty, D. A. (2007) Chemical-scale studies on the role of a conserved aspartate in preorganizing the agonist binding site of the nicotinic acetylcholine receptor, *Biochemistry* 46, 630-639.
87. Cashin, A. L. (2006) Chemical scale investigations of drug-receptor interactions at the nicotinic acetylcholine receptor., in *Chemistry and Chemical Engineering*, California Institute of Technology, Pasadena.
88. Chen, H. S., Pellegrini, J. W., Aggarwal, S. K., Lei, S. Z., Warach, S., Jensen, F. E., and Lipton, S. A. (1992) Open-channel block of N-methyl-D-aspartate (NMDA) responses by memantine: therapeutic advantage against NMDA receptor-mediated neurotoxicity, *J Neurosci* 12, 4427-4436.
89. Chen, H. S., and Lipton, S. A. (1997) Mechanism of memantine block of NMDA-activated channels in rat retinal ganglion cells: uncompetitive antagonism, *J Physiol* 499 (Pt 1), 27-46.
90. Lipton, S. A., and Chen, H. S. (2005) Paradigm shift in NMDA receptor drug development, *Expert Opin Ther Targets* 9, 427-429.
91. Kashiwagi, K., Masuko, T., Nguyen, C. D., Kuno, T., Tanaka, I., Igarashi, K., and Williams, K. (2002) Channel blockers acting at N-methyl-D-aspartate receptors: differential effects of mutations in the vestibule and ion channel pore, *Mol Pharmacol* 61, 533-545.
92. Chen, H. S., and Lipton, S. A. (2005) Pharmacological implications of two distinct mechanisms of interaction of memantine with N-methyl-D-aspartate-gated channels, *J Pharmacol Exp Ther* 314, 961-971.
93. Sobolevsky, A. I., Koshelev, S. G., and Khodorov, B. I. (1998) Interaction of memantine and amantadine with agonist-unbound NMDA-receptor channels in acutely isolated rat hippocampal neurons, *J Physiol* 512 (Pt 1), 47-60.
94. Sobolevsky, A., and Koshelev, S. (1998) Two blocking sites of amino-adamantane derivatives in open N-methyl-D-aspartate channels, *Biophys J* 74, 1305-1319.
95. Bresink, I., Benke, T. A., Collett, V. J., Seal, A. J., Parsons, C. G., Henley, J. M., and Collingridge, G. L. (1996) Effects of memantine on recombinant rat NMDA receptors expressed in HEK 293 cells, *Br J Pharmacol* 119, 195-204.
96. Blanpied, T. A., Boeckman, F. A., Aizenman, E., and Johnson, J. W. (1997) Trapping channel block of NMDA-activated responses by amantadine and memantine, *J Neurophysiol* 77, 309-323.
97. Antonov, S. M., and Johnson, J. W. (1996) Voltage-dependent interaction of open-channel blocking molecules with gating of NMDA receptors in rat cortical neurons, *J Physiol* 493 (Pt 2), 425-445.
98. McMenimen, K. A., Dougherty, D. A., Lester, H. A., and Petersson, E. J. (2006) Probing the Mg²⁺ blockade site of an N-methyl-D-aspartate (NMDA) receptor with unnatural amino acid mutagenesis, *ACS Chem Biol* 1, 227-234.

99. Wrighton, D. C., Baker, E. J., Chen, P. E., and Wyllie, D. J. (2008) Mg²⁺ and memantine block of rat recombinant NMDA receptors containing chimeric NR2A/2D subunits expressed in *Xenopus laevis* oocytes, *J Physiol* 586, 211-225.
100. Nowak, M. W., Gallivan, J. P., Silverman, S. K., Labarca, C. G., Dougherty, D. A., and Lester, H. A. (1998) In vivo incorporation of unnatural amino acids into ion channels in *Xenopus* oocyte expression system, *Methods Enzymol* 293, 504-529.
101. Spier, A. D., and Lummis, S. C. (2000) The role of tryptophan residues in the 5-Hydroxytryptamine(3) receptor ligand binding domain, *J Biol Chem* 275, 5620-5625.
102. Lummis, S. C., Beene, D. L., Lee, L. W., Lester, H. A., Broadhurst, R. W., and Dougherty, D. A. (2005) Cis-trans isomerization at a proline opens the pore of a neurotransmitter-gated ion channel, *Nature* 438, 248-252.
103. Boys, S. F. a. B., F. (1970) *Molecular Physics*, 553-557.
104. Frisch, M. J. T., G. W.; Schlegel, H. B.; Scuseria, G. E.; Robb, M. A.; , Cheeseman, J. R. Z., V. G.; J. A. Montgomery, J.; Stratmann, R. E.; Burant, J. C.; Dapprich, S. M., J. M.; Daniels, A. D.; Kudin, K. N.; Strain, M. C.; Farkas, O.; , Tomasi, J. B., V.; Cossi, M.; Cammi, R.; Mennucci, B.; Pomelli, C.; Adamo, C.; , and Clifford, S. O., J.; Petersson, G. A.; Ayala, P. Y, et al. (1998) Frisch, M. J.; Trucks, G. W.; Schlegel, H. B.; Scuseria, G. E.; Robb, M. A.; Cheeseman, J. R.; Zakrzewski, V. G.; J. A. Montgomery, J.; Stratmann, R. E.; Burant, J. C.; Dapprich, S.; Millam, J. M.; Daniels, A. D.; Kudin, K. N.; Strain, M. C.; Farkas, O.; Tomasi, J.; Barone, V.; Cossi, M.; Cammi, R.; Mennucci, B.; Pomelli, C.; Adamo, C.; Clifford, S.; Ochterski, J.; Petersson, G. A.; Ayala, P. Y, in *Gaussian 98 Revision A.9* ed., Gaussian Incorporated, Pittsburgh, PA.

Chapter 3: Studies of Partial Agonist Interactions in the Binding Site of Glutamate Receptors using Unnatural Amino Acid Mutagenesis

3.1 Introduction

Ionotropic glutamate receptors are multi-subunit, allosteric, ligand-gated ion channels (LGICs) that undergo agonist-induced conformational changes between an open and closed state. Early studies of many LGICs have demonstrated a step-wise mechanism that controls this conformational change. One intriguing feature of many LGICs is that the relatively small neurotransmitter generally binds in an extracellular domain, often 50Å away from the channel pore. The ensuing conformational changes required to transmit the signal of agonist binding to ion channel gating span a large distance and alter the conformation of a large, multi-subunit protein complex. Exploration of how the binding of a small molecule triggers these structural changes remains a topic of great interest. Structural studies such as x-ray crystallography and NMR spectroscopy are commonly employed to gather molecular level details of these interactions. However, information is sparse due to the difficulty of using these methods on full-length transmembrane receptors. Another approach utilizes chemistry-based methods to obtain information about receptor structure, often by varying the structure of the ligand and/or varying the structure of the receptor by mutagenesis. This method is useful in that full-length receptors are studied and generate results using many structure-function assays. We will employ the second method, utilizing functional, full-length glutamate receptors in concert with several agonists and partial agonists to create a novel functional assay of ligand binding in ionotropic glutamate receptors.

α -amino-3-hydroxy-5-methyl-4-isoxazolepropionic acid (AMPA) and N-methyl-D-aspartate (NMDA) receptors are the two main types of glutamate-gated ion channels that couple the energy of glutamate binding to the ligand-binding domain with the opening of the transmembrane ion channel domain (*I*). AMPA receptors mediate most of the fast excitatory neurotransmission in the mammalian brain upon glutamate activation. NMDA receptors play a unique role as ligand-gated ion channels as they require the

binding of both glutamate and glycine to couple to ion channel function and membrane depolarization for release of the magnesium block (2). The prerequisite for both chemical and electrical stimuli, coupled with the calcium permeability of NMDA receptors, establishes the key differences between them and the other ionotropic glutamate receptor (iGluR) subtypes (Figure 3.1). Although members of the the iGluR family have unique biological roles, they are all implicated in learning and memory under normal conditions and several disease states (including stroke, schizophrenia, and neurodegenerative diseases), and identifying agonists that modulate their function could be a useful treatment strategy (3-5).

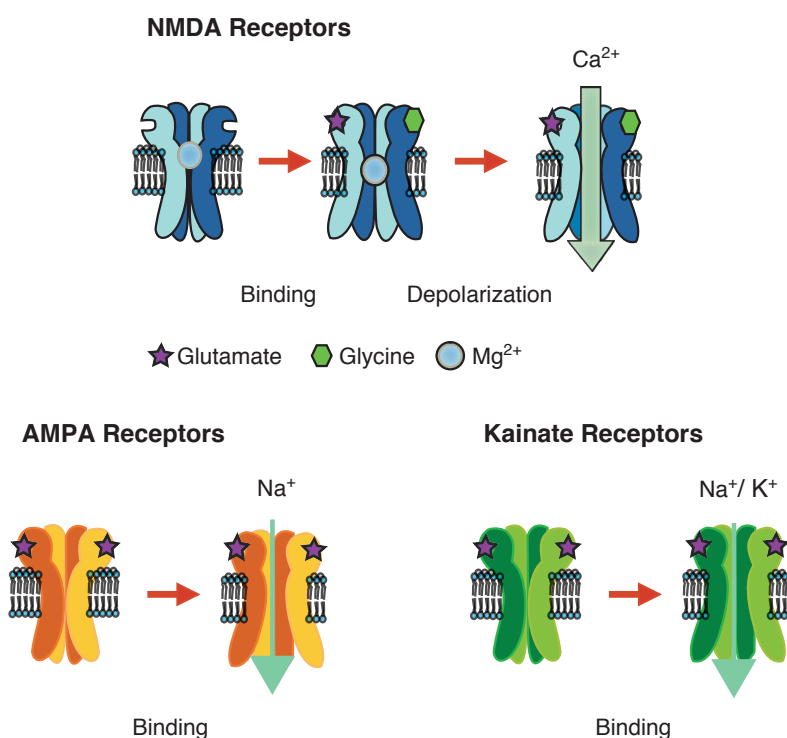


Figure 3.1 iGluR Families, NMDARs, AMPARs, and KA Receptors.

The goal is to determine the interactions that guide the binding of glutamate to these different receptors and map the interactions that remain conserved across the family and the interactions that are different between NMDA and AMPA receptors. In particular, we want to identify the chemical-scale interactions that influence the NMDA NR1 subunit preference for glycine and the NR2 subunit preference for glutamate. Our

studies will begin by focusing on the NR2 ligand-binding domain and its interactions with several agonists.

3.1.1 The Mechanism of Partial Agonist Action on Glutamate Receptors

Direct structural studies of full-length ion channels remain elusive, yet recent studies have developed “tricks” to gain insight into these complicated transmembrane proteins. Since 1998, a plethora of structural evidence for ligand interaction with the ligand-binding domain of iGluRs has erupted. A methodology developed by Gouaux and co-workers enabled the generation of high-resolution crystal structures of the ligand-binding domain (LBD) of all types (AMPA, NMDA, and Kainate) of iGluRs in complex with agonists, partial agonists, and antagonists (6). These structural studies have provided many insights into the mechanism of agonist interactions with the different iGluR subtypes. Additionally, crystal structures of many iGluR LBDs in complex with partial agonists have provided insight into the mechanism of partial agonism of iGluRs. Another important result of many of these studies is that although the iGluRs have structural similarities in overall topology and specifically in their LBDs, there are many subtle underlying differences between the subtypes within a family (e.g., GluR2 vs. GluR4) and between families (e.g., AMPAR vs. NMDAR).

These structural studies are incredibly useful because they provide direct images of the LBD from mammalian iGluRs, however they are not the full-length receptors and do not directly correlate to functional representations of iGluR LBDs. These caveats are important to remember when constructing hypotheses and conclusions about the function of iGluRs that are solely based on these structural images. Additionally, it is important to remember that differences exist between iGluR subtypes, and the conclusions made regarding one type of receptor will not always translate to another subtype. Nevertheless, these crystal structures form a basis for our investigations into the mechanism of agonist action with full-length iGluRs.

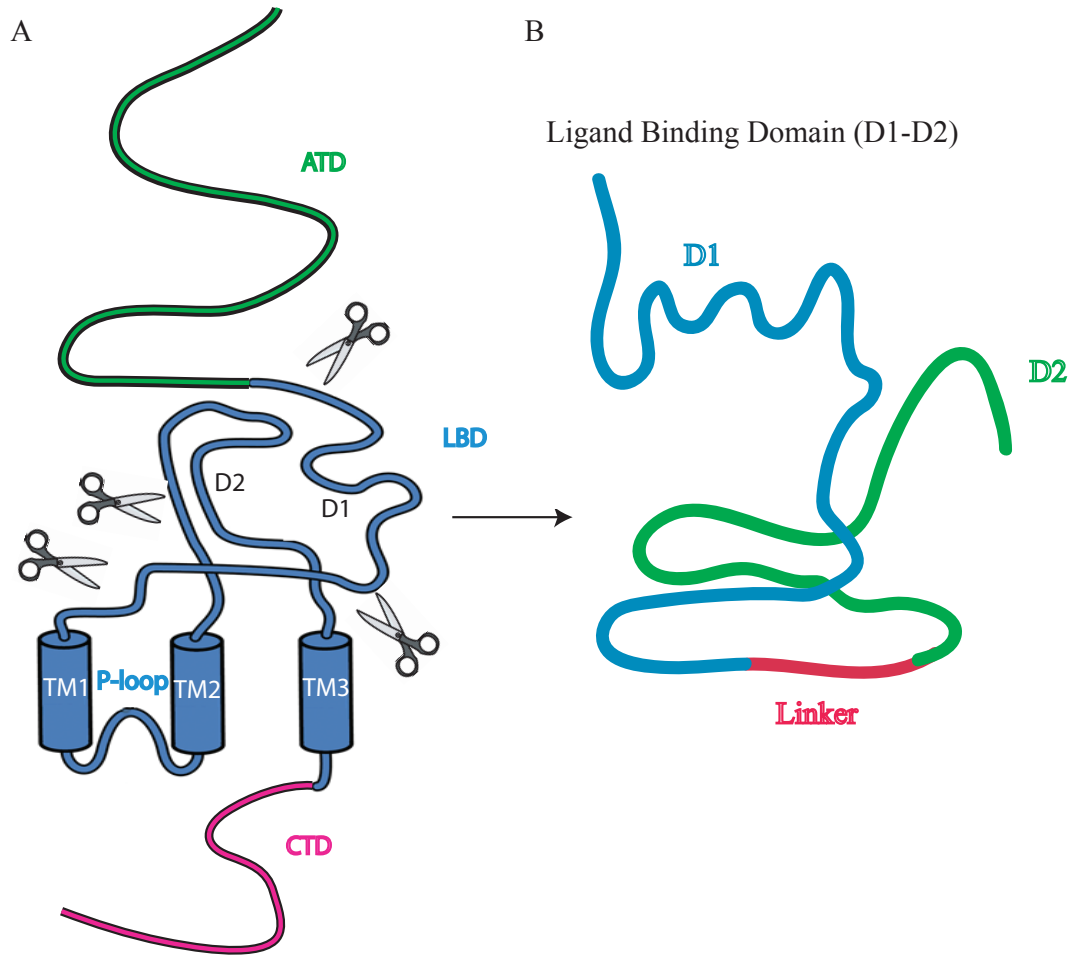


Figure 3.2 A) Topology of iGluR subunit containing an amino-terminal domain (ATD), ligand-binding domain (LBD), and three trans-membrane domains with a re-entrant P-loop followed by the carboxy-terminal domain (CTD). The scissors depict where PCR reactions were used to isolate fragments of S1 and S2 to produce a new ligand binding construct (called S1S2) used in x-ray crystallography. B) Ligand-binding domain clamshell resulting from the D1 (blue) and D2 (green) portions connected by a linker region (red).

Prior to the crystallographic studies, several key experiments suggested that the agonist-binding core consisted of two domains, similar to bacterial periplasmic proteins. The first experiment inserted N-glycosylation and proteolytic sites into the protein, digested the protein enzymatically, and analyzed the resultant fragments by gel shift to indicate domain topology (7-10). The second experiment used that evidence in combination with homology modeling to demonstrate that the agonist-binding domain

had structural similarity to the crystallized bacterial periplasmic proteins (11-13).

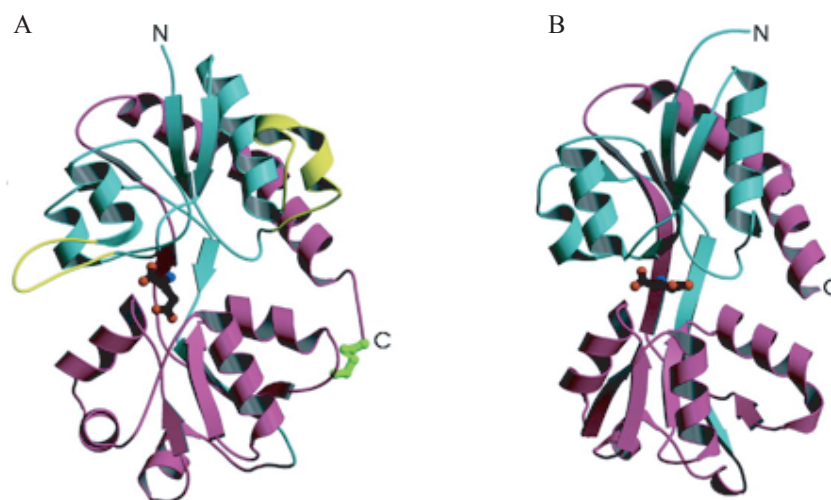


Figure 3.3 A) Topology of ligand-binding domain of GluR2 with glutamate bound in the cleft between D1 (blue) and D2 (purple). B) Topology of LBD of GluR0 with glutamate bound in cleft although in a different orientation from (A). Adapted from reference (14).

These studies suggested that by using protein engineering, it would be possible to isolate the ligand-binding domains. The isolated domains were water-soluble and retained the agonist binding characteristics specific for AMPA receptors. The ATD was removed, and the D1 and D2 portions of the LBD, normally separated by several of the trans-membrane domains, were hooked together with a linker (Figure 3.2). Initial studies performed in *Escherichia coli* (*E. coli*) yielded the excised soluble D1-D2 connected domains of the GluR4 AMPA receptor subtype (15), yet the soluble LBD was not optimized for crystallization. Continued protein engineering and use of a special *E. coli* strain, optimal for proteins containing disulfide bonds, generated high resolution structures (1.5Å) of the GluR2 AMPAR subunit in complex with the agonist kainate (6, 16, 17). These results spurred the isolation of other glutamate-binding cores from the bacterial GluR0 subunit, mammalian GluR4, GluR6, NR2A, and the glycine-binding NR1 subunit (Figure 3.3) (18-21).

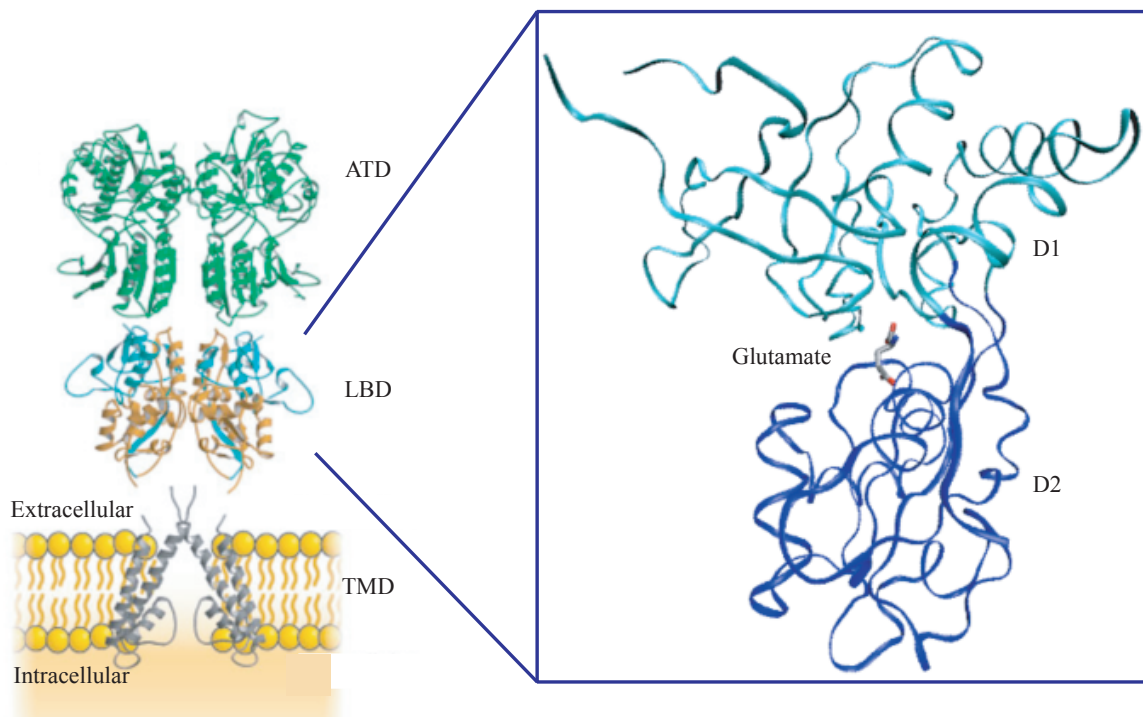


Figure 3.4 Extracellular ligand-binding domain of GluR2 AMPA receptor subunit co-crystallized with the agonist glutamate. The ligand binds to a cleft formed between D1 and D2 of the LBD. The GluR2 PDB file, 1FTJ, adapted from reference (22).

Not surprisingly, the results from the LBD crystal structures demonstrate a bi-lobed domain topology with D1 and D2 enclosing a cleft where the agonist binds. The D1 portion (pre-TM1) forms the top portion of the cleft and D2 (post-TM2) encloses the bottom of the cleft. The overall topology resembles a clamshell and is often referred to as such. Initial structures were crystallized in the presence of kainate(6), but further studies produced the clamshell in a ligand-free (apo) state and with many agonists, partial agonists, and antagonists binding in the cleft between D1 and D2 (Figure 3.4) (18, 19, 22). Currently, there are more than 20 structures, and all iGluR subtypes (AMPA, NMDA, and Kainate) are represented, each in complex with many different ligands. Additionally, to complement the static images of the LBD, NMR was used to obtain dynamic data on the GluR2 LBD (23). The first and most studied iGluR LBD is the GluR2 AMPAR subunit, which has provided the first mechanistic insights into ligand binding.

A globular protein consisting of two-domains, each representing a lobe of a

clamshell, encloses a cleft that characterizes the extracellular LBD (Figure 3.4). The two lobes are connected by two anti-parallel β -strands and are structurally similar to a periplasmic glutamine-binding protein, GlnBP (24). Interestingly, the domains are formed from peptide segments of both S1 and S2. The S1 segment corresponds to the peptide from the pre-M1 domain and S2 is the peptide fragment corresponding to the post-TM2/pre-TM3 segment. Both S1 and S2 contribute to D1 and D2 demonstrating that these peptides are not discreet domains within the LBD (6).

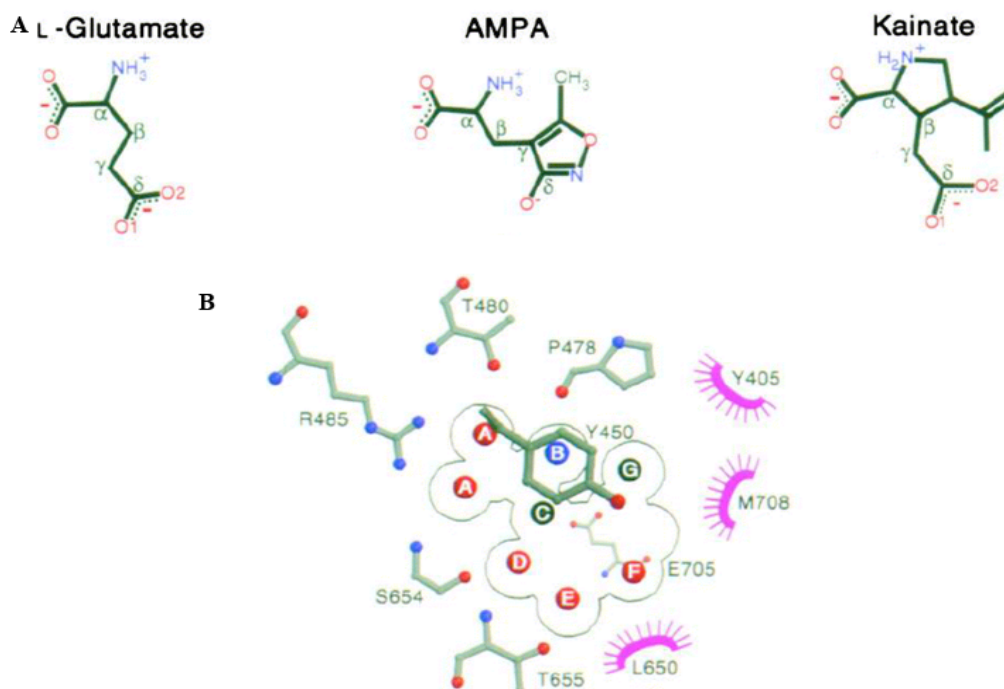


Figure 3.5 A) The agonists L-glutamate, AMPA, and Kainate with labeled carbon architecture. B) Amino acid side chains involved in ligand recognition in GluR2 subunit. The figure was adapted from reference (22).

Crystallization of the GluR2 LBD with the agonists glutamate and AMPA, the partial agonist, kainate, and the apo state established the specific interactions that are important for ligand activity and demonstrated that a large conformational change occurs upon ligand binding (22, 25). The structural evidence coupled with additional biochemical investigations (26) suggests a two-step process leading to channel activation. The first step, ligand docking, occurs as the ligand binds to D1 (top lobe) amino acids via

the α -amino and α -carboxy groups in the cleft between D1 and D2 (Figure 3.5A). Then the γ -carboxyl group interacts electrostatically with the base of helix F, the N-terminal dipole of which points into the cleft (Figure 3.5B). This interaction is referred to as the “locking” step and involves the movement of D2 toward D1, which closes or clamps the binding cleft (14). The structures with bound glutamate and AMPA demonstrated cleft closure involving a rotation of D2 towards D1 by $\sim 21^\circ$ compared to the open-cleft apo structure (22).

The ligand-binding domains form dimers with the S1-S2 linkers that replace the ion channel pore positioned on the same side of the dimer interface. The dimers make contact exclusively through D1, and the knowledge of this interaction combined with agonist binding that involves D2 rotation towards D1 suggested a mechanism that would open the ion channel. The dimers are connected such that each agonist binding cleft points outward from the dimer interface and upon agonist binding the closed cleft conformation is stabilized, and the linker regions of S1-S2 (on D2) swing apart from one another. As D2 moves closer to D1 to close the cleft, it pulls or twists the ion channel domain open (Figure 3.6).

The interactions that occur at the dimer interface also translate to differences between the desensitization kinetics of each ion channel. Desensitization refers to a physical state of the receptor where ligand is bound to the LBD, but the ion channel is in a non-conducting state. The interactions that contribute to ion channel gating also affect desensitization. Again, there are many structural similarities between the dimer interfaces of all the iGluR subunits, however more subtle features contribute to varying degrees of desensitization observed for each receptor. For example, most AMPARs undergo rapid desensitization whereas NMDARs experience much slower desensitization and some do not desensitize at all. Many of these features can be attributed to chemical-scale interactions at the dimer interface.

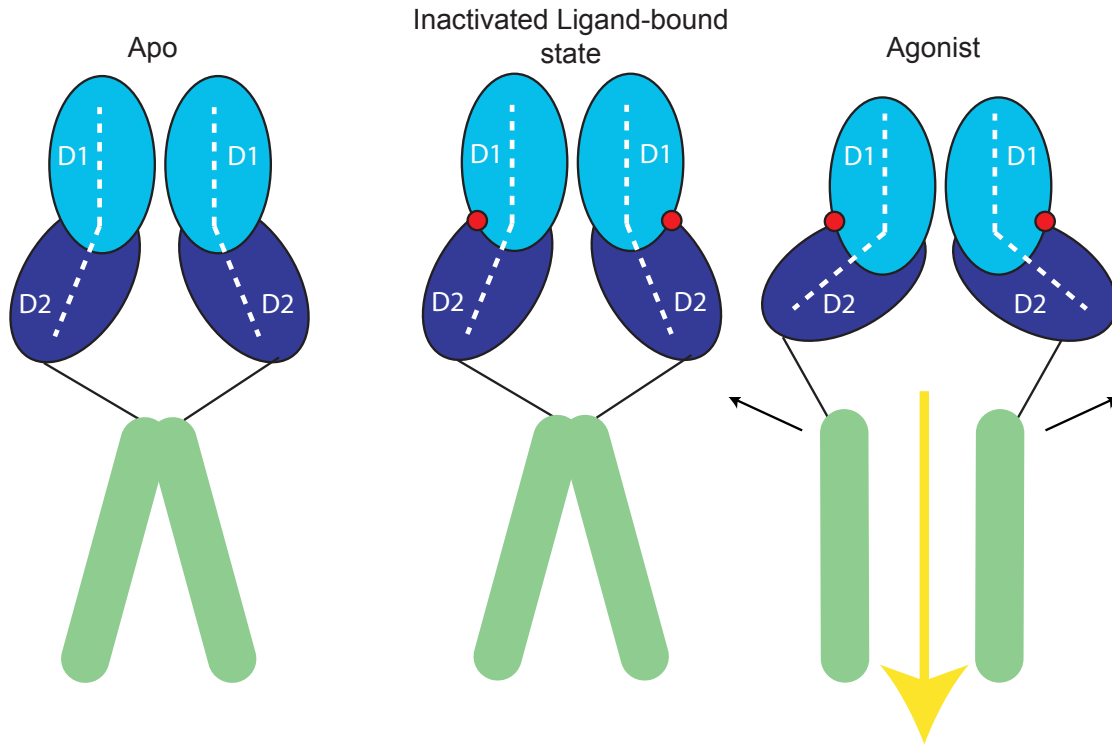


Figure 3.6 Diagram for proposed ligand-induced activation. The ligand-binding core is attached to the ion channel domain via a linker and as D2 moves toward D1, a conformational change opens the channel pore domain.

Crystallographic evidence supports the assembly of dimers for GluR2 AMPARs, the GluR0 bacterial homologue, and the NR1/NR2 NMDARs. This feature is unique since the structurally related bacterial periplasmic-binding proteins do not assemble into dimers in solution or in crystals. Additionally, the dimer interface of iGluRs is mostly hydrophobic, whereas the homologous surface of the periplasmic proteins contains many charged amino acids that do not establish complementary contacts when superimposed as a dimer (21). The iGluR dimer interface has evolved to support a structure that requires subtle conformational changes during ion channel activation and desensitization and remains a target for many different structural studies.

The extent to which these structural studies have expanded our knowledge of iGluR structure, activation, and function cannot be expressed enough. Although all of the iGluR families are related, the subtle features of each family do not always translate to another, so we must perform biochemical experiments for all of the different iGluRs to understand

them fully. We cannot assume that a mechanism that applies to one type of receptor will automatically apply to another, as we will demonstrate below.

Another caveat to structural studies is that although they provide precise molecular-level details, they do not assess the receptor in its native state or the full protein conformation. This is where our functional studies are key. We will use the structural evidence to guide our experiments and produce functional data for these ion channels.

3.1.2 Previous Studies of Partial Agonism and Structural Evidence for the Clamshell Model of Partial Agonism in AMPA-Selective Receptors

The methodology developed by Gouaux and co-workers is not solely applied to studying full agonists. Many studies have been performed using the S1-S2 LBD in complex with competitive antagonists and partial agonists. Competitive antagonists bind to the agonist recognition site but do not activate a receptor according to classical receptor models (27). Studies of AMPA-selective receptors were first performed on the GluR2 S1-S2 LBD structure, and we will summarize the observations of this receptor subtype, as they formed the basis of analysis on additional receptors. The iGluR competitive antagonists are generally larger in size than the agonists, and therefore the basic assumption is that they prevent ion channel activation via steric interference. Two GluR2 competitive antagonists, DNQX (6,7-Dinitroquinoxaline-2,3-dione) and ATPO ((*R,S*)-2-amino-3-[5-*t*-butyl-3-(phosphonomethoxy)-4-isoxazolyl]propionic acid), were crystallized with the GluR2 S1-S2 LBD and both prevent receptor activation by steric interference, a mechanism often referred to as the “foot in the door” (22, 28). From a chemical standpoint these antagonists are unrelated; DNQX is a quinoxalinedione and ATPO is an isoxazole (Figure 3.7). The 7-nitro group of DNQX is the likely “foot” that interacts with threonine 686 in D2. ATPO is structurally similar to AMPA and binds in a similar orientation. However, the 3-phosphono-methoxy moiety interacts with the base of helix F as the “foot” since it is a more extended structure than AMPA. The resulting domain closure is between 2.5 and 6.0°, insufficient for wild type receptor activation (compared to ~21° for AMPA and glutamate). The main conclusion from the experiments with antagonists is that they interact with pre-organized residues primarily in D1 and stabilize the open-cleft state of the clamshell, similar to the apo structure.

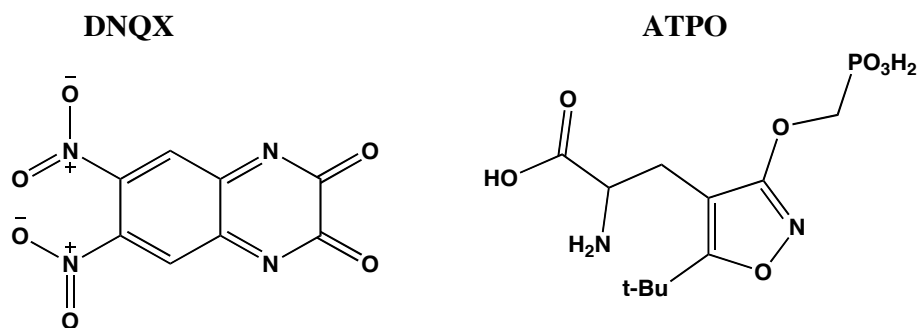


Figure 3.7 AMPA receptor antagonists, DNQX and ATPO.

The studies of GluR2 with full agonists and antagonists demonstrated a correlation between activation of the ion channel and the amount of agonist-induced cleft-closure between D1 and D2. The results with the partial agonist kainate provided more insight into the mechanism of agonist action in iGluR LBDs. Ion channel activation is characterized by at least two separate steps at the atomic level, the ligand-binding step, dependent on the receptor's affinity for the ligand, and the activation step described in terms of agonist efficacy, its ability to activate the receptor. Partial agonists are very useful molecules because they can probe the relationships among agonist binding, conformational changes of the protein, and receptor activation. Partial agonists were first described by del Castillo and Katz as ligands that have an open channel probability of less than 1 despite occupying all of the ligand-binding sites (29). In the absence of direct structural data, several models have been developed to explain the basis of partial agonism.

The most common method is based on the Monod-Wyman-Changeux (MWC) model for allosteric proteins (30). This model suggests that ligand-gated ion channels have two possible states, the closed or resting state (T) and the active or open state (R), which exist in equilibrium with each other. Agonists would shift this equilibrium in the direction of the open state. Full agonists, the most efficacious, are maximally effective at shifting the equilibrium to the open state, and partial agonists are less effective at shifting this equilibrium (31). This model provides a clear, but simple explanation of efficacy. However, this model may be too simple and unable to account for the ability of partial agonists to activate a spectrum of receptor efficacies (14).

Crystal structures demonstrating the mechanism of partial agonism in GluR2 AMPARs were solved for a variety of partial agonists. The first structures were with kainate and quisqualate, followed by willardiine (and the derivatives, 5-F-willardiine, 5-Cl-willardiine, 5-Br-willardiine, and 5-I-willardiine) (Figure 3.8), and an isoxazole series ((S)-2-Me-Tet-AMPA, (S)-ACPA, (S)-Br-HIBO) (28, 32, 33). One key attribute of the partial agonists is that when they bind in the closed-cleft GluR2 LBD, some of the structural water molecules that are present when glutamate is bound are excluded to support the expanded ligand structure, and some of the full and partial agonists do not bind in the same orientation as glutamate. However, this does not directly correlate with agonist efficacy. For example, AMPA and glutamate bind in a similar orientation within the cleft and are full agonists, however, the full agonists 2-Me-Tet-AMPA, quisqualate, and ACPA all bind with different orientations (28, 33). This suggests that the orientation of the agonist within the binding cleft is not as important for determining agonist activity as the orientation of the binding cleft itself. In other words, the receptor responds to how “full” the binding pocket is instead of how it is filled.

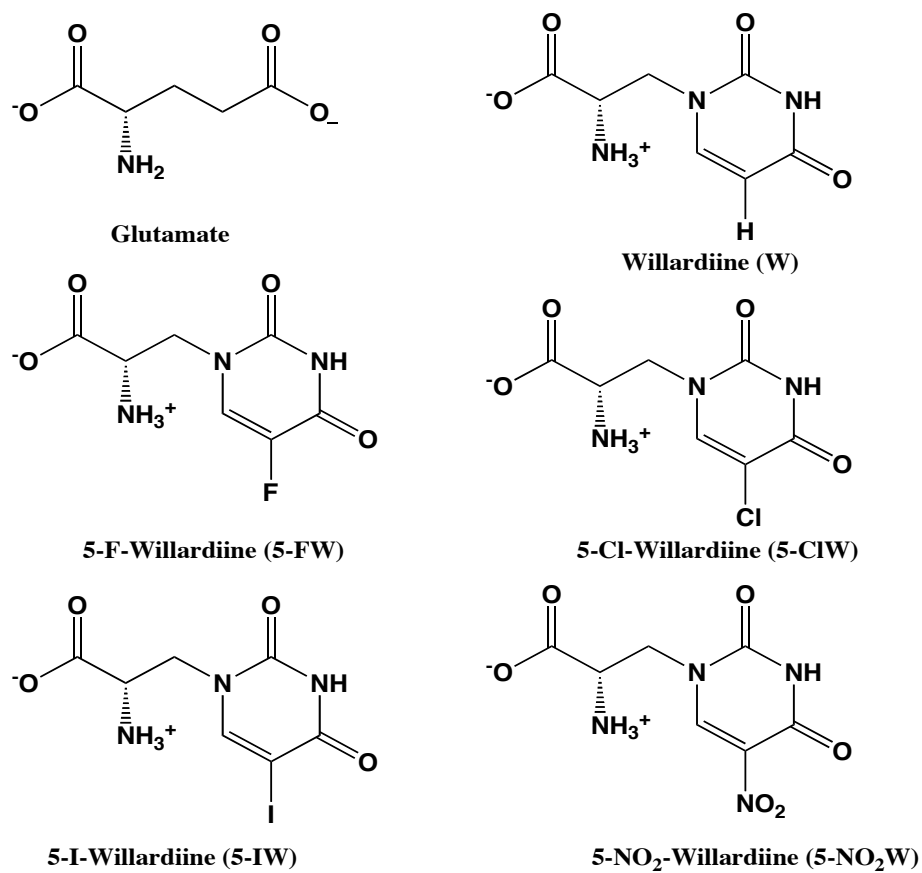


Figure 3.8 Structures of the willardiine series of GluR2 partial agonists.

The structural studies demonstrate that there is a correlation between agonist efficacy and the degree of cleft closure. The full agonists, AMPA and glutamate, induce ~20° of domain closure and kainate, a partial agonist, induces only 12° of domain closure, relative to the apo conformation. These results suggest that the amount of domain closure is related to the activity of the ion channel. Further studies with the willardiine series (Figure 3.8) were performed and acted as an ideal test case since they bind to the cleft in an orientation similar to glutamate. The willardiines act as partial agonists due to the substitution of the 5-substituent on the uracil ring, which sterically interferes with GluR2 Met708 preventing full cleft closure. The substituted willardiines, 5-H, F, Br, and I were studied (Figure 3.8) and as the size of the 5-substituent increases, the extent of activation of the ion channel diminished (i.e., agonist efficacy decreases) (32).

The extent of cleft closure in the GluR2 dimer was measured by evaluating the

distance between the protomer linker regions. An increase in domain closure correlates to an increase in the distance between the protomer linkers. The linkers replace the region corresponding to the ion channel pore domain of the full-length receptor; therefore an increase in the distance between the linkers suggests a physical mechanism for channel activation. To demonstrate the correlation between agonism and domain closure, plots were generated with relative agonist efficacy on the x-axis and linker separation (Å) on the y-axis (Figure 3.9) (28, 32, 34). One feature of these plots demonstrates a linear correlation between agonist efficacy and linker separation, consistent with the domain-closure hypothesis (Figure 3.9).

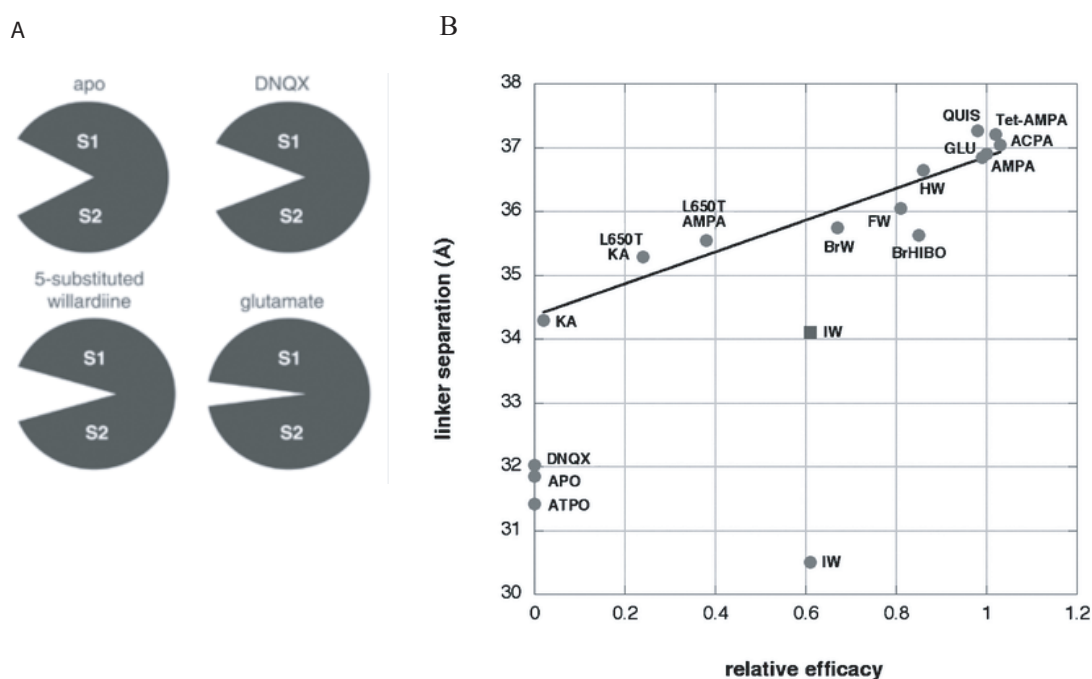


Figure 3.9 A) Schematic representing the degree of domain closure induced by full and partial agonists. Full agonists induce more domain closure relative to the apo state than partial agonists. B) Plot of the relative efficacy of different agonists vs. the distance of linker separation measured from the GluR2 S1-S2 crystal structures (Å). Adapted from references (28, 32, 34).

Single-channel analysis of full-length ion channels suggests how structural changes in the binding core couple to ion channel activation. Several conductance states have been identified for iGluRs, some conducting more than others. Conductance states are

open-state conformations of the ion channel defined by a particular ion flux. iGluR partial agonists preferentially activate lower conductance states, and full agonists activate higher conductance states. The existence of multiple conducting states for the ion channel suggests that the degrees of domain closure exist along a continuum. More importantly, it suggests that the conformational changes signaled to the ion channel domain by the ligand binding domain exist as specific states along this continuum. In other words, the degree of ligand binding domain closure promotes population of specific conductance states (32) presumably that coincide with specific amount of ion channel opening (Figure 3.10). Another study supporting this idea involved mutation of GluR2 Leu650 to Thr. The L650T mutation decreased AMPA efficacy without a change in domain closure, but kainate efficacy increased, becoming a full agonist with an increase in domain closure (25). These studies imply that agonists induce ion channel activation via several mechanisms. However, further investigation of the structure and function of iGluRs with partial agonists are necessary for a better, more complete understanding of these mechanisms.

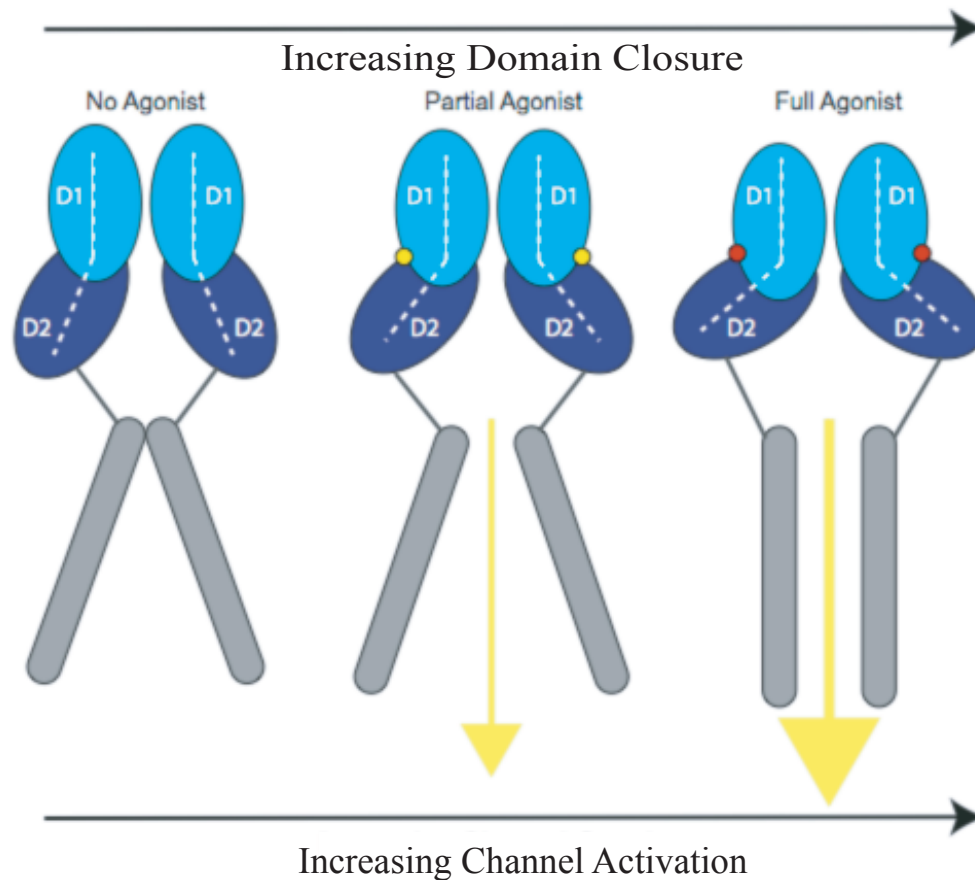


Figure 3.10 Schematic representing the partial ion channel opening induced by partial agonists and a larger channel opening induced by full agonists.

3.1.3 Structural Studies of NMDA-Selective Receptors

NMDA receptors are unique in the glutamate family of ion channels for many reasons, but they are especially peculiar in terms of ligand binding, since the endogenous ligand for the NR1 subunit (a requirement for channel function) is glycine or D-serine, not glutamate (1). The first structural understanding of NMDA receptors came from crystal structures of the S1-S2 region of the NR1 glycine-binding domain (18). Gouaux and coworkers demonstrated that similar to bacterial periplasmic proteins, bacterial GluR0, and mammalian GluR2 and GluR6, the NR1 LBD folds into a D1-D2 clamshell. Several years after these structures were solved, the soluble S1-S2 NR1-NR2A heterodimer was characterized (19) in the presence of glutamate and glycine (Figure 3.11). These studies and biochemical studies, with disulfide crosslinked NR1-NR2 receptors, demonstrated that the native NMDAR forms a dimer of heterodimers instead

of a composite of NR1 homodimers and NR2 homodimers (19). Uniquely, NMDA receptor dimer assemblies involve allosteric coupling between the two different subunits. The heterodimer suggests that unlike the AMPAR LBD dimers, the NMDAR dimer interface consists of both D1 and D2 contacts. This could be one contributing factor affecting the differences observed among NMDA receptor assemblies (35, 36).

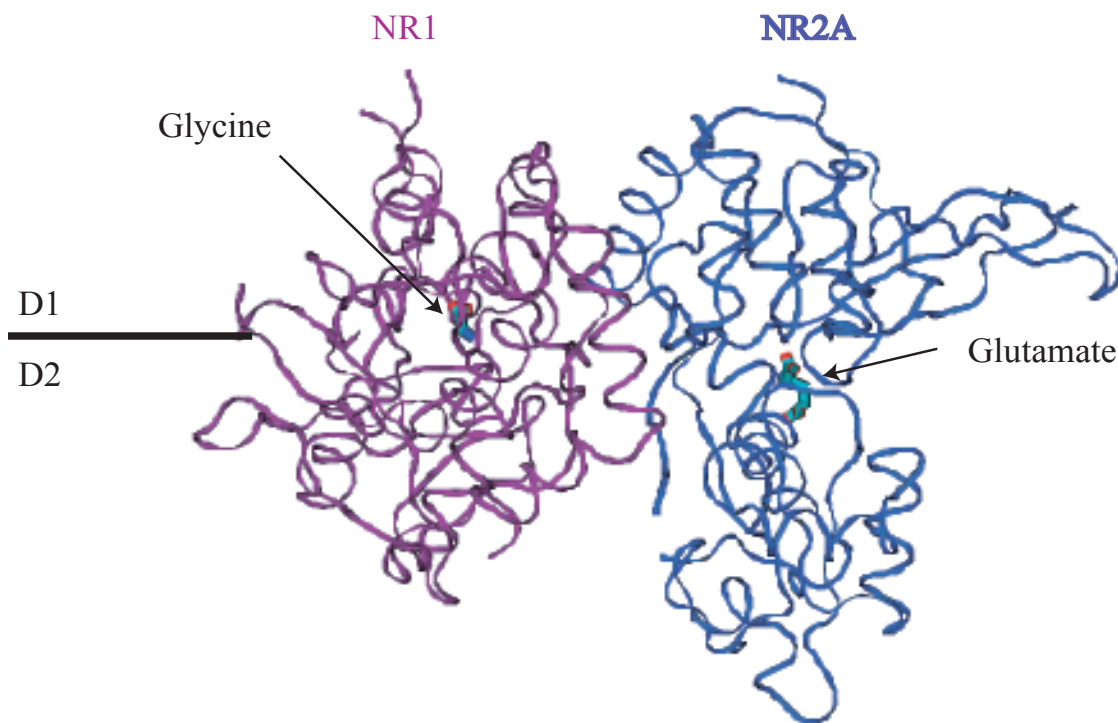


Figure 3.11. NR1-NR2A heterodimer structure. Glycine is bound to the NR1 subunit and glutamate is bound to the NR2A subunit. The dimer interface is composed of both D1 and D2 contacts. PDB file: 2A5T (19).

The NMDAR glutamate and glycine agonist-binding domains share several characteristics with the GluR S1-S2 structures, including conserved residues that appear in all of the iGluR families. An arginine in Helix D forms the major binding site for the α -carboxyl group of the ligand. Helix F contains a conserved threonine or serine, which makes a hydrogen-bond contact with the γ -carboxyl group (e.g., in NMDARs it contacts the main-chain peptide bond). The α -amino group makes contact with a conserved glutamate residue in AMPA and KA receptors, and in NMDA receptors it makes a

solvent-mediated contact with an aspartate residue (Figure 3.12).

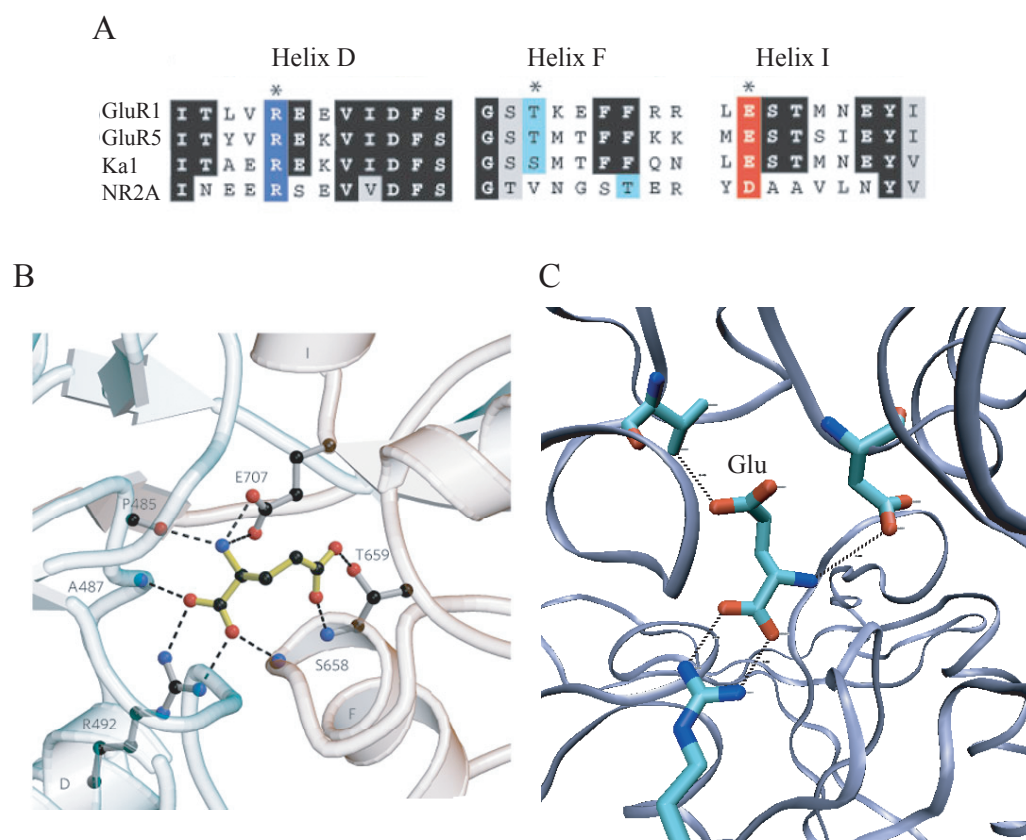


Figure 3.12 A) Sequence alignment of helices D, F, and I, which are involved in ligand binding. B) Conserved structural contacts between helices and glutamate (GluR6 S1-S2 domain), adapted from reference (37). C) NR2A binding site with conserved residues highlighted, PDB file 2A5T.

These structures demonstrate that in all of the binding pockets there is more than enough room to accommodate glutamate and related structures with the exception of NR1, which is just large enough to accommodate glycine and excludes the larger glutamate residue (18). The D2 portion of the clamshell provides subunit specificity for different ligands. In all iGluRs, D1 has conserved structure and binding interactions with the α -carboxyl and α -amino groups from the ligands. The most important theme, which we will revisit in our studies, is that the amount of agonist-induced domain/clamshell closure varies between each of the receptor subtypes, as well as for individual agonists, antagonists, and partial agonists (18, 20, 22, 27, 28, 38).

3.1.4 Previous Studies of Partial Agonism and the Clamshell Model of Partial Agonism in NMDA Receptors: The NR1 Glycine-Binding Subunit

Partial agonism studies were performed on the NR1 S1-S2 LBD prior to the characterization of the heterodimer complex. These studies paralleled those of GluR2, but with NR1 specific partial agonists, 1-aminocyclopropane-1-carboxylic acid (ACPC), 1-aminocyclobutane-1-carboxylic acid (ACBC), and D-cycloserine (D-CS) (Figure 3.13) and the antagonist, cycloleucine. The first study demonstrated that the partial agonist, D-CS, induced similar domain closure to glycine, an unexpected result based on the previous partial agonist studies with GluR subunits (18). This study prompted a more thorough investigation of NR1 partial agonism using additional partial agonists and antagonists.

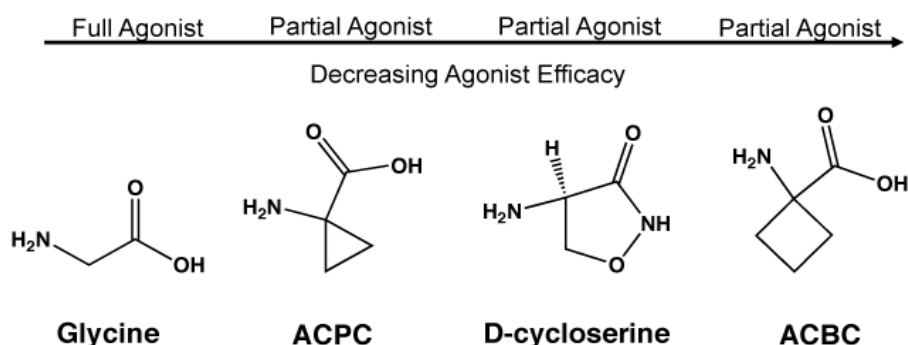


Figure 3.13 Chemical structures of NR1 ligand-binding domain partial agonists.

The study used these different partial agonists, which increase in volume by $\sim 11 \text{ \AA}^3$ per molecule (18). The conclusion of the study was that the NR1 S1-S2 core behaves differently than the AMPA-sensitive ligand-binding core in the presence of partial agonists. The NR1 glycine-selective subunit ligand-binding domain undergoes the same degree of clamshell closure for partial agonists as it does for full agonists (39) (Figure 3.14). Previously established models depicting the interactions between ligand-binding domain conformational states and how they translate to ion channel activity are complicated by these results (32). Full agonists for AMPA-selective receptors appear to shift the equilibrium towards the open state, with partial agonists stabilizing intermediate states, but the NR1 partial agonists do not fit this model. An alternative model for ion

channel activation is a two-state model in which both the ligand-binding domain and the pore domain have two states, either closed or open. Full agonists are more effective at populating an agonist-bound, open channel state than partial agonists, which are not as effective at shifting the equilibrium constant (K_{eq}) from the agonist-bound, closed channel state to the agonist-bound, open channel state (31). The second model can account for the observations in the NR1 partial agonist bound LBD structures, but differs from the mechanism thought to occur in GluR2 receptors (Figure 12).

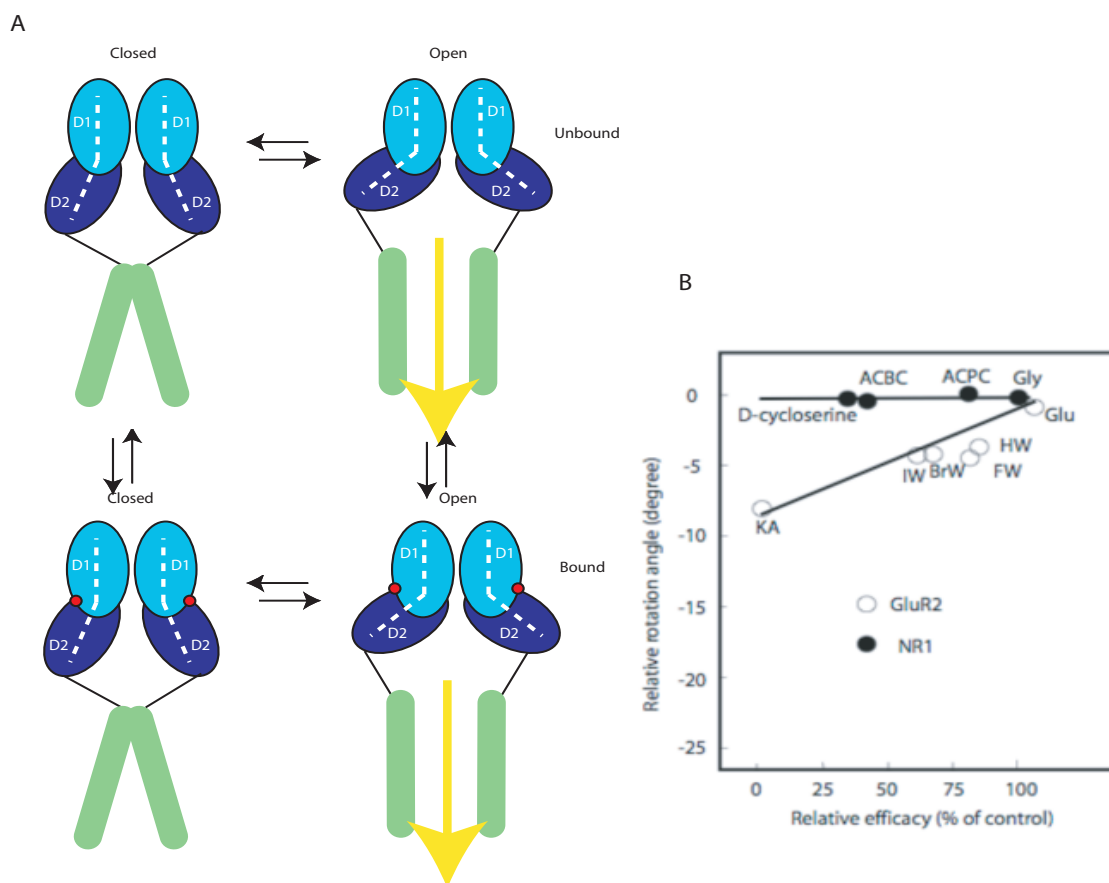


Figure 3.14 A) Scheme of model depicting NR1 agonist efficacy and channel activation. B) Graph of relative agonist efficacy versus S1-S2 domain closure for NR1 and GluR2 receptors. No correlation is observed for NR1 compared to the GluR2 subunit, adapted from reference (31).

To understand the binding of partial agonist to NR1, Gouaux and co-workers analyzed the contacts between D1-D2 and the agonists. All of the agonists- glycine, ACPC, and ACBC- interact with a similar hydrogen bond scheme among the domains

and the carboxy and amino groups. A hydrophobic surface of the LBD (Phe484, Val689, and Trp731) interacts with the rest of the hydrophobic portion of the ligands and since it is primarily composed of D2 residues, it is possible that these residues “sense” the size of the ligand and undergo localized conformational changes in the clamshell that translate to receptor activation (39). D-CS interacts similarly to glycine with a couple of subtle differences. The nitrogen and exocyclic oxygen interact with Arg523 similarly to the glycine α -carboxylate of glycine. The isoxazolidinone ring oxygen interacts with Ser688 instead of the α -carboxylate oxygen (in glycine structure) (18). NR1 Val689 is implicated in changing the conformation of helix F and the inter-domain β strand, believed to be implicated in receptor activation. It is possible that NR1 compensates for increasing the ligand size, using a different mechanism than glutamate-gated subunits (40). Since the amount of clamshell closure is not as important for NR1 subunits, this suggests that the other regions of the protein (possibly the dimer interface) are more important for translating conformational changes induced upon agonist binding. The conclusion from the structural studies is that even though NR1 partial agonists induce the same domain closure as full agonists, they do not stabilize the closed-clamshell as well as full agonists, as evidenced by their efficacy.

3.1.5 Previous Studies of Partial Agonism and the Clamshell Model of Partial Agonism in NMDA Receptors: The NR2 Glutamate-Binding Subunit

The S1-S2 heterodimer containing both NR1 and NR2A subunits is the only current structural characterization of any NR2 subunits. Crystal structures of the NR2 agonist-binding clamshell with partial agonist bound remain elusive. However, there has been a plethora of biochemical and *in silico* studies performed on NR2 subunits. As mentioned above, residues that interact directly with the ligands across all iGluRs are highly conserved, and an increase in solvent-mediated interactions distinguishes the NR2 agonist binding cleft. The α -amino group of glutamate interacts with NR2A Asp712 (mature protein numbering) through a water-mediated interaction.

In addition, several hydrogen bonds have been identified between D1 and D2 residues that are thought to contribute to agonist-induced activation of the ion channel. The Asp (712) residue also makes an inter-domain interaction with Tyr742. Another D2

residue, Tyr711 (NR2A mature protein numbering), interacts with a D1 residue, Glu394, as well as the γ -carboxylate of the ligand (34, 41) (Figure 3.15). Mutagenesis studies were performed on several of these residues, most notably a mutation in NR2B, Tyr705Ala (NR2AY711 equivalent), which resulted in a >400-fold shift in glutamate EC₅₀ (42). Additional kinetic experiments also demonstrated that this residue was important for receptor activation, possibly through inter-domain interactions. These studies provide clear evidence that although crystal structures are useful for understanding the nature of chemical-scale interactions, without full-length, functional ion channels we cannot get a clear understanding of how structure relates to function, and thus it is important to correlate mutagenesis with structural studies.

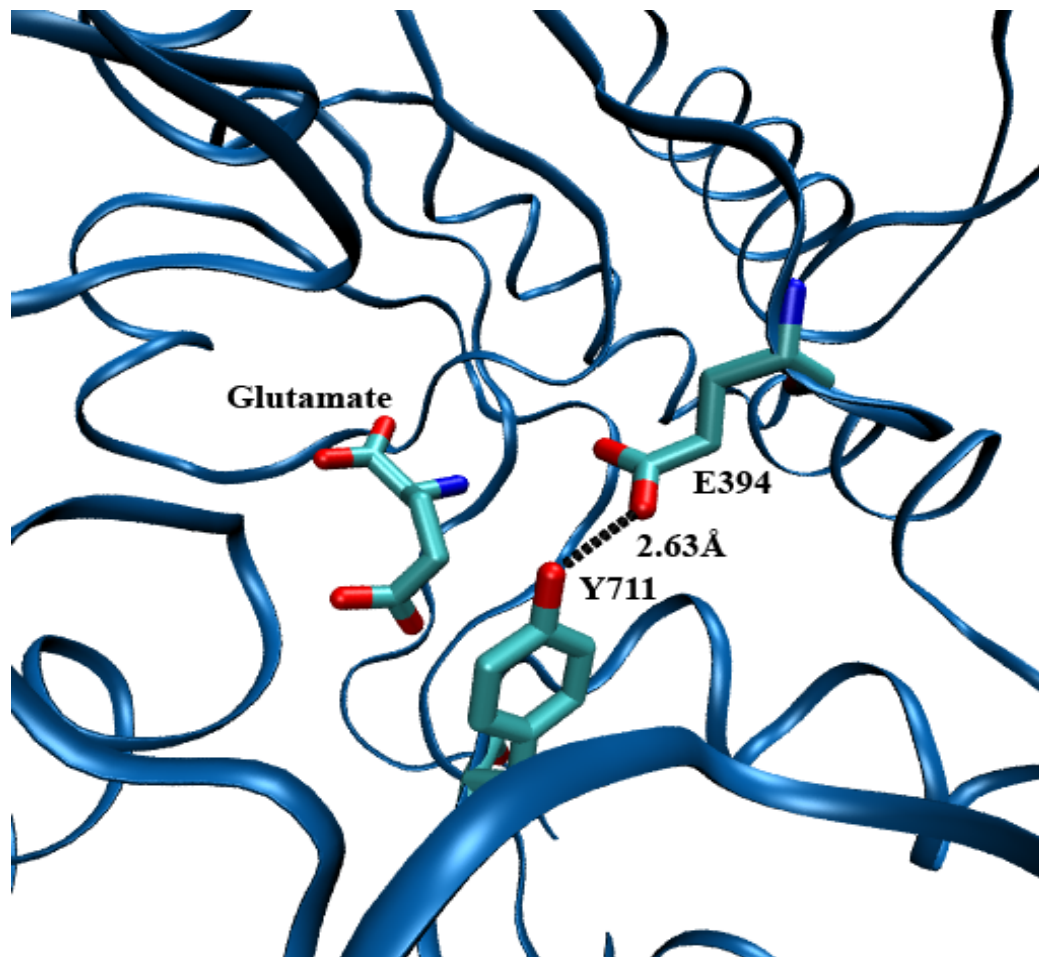


Figure 3.15 Ligand-binding domain of the NR2A subunit (PDB file 2A5T). The ligand, glutamate, is highlighted and an inter-domain hydrogen bond between E394 (D1 residue) and Y711 (D2 residue) is labeled.

3.2 NMDA Receptor Ligand-Binding Domain Studies

3.2.1 Project Overview

To further explore the relationship between structure and function, we decided to incorporate unnatural amino acids into the ligand-binding site of the NR2B glutamate-binding subunit of the NMDA receptors. We hypothesized that amino acids that lie at the agonist-cleft interface could interact with the agonist and induce ion channel activation. Since previous studies had implicated NR2BY705 (NR2AY711, Figure 3.15) in an ion-pair interaction with NR2BE387 (NR2AE394, Figure 3.15), we decided to begin our studies with these residues (all numbering will be for the mature protein). In particular, we sought an alternative probe of the clamshell mechanism, one based on receptor *function*, rather than a series of structures of receptor fragments. Along with complementing the structural work, such an approach could be more generally applicable to a wide range of receptors. Our focus is on residues at the D1-D2 interface that have been implicated to be important in receptor function, and that, based on the structural studies, appear to be in a critical position with regard to clamshell closure. Using unnatural amino acid mutagenesis, we have influenced clamshell closure by inserting a “stick” in the clam to prop it open, and we then evaluated the impact on activation of the receptor by agonists and partial agonists.

3.2.2 Studies of an Ion-Pair Interaction at the NR2B D1-D2 Interface

To examine the inter-domain interactions, we utilized nonsense suppression to incorporate Tyr, Phe, 4-Me-Phe, and 4-MeO-Phe at NR2BY705 (Figure 3.16). We analyzed full-length functional receptors to measure whole-cell currents and determine EC_{50} values and relative efficacies for each of the mutant receptors. Relative efficacies were determined by measuring the I_{\max} partial agonist/ I_{\max} L-glutamate. Also, responses to all of the NR2B agonists were measured in the presence of 10 μ M glycine. As mentioned above, a previous study indicated that the conventional mutation, NR2BY705A, resulted in >400-fold shift in L-glutamate EC_{50} (42). This result is not surprising since the alanine mutation completely obliterates the side chain, a non-subtle mutation eliminating a hydrogen bond donor and acceptor and aromaticity.

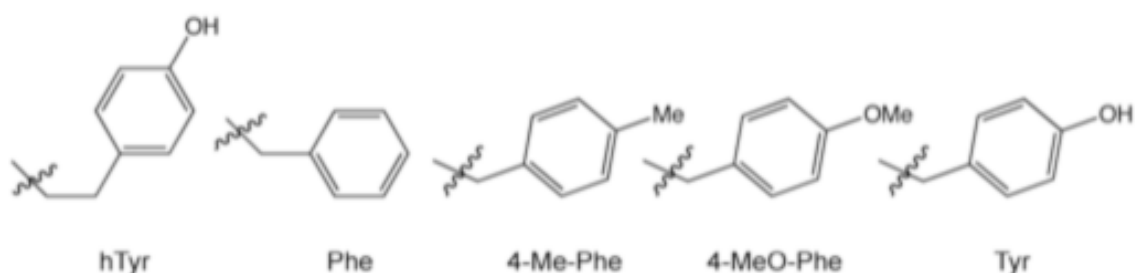


Figure 3.16 Conventional and unnatural amino acid side chain analogs of Tyr, homo-tyrosine (hTyr), phenylalanine (Phe), 4-methyl-phenylalanine (4-Me-Phe), and 4-methoxy-phenylalanine (4-MeO-Phe).

The more subtle mutations Phe, 4-Me-Phe, and 4-MeO-Phe produced functional receptors with manageable EC_{50} shifts of 14-, 10-, and 9-fold for glutamate and 23-, 9-, and 15-fold for NMDA respectively (Table 1). Overall, there are no significant differences among these mutations. All mutations remove the hydrogen bond donating ability of Tyr, but 4-MeO-Phe retains the hydrogen bond accepting ability. Our results thus suggest that an important role of Y705 is to donate a hydrogen bond. Additionally, each of these mutations produces a significant decrease in efficacy for NMDA with respect to glutamate (Figure 3.17A). Compared to wild type, where NMDA shows an efficacy of 0.88, the relative efficacies for the Phe, 4-Me-Phe, and 4-MeO-Phe mutants drop to 0.14, 0.37, and 0.26, respectively (Table 1). The drops in efficacy suggest that the hydrogen bond donating ability of Y705 is important for gating interactions that stabilize the closed, ligand-bound conformation of the clamshell. The efficacy studies also suggest that the Y705 hydrogen-bond donor is more important for stabilizing the partial agonist, NMDA, compared to glutamate, although the presence of electron density at the 4-position is important for function, even if there are no hydrogen bond donors or acceptors, as evidenced by the relative efficacy with 4-Me-Phe (Table 3.1).

Table 3.1 EC₅₀ and relative efficacy for NR2B D1-D2 interface mutations with L-glutamate and NMDA (N.E. is no expression). NMDA relative efficacy is compared to L-glutamate, (S.E.M.= standard error measurement).

Receptor	Glutamate EC ₅₀ μ M \pm S.E.M. (n)	Glu Hill	NMDA EC ₅₀ μ M \pm S.E.M. (n)	NMDA Hill	NMDA Efficacy
wildtype (1a/2B)	2.6 \pm 0.6 (8)	1.2	20 \pm 1.3 (15)	1.6	0.88 \pm 0.009
1a/2BY705 Phe	36 \pm 1.3 (6)	2.0	460 \pm 52 (5)	2.1	0.14 \pm 0.01
1a/2BY705 4-MePhe	27 \pm 2.3 (12)	1.5	190 \pm 23 (5)	2.0	0.37 \pm 0.01
1a/2BY705 4-MeOPhe	24 \pm 1.1 (7)	1.4	310 \pm 24 (6)	1.2	0.26 \pm 0.01
1a/2BY705 hTyr	43 \pm 2.4 (5)	1.5	31 \pm 2.6 (7)	1.5	0.79 \pm 0.01
1a/2BE387D	50 \pm 0.9 (5)	2.4	490 \pm 110 (6)	1.4	0.29 \pm 0.05
1a/2BE387Nha	92 \pm 8.2 (10)	1.8	220 \pm 21 (10)	1.9	0.39 \pm 0.02
1a/2BE413DY705 hTyr	N.E.		N.E.		

E387 is the proposed D1 partner of Y705. Mutation of the glutamate side chain to alanine was detrimental, producing a >200-fold shift in EC₅₀ (42). We again sought a more insightful evaluation of the importance of the glutamate side chain, using more subtle mutations. We introduced Asp, which contains the same charge as Glu but a shorter side chain. This subtle mutation significantly affected EC₅₀, raising it by ~20-fold for both glutamate and NMDA. We next introduced the unnatural amino acid nitrohomoalanine (Nha) (Figure 3.17B). Nha acts as an isosteric and isoelectronic analogue of a Glu, but it lacks the negative charge and is also a significantly weaker hydrogen-bond acceptor (43). Large increases in EC₅₀ were again seen, but in this case the effect was more than 3-times larger for glutamate than for NMDA. This suggests that E387 may play an important role in distinguishing different agonists.

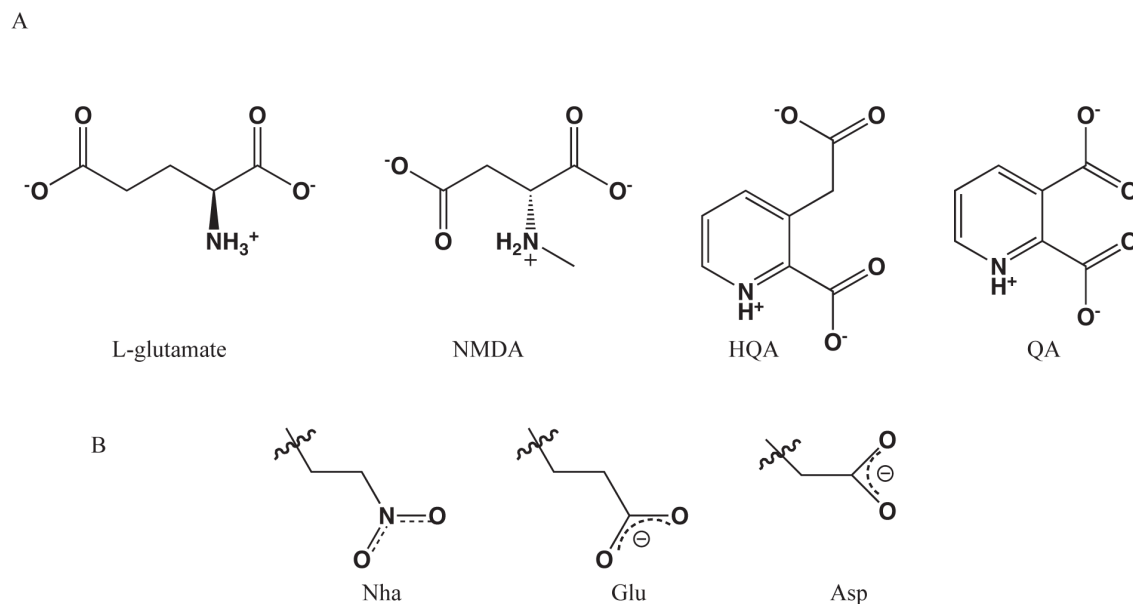


Figure 3.17 A) NR2B full and partial agonists used to study receptor function, L-glutamate, NMDA, homoquinolinic acid (HQA), and quinolinic acid (QA). B) Analogs of glutamate (Glu), aspartate (Asp), and nitrohomoalanine (Nha).

As with mutations at Y705, a drop in relative efficacy was observed for NMDA with each glutamate mutation. The effects were similar to those seen at the tyrosine, with NMDA efficacies relative to glutamate dropping to 0.29 for E387D and 0.39 for E387Nha (Table 3.1) (Figure 3.17B). All of the mutations result in a drop in relative efficacy for NMDA, suggesting that the inter-domain hydrogen bond between E387 and Y705 is directly involved in conferring changes induced by agonist binding to ion channel activation.

It has been proposed that E387 interacts electrostatically with the amino group of glutamate (41). The stereochemical difference between L-glutamate and NMDA suggests caution in directly comparing their binding behaviors, but the comparable responses of the two agonists to the E387D mutation suggests that the ammonium groups may be similarly positioned. Another difference between the two agonists concerns the nature of the positive charge on the agonist. The added methyl group of NMDA creates a more diffuse positive charge that spreads onto the N⁺-methyl hydrogens (34, 44, 45). In contrast, L-glutamate has a more localized charge, focused primarily on its ammonium

group. The more focused positive charge on glutamate should experience a stronger electrostatic interaction with a nearby negative charge, and hence the Nha mutation is more deleterious for glutamate. We propose that both agonists experience an electrostatic interaction with E387. The penalty for the E387D mutation primarily reflects the adjustments to protein structure and/or agonist orientation in response to shortening the side chain, and both agonists are penalized to the same degree. However, with Nha, for which no such adjustment is required, the larger penalty for glutamate indicates that the intrinsic electrostatic interaction to E387 is larger for glutamate. This is consistent with expectations based on the differing electrostatics for the higher charge density of the R-NH_3^+ of glutamate compared to the lower charge density of the $\text{R-N(CH}_3\text{)H}_2^+$ of NMDA.

3.2.3 Homo-tyrosine Incorporation at Y705

Having confirmed that Y705 and E387 are important for receptor function, we wished to use them as a probe of the clamshell motion. The simple idea was to increase the size of one of the residues by introducing the one-carbon homologue, in this case homotyrosine (hTyr, Figure 3.16). This would be like inserting a stick in the clamshell, preventing full cleft closure. We anticipated that full agonists would be more strongly influenced by the stick than partial agonists, because the latter do not induce full clamshell closure according to the GluR2-based structural model. Having established that the hydroxyl group of Y705 is essential for proper receptor function, it is clear that hTyr is a superior choice to other possible bulky residues, highlighting the value of the unnatural amino acid methodology. In fact, this is the only method that could test our hypothesis without making a less subtle mutation.

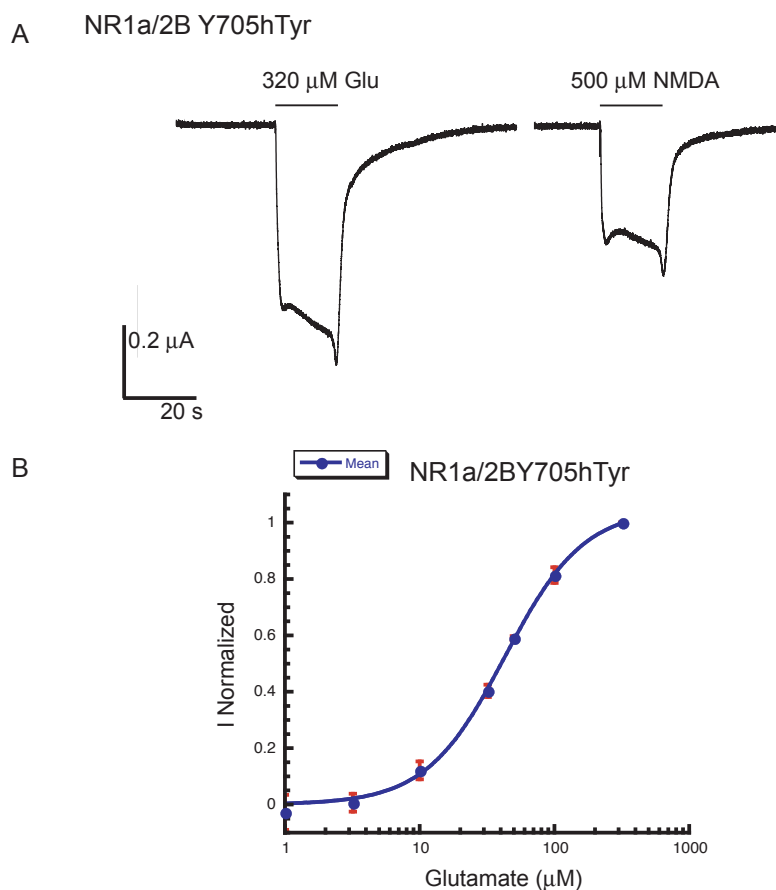


Figure 3.18 A) Electrophysiology traces of the NR1a/NR2BY705hTyr receptor. The currents were induced by glutamate and NMDA doses, as labeled. B) Example dose-response relationship for the NR1a/NR2BY705hTyr receptor and glutamate.

Initially, we measured EC_{50} values for the Y705hTyr mutant with glutamate and NMDA (Fig. 3.18). The respective EC_{50} s were shifted 16- and 1.5-fold, respectively (Table 3.1), the largest distinction between the two agonists we have seen and a result much different from the other Tyr mutants we evaluated. We considered the possibility that the new side chain geometry was affecting D1-D2 clamshell closure and that partial agonists would respond depending on their relative efficacy.

Table 3.2 EC₅₀ and relative efficacy for NR2B D1-D2 interface mutations with homoquinolinic acid (HQA) and quinolinic acid (QA). HQA and QA relative efficacies are compared to L-glutamate.

Receptor	HQA			QA		
	EC ₅₀ μ M \pm S.E.M. (n)	Hill	Efficacy	EC ₅₀ μ M \pm S.E.M. (n)	Hill	Efficacy
wildtype (1a/2B)	8.1 \pm 1.0 (16)	2.2	0.96 \pm 0.002	650 \pm 90 (7)	1.9	0.86 \pm 0.005
1a/2BY705 hTyr	49 \pm 4.3 (11)	2.1	0.83 \pm 0.008	720 \pm 90 (5)	2.4	0.32 \pm 0.009
1a/2BE387D	69 \pm 2.3 (16)	2.3	0.77 \pm 0.02	690 \pm 120 (10)	2.0	0.02 \pm 0.003
1a/2BE387Nha	85 \pm 6.1 (11)	1.8	0.86 \pm 0.006			

To further investigate the effect of Y705hTyr, we studied two additional partial agonists, homoquinolinic acid and quinolinic acid (Fig. 3.17A), with relative efficacies in the wild type receptor of 0.96 and 0.86 compared to glutamate. In response to homoquinolinic acid, Y705hTyr produced a 6-fold shift in EC₅₀, while the Y705hTyr mutation essentially did not affect the EC₅₀ of quinolinic acid (Table 3.2). A trend was observed: increased efficacy of the agonist in the wild type receptor correlated with a larger shift in EC₅₀ in response to the Y705hTyr mutant. These results produced a compelling relationship between agonist efficacy and receptor response (Figure 3.19). The plot is similar to ones produced for other iGluR systems, except now the y-axis is a measure of receptor *function*, rather than a structural parameter.

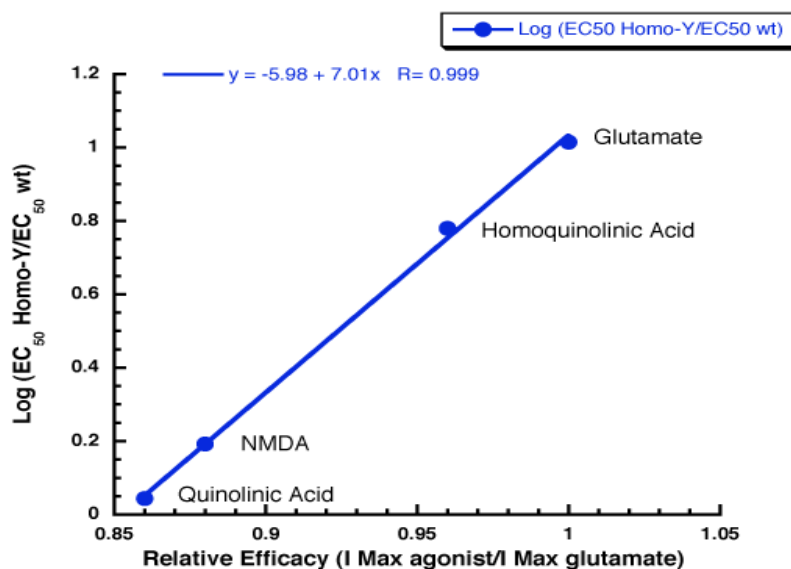


Figure 3.19 Activity of partial agonists at the NR1a/NR2BY705hTyr receptor compared to each agonists relative efficacy. A linear relationship is observed between receptor function and agonist activity. Partial agonists are less affected by the mutation than full agonists.

Since E413 and Y705 are proposed to interact directly through a hydrogen bond, we investigated whether the increased side chain length of the Y705hTyr mutation could be compensated for by the comparably decreased chain length of the E413D mutation. The double mutant E413DY705hTyr was prepared, but no electrophysiological responses were seen. Studies involving anti-NR2B receptor antibody labeling established that receptors were not trafficked to the surface of the oocytes (Figure 3.20), thwarting efforts to evaluate this double mutant.

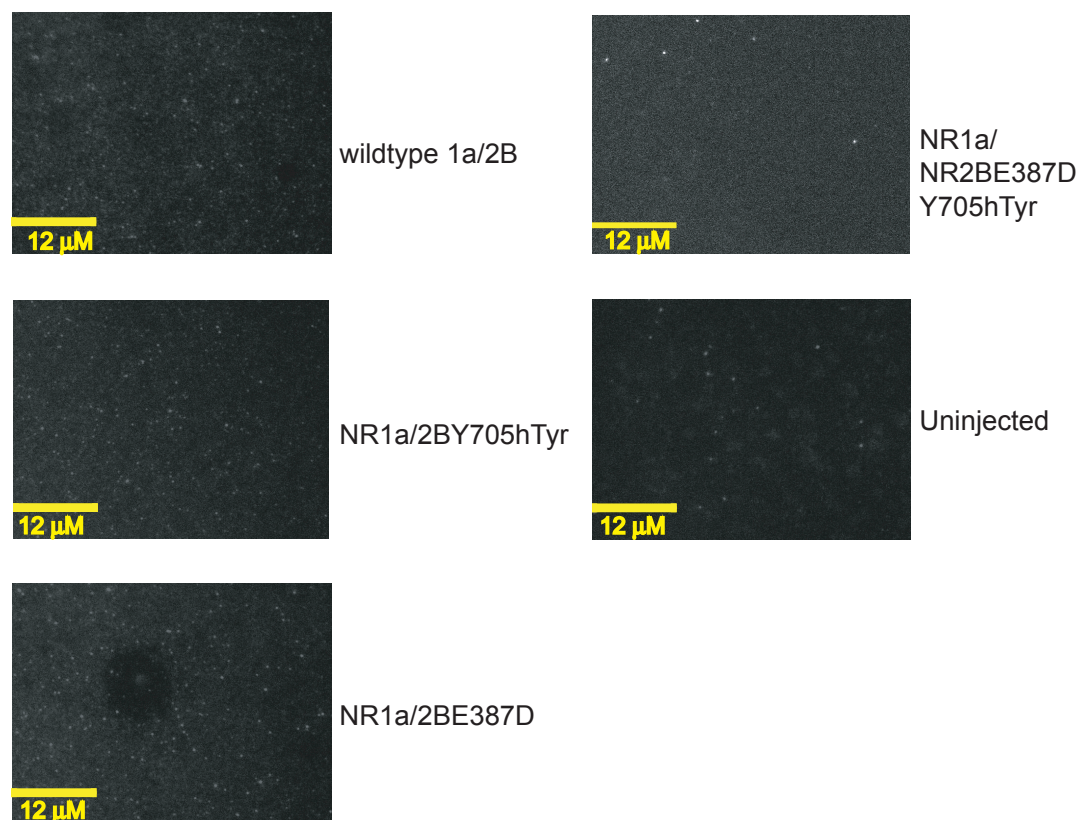


Figure 3.20 TIRF images of *Xenopus laevis* oocytes injected with wild type and mutant NMDA receptors. NR2B antibodies were used to label the NMDA receptors on the oocyte membranes.

3.2.4 Inter-domain Contacts and Mutations in the Glycine-Binding NR1 Subunit

There are many structural differences between the NR2 and NR1 subunits of the NMDA receptor. In fact, there is approximately a 20% sequence identity between the subunits (46), and the currently available structural information about NR1 does not correlate as well with the previously mentioned GluR2 structures as the NR2 structures do. Additionally, previous studies of the NR1 ligand binding domain in complex with full and partial agonists suggest that cleft closure around the agonist does not correlate with agonist activity. However, studies with an antagonist, cycloleucine, suggest that an open-cleft conformation contributes to receptor inactivation, similar to studies performed on the AMPA receptor formed from homomeric GluR2 (39). Clearly, there is not much consensus on the mechanism relating NR1 partial agonism to channel activation. Previous structural studies of NR1, the glycine binding subunit, suggested that the

clamshell effect was much less pronounced. As noted above, the homology between NR1 and NR2 subunits is not high, and certainly glycine and glutamate are structurally quite different. As such, we felt that applying the unnatural amino acid approach, lengthening amino acid side chains in the NR1 subunit, would provide a good test of the method and an opportunity to confirm previous structural studies.

The NR1 residues that correspond (based on sequence alignments) to the NR2 hydrogen bonding residues discussed above are Q403 and W731. Responses to the full, co-agonist glycine and the partial co-agonists- ACPC (1-aminocyclopropane-1-carboxylic acid), D-CS (D-cycloserine), and ACBC (1-aminocyclobutane-1-carboxylic acid) (Figure 3.13) were measured for functional NR1a/NR2B receptors containing the NR1 mutations Q403N, Q403E, and W731F (numbering for the mature receptors) always in the presence of 100 μ M glutamate (Figure 3.21).

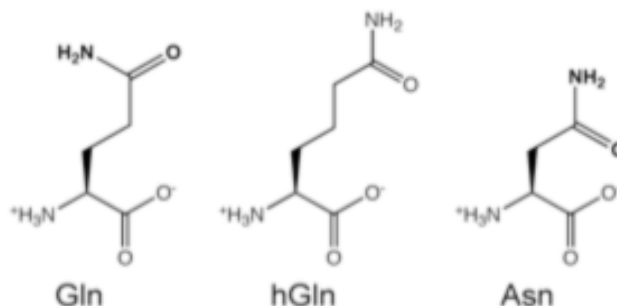


Figure 3.21 Analogs of glutamine (Gln) used in NR1 ligand binding studies, homoglutamate (hGln) and asparagine (Asn).

The ligand-binding domain mutation, Q403N, produced EC_{50} shifts of up to 17-fold (with D-cycloserine and ACPC), suggesting that the length of the side chain in that position of the ligand-binding domain significantly influences receptor activation. The Q403N mutation also influenced the relative efficacies of both D-cycloserine and ACPC, with a slight decrease in relative efficacy being observed for both partial agonists. The mutations introduced at NR1Q403 produced several shifts in relative efficacy for the partial agonist ACBC as well, with a large decrease in overall efficacy observed for the NR1Q403N mutation, without a large shift in EC_{50} (Tables 3.3 and 3.4).

Table 3.3 EC₅₀ and relative efficacy for NR1 D1-D2 interface mutations with glycine and (ACPC). Relative efficacy for ACPC is compared to glycine.

Receptor	Glycine EC ₅₀ ± SEM	Gly Hill	Gly n	ACPC EC ₅₀ ± SEM	ACPC Hill	ACPC n	ACPC Efficacy
wildtype (1a/2B)	0.98 ± 0.11	1.2 ± 0.13	8	0.28 ± 0.033	1.13 ± .12	12	0.86 ± 0.011
NR1aQ403N/2B	5.85 ± .13	2.3 ± 0.09	6	4.97 ± .40	1.28 ± 0.081	7	0.27 ± 0.0085
NR1aQ403E/2B	No Current			No Current			
NR1aW731F/2B	4.37 ± .11	2.9 ± 0.19	4	0.43 ± 0.08	1.43 ± .37	5	1.31 ± 0.04
NR1aQ403hGln	5.78 ± 1.058	1.31 ± 0.256	5	1.32 ± 0.36	0.74 ± 0.12	6	0.56 ± 0.04

Table 3.4 EC₅₀ and relative efficacy for NR1 D1-D2 interface mutations with ACBC and D-cycloserine (D-CS). Relative efficacy for ACBC and D-CS is compared to glycine.

Receptor	ACBC EC ₅₀ ± SEM	ACBC Hill	ACBC n	ACBC Efficacy
wildtype (1a/2B)	13.9 ± 1.61	1.16 ± 0.12	9	0.43 ± .008
NR1aQ403N	38.3 ± 7.1	1.64 ± 0.37	6	0.028 ± 0.0008
NR1aQ403E	25.7 ± 2.4	0.90 ± 0.06	4	0.37 ± 0.011
NR1aW731F	101.59 ± 6.8	1.28 ± 0.09	5	0.87 ± 0.02
NR1aQ403hGln	18.6 ± 7.0	1.13 ± 0.38	6	0.075 ± 0.0033
Receptor	D-CS EC ₅₀ ± SEM	D-CS Hill	D-CS n	D-CS Efficacy
wildtype (1a/2B)	6.02 ± 0.41	1.13 ± 0.08	9	0.66 ± 0.05
NR1aQ403N	99.6 ± 9.19	1.68 ± 0.21	12	0.50 ± 0.018
NR1aQ403E	87.4 ± 4.28	1.89 ± 0.15	5	0.42 ± 0.0197
NR1aW731F	78.8 ± 6.1	1.74 ± 0.18	5	0.57 ± 0.044
NR1aQ403hGln	13.5 ± 2.66	1.06 ± 0.21	5	0.60 ± 0.022

The NR1Q403E mutation produces significant perturbations. The two agonists with the highest efficacy, glycine and ACPC, are no longer agonists for this mutant receptor (Table 3.3). However, the other two partial agonists, D-CS and ACBC, still activate the receptor, with reduced potency. It is possible that the introduction of a negative charge on the side chain and/or the loss of a hydrogen bond donor in the glutamine side chain are important for agonist efficacy (Table 3.4).

Considering the D2 section of the NR1 ligand-binding domain, we evaluated W731F, a relatively severe mutation compared to the others considered here. For this mutant, the functional receptors lost potency with all of the agonists, producing a 5-fold shift for glycine and up to a 14-fold shift with D-CS (Table 3.4). This mutation not only alter the sterics of the side chain, but also removes a hydrogen bond donor. Both of these chemical aspects likely contribute to the decreased potency for all the agonists in the experiment.

3.2.5 Homo-glutamine Incorporation at NR1 Q403

Studies with the conventional mutation Q403N suggested that this site could be a candidate for the “stick in the clam” strategy. In order to probe clamshell closure around different ligands, we incorporated homo-glutamine, hGln, at NR1 Q403. As discussed above, introducing an additional methylene group to the side chain should disrupt clamshell closure. Along with glycine, we considered the three partial agonists, with efficacies at the wild type receptor ranging from 0.43 to 0.86. As shown in Tables 3.3 and 3.4, there is again a correlation between the change in EC_{50} for the hGln mutant and the efficacy of the partial agonist (Figure 3.22, 3.23).

However, it is clear that the NR1 subunit is much less sensitive than the NR2 subunit. The plot in Figure 3.23 reveals that there is indeed a strong correlation between the efficacy of a given agonist on the wild type receptor and the magnitude of the perturbation of EC_{50} induced by the hTyr mutation. As anticipated, the stick in the clam has a larger effect on full agonists, which require full closure, than on partial agonists. In fact, our results demonstrate that it is important to study full-length, functional ion channels especially when trying to determine the molecular-level interactions that govern overall conformational changes in the protein. Additionally, we have demonstrated that our method of studying the functional ion channel is much more sensitive to smaller structural changes that affect the glycine-binding NR1 subunit.

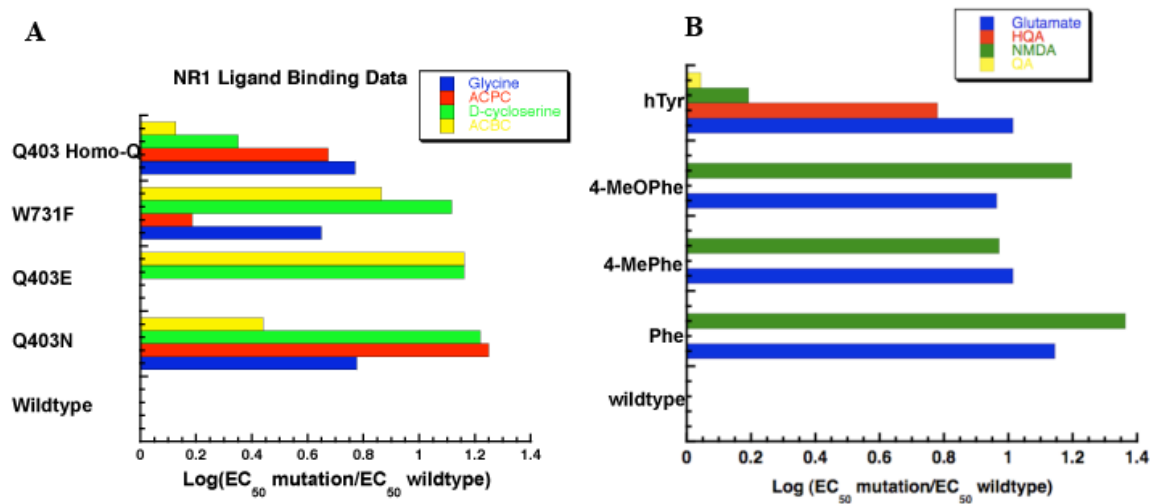


Figure 3.22 Shifts in EC_{50} for each mutant NR1a(A)/NR2B(B) receptor compared to wild type.

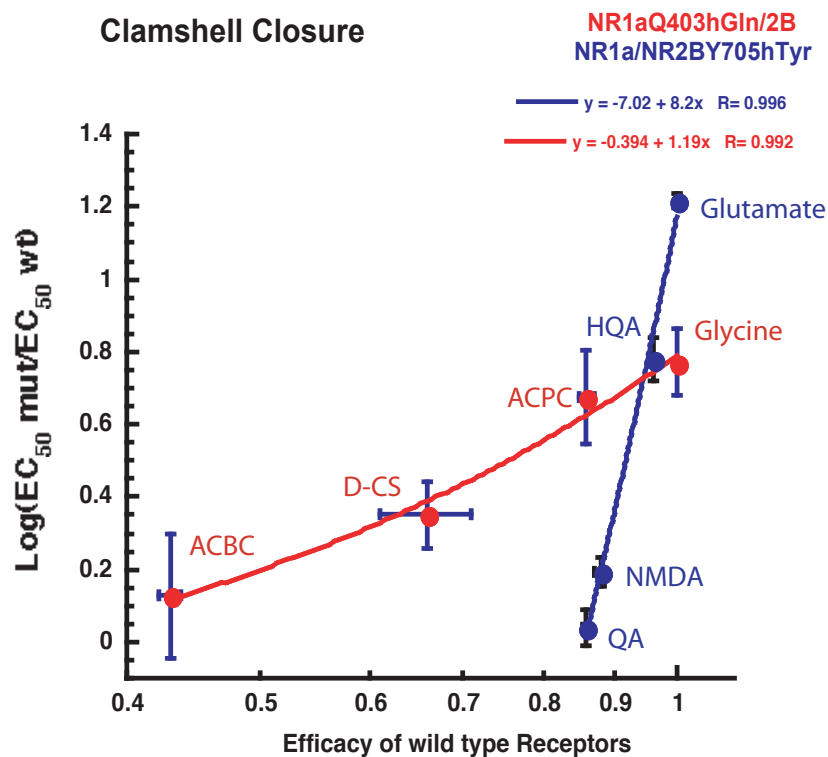


Figure 3.23 The functional probe of clamshell closure: The relationship between partial agonist efficacy for the wild type receptor and Log (EC_{50} responses mut/ EC_{50} responses WT) for NR1a/2BY705hTyr and NR1aQ403hGln/NR2B receptors. The relationship between relative efficacy and Log (EC_{50} ratios) demonstrates a measurable energetic relationship between clamshell closure and agonist efficacy. The steepness of the slope is related to the degree of clamshell closure.

3.2.6 GluR2 Structural Study Correlation

The experimental results obtained from the study of the NMDAR binding sites are supported by the available structural data on the homotetrameric GluR2 (AMPA) receptor. The GluR2 residues E402 and L704 are homologous to Q403 and Y705. Distances were measured between the α -carbons of these residues in GluR2 in structures that were 14.7Å unactivated (apo), 13.3Å partially activated (willardiine (HW) and 12.9Å 5-iodowillardiine (IW)), and 12.5Å fully activated (glutamate-bound) (Figure 3.24). From the apo to the glutamate bound structure, as the relative efficacy of the agonist increased, the distance between the α -carbons of E402 and L704 decreased (Figure 3.24). Additionally, the NR2A/glutamate and GluR2/glutamate structures were overlaid, and the

relevant C $_{\alpha}$ -C $_{\alpha}$ distances for the two glutamate-bound structures are very similar.

Therefore, we feel justified in relating our functional studies on the NMDA receptor to the structural studies of GluR2.

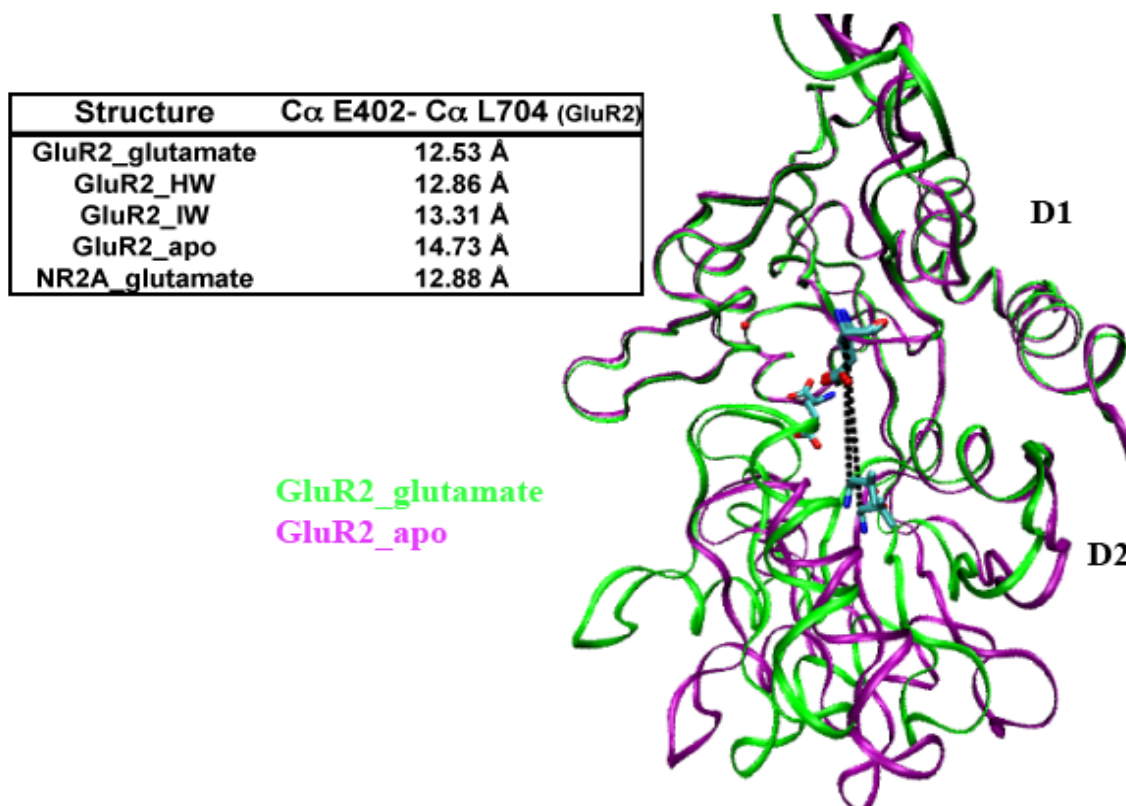


Figure 3.24 Distances between alpha carbons of E402 and L704 in various GluR2 structures (data from PDB files, 1FTJ, IMQJ, 1MQG, 1FTO, and 2A5S). E402 and L704 in GluR2 are homologous to NR2B E387 and Y705. Efficacy values from Jin, *et al.* (32).

3.2.7 Implications for the Functional Study of the Clamshell Mechanism of Agonist Action

The most compelling structural studies of clamshell closure have been performed in the homotetrameric AMPA and kainate receptors. It is not clear, however, the extent to which observations for one member of a large class of receptors will apply to all the members of the superfamily. In these studies, we sought an alternative way to evaluate the clamshell mechanism seen in select iGluRs with several specific aims. First, although

there is no denying the compelling images produced by structural biology, there is always value in having complementary functional studies on intact receptors in biologically relevant environments. Secondly, functional measurements allow for the study of a wider range of structures than lower throughput crystallographic approaches. This also allows us to address the third issue related to the risks of extrapolating mechanistic insights from one receptor to all the members of the family.

Conceptually, the approach is straightforward. We engineer into the hinge region of the clamshell a partial occlusion that will prevent full closure. A full agonist, that requires full closure for maximal activation, should be quite sensitive to such an effect. However, such a change should have a lesser impact on a partial agonist, which does not require full clamshell closure to reach its maximum in activation. The approach relies on the power of the nonsense suppression method for site-specifically incorporating unnatural amino acids into receptors and ion channels expressed in vertebrate cells. The subtlety and control that the method enables are essential to producing meaningful results.

The goal of the method was to produce a plot as in Figure 21. We would expect to see a clear correlation between GluR2 function and agonist efficacy, similar to that observed for both NMDA subunits. Here the x-axis is *identical* to that used in the structural studies, the innate efficacy of the agonist on the wild type receptor. But for the y-axis, instead of a structural measure – a distance – we employ a measure of receptor function. If the mechanistic model implied by the GluR2 structural studies is correct, the structural changes must be accompanied by a comparable functional change. The functional measure we use, EC_{50} , is a composite number that reflects both agonist binding and channel gating. The present analysis assumes that, for the sites considered here, mutations affect EC_{50} primarily through changes in gating behavior. Earlier mutagenesis studies (41) of these residues and their analogues in other receptors have reached just this conclusion.

Our strategy was to introduce homo-tyrosine, hTyr, at position 705. As illustrated in Figure 3.25, the added CH_2 of hTyr extends the chain and can significantly expand the effective size of the residue depending on the side chain geometry. The addition of a

methylene group may not appear to be that significant at first glance, however, depending on the adopted side chain geometry, a difference in several angstroms exists between the Tyr and hTyr (Figure 3.25). The difference that this methylene unit makes would be the “stick” that would block clamshell closure. It should be noted that all the functionality of the natural residue Tyr is present; it has just been repositioned. The unnatural amino acid hTyr was well-tolerated in the receptor (Figure 3.25), and it produced intriguing results. As shown in Tables 3.1 and 3.2, the effect on EC_{50} ranged from ~17-fold for glutamate to essentially no effect for the partial agonist quinolinic acid (QA). Introduction of a similar residue, homo-glutamine, at NR1Q403, produced a similar result, although the magnitude of the perturbation was attenuated compared to that of hTyr.

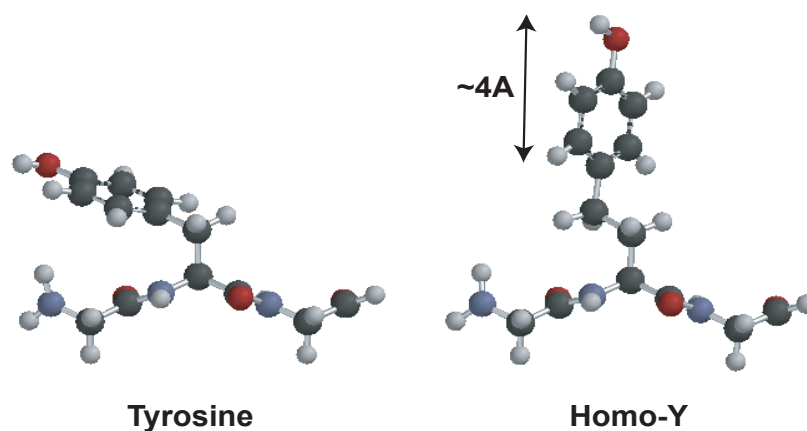


Figure 3.25 Side chain geometries of Tyr and hTyr minimized in GYG/GhTyrG peptides.

Our functional method has resulted in a new probe of the clamshell. By expanding the size of a specific amino acid side chain, while keeping all functionality the same, the importance of a clamshell-like domain closure can be probed. This “stick-in-the-clam” approach using the one-carbon homologue of the natural amino acid should be more consequential for full agonists – which require full clamshell closure – than for partial agonists, which require only partial closure. We find for the glutamate-binding NR2 domain of the NMDA receptor a very strong correlation between agonist efficacy and the impact of the homology experiment. A similar correlation was observed for

the glycine-binding NR1 domain, however, now the slope is *much* smaller, suggesting that clamshell closure of the NR1 subunit is less critical to receptor function than it is in the NR2 subunit. This, of course, agrees with structural studies, which found no effect in the NR1 subunit. The non-zero slope of Figure 3.23 suggests that perhaps there is a small but significant clamshell effect in NR1, but one that may be too subtle to be revealed in the crystal structures. These results are intriguing, particularly because they suggest that glycine-binding subunits use an attenuated version of the clamshell mechanism to induce structural changes correlating to ion channel activation. More importantly though, along with providing valuable insights into the function of the NMDA receptor, this work introduces a potentially generalizable strategy for probing structural changes associated with receptor activation.

3.3 AMPA Receptor Ligand-Binding Domain Studies

In order to test the generality of our new functional test of the clamshell mechanism in iGluRs, we decided to expand our repertoire of glutamate receptor studies to the homomeric GluR2 receptor. Our goal was to use the nonsense suppression methodology to incorporate the $-\text{CH}_2$ elongated amino acid residues that lie at the interdomain hinge region of the ligand binding site. Based on previous GluR2 structural studies, we hypothesized that we would obtain a similar trend as observed above in the NR2BY705 studies. Our studies will parallel those performed by Gouaux and co-workers with the partial agonist series of substituted willardiines.

We acquired the GluR2 construct containing the “flip” sequence. The flip/flop sequence is an alternatively spliced exon consisting of 38 amino acids just prior to the final transmembrane domain and is involved in determining receptor kinetics (47, 48). We also use a GluR2 construct containing the unedited glutamine at the Q/R site, which determines the Ca^{2+} permeability of the receptor. The Q-containing receptor is Ca^{2+} permeable. The GluR2 construct also contains the mutation L483Y (504 in the immature protein). This is a non-desensitizing mutation that is thought to stabilize the closed-cleft ligand binding domain (24, 49). Our construct is a non-desensitizing, Ca^{2+} permeable GluR2 subunit that forms homotetrameric ion channels.

3.3.1 Mutational Probe of the GluR2 Clamshell

We began our GluR2 investigations by testing the wild type receptor response to glutamate (Figure 3.26). For consistency, we decided to mutate the D1 and D2 amino acids that corresponded to those in our previous NR1 and NR2B studies (Figure 3.15). The corresponding GluR2 D1 amino acid is E402 (mature protein numbering) and the D2 amino acid is not a tyrosine, but L704. These two amino acids cannot interact via a hydrogen bond as in NR2B, but if our hypothesis is based on the size of the amino acid side chain and its ability to “put a stick in the clam,” then our method should work for the GluR2 receptor.

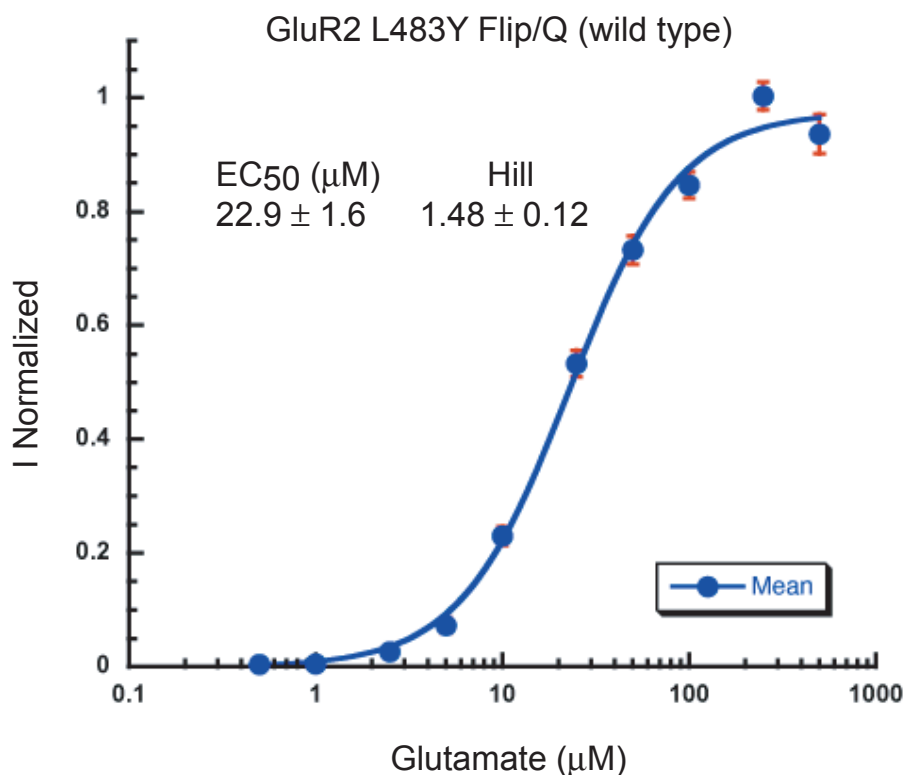


Figure 3.26 Dose-response relationship obtained for wild type GluR2 homomeric channels in response to glutamate.

The first mutations we introduced into GluR2 were at E402- Asp, Asn, homoglutamine (hGln), and nitrohomocysteine (Nha). hGln was incorporated into the

receptor instead of hGlu due to synthetic availability. We also made the L704A mutation, which we felt was appropriately different from Leu in that it is a sterically, much smaller amino acid, but still hydrophobic. One goal of this study was to determine the EC₅₀ and efficacy sensitivity of the full and partial agonists at these sites upon mutagenesis. We first recorded responses of all of the homomeric GluR2 receptors to glutamate (Table 3.5).

Table 3.5 EC₅₀ values and Hill coefficients for homomeric GluR2 AMPA receptors (n= number of oocytes).

Receptor	Glutamate EC ₅₀ ± S.E.M.	Glutamate Hill	Glutamate n
wildtype GluR2 (L483Y)	22.3 ± 1.16	1.4 ± .08	11
E402D	20.9 ± 1.81	1.62 ± 0.18	5
E402N	246 ± 21	1.9 ± 0.21	9
E402TAG hGln	2020 ± 1060	0.90 ± 0.18	20
E402TAG Nha	>3000 ± 1060	0.58 ± 0.16	8
L704A	5.47 ± 0.31	1.91 ± 0.19	13

Not surprisingly, the conservative mutation from Glu to Asp at GluR2402 resulted in no shift in EC₅₀ value; however, the mutation to Asn resulted in a ~20-fold shift in EC₅₀ (Table 3.5). Clearly, the negatively charged side chain at position 402 is required for proper interaction with the agonist. We also incorporated the unnatural amino acids homoglutamine (hGln) and nitrohomalanine (Nha), which expanded the Gln side chain by one methylene group (in the case of hGln) and neutralized the charge on the side chain of Glu with an isosteric nitro group (in the case of Nha). Both of these mutations drastically shifted EC₅₀ by ~100-fold, indicating glutamate is very sensitive to the charge and the size of the amino acid at this position of the GluR2 binding site. Previous studies have also indicated that mutation of E402 results in shifts in EC₅₀ values and glutamate affinity (26, 50-53). These studies suggest that E402 is involved in an inter-domain hydrogen bond with Thr686. The stability of clamshell closure around the agonist is directly correlated with the affinity of the agonist. We also made the conventional mutation L402A, which maintains the hydrophobicity of the side chain, but reduces the size. A little surprisingly, this mutation appears to increase agonist affinity and reduces

EC₅₀ by ~3.5-fold. It is possible that the smaller side chain, L402A, allows glutamate to fit into the binding site and make more favorable interactions with the receptor.

In order to study the effects of these mutations on partial agonism, we decided to use the willardiine series of partial agonists that were used in the structural studies of GluR2 (Figure 3.9). In addition to the structural work, studies of willardiine action at the GluR2 subunit have been examined using FRET (fluorescence resonance energy transfer) analysis (54). The FRET studies determined that the interactions between the LBD and the α -amine group of the agonist contributed to clamshell closure, however this is probably not the only contributing factor. According to the previous GluR2 ligand binding domain studies, the order of partial agonism affinity for the willardiines is: HW~FW>CIW>IW, with HW, FW, CIW, and IW producing 62%, 60%, 53%, and 24% of the currents produced by glutamate, respectively. Overall, this trend follows that as the size of the 5-substituent increases, ion channel activation decreases (33, 54).

Table 3.6 EC₅₀ values and efficacy measurements for the willardiines in GluR2 receptors.

Efficacy measurements are always compared to the full agonist, glutamate. (SEM = standard error measurement)

Receptor	5-FW EC₅₀ ± SEM	5-FW Hill	5-FW n	5-FW Efficacy ± SEM
wildtype GluR2 (L483Y)	0.44 ± 0.031	1.79 ± 0.20	14	0.984 ± 0.028
E402D	0.97 ± .112	1.34 ± 0.154	7	0.943 ± 0.047
E402N	1.32 ± 0.024	1.75 ± 0.04	7	0.998 ± 0.013
E402TAG hGlu	0.15 ± 0.016	1.43 ± 0.17	1	
L704A	0.098 ± 0.005	1.74 ± 0.13	12	0.913 ± 0.0093
Receptor	(S)-HW EC₅₀ ± SEM	(S)-HW Hill	(S)-HW n	(S)-HW Efficacy ± SEM
wildtype GluR2 (L483Y)	15.80 ± 0.33	1.94 ± 0.06	13	0.936 ± 0.014
E402D	57.9 ± 10.7	1.25 ± 0.17	11	0.922 ± 0.073
E402N	No Current	No Current	8	0.0 ± 0.016
L704A	8.24 ± 0.355	1.44 ± 0.0753	12	0.936 ± 0.012
Receptor	5-CW EC₅₀ ± SEM	5-CW Hill	5-CW n	5-CW Efficacy ± SEM
wildtype GluR2 (L483Y)	1.323 ± 0.053	1.321 ± 0.056	13	0.617 ± 0.010
E402D	5.864 ± 1.171	0.873 ± 0.111	7	0.716 ± 0.020
E402N	76.89 ± 8.60	1.521 ± 0.151	5	0.501 ± 0.016
L704A	1.018 ± 0.13	1.141 ± 0.139	6	1.365 ± 0.126
Receptor	5-IW EC₅₀ ± SEM	5-IW Hill	5-IW n	5-IW Efficacy ± SEM
wildtype GluR2 (L483Y)	4.11 ± 0.28	1.63 ± 0.15	16	0.34 ± 0.005
E402D	13.64 ± 1.08	1.55 ± 0.11	11	0.46 ± 0.008
E402N	115.6 ± 80.0	1.30 ± 0.143	8	0.097 ± 0.010
L704A	4.51 ± 0.29	1.37 ± 0.09	8	0.57 ± 0.012

Our results are summarized in Table 6, and demonstrate a similar trend for the willardiine series, with 5-HW~5-FW > 5-CIW > 5-IW at wild type GluR2 receptors. The mutations at E402 do not drastically shift efficacy for any of the willardiines, however several of the EC₅₀ values do shift. The E402N mutation results in ~70-fold shift in EC₅₀ for 5-CIW, yet efficacy only decreases slightly (Table 3.6). Our results indicate that these conventional mutations are implicated in the affinity of ligand binding to GluR2 more than they are implicated in ion channel activation. Alternatively, since relative efficacy is measured for each partial agonist against glutamate, and the conformation of

the closed cleft conformation depends on the mutation and not the agonist, the effects on agonist affinity would be evident by EC_{50} , but the relative efficacy would not change because it reflects the effect that the mutation has on both glutamate and the partial agonist.

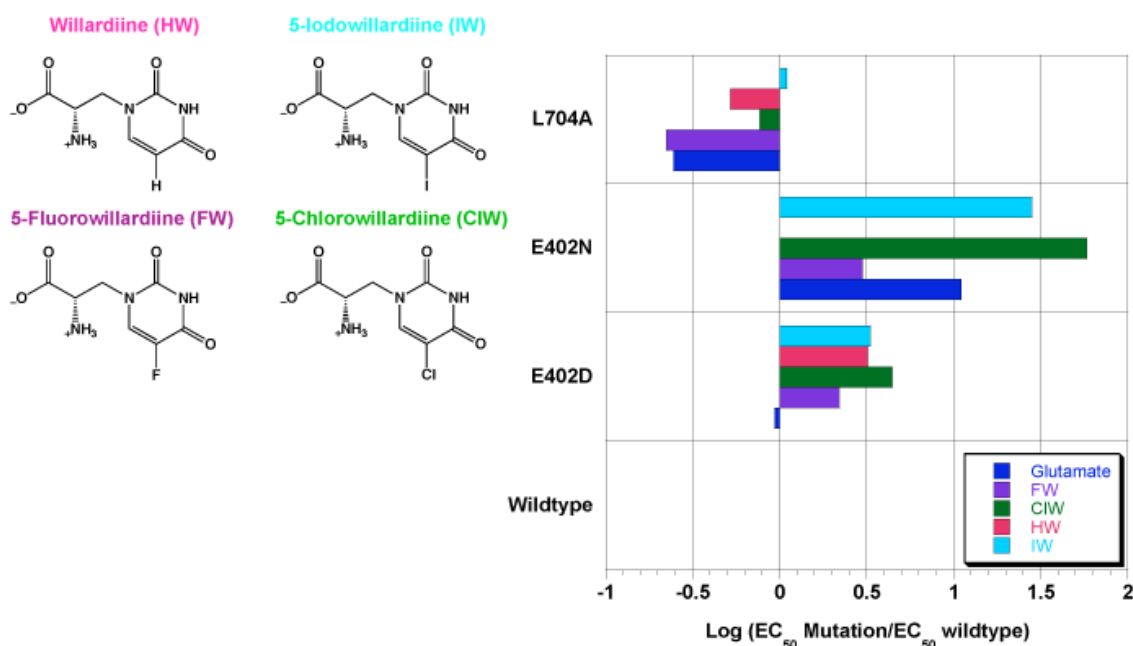


Figure 3.27 Shifts in EC_{50} values for mutations in the GluR2 ligand binding domain with the willardiine partial agonists.

Overall, our first studies of the GluR2 binding site are intriguing in that all of the partial agonists, except for 5-IW, respond more favorably to the L704A mutation (Figure 3.27). This is likely due to the positioning of the 5-substituent on the willardiines, which the alanine mutation can accommodate more easily than the leucine side chain. There is precedent for this type of accommodation where previous structural evidence has demonstrated that a GluR2 methionine side chain, M708, swings out of the binding cleft to prevent a steric clash with 5-IW (32). Additionally, our results demonstrate larger EC_{50} increases for the asparagine mutation versus the aspartate mutation; so clearly, maintaining the charge at E402 is necessary for optimal agonist binding.

Our initial studies incorporating the unnatural amino acids, hGln and Nha, at GluR2 E402, resulted in significant EC₅₀ shifts for glutamate (Table 3.5) of approximately 100-fold. These measurements become difficult to accurately determine since we have to use very large concentrations of glutamate in order to get full receptor activation. Further studies by a new lab member, Maggie Thompson, using the willardiine partial agonists in combination with hGln and hGlu will determine if our model for the clamshell mechanism of iGluR activation is upheld in the GluR2 receptor.

3.3.2 Studies of Ligand Binding Domain Hinge Residues Involved in Receptor Activation

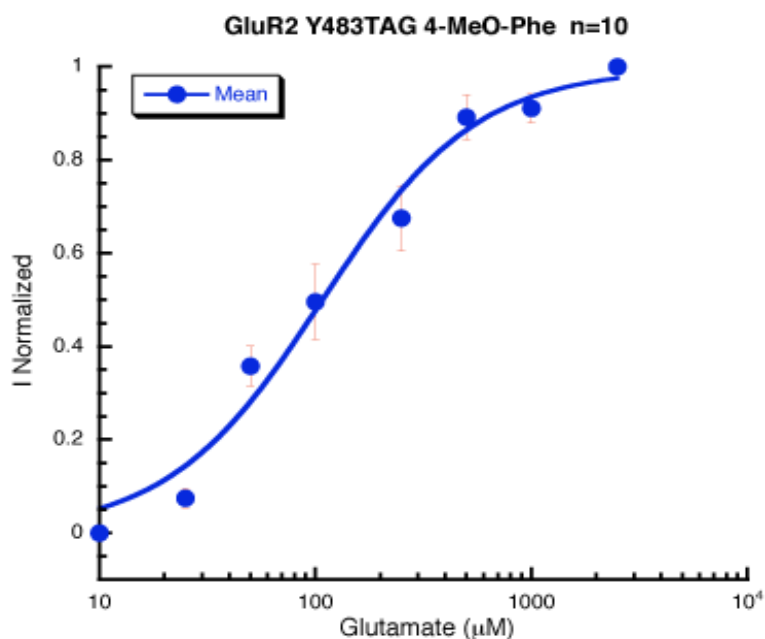
Studies of the stability of the ligand binding domain dimer, measured by equilibrium centrifugation, correlate with the degree of desensitization of the ion channel (55). As the stability of the ligand-binding domain dimer increases, the amount of receptor desensitization decreases. These observations have led to the proposal that a rearrangement of the dimer conformation is required for desensitization to occur (55). Further mutational analysis found the non-desensitizing mutation, GluR2L483Y, an interfacial residue thought to stabilize the dimer through a potential cation- π interaction. Corresponding mutations have also been identified in the GluR3 and GluR6 subunits as well (56, 57).

In GluR2, the suggested binding partners for the L483Y mutation are L748 and K752. In GluR2, L/Y483 interacts with K752 across the dimer interface. This is the non-desensitizing mutation that we use for our wild type GluR2 receptor. However, we thought that by using the nonsense suppression methodology, we could subtly probe the residues at the dimer-dimer interface to determine the chemical-scale interactions that contribute to dimer stability. We began by studying L/Y483 and incorporating a series of unnatural amino acids that would probe the nature of the proposed electrostatic and or hydrophobic interaction at this site. We incorporated Phe (both with conventional mutagenesis and nonsense suppression), 4-Me-Phe, 4-MeO-Phe, and Cha. We expected that both the kinetics and potency of the agonist could be altered by the mutations.

Table 3.7 EC₅₀ values for mutations at GluR2L/Y483 (S.E.M.= standard error measurements).

Receptor	Glutamate EC ₅₀ $\mu\text{M} \pm \text{SEM}$	Glutamate Hill	Glutamate N
wildtype GluR2 (L483Y)	22.3 \pm 1.16	1.4 \pm .08	11
Y483F	47.6 \pm 5.6	1.2 \pm .19	14
Y483TAG Phe-THG73	60.4 \pm 6.2	1.4 \pm 0.19	12
Y483 4-Me-Phe	33.5 \pm 5.4	1.8 \pm .48	10
Y483 4-MeO-Phe	107 \pm 21	1.2 \pm .23	10
Y483 Cha	>2500		5

Our initial studies show an ~2-fold shift when Phe is incorporated at this site. Interestingly, eliminating the 4-position hydroxyl group doesn't drastically alter EC₅₀. Additionally, replacing the hydroxyl group with a methyl (4-Me-Phe) produces results similar to the wild type receptor and adding the methoxy group (4-MeO-Phe) increases EC₅₀ ~5-fold. The largest shift in EC₅₀ value was observed for the Cha mutation, which results in an almost non-functional receptor (Table 3.7).

**Figure 3.28** Dose-response curve for glutamate at the GluR2 Y483 4-MeO-Phe mutant.

Based on our first observations with unnatural amino acid mutagenesis at the L/Y483 site and using previous knowledge that this site possibly interacts with the hydrophobic L748 and the positively charged K752, we can infer that there are hydrophobic and or electrostatic interactions at the dimer-dimer interface. If a cation- π interaction were involved between Y783 and K752, we would expect to see the largest shift with the Cha mutation. In fact, we see the expected outcome, where mutation to a side chain with similar sterics to Phe but no aromatic component, results in an ~100-fold shift in EC_{50} . In addition, the shift in EC_{50} obtained with the 4-MeO-Phe analog is somewhat expected since the oxygen would draw electron density out of the aromatic ring, reducing its cation- π binding ability with the positively charged lysine (Table 3.7).

Although these results are preliminary, they are suggestive of the power of the unnatural amino acid mutagenesis to determine the chemical-scale interactions involved in regulating the function of iGluRs. We have established a method for unnatural amino acid incorporation into several iGluR receptors and further work in the group by Maggie Thompson will continue to evaluate the ligand-binding domain of GluR2 AMPARs.

3.4 Conclusions and Future Work

We have demonstrated that we are able to incorporate unnatural amino acids into both the NMDA and AMPA families of iGluRs. We have also introduced a new probe of receptor function that utilizes unnatural amino acid mutagenesis. We expanded the side chains of NR2BY705 and NR1aE403 and demonstrated that clamshell-like domain closure around an agonist is more important for full agonists and less so for partial agonists, which required only partial domain closure. We find for the glutamate-binding NR2 domain of the NMDA receptor a very strong correlation between agonist efficacy and the impact of the homologation experiment. This provides a *functional* evaluation of the clamshell mechanism. Interestingly, the analogous experiment performed on the glycine-binding NR1 domain shows a much weaker correlation. These results are consistent with current structural studies and demonstrate a more precise probe of partial agonist action, particularly with the NR1 subunit. Along with providing valuable insights into the

function of the NMDA receptor, this work introduces a potentially generalizable strategy for probing structural changes associated with receptor activation.

In addition, we have begun studies in the AMPA-binding GluR2 receptor. Our initial characterization of interactions in the LBD demonstrates the importance of several residues, i.e., E402 and L704, in determining ligand affinity for the receptor.

Additionally, we have evaluated a Tyr mutant (Y483), which lies at the dimer-dimer interface within the ligand binding domain of GluR2 and alters ion channel kinetics resulting in a non-desensitizing receptor. Our initial experiments at this site indicate a potential cation- π interaction with a positively charged arginine in the complementary ligand binding domain, K752. These experiments suggest that a cation- π interaction introduces enough stability at the LBD dimer interface to stabilize the open channel conformational state of the receptor, preventing a shift to a desensitized state. Continued studies by other lab members will confirm the interactions at the dimer interface. In addition, future studies could examine similar interactions in related iGluRs, such as GluR6 that is a KA receptor, which also contains a homologous non-desensitizing Tyr mutation (56, 57). Our studies demonstrate the importance of studying these interactions on the chemical-scale with a precise probe, unnatural amino acids, in combination with functional electrophysiology analysis. We are able to expand our repertoire of investigations to a new family of ion channels, with the potential for many further investigations.

3.5 Methods

3.5.1 Electrophysiology

Stage V-VI *Xenopus laevis* oocytes were injected with 50nL/cell of mRNA/tRNA mixtures. NMDAR subunits are cloned into the pAMV vector as described previously, and the GluR2 subunit was obtained from Dr. Yael Stern-Bach in the pGEMHE expression vector. Oocytes with NMDARs injected were evaluated in a Mg^{2+} and Ca^{2+} free saline solution (96 mM NaCl, 5 mM HEPES, 2 mM KCl, and 1 mM $BaCl_2$). The receptors were activated in a Mg^{2+} and Ca^{2+} free solution containing 10 μ M glycine (Aldrich) or 100 μ M glutamate (Aldrich) and 100 mM niflumic acid (to reduce activity of

Ca²⁺ activated Cl⁻ channels, Sigma) depending on the mutations being studied. For oocytes containing AMPARs, we utilized a standard Ca²⁺ free saline solution (96 mM NaCl, 5 mM HEPES, 2 mM KCl, and 1 mM MgCl₂). All oocyte recordings were made 48 hours after initial injection in two-electrode voltage clamp mode using the OpusXpress 6000A (Molecular Devices). Solutions were perfused at flow rates of 1 and 4 mL/min during agonist application and 3 mL/min during wash. Data were sampled at 125 Hz and filtered at 50 Hz. Eight oocytes were simultaneously voltage clamped at -60 mV, and dose-response relationships were obtained by delivery of increasing concentrations of L-glutamate, NMDA, homoquinolinic acid, or quinolinic acid in 1 mL aliquots for 15s for the NR2B mutations. Increasing concentrations of glycine, ACPC (Sigma), ACBC (Sigma), and D-cycloserine (Sigma) in 1 mL aliquots for 15s were applied to the NR1 mutations. Increasing concentrations of 5-HW, 5-FW, 5-CIW, and 5-IW were applied to the GluR2 mutations. (*S*)-5-Fluorowillardiine (FW), (*S*)-5-Chlorowillardiine (CIW), and (*S*)-Willardiine (HW) were obtained from Ascent Scientific (Somerset, England, United Kingdom), and (*S*)-5-Iodowillardiine (IW) was obtained from Tocris Bioscience (Ellisville, MO). All agonists were prepared in sterile ddi water and diluted in Mg²⁺, Ca²⁺ free saline solutions (Ca²⁺ free solutions for GluR2). Additionally, all of the drug solutions were maintained at a pH of 7.5. L-glutamate, glycine, NFA, quinolinic acid, and NMDA were all purchased from Sigma Aldrich RBI. Homoquinolinic acid was purchased from Tocris. The data were analyzed using Clampfit 9.0 software (Axon Instruments).

The Hill equation was used to fit data: $I = I_{\max} / (1 + (EC_{50} / [A])^{n_H})$, where *I* is peak current at drug concentration (*A*), EC₅₀ is the concentration of drug that evokes 50% of the maximal response, and *n_H* is the Hill coefficient. Efficacy values were measured for all agonists relative to the maximal glutamate currents evoked on the same cell. Standard error was calculated for both EC₅₀ and relative efficacy values.

3.5.2 Mutagenesis and preparation of cRNA and Unnatural Amino Acid Suppression

Mutant NR2B and NR1 constructs were made following the QuickChange mutagenesis protocol (Stratagene). All mutant and wild type cDNAs were linearized with *NotI*, and

mRNA was synthesized by in vitro runoff transcription using the T7 mMESSAGE mMACHINE kit (Ambion). All NR2B mutant mRNA was injected with wild type NR1a mRNA in a NR1a:NR2B (1:5) ratio. All NR1 mutant mRNA was injected with wild type NR2B mRNA in a NR1a:NR2B (5:2) ratio. Wild type receptors were injected in a NR1a:NR2B (1:1) ratio. Synthetic amino acids were ligated to truncated 74 nt tRNA as described previously (58). As a negative control for suppression, dCA was ligated to tRNA and co-injected with mRNA. No currents were observed in these experiments. The aminoacyl tRNA was deprotected by photolysis immediately prior to co-injection with mRNA (58, 59). Typically, 5 ng mRNA and 25 ng tRNA-aa were injected into oocytes in a total volume of 50 nL.

3.5.3 Immunolocalization of Wild type and Mutant NMDA Receptors

These experiments were performed by adapting previously reported procedures. *Xenopus laevis* oocytes were injected as reported above. Cells were incubated at 16°C for 2 days. The primary antibody, anti-NMDAR2B (Invitrogen; 0.5 mg/mL dilution in phosphate-buffered saline) was used with the Zenon Rabbit IgG Labeling Kit (Molecular Probes) as per labeling instructions. The cells were incubated with primary antibody for 1 h at room temperature. Cells were washed (3x) with phosphate-buffered saline and stored in Mg^{2+} , Ca^{2+} free saline. Oocytes were placed into a hypertonic solution (96 mM NaCl, 5 mM HEPES, 2 mM KCl, 1 mM $MgCl_2$, 1.8 mM $CaCl_2$, and 200 mM Sucrose) for 10 min and the vitelline membrane was removed with fine tweezers. Alexa-Fluor 488 labeled receptors on the oocyte membrane were analyzed using TIRF microscopy.

3.6 Cited References

1. Dingledine, R., Borges, K., Bowie, D., and Traynelis, S. F. (1999) The glutamate receptor ion channels, *Pharmacol Rev* 51, 7-61.
2. Cull-Candy, S., Brickley, S., and Farrant, M. (2001) NMDA receptor subunits: diversity, development and disease, *Curr Opin Neurobiol* 11, 327-335.
3. Coyle, J. T., Tsai, G., and Goff, D. C. (2002) Ionotropic glutamate receptors as therapeutic targets in schizophrenia, *Curr Drug Targets CNS Neurol Disord* 1, 183-189.
4. Nakazawa, K., Quirk, M. C., Chitwood, R. A., Watanabe, M., Yeckel, M. F., Sun, L. D., Kato, A., Carr, C. A., Johnston, D., Wilson, M. A., and Tonegawa, S. (2002) Requirement for hippocampal CA3 NMDA receptors in associative memory recall, *Science* 297, 211-218.
5. Tsai, G., and Coyle, J. T. (2002) Glutamatergic mechanisms in schizophrenia, *Annu Rev Pharmacol Toxicol* 42, 165-179.
6. Armstrong, N., Sun, Y., Chen, G. Q., and Gouaux, E. (1998) Structure of a glutamate-receptor ligand-binding core in complex with kainate, *Nature* 395, 913-917.
7. Bennett, J. A., and Dingledine, R. (1995) Topology profile for a glutamate receptor: three transmembrane domains and a channel-lining reentrant membrane loop, *Neuron* 14, 373-384.
8. Hollmann, M., Maron, C., and Heinemann, S. (1994) N-glycosylation site tagging suggests a three transmembrane domain topology for the glutamate receptor GluR1, *Neuron* 13, 1331-1343.
9. Wo, Z. G., and Oswald, R. E. (1994) Transmembrane topology of two kainate receptor subunits revealed by N-glycosylation, *Proc Natl Acad Sci U S A* 91, 7154-7158.
10. Wo, Z. G., and Oswald, R. E. (1995) A topological analysis of goldfish kainate receptors predicts three transmembrane segments, *J Biol Chem* 270, 2000-2009.
11. O'Hara, P. J., Sheppard, P. O., Thogersen, H., Venezia, D., Haldeman, B. A., McGrane, V., Houamed, K. M., Thomsen, C., Gilbert, T. L., and Mulvihill, E. R. (1993) The ligand-binding domain in metabotropic glutamate receptors is related to bacterial periplasmic binding proteins, *Neuron* 11, 41-52.
12. Quirocho, F. A., and Ledvina, P. S. (1996) Atomic structure and specificity of bacterial periplasmic receptors for active transport and chemotaxis: variation of common themes, *Mol Microbiol* 20, 17-25.
13. Stern-Bach, Y., Bettler, B., Hartley, M., Sheppard, P. O., O'Hara, P. J., and Heinemann, S. F. (1994) Agonist selectivity of glutamate receptors is specified by two domains structurally related to bacterial amino acid-binding proteins, *Neuron* 13, 1345-1357.
14. Mayer, M. L., and Armstrong, N. (2004) Structure and function of glutamate receptor ion channels, *Annu Rev Physiol* 66, 161-181.
15. Kuusinen, A., Arvola, M., and Keinänen, K. (1995) Molecular dissection of the agonist binding site of an AMPA receptor, *Embo J* 14, 6327-6332.
16. Chen, G. Q., and Gouaux, E. (1997) Overexpression of a glutamate receptor (GluR2) ligand binding domain in Escherichia coli: application of a novel protein folding screen, *Proc Natl Acad Sci U S A* 94, 13431-13436.

17. Chen, G. Q., Sun, Y., Jin, R., and Gouaux, E. (1998) Probing the ligand binding domain of the GluR2 receptor by proteolysis and deletion mutagenesis defines domain boundaries and yields a crystallizable construct, *Protein Sci* 7, 2623-2630.
18. Furukawa, H., and Gouaux, E. (2003) Mechanisms of activation, inhibition and specificity: crystal structures of the NMDA receptor NR1 ligand-binding core, *Embo J* 22, 2873-2885.
19. Furukawa, H., Singh, S. K., Mancusso, R., and Gouaux, E. (2005) Subunit arrangement and function in NMDA receptors, *Nature* 438, 185-192.
20. Mayer, M. L. (2005) Crystal structures of the GluR5 and GluR6 ligand binding cores: molecular mechanisms underlying kainate receptor selectivity, *Neuron* 45, 539-552.
21. Mayer, M. L., Olson, R., and Gouaux, E. (2001) Mechanisms for ligand binding to GluR0 ion channels: crystal structures of the glutamate and serine complexes and a closed apo state, *J Mol Biol* 311, 815-836.
22. Armstrong, N., and Gouaux, E. (2000) Mechanisms for activation and antagonism of an AMPA-sensitive glutamate receptor: crystal structures of the GluR2 ligand binding core, *Neuron* 28, 165-181.
23. McFeeters, R. L., and Oswald, R. E. (2002) Structural mobility of the extracellular ligand-binding core of an ionotropic glutamate receptor. Analysis of NMR relaxation dynamics, *Biochemistry* 41, 10472-10481.
24. Sun, Y. J., Rose, J., Wang, B. C., and Hsiao, C. D. (1998) The structure of glutamine-binding protein complexed with glutamine at 1.94 Å resolution: comparisons with other amino acid binding proteins, *J Mol Biol* 278, 219-229.
25. Armstrong, N., Mayer, M., and Gouaux, E. (2003) Tuning activation of the AMPA-sensitive GluR2 ion channel by genetic adjustment of agonist-induced conformational changes, *Proc Natl Acad Sci U S A* 100, 5736-5741.
26. Abele, R., Keinänen, K., and Madden, D. R. (2000) Agonist-induced isomerization in a glutamate receptor ligand-binding domain. A kinetic and mutagenetic analysis, *J Biol Chem* 275, 21355-21363.
27. Wyllie, D. J., and Chen, P. E. (2007) Taking the time to study competitive antagonism, *Br J Pharmacol* 150, 541-551.
28. Hogner, A., Kastrup, J. S., Jin, R., Liljefors, T., Mayer, M. L., Egebjerg, J., Larsen, I. K., and Gouaux, E. (2002) Structural basis for AMPA receptor activation and ligand selectivity: crystal structures of five agonist complexes with the GluR2 ligand-binding core, *J Mol Biol* 322, 93-109.
29. Del Castillo, J., and Katz, B. (1957) Interaction at end-plate receptors between different choline derivatives, *Proc R Soc Lond B Biol Sci* 146, 369-381.
30. Monod, J., Wyman, J., and Changeux, J. P. (1965) On The Nature Of Allosteric Transitions: A Plausible Model, *J Mol Biol* 12, 88-118.
31. Li, J., Zagotta, W. N., and Lester, H. A. (1997) Cyclic nucleotide-gated channels: structural basis of ligand efficacy and allosteric modulation, *Q Rev Biophys* 30, 177-193.
32. Jin, R., Banke, T. G., Mayer, M. L., Traynelis, S. F., and Gouaux, E. (2003) Structural basis for partial agonist action at ionotropic glutamate receptors, *Nat Neurosci* 6, 803-810.

33. Jin, R., Horning, M., Mayer, M. L., and Gouaux, E. (2002) Mechanism of activation and selectivity in a ligand-gated ion channel: structural and functional studies of GluR2 and quisqualate, *Biochemistry* 41, 15635-15643.
34. Chen, P. E., and Wyllie, D. J. (2006) Pharmacological insights obtained from structure-function studies of ionotropic glutamate receptors, *Br J Pharmacol* 147, 839-853.
35. Laurie, D. J., and Seeburg, P. H. (1994) Ligand affinities at recombinant N-methyl-D-aspartate receptors depend on subunit composition, *Eur J Pharmacol* 268, 335-345.
36. Monyer, H., Burnashev, N., Laurie, D. J., Sakmann, B., and Seeburg, P. H. (1994) Developmental and regional expression in the rat brain and functional properties of four NMDA receptors, *Neuron* 12, 529-540.
37. Mayer, M. L. (2006) Glutamate receptors at atomic resolution, *Nature* 440, 456-462.
38. Jin, R., and Gouaux, E. (2003) Probing the function, conformational plasticity, and dimer-dimer contacts of the GluR2 ligand-binding core: studies of 5-substituted willardiines and GluR2 S1S2 in the crystal, *Biochemistry* 42, 5201-5213.
39. Inanobe, A., Furukawa, H., and Gouaux, E. (2005) Mechanism of partial agonist action at the NR1 subunit of NMDA receptors, *Neuron* 47, 71-84.
40. Madden, D. R., Cheng, Q., Thiran, S., Rajan, S., Rigo, F., Keinänen, K., Reinelt, S., Zimmermann, H., and Jayaraman, V. (2004) Stereochemistry of glutamate receptor agonist efficacy: engineering a dual-specificity AMPA/kainate receptor, *Biochemistry* 43, 15838-15844.
41. Laube, B., Hirai, H., Sturgess, M., Betz, H., and Kuhse, J. (1997) Molecular determinants of agonist discrimination by NMDA receptor subunits: analysis of the glutamate binding site on the NR2B subunit, *Neuron* 18, 493-503.
42. Laube, B., Schemm, R., and Betz, H. (2004) Molecular determinants of ligand discrimination in the glutamate-binding pocket of the NMDA receptor, *Neuropharmacology* 47, 994-1007.
43. Cashin, A. L., Torrice, M. M., McMenimen, K. A., Lester, H. A., and Dougherty, D. A. (2007) Chemical-scale studies on the role of a conserved aspartate in preorganizing the agonist binding site of the nicotinic acetylcholine receptor, *Biochemistry* 46, 630-639.
44. Chen, P. E., Geballe, M. T., Stansfeld, P. J., Johnston, A. R., Yuan, H., Jacob, A. L., Snyder, J. P., Traynelis, S. F., and Wyllie, D. J. (2005) Structural features of the glutamate binding site in recombinant NR1/NR2A N-methyl-D-aspartate receptors determined by site-directed mutagenesis and molecular modeling, *Mol Pharmacol* 67, 1470-1484.
45. Sun, A., Lankin, D. C., Hardcastle, K., and Snyder, J. P. (2005) 3-Fluoropiperidines and N-methyl-3-fluoropiperidinium salts: the persistence of axial fluorine, *Chemistry* 11, 1579-1591.
46. Monyer, H., Sprengel, R., Schoepfer, R., Herb, A., Higuchi, M., Lomeli, H., Burnashev, N., Sakmann, B., and Seeburg, P. H. (1992) Heteromeric NMDA receptors: molecular and functional distinction of subtypes, *Science* 256, 1217-1221.

47. Lomeli, H., Mosbacher, J., Melcher, T., Hoyer, T., Geiger, J. R., Kuner, T., Monyer, H., Higuchi, M., Bach, A., and Seeburg, P. H. (1994) Control of kinetic properties of AMPA receptor channels by nuclear RNA editing, *Science* 266, 1709-1713.
48. Mosbacher, J., Schoepfer, R., Monyer, H., Burnashev, N., Seeburg, P. H., and Ruppersberg, J. P. (1994) A molecular determinant for submillisecond desensitization in glutamate receptors, *Science* 266, 1059-1062.
49. Hansen, K. B., Yuan, H., and Traynelis, S. F. (2007) Structural aspects of AMPA receptor activation, desensitization and deactivation, *Curr Opin Neurobiol* 17, 281-288.
50. Uchino, S., Sakimura, K., Nagahara, K., and Mishina, M. (1992) Mutations in a putative agonist binding region of the AMPA-selective glutamate receptor channel, *FEBS Lett* 308, 253-257.
51. Lampinen, M., Pentikainen, O., Johnson, M. S., and Keinänen, K. (1998) AMPA receptors and bacterial periplasmic amino acid-binding proteins share the ionic mechanism of ligand recognition, *Embo J* 17, 4704-4711.
52. Mano, I., Lamed, Y., and Teichberg, V. I. (1996) A venus flytrap mechanism for activation and desensitization of alpha-amino-3-hydroxy-5-methyl-4-isoxazole propionic acid receptors, *J Biol Chem* 271, 15299-15302.
53. Robert, A., Armstrong, N., Gouaux, J. E., and Howe, J. R. (2005) AMPA receptor binding cleft mutations that alter affinity, efficacy, and recovery from desensitization, *J Neurosci* 25, 3752-3762.
54. Mankiewicz, K. A., Rambhadrar, A., Wathen, L., and Jayaraman, V. (2008) Chemical interplay in the mechanism of partial agonist activation in alpha-amino-3-hydroxy-5-methyl-4-isoxazolepropionic acid receptors, *Biochemistry* 47, 398-404.
55. Sun, Y., Olson, R., Horning, M., Armstrong, N., Mayer, M., and Gouaux, E. (2002) Mechanism of glutamate receptor desensitization, *Nature* 417, 245-253.
56. Nanao, M. H., Green, T., Stern-Bach, Y., Heinemann, S. F., and Choe, S. (2005) Structure of the kainate receptor subunit GluR6 agonist-binding domain complexed with domoic acid, *Proc Natl Acad Sci U S A* 102, 1708-1713.
57. Stern-Bach, Y., Russo, S., Neuman, M., and Rosenmund, C. (1998) A point mutation in the glutamate binding site blocks desensitization of AMPA receptors, *Neuron* 21, 907-918.
58. Nowak, M. W., Gallivan, J. P., Silverman, S. K., Labarca, C. G., Dougherty, D. A., and Lester, H. A. (1998) In vivo incorporation of unnatural amino acids into ion channels in *Xenopus* oocyte expression system, *Methods Enzymol* 293, 504-529.
59. Li, L., Zhong, W., Zacharias, N., Gibbs, C., Lester, H. A., and Dougherty, D. A. (2001) The tethered agonist approach to mapping ion channel proteins--toward a structural model for the agonist binding site of the nicotinic acetylcholine receptor, *Chem Biol* 8, 47-58.

Chapter 4: Studies of the Binding Site of the Mouse Muscle Nicotinic Acetylcholine Receptor[†]

4.1. Introduction

This chapter describes initial studies of the prototypical nicotinic acetylcholine receptor (nAChR), the mouse muscle nAChR. These studies were performed several years ago, and since then many advances and experiments have obtained a much more thorough understanding of the structure and function of the nAChR. A current description of these receptors is outlined along with the reasoning behind our studies of this receptor. Additionally, we incorporated computational models of the nAChR to enhance our understanding of the functional studies we performed on the receptor. In addition, background information regarding previous computational models of the receptor will be provided. There will be a discussion of how these contribute to our understanding of these ligand-gated ion channels.

4.1.1. *The Nicotinic Acetylcholine Receptor*

The nAChR is a ligand-gated ion channel in the Cys-loop family of ion channels. The Cys-loop family also encompasses the serotonin receptors, glycine, and γ -aminobutyric acid (GABA) receptors (1-4). The nAChR is the prototypical Cys-loop receptor, and it is active in both the central nervous system and at the neuromuscular junction. This receptor is the target of acetylcholine, but also responds to nicotine (Nic) and many pharmaceuticals aimed at memory enhancement and Parkinson's disease (5). The nAChR became the prototype for ion channel studies in part due to its natural abundance in the *Torpedo* ray *electroplax* (where the receptors provide the ray's electrical shock), which allowed for the first cloning in 1982 (6-8). Further biochemical studies by Unwin have produced cryo-electron micrograph (cryo-EM) images of the full-length receptor (9).

[†]Reproduced in part with permission from Cashin, A.L., Torrice, M.M., McMenimen, K.A., Lesater, H.A., Dougherty, D.A. *Biochemistry* **2007**, *46*, 630–639. Copyright 2007 American Chemical Society

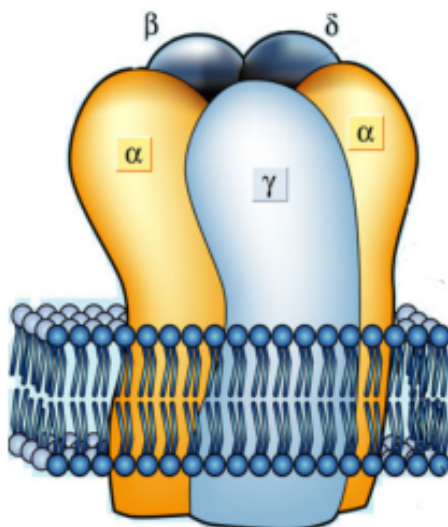


Figure 4.1 Pentameric architecture of the muscle-type nAChR with α , β , δ , α , and γ subunit arrangement.

The Cys-loop receptors all have a cylindrical, pentameric assembly and are sometimes referred to as the pentameric LGICs (Figure 4.1). The five subunits (approximately 400 amino acids in size) are pseudosymmetrically arranged around the ion-conducting pore (10). There are several different subunits- α , β , δ , γ , and ϵ - that assemble in different configurations depending on the type of α subunit present. The α subunit is required for assembly and to date there are 10 types of α subunits ($\alpha 1$ - $\alpha 10$); similarly, there are four types of β ($\beta 1$ -4). The nAChRs found at the neuromuscular junction are referred to as the muscle-type receptor and are composed of two $\alpha 1$ subunits, and one $\beta 1$, δ , and γ subunits. The neuronal nAChRs are composed of different combinations of α and β subunits; for example, several common neuronal nicotinic receptors are the homopentameric $\alpha 7$ receptors and the $\alpha 4\beta 2$ receptors, which demonstrate the diversity of these receptors (4). Topology is conserved for all subunit types, with each containing an extracellular, N-terminal ligand-binding domain (LBD) followed by four transmembrane spanning helices (TM1-4), and a short extracellular C-terminus. Structural analysis of a homologous protein, acetylcholine binding protein (AChBP), has provided much of the structural analysis of the LBD and will be discussed below (11). The LBD also contains the conserved Cys-loop, for which these receptors are named (Figure 4.2). Although the arrangement of the transmembrane domains

around the pore are not conclusively determined, a lot of biochemical evidence suggests that TM2 is the pore-lining helix and TM4 is aligned closest to the membrane (Figure 4.2).

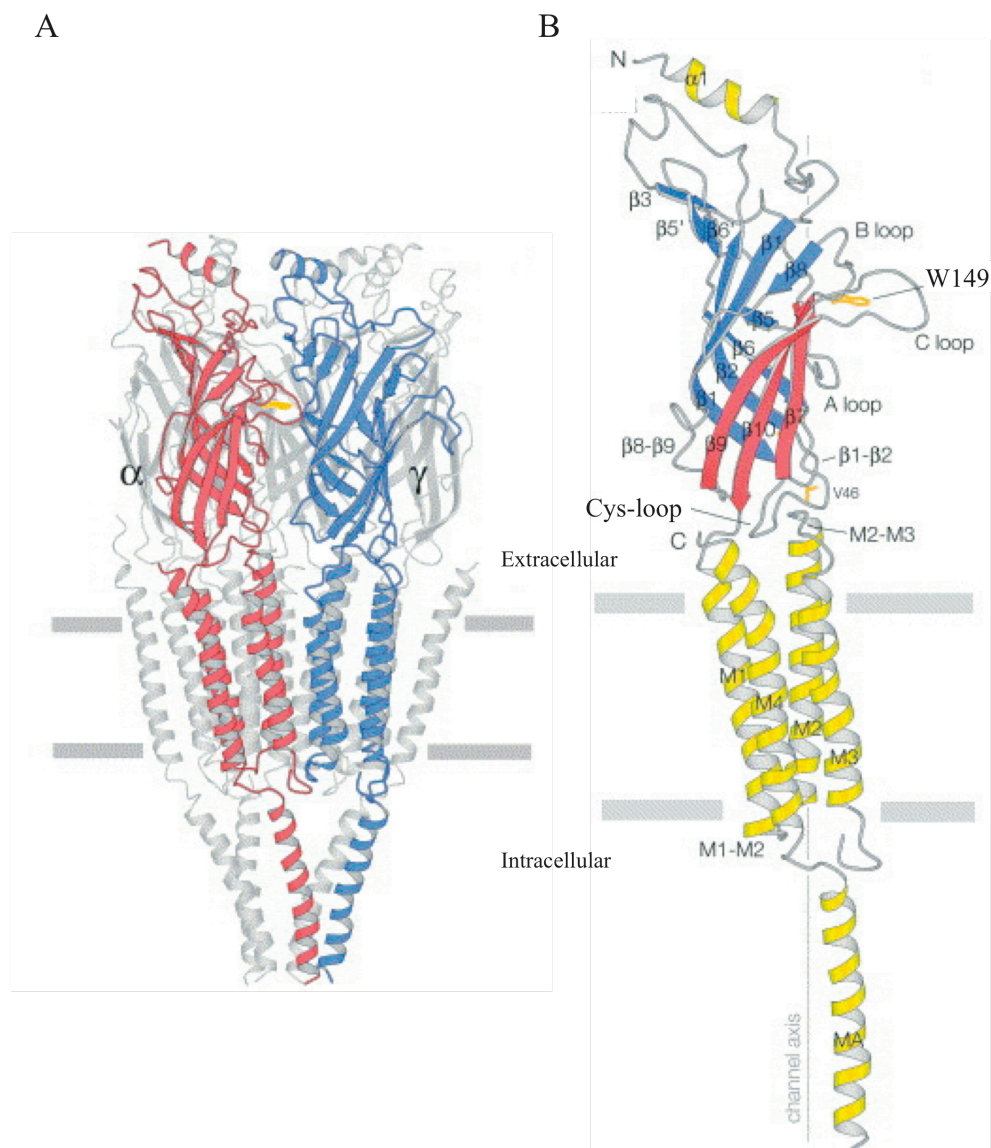


Figure 4.2 A) Structural topology of the muscle-type nAChR. B) Subunit topology of nAChR with the Cys-loop in the extracellular domain and the four TM helices, adapted from reference (12).

All of the experiments described were performed on the muscle-type receptor and will be the focus of the discussion. The early studies of the nAChR using unnatural

amino acids were preceded by many biochemical studies of the muscle-type receptor. These biochemical studies identified key residues likely to contribute to the ligand-binding sites in the receptor. The muscle-type receptor has two ligand-binding sites, which are located at the α/γ and α/δ subunit interfaces (4, 13, 14). Near the agonist binding site is a conserved disulfide bond (Cys192-Cys193, mouse muscle numbering), which was discovered by Karlin and co-workers (15). Several conserved loops are present in the extracellular domain and contribute to the agonist-binding site. The primary face of the binding site is located on the α -subunits and presents residues from loops A, B, and C (Figure 3). The complementary binding face is located on the δ/γ subunit and contributes loops D, and possibly E and F, to the binding site (Figure 4.2) (16).

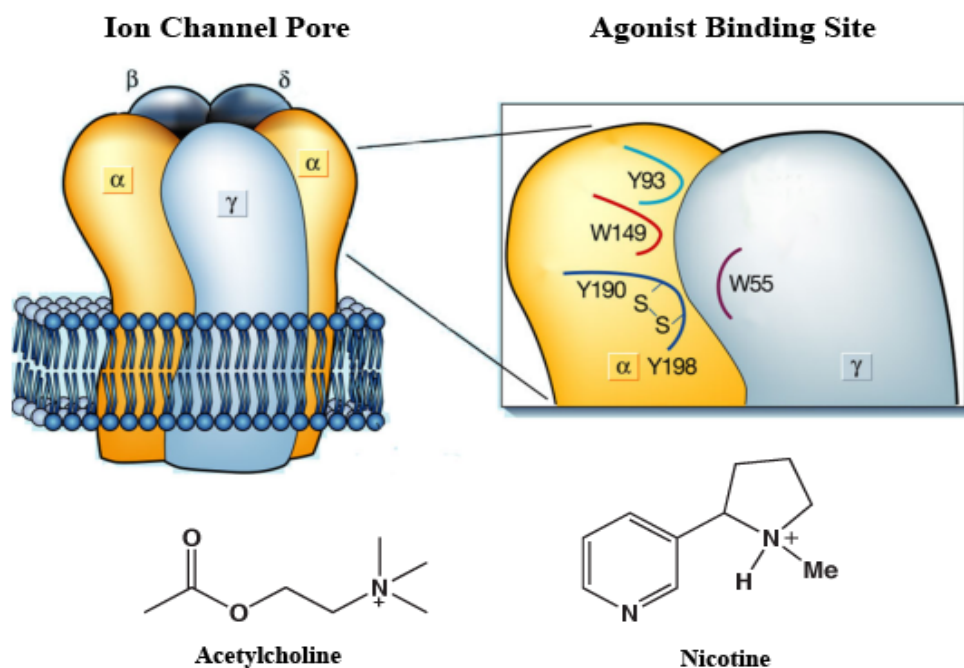


Figure 4.3 The agonist binding site is primarily comprised from α -subunit residues in loops A, B, and C. The γ -subunit contributes to the complementary face and the ligands, acetylcholine and nicotine, bind to this site.

4.1.2. Acetylcholine Binding to the nAChR

Pioneering work by Changeux using photoaffinity labeling and radio-ligand binding

studies identified many aromatic residues near the agonist binding site (17-19). This plethora of aromatic residues suggested that a cation- π interaction between the aromatic residues and the quaternary ammonium group of acetylcholine (ACh) may be contributing to ligand binding. We have previously demonstrated the cation- π interaction is primarily electrostatic and involves a cation binding to the electron-rich face of an aromatic ring (20). All of the tyrosine (Tyr) and tryptophan (Trp) residues in the binding site were evaluated for a cation- π interaction, however only Trp149 in loop B of the α subunit (Figure 4.3) was involved in the interaction with acetylcholine, as demonstrated by Zhong *et. al* (21). Incorporation of the fluorinated tryptophan series (introduced in Chapter 2) resulted in increasing EC_{50} shifts for ACh (Figure 4.4). These studies established that Trp 149 in the “aromatic box” contributes to ligand binding through a cation- π interaction.

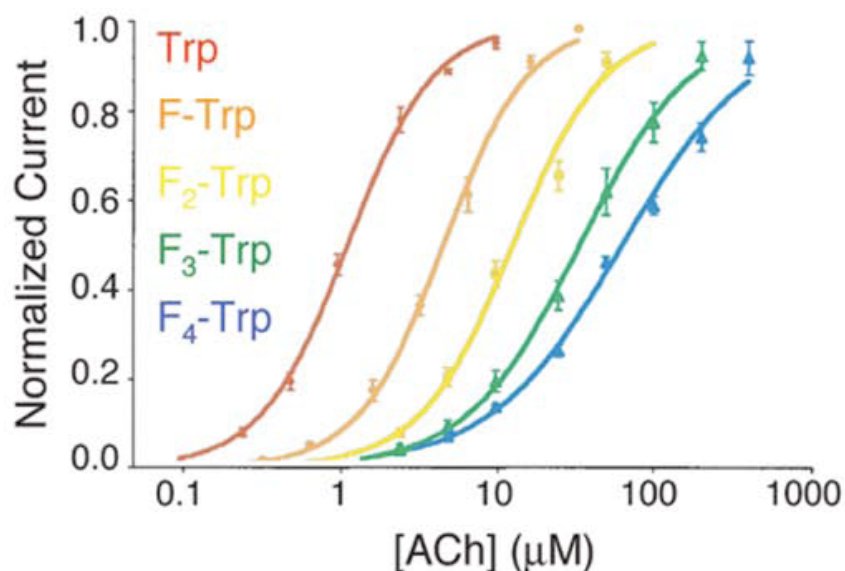


Figure 4.4 EC_{50} shifts for ACh at the mouse muscle nAChR with F_n-Trp incorporation at Trp149.

Further evidence for the aromatic box, along with more detail about the structure of the ligand binding domain of nAChRs, was established due to crystallography on the acetylcholine binding protein (AChBP), which is homologous to the extracellular ligand binding domain of nAChRs (11, 22). AChBP is a soluble, homopentameric protein found in snail glial cells and is 20-26% identical in sequence to nAChR LBDs and most similar

to the homomeric $\alpha 7$ receptor (11, 22). Crystal structures of AChBP, complexed with different ligands, demonstrated the presence of the “aromatic box” containing five aromatic amino acids that form a cavity where the cationic ligand binds (Figure 4.5).

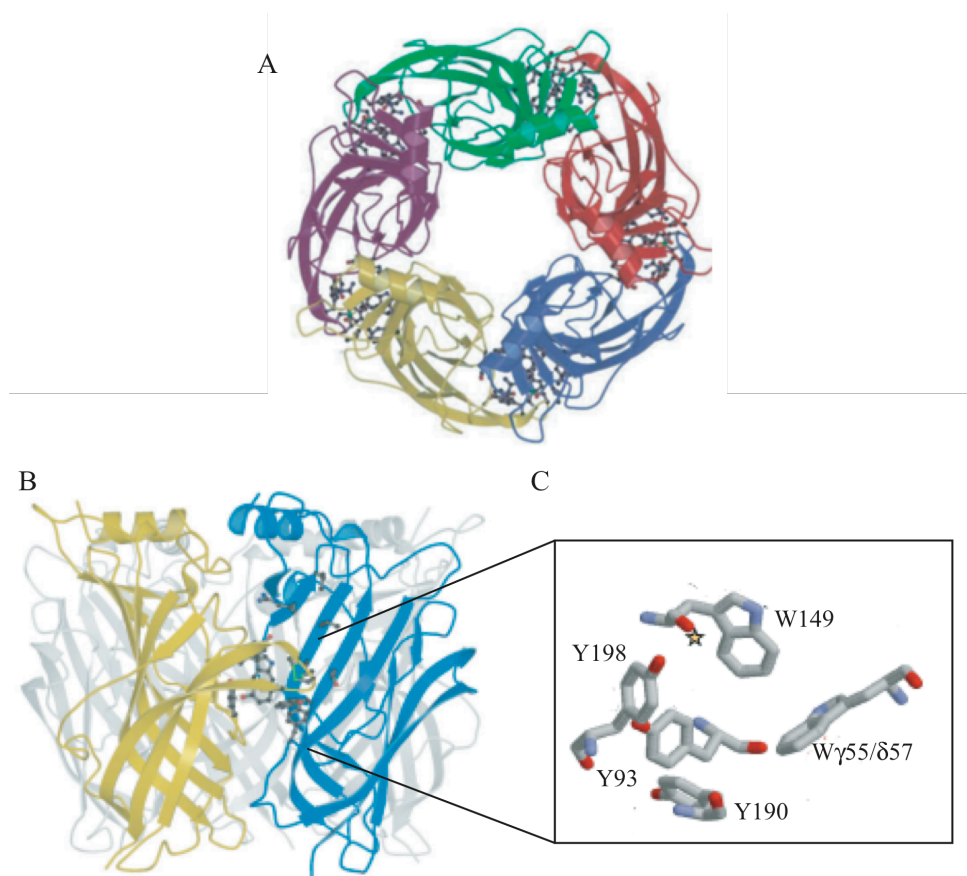


Figure 4.5. A) Pentameric structure of AChBP. B) Agonist binding site in AChBP. C) The aromatic box residues that create the binding pocket in AChBP, adapted from reference (23).

Currently, there are no crystal structures of any nAChRs. Therefore it is important that when we use AChBP as a guide for designing experiments, it serves as a model for the receptor with the caveat that it is *only* a model and not necessarily an accurate representation of the true receptor. The loops previously identified in biochemical experiments that contribute to the agonist binding site overlap well with those in the AChBP structure (22, 23). Additionally, in the original AChBP crystal structures, a molecule of HEPES, a cationic buffer, was positioned in the agonist binding

site cavity where the cationic portion of the molecule was in close proximity with AChBP Trp 143 (homologous to Trp 149 in mouse muscle) (22, 23).

4.1.3. Nicotine Binding to the nAChR and Ligand Discrimination

The initial studies confirming the presence of a cation- π interaction between ACh and the muscle nAChR were intriguing and led us to pursue the presence of additional cation- π interactions involved in recognition of other nAChR agonists. Due to the cationic nature of (-)-nicotine (Figure 4.3), it was hypothesized to bind the nicotinic acetylcholine receptor in a similar manner to ACh (i.e., via a cation- π interaction) (24). Cohen *et al.*, used photoaffinity labeled nicotine analogs to investigate how nicotine binds to the muscle nAChR. Interestingly, these experiments identified the same aromatic residues involved in ACh binding, suggesting that ACh and nicotine utilize the same residues for agonist binding (25). However, incorporation of the F_n-Trp derivatives at Trp149 of the muscle receptor did not produce a similar trend in the fluorination plot compared to ACh binding, which suggested that nicotine does not utilize a cation- π interaction (26). The other residues within the agonist binding box were also tested for the presence of a cation- π interaction, but did not demonstrate the interaction (Figure 4.6).

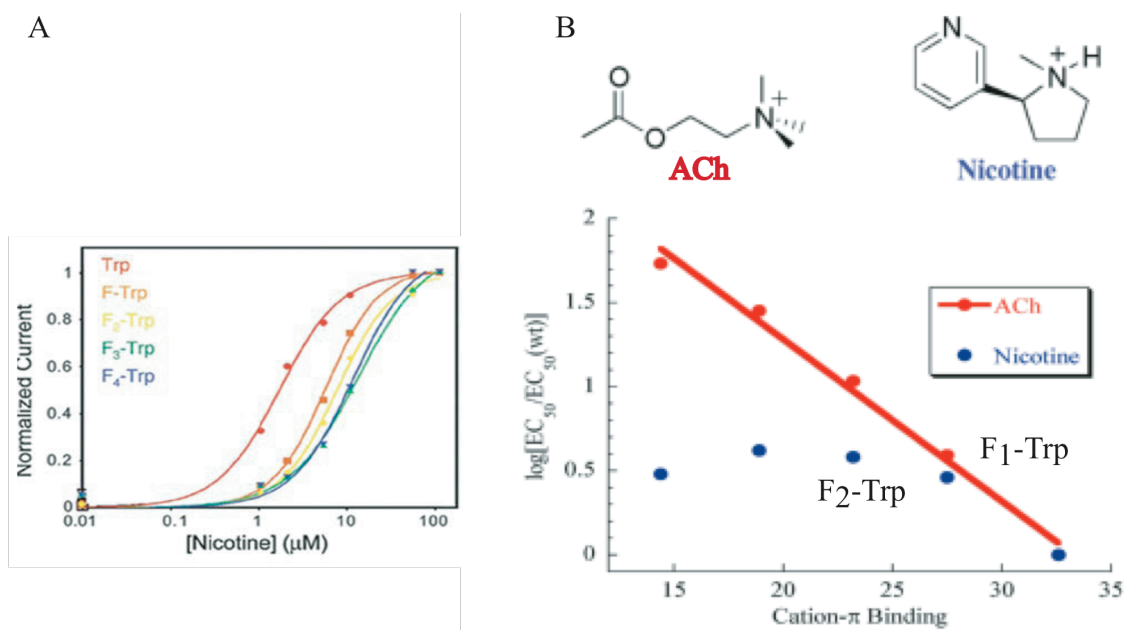


Figure 4.6. A) EC₅₀ shifts for F_n-Trp incorporation at α149 in mouse muscle nAChR. No shift is observed after F₁-Trp incorporation. B) Fluorination plot for ACh and nicotine binding to muscle nAChR. A linear relationship is observed for ACh but not for nicotine, indicating the absence of a cation-π interaction.

Previously, all cationic agonists were believed to interact with the receptor in a similar way. However, these results separated the ligands into two classes, the “cholinergic” agonists such as ACh, and the “nicotinic” agonists that bind similarly to nicotine. One intriguing feature of the nicotine fluorination plot is that it begins with a shift in EC₅₀, like the cholinergic agonists, and then changes its path. These plots correspond to a Hammett-like plot and the “break” in the curve (two different slopes) suggests that nicotine binds using one mechanism and then fluorination of α149 could result in a change in the binding mechanism. On the other hand, it is possible that nicotine never interacts with the binding site through a cation-π interaction at the muscle nAChR. Another noticeable difference between ACh and nicotine binding to the muscle nAChR is that nicotine is approximately 100-fold less potent than ACh, indicating that other interactions are involved in the binding and/or gating mechanisms for Nic. This establishes that the receptor is able to discriminate between different types of ligands. Previous modeling studies suggested that nicotine makes a hydrogen bond between the N⁺-H to the backbone carbonyl of αTrp149 (27, 28). Sixma and co-workers

simultaneously published a crystal structure of AChBP with nicotine bound, confirming the presence of the hydrogen bond between nicotine and the backbone carbonyl of α Trp149 (29). Although both ACh and nicotine agonists bind to the same site in the receptor, they utilize different non-covalent interactions to do so.

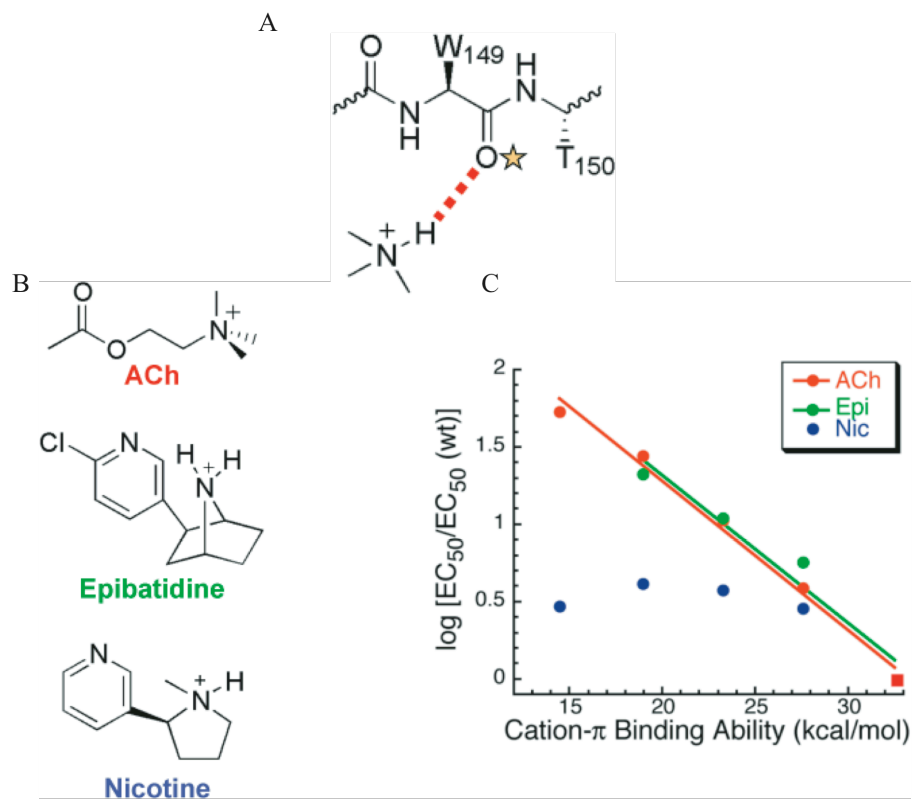


Figure 4.7. A) Schematic of the hydrogen bond between the tertiary ammonium ion of nicotine and the backbone carbonyl of α Trp149. B) Structures of three different nAChR ligands. C) Fluorination plots for ACh, epibatidine, and Nic, demonstrating the presence and absence of a cation- π interaction.

Given the previous experiments, additional agonists were investigated to further explore the difference between cholinergic and nicotinic ligand binding to the nAChR. As stated before, nicotine is a low affinity agonist at the muscle-type nAChR although it is much more potent for several of the neuronal receptors (30, 31). Therefore, the highly potent agonist at both muscle and neuronal nAChRs (30, 32), epibatidine (Epi), was also studied using the F_n -Trp series and demonstrated the presence of a cation- π interaction at

α Trp149 (33). As such, epibatidine serves as a probe of “nicotinic” interactions for the nAChR. It is similar in structure to nicotine although it contains the potency of ACh, making it an appropriate probe for studying nicotinic interactions at the binding site (Figure 4.7).

4.1.4 Computational Modeling of nAChRs

Many advances since the early 1970’s allow for detailed experimentation exploring structure/function relationships in ion channels. The use of unnatural amino acids provides one of these tools, which helps us gain a more thorough understanding of these proteins. Another method of analysis involves using computational (*in silico*) models of either the entire LGIC or portions of the LGIC. Several types of modeling are often employed, varying in both computational intensity and accuracy. Some of those used in our lab are *ab initio* quantum mechanics (QM) and molecular mechanics force fields resulting in molecular dynamics (MD) simulations. QM calculations are very precise, computationally intensive calculations that allow for the calculation of interactions between individual molecules. On the other hand, MD simulations are much less precise, but allow for calculations on larger proteins and solvent molecules (34, 35). One major drawback to MD simulations is the reliance on MM force fields, which do not accurately represent many non-covalent interactions because they do not explicitly treat electrons (36, 37). Nevertheless, we generated models of the extracellular domains for both the neuronal $\alpha 7$ nAChR and the mouse muscle nAChR utilizing the most recent AChBP crystal structure and produced MD runs using these models. These models provided “dynamic” information about different chemical-scale interactions involved in maintaining the structure of the agonist binding site. In particular, we explored the role of a conserved aspartate, α D89, in shaping the aromatic box.

4.1.5 Project Goals

A critical feature of nicotine as an agonist is the extreme difference in potency between the muscle and neuronal nAChRs (32, 38). Nicotine is a very potent agonist for the neuronal nAChRs and has been implicated in a number of neurological diseases. In addition to its obvious role in nicotine addiction, it also plays a role in Alzheimer’s and

Parkinson's disease, making it an interesting drug target (39). Nicotine and ACh have similar EC_{50} values (concentration of drug required to activate 50% of the channel current) for the neuronal receptors, particularly $\alpha 4\beta 2$ (40, 41). However, nicotine is not a potent agonist for the muscle nAChR. The EC_{50} for nicotine at the muscle receptor is approximately 70-fold greater than that of ACh (Table 4.1) (32).

Table 4.1 EC_{50} Values for wild type muscle and neuronal nAChRs. The mouse muscle data was acquired in the Dougherty lab (33) and the Human $\alpha 4\beta 2$ data was obtained from references (41)^a and (42)^b.

Ligand	Mouse Muscle	Mouse Muscle $\beta 9'$	Human $\alpha 4\beta 2$
ACh	50 μ M	0.33 μ M	3.3 μ M ^a
Nic	>500 μ M	30 μ M	3.9 μ M ^a
Epi	13 μ M	0.6 μ M	43 nM ^b

Unfortunately, the low affinity of the muscle nAChR for nicotine is a complication that makes experimentation on this receptor with nicotine difficult due to the high concentrations of nicotine required in order to obtain electrophysiological data. The binding difference between the agonists complicates the challenge of understanding the binding modes of these small molecules to the receptor, which is important when designing drugs to modulate receptor function. The goal of these studies was to determine the residues underlying subunit specificity for nicotine binding to allow for better drug design that could target each receptor subtype. At the time of the study expression of neuronal receptors in the heterologous *Xenopus* oocyte was not feasible. However, recent advances have allowed incorporation of unnatural amino acids into several neuronal nAChRs (43).

4.2 Results

4.2.1 Conventional Mutations of the Outer Shell of the mouse muscle nAChR Binding Box

The first approach taken to determine the subunit specificity of nicotine binding involved scanning the sequence alignment between the neuronal and muscle nAChR subunits (Figure 4.8). The focus of our experiments was directed on the α subunit, which contributes to the primary face of the binding site. We used sequence alignments to determine residues that were significantly different between the receptor types, for example if there was a charged amino acid in place of a hydrophobic residue, etc. Since the aromatic binding box is conserved throughout all types of nAChRs, this would suggest that there are structural subtleties introduced by amino acids other than those directly contributing to the binding pocket. As such, it is likely that the residues that form the binding site involve a more complex organization of interactions that help to shape the “aromatic box” in such a way that facilitates or destabilizes certain binding interactions. Further, these residues may be key to understanding the difference in agonist potency and specificity between the muscle and neuronal receptors, or even between the different neuronal subunits.



Figure 4.8 Alignment of nAChR subunits including several α subunits (muscle and neuronal) and β 2, δ , and γ . We introduced mutations at the residues denoted by a red asterisk.

When studying low potency agonists or nAChRs where mutations reduce receptor activation, we introduce a “background” mutation that compensates for this decrease in ligand potency. A Leu-to-Ser mutation in the M2 transmembrane region of the β subunit

at a position known as 9' produces a hypersensitive receptor (44-46). The $\beta 9'$ (a distinction between $\beta 9'$ and "regular" wt is made) mutation is almost 50Å from the agonist binding site, located in the channel pore and has been shown to lower agonist EC_{50} values by 40-fold without altering any other trends (45). As such, it is important to remember that EC_{50} is a measure of channel function and is representative of equilibria between binding and gating, not just a measure of agonist affinity. Often the trends that we observe in EC_{50} are a result of changes that are due to the agonist binding interaction and not due to gating processes.

Previous studies indicate that the amino acids surrounding the aromatic box are clearly involved in determining the potency of different agonists and likely influence the binding of the same agonist at different receptor subtypes (30). Amino acids directly adjacent to the conserved aromatic box were evaluated for conservation of charge, size, and chemical properties. Residues $\alpha S191$, $\alpha T196$, and $\delta D59/\gamma E57$ are all physically near the aromatic box based on the AChBP structure. Additionally, these residues are not conserved between nAChR subunits, such as $\alpha 4\beta 2$, as seen in the subunit alignment (Figure 8). Conventional mutagenesis was used to mutate these residues to the corresponding amino acids of the $\alpha 4\beta 2$ subunits. Since $\alpha 4\beta 2$ receptors bind nicotine with a greater potency than muscle, we hypothesized that the mutations would allow the muscle receptor to have an equal potency for nicotine and ACh (i.e. increase the potency of nicotine relative to ACh). The mutant receptors were characterized by electrophysiology (Figure 4.9).

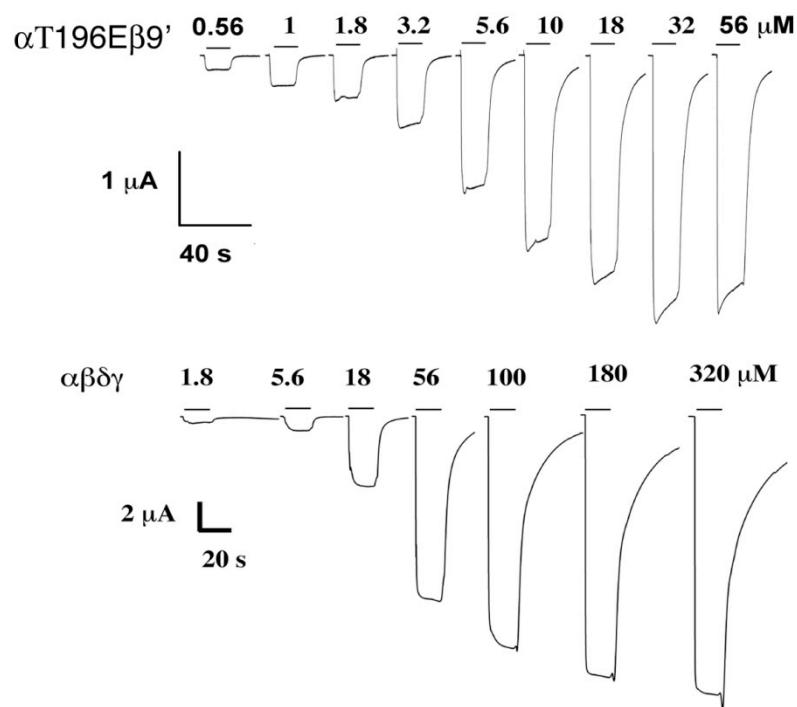


Figure 4.9 Electrophysiology traces of the inward current produced from mutant receptors $\alpha T196E\beta 1\delta\gamma$ receptors and wild type muscle nAChRs in response to increasing doses of ACh.

Mouse muscle nAChR $\alpha S191$ and $\alpha T196$ are polar and hydrophilic groups containing hydroxyl side chains that have the potential to hydrogen bond. However, in the neuronal nAChRs, $\alpha 191/196$ are acidic residues, mostly glutamate (Figure 4.8). We hypothesized that introducing a charged side chain at these sites could create ionic interactions that shape the box allowing nicotine to be a more potent agonist. One goal of these experiments is to increase nicotine potency at the muscle nAChR relative to ACh. This approach examines the significant differences among the side chains near the aromatic box to determine their potential contributions towards agonist binding. Additionally, residues in the δ/γ subunits near the complementary face of the binding box were also significantly different when comparing the muscle and neuronal receptors. The residues $\delta D59$ and $\gamma E57$, which are both acidic, were mutated to glutamine, a polar and hydrophilic amino acid that does not contain a negative charge. In the crystal structure of AChBP the amino acids in the α subunit are facing the extracellular matrix, however these residues are likely not aligned identically in the muscle type nAChR. In fact, these

residues may be able to participate in non-covalent interactions with other residues that surround the aromatic box, shaping the binding pocket.

We introduced several side chain mutations at these sites, the single mutations α S191E and α T196E, the double mutation α S191E T196E, and we combined the α -subunit mutations with those in δ/γ , δ D59Q and γ E57Q. By combining the α -subunit mutations with the δ/γ mutations we were able to study the combined effects of mutations to both faces of the agonist binding site for ACh and nicotine. These recordings were made in the presence and absence of the β 9' mutation as well, to ensure that we were recording accurate responses from the mutant receptors with both traditional wild type and the β 9' wild type (Table 4.2). Plots of the ratio of EC_{50} for the mutant receptors compared to the EC_{50} for the wild type receptor demonstrate the change in receptor potency for both ACh and nicotine (Figure 4.10). As a reference the EC_{50} values for α 4 β 2 wild type receptors were also plotted against the muscle receptor. This provides a “baseline” for which we can compare our mutated muscle receptors since one goal is to make a muscle receptor respond to nicotine similarly to the neuronal nAChRs.

Table 4.2 EC_{50} data for mutations of the outer shell residues near the muscle nAChR binding site.

Mutations	EC_{50} μ M ACh	Hill Value (ACh)	EC_{50} μ M Nic	Hill Value (Nic)
WT	57	1.17	>500	N/A
α T196E	2.5	1.65	75	1.48
α S191E	2	1.01	82.2	0.88
α S191E T196E	10.5	1.45	350	0.93
α T196E δ γ E57Q	3.6	1.95	101	1.76
α T196E δ D59Q γ	7.5	1.34	135	1.41
α T196E δ D59Q γ E57Q	11.3	2.04	111.5	2.21
WT β 9'	0.33	1.34	30	1.52
δ D59Q β 9'	-	-	77	1.26
γ E57Q β 9'	-	-	75	1.76
α T196E β 9'	0.35	1.7	3.8	1.43
α S191E β 9'	0.42	0.89	6.5	2.07

All of the mutations introduced into the α -subunit and the δ/γ subunits resulted in a decrease in EC_{50} value for both ACh and nicotine (Figure 4.10). However, using α 4 β 2 wild type values for comparison, none of the mutations resulted in producing a muscle

receptor with the same potency for ACh or nicotine as a neuronal receptor. The goal of these studies was to obtain a mutant receptor that had the same EC_{50} for ACh and Nic, making them more neuronal-like in function. The largest shift was obtained for the α T196E mutation, which resulted in a 8-fold shift for nicotine and 12-fold shift for ACh. Interestingly, this site appears to affect ACh more than Nic, and turns ACh into a more potent agonist than it is at the wild type $\alpha 4\beta 2$ receptor (Figure 4.10).

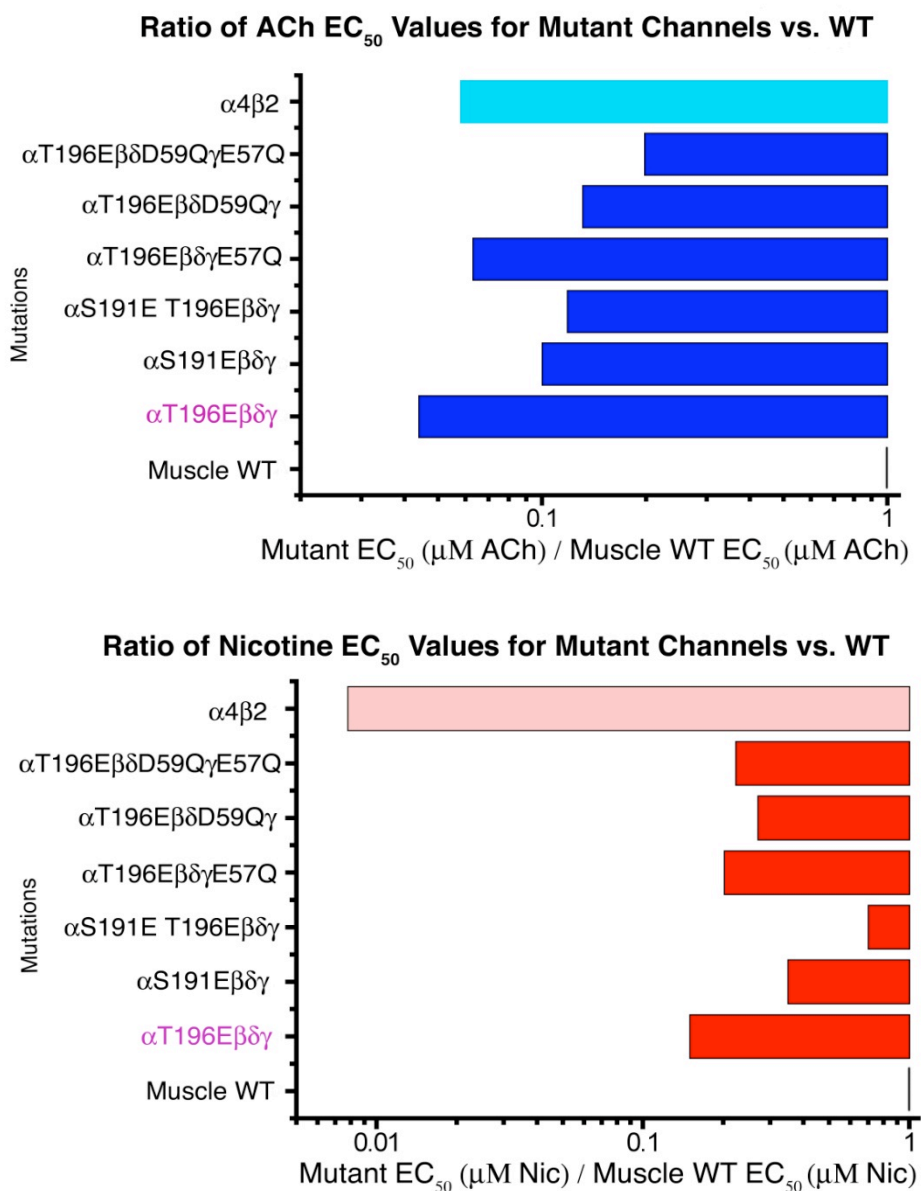


Figure 4.10 Ratio of EC_{50} values for binding site mutants vs. wild type muscle nAChR in response to ACh (blue) and nicotine (red). The EC_{50} for wild type $\alpha 4\beta 2$ is shown (light blue and red, respectively) as a reference.

Combining the α -subunit mutations with δ/γ mutations generally resulted in larger decreases in EC_{50} (increase nicotine and ACh potency) than with the single mutations. This was particularly evident by the α T196E mutant, which shifted more when combined with other mutations (Table 4.2, Figure 4.10). Residues homologous with α 196 lie directly behind α 198 in the AChBP crystal structure, and α 198 is one of the aromatic box residues that make direct contact with the agonist (22). In AChBP the α T196 homologue is exposed to solvent, which suggests that a charged side chain such as glutamate would be even more stable than threonine in the solvent-exposed hydrogen-bonding environment. The crystal structure does not indicate a clear bonding partner for α 196, however it remains a possibility that the muscle receptor residues in this area are not solvent exposed, but instead making intrasubunit contacts. We assume that the structure of muscle nAChR is similar to AChBP, but it is not likely that all the side chains are oriented in the same direction in both proteins. This does not explain the decrease in EC_{50} values we observe for both ACh and Nic, and there is no obvious reason why mutating α T196 alters ligand potency.

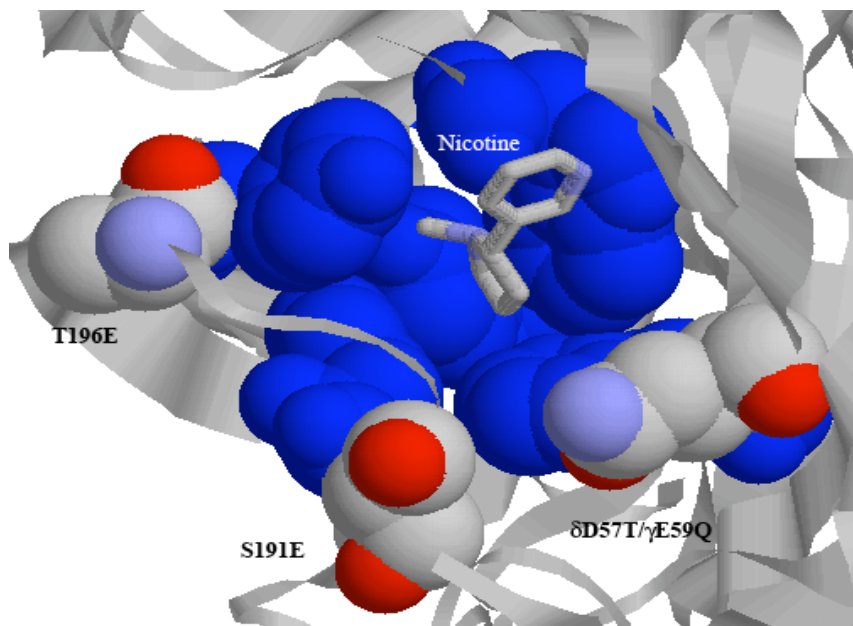


Figure 4.11. Binding site of AChBP with nicotine bound to the aromatic box. Mutations are shown in CPK colors and the aromatic box residues are blue.

There are additional reports that other non- α subunit residues, δ D59N and γ G57S (similar to the above reported mutations), when mutated, demonstrate decreased affinity for ACh (32). Interestingly, these non- α amino acids form the lower part of the binding site, according to the AChBP structure (Figure 4.11). Carbamylcholine (another choline agonist) binding is influenced by δ D59 and γ E57, but that amino acid does not appear to influence ACh or nicotine binding (47). However, our mutations in δ/γ did not result in a large increase (or decrease) in ACh or nicotine potency.

4.2.2. Chimera Experiments Between Mouse Muscle and Neuronal nAChRs

Although the α 196 mutant increased muscle nAChR potency for nicotine, it did not increase the potency to equal that of the neuronal receptors. We thought that expanding our region of analysis to include additional residues in the outer binding shell could result in larger EC₅₀ shifts. To investigate whether the effects of larger scale alterations to the outer shell of the binding pocket would induce a larger shift in potency we examined several “loop” areas in the extracellular domain previously implicated in determining agonist specificity and generated chimeras (mutant receptors containing segments from at least two different subunits) between the muscle and neuronal receptors.

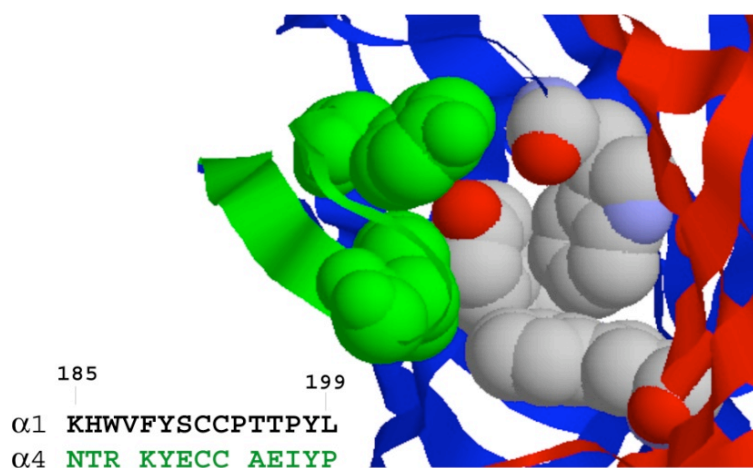


Figure 4.12 Alignment of β 9- β 10 loop from muscle α 1 and neuronal α 4 subunits. The loop is highlighted in green in the AChBP structure and is directly adjacent to the aromatic box, and includes α Y190 and α Y198, two aromatic box residues.

Previous experiments constructed chimeras between the $\alpha 4$ and $\alpha 7$ neuronal nAChR subunits (4). These chimeras focused on residues $\alpha 186$ - $\alpha 194$, which are in a loop identified to contribute in part to some of the differences in agonist specificity between the neuronal $\alpha 7$ and $\alpha 4\beta 2$ receptors (4). This loop, the $\beta 9$ - $\beta 10$ loop, contains the $\alpha 196$ residue described above which we found to alter nicotine potency, therefore it is reasonable to infer that this region shapes the agonist “box” and could make the mouse muscle receptor more sensitive to nicotine.

To increase agonist potency at the muscle type nAChR, we constructed a chimera between mouse muscle $(\alpha 1)_2\beta 1\delta\gamma$ and the human $\alpha 4\beta 2$ receptor at the $\beta 9$ - $\beta 10$ loop area (Figure 4.12). The α subunit chimera was expressed in oocytes with wild type β , δ , and γ subunits. Unfortunately, protein expression was very low for these receptors and responses to ACh and nicotine could not be reliably obtained. One possibility is that this loop is important for receptor assembly, therefore substantial mutations prevent proper ion channel formation. Additionally, it is possible that this region of the protein is important for receptor trafficking, and our mutations prevented the ion channels from reaching the cell surface. Since the chimera did not express we decided to make several point mutations within the chimera loop. We wanted to explore the role of several nonconserved amino acids in shaping the aromatic box. The mutations $\alpha V188L$, $\alpha V188K$, and $\alpha L199P$ were constructed, however all of these mutations produced ion channels with little to no expression in response to ACh or nicotine.

4.2.3 Unnatural Amino Acid Mutagenesis of Outer Shell Amino Acids

Our previous efforts to understand how contributions from the outer binding shell amino acids contribute to agonist specificity remained unclear; therefore we turned to exploring the role of hydrogen bonds in shaping the aromatic box. Using unnatural amino acid mutagenesis we can introduce subtle mutations to alter hydrogen-bonding properties of the amino acid side chains. A nAChR conserved Trp, $\alpha W86$, was previously studied for its role in a potential cation- π interaction with ACh (none was found), but the hydrogen bonding potential of the indole N-H was not investigated. $\alpha W86$ is in close proximity to another conserved residue, $\alpha D89$, in the AChBP crystal structure, which has been

implicated in shaping the binding site (29). We were interested in exploring the potential hydrogen bond between α W86 and α D89 in mouse muscle nAChR (Figure 4.13).

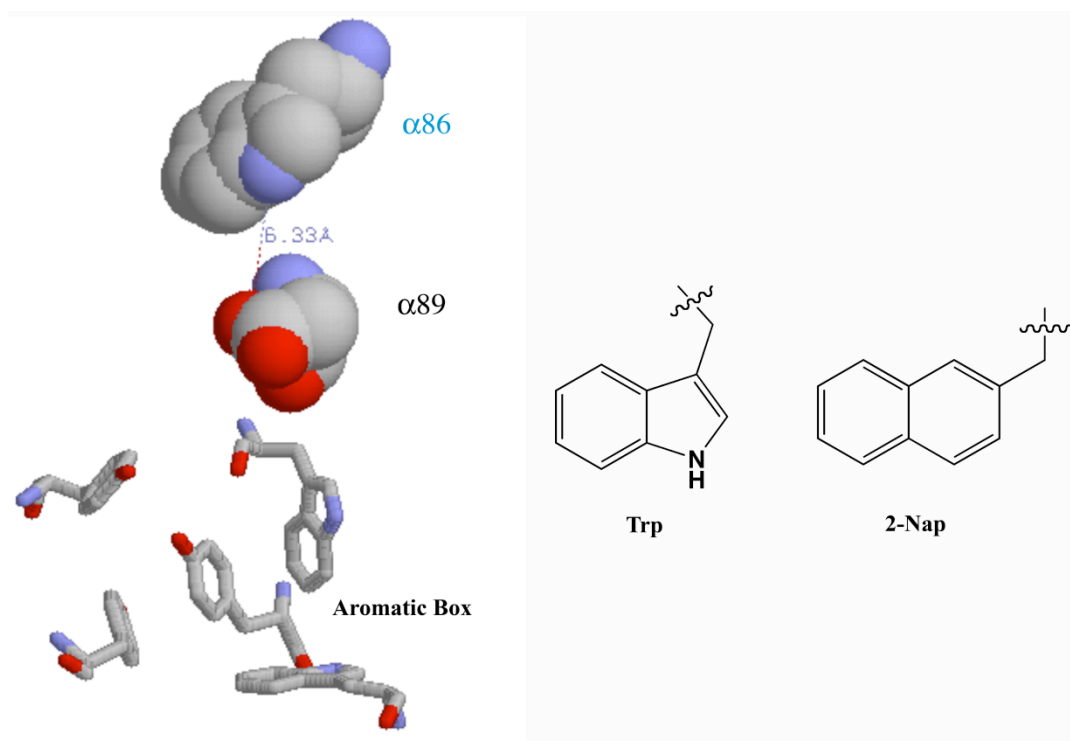


Figure 4.13 Potential hydrogen bond between α W86 and α D89 involved in shaping aromatic box. Hydrogen bonds in Trp can be probed by introducing the unnatural amino acid 2-naphthylalanine (2-Nap).

A Trp derivative, 2-naphthylalanine (2-Nap, Figure 4.13) was incorporated into the α W86 residue of mouse muscle nAChR to investigate the importance of this position as a hydrogen bond donor with its potential proximal partner, α D89. The derivative, 2-Nap is similar in size and structure to Trp, but does not contain the hydrogen bond donor (N-H) in the indole ring. However, 2-Nap retains the aromaticity of the natural Trp sidechain, and allows us to probe the hydrogen bond characteristics of α W86 without significantly altering the electronic aspects of the side chain.

Incorporation of α W86 2-Nap did not result in an EC_{50} shift for ACh. If the hydrogen bond were important for shaping the aromatic box we would expect a rightward shift in EC_{50} , which was not observed (Figure 4.14). One difference upon 2-Nap incorporation is an increase in the Hill coefficient, which is an indication of the

cooperativity between the binding sites of the receptor. This higher Hill coefficient suggests that there is more cooperativity between the binding sites when 2-Nap is incorporated compared to Trp. This suggests that this residue may be important for gating interactions or conferring conformational changes between subunits of the receptor. Hydrogen bonding and the cation- π interaction are not requirements of α W86, yet this Trp is conserved in all α subunits, suggesting that this residue plays a role in maintaining correct protein structure. To test this hypothesis we incorporated an alanine residue at α 86, which completely obliterates the side chain. The α W86A mutation drastically decreased the amount of currents generated in response to ACh, suggesting that this is a structural residue, however EC_{50} values could not be determined. This result is consistent with the hypothesis that a large, hydrophobic amino acid is structurally important at this highly conserved site.

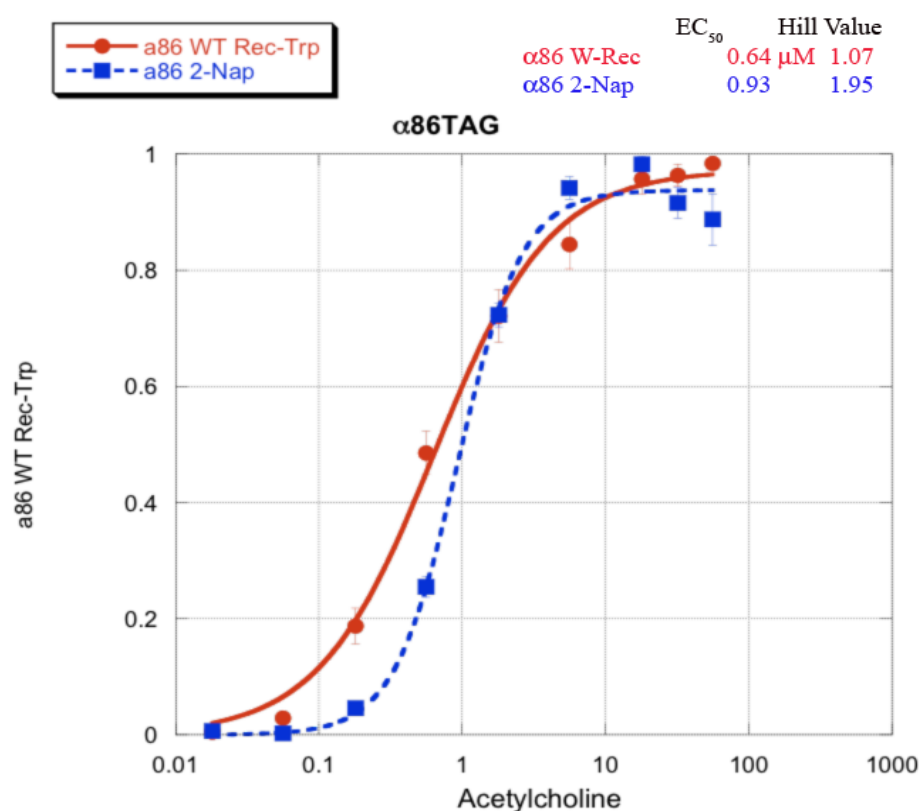


Figure 4.14 EC_{50} plot of α 86 wild type recovery and α 86 2-Nap data demonstrating no shift in EC_{50} .

Two additional, highly conserved residues that physically surround the aromatic box were also examined in the α subunit. The residues, α P21 and α Y151 were mutated in order to determine the importance of their conservation in receptor function. These residues are positioned on either side of α 86 in the AChBP structure, suggesting that these conserved residues could interact with one another during agonist binding and/or the receptor gating process.

We perturbed α Y151 by incorporating the unnatural amino acid 4-Me-Phe which is sterically similar to Tyr but unable to form hydrogen bonds since it lacks both a hydrogen bond donor and acceptor. Tyr is conserved at this position throughout all nAChRs as well as several other Cys-loop family receptors. Since Tyr is both a hydrogen bond acceptor and donor we wanted to test the implications of altering these characteristics at this site by replacing the hydroxyl with a methyl group. We hypothesized that α T151 4-Me-Phe would be worse at structuring the aromatic box, resulting in EC_{50} shifts to the right (decreasing agonist potency). Replacement of the hydroxyl with a methyl group did shift EC_{50} rightward approximately 5-fold for both ACh and nicotine (Table 4.3). This suggests that the hydroxyl plays an important role in hydrogen bonding at that site, possibly influencing the general shape of the aromatic box for both cholinergic and nicotinic agonists.

Table 4.3 EC_{50} data for mutations of conserved residues, α 151 and α 21 in mouse muscle nAChR.

Mutations	EC_{50} μ M ACh	Hill Value (ACh)	EC_{50} μ M Nic	Hill Value (Nic)
WT β 9'	0.33	1.34	30	1.52
α Y151TAG β 9' Phe	3.8	2.08	-	-
α Y151TAG β 9' 4-Me-Phe	2.04	1.71	154.6	1.86
α P21F β 9'	1.05	2.45	100.5	1.68
α P21G β 9'	0.7	1.51	13.9	1.47

The conserved proline, α 21, is present in all Cys-loop family receptors. The orientation of α P21 above α W86 (in AChBP) suggests that α P21 is another structural residue that holds the formation of the residues in the outer shell of the binding box in

place. In general, prolines are rigid and often found in protein turns because they can induce a kink within helices. Since proline residues provide a distinct structure-function relationship, we were interested in determining if this proline residue played a role in structuring the agonist binding site. We introduced the conventional mutations, Phe and Gly, at $\alpha 21$. Incorporation of the large, aromatic group, $\alpha P21F$, resulted in a 3-fold shift in EC_{50} for both ACh and Nic. The more interesting effect came with the $\alpha P21G$ mutation, which resulted in a 2-fold increase in EC_{50} for ACh while lowering that of nicotine 2-fold. These results suggest that “locking” the binding site into one conformation (Phe mutation) reduces overall agonist potency while introducing a more flexible residue (Gly mutation) is more beneficial for nicotine binding, possibly allowing the binding site to accommodate the different steric constraints of nicotine. The mutation $\alpha P21G$ results in an increase in nicotine potency, which suggests that nicotine might require a larger box structure in order to bind more tightly to the receptor. Proline could constrain the binding site and the increased flexibility introduced by glycine may allow the binding site to reorient around nicotine for a better “fit.” The conservation of $\alpha P21$ in all nAChR subtypes suggests that although this amino acid is important for structuring the aromatic box, it does not likely define subtype specificity between muscle and neuronal nAChRs.

4.2.4 A Computational Model of Extracellular Domain of Mouse Muscle nAChR

The goal of these experiments was to generate models of the entire binding site (all outer shell residues) of the nAChR. The structure of AChBP provides a good model for the extracellular domain, yet there is good reason to believe that it does not accurately describe the structure of the binding site in the nAChRs, especially the heteromeric receptors. Previous models have been generated using different templates, alignments, and structural refinements; producing similar yet subtly different results (27, 28, 48-50). The variations in the binding between ACh, nicotine, and epibatidine for the different receptor subtypes also indicate that many differences must be present in each receptor. Ideally, we could generate models of the binding site that take into account these differences and not just evaluate the conserved aromatic residues. We need to account

for the outlying residues, the equivalent to the first and second solvation shell of a small molecule, which impart the differences contributing to ligand specificity.

A model for the human $\alpha 7$ homomeric nAChR extracellular domain was generated by E.J. Petersson (51). This model used the backbone architecture of the AChBP structure as a basis for “threading” on the $\alpha 7$ subunit sequence. The $\alpha 7$ homology model was generated using the AChBP structure with nicotine bound (Subunit A, of 1UW6). Refinements were made to the structure and then MD simulations were performed to generate several nanoseconds of movement of the extracellular domain of the $\alpha 7$ LBD. We utilized this model of $\alpha 7$ as a guide to generate a model of the mouse muscle extracellular domain $\alpha 1_2\beta\delta\gamma$.



Figure 4.15 A) Alignment of the alpha subunit from *Torpedo marmorata* with $\alpha 1$ mouse. The beginning and end of the LBD sequence in the final PDB file is denoted by (*).

We constructed sequence alignments between *T. marmorata* from Unwin’s model of the nicotinic receptor (12) and the different mouse muscle subunits using the program T-coffee (52); Figure 4.15 has examples of the α subunit alignments. *T. marmorata* has almost exact sequence homology to the mouse muscle receptor subunits therefore, the fit was ideal. The program Prime, part of the Schrodinger (53) suite of software, was used to develop a homology model based on the *T. marmorata* structural model, PDB file 2BG9 (10, 12). We generated three models of $\alpha 7$ and mouse muscle (mm_nachr), one without ligand, one with nicotine bound, and one with carbamylcholine (CCh) bound.

A single subunit of *T. marmorata* (without ligand) was used as a template for generating mm_nachr. During the build step side chains were allowed to move. Each subunit was built and exported individually and exported as a PDB file. A pentamer was built in Swiss PdbViewer (54) by aligning each subunit onto the *T. marmorata* pentamer. The pentamer was exported back into Prime, where loop refinement algorithms and side chain predictions were performed. We performed refinements for the C loop, which is directly implicated in forming the binding site in nAChRs. Residues homologous among the mm_nachr subunits and *T. marmorata* were held fixed. The final chain assignments were made, Chain A ($\alpha 1$), Chain B (δ), Chain C (β), Chain D (α), and Chain E (γ). Chain A of the Torpedo structure was used as the template for both of the α subunits of the mouse muscle nAChR. This pentamer was then exported as a PDB file to GROMACS for molecular mechanics minimizations (54).

The mm_nachr heteropentamer was converted to a GROMACS format for molecular mechanics. The pentamer was placed in a hexagonal periodic box with 7 Å gaps between the edge of the box and the protein. Explicit solvation was added to the box using SPC water molecules (55), followed by the addition of ions (Na^+ and Cl^-) to the box at a concentration of 150 mM. Extra Na^+ ions were added to the box to neutralize the -62 total charge of the protein.

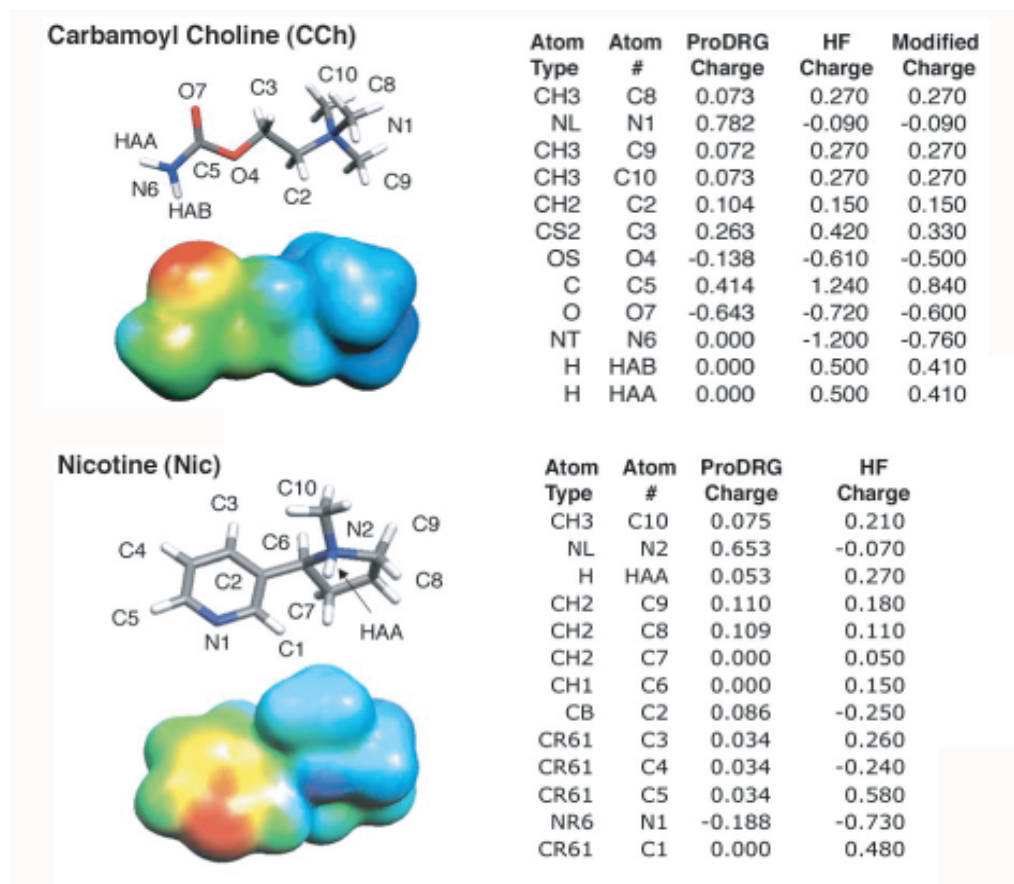


Figure 4.16 Charges generated for the agonists, CCh and Nic. The ProDRG charges are listed and the modified charge determined using Hartree-Fock (HF) calculations, which were determined by HF/6-31G** computations. These also produced the electrostatic potential surfaces that correspond to an energy range of $+10$ to $+130$ kcal/mol (blue is more positive and red is less positive).

We generated three separate mm_nachr models, one without ligand, and two with ligands (Nic and CCh). Into the mm_nachr model we inserted either nicotine or CCh at the two binding sites, α/δ and α/γ . This was performed by aligning the binding site of the AChBP structure with nicotine (1UW6) and CCh (1UV6) with the mm_nachr pdb file. We generated the parameters for nicotine and CCh using the ProDRG (<http://davapc1.bioch.dundee.ac.uk/programs/prodrg/>) website, although the charges it generated were determined to be unacceptable because it placed most of the positive charge on the nitrogen atoms of the ammonium groups (56), therefore modified charges were used (Figure 4.16). The modified CHELPG charges from HF/6-31G** calculations

were used for nicotine (57). In the case of CCh, the partial charges generate large intramolecular forces between carbamyl oxygens and protons, which GROMACS cannot resolve. Therefore these charges were lessened and labeled as the “Modified Charge” in Figure 4.16. The Nic-bound and CCh-bound mm_nachr proteins were also placed in periodic boxes containing solvation and counterions, as described above.

The three mm_nachr proteins (apo, Nic, and CCh bound) began with seven minimizations prior to the MD simulations:

- Minimization 1: Identical residues frozen, protein (ligand) strongly restrained
- Minimization 2: Identical residues frozen, protein backbone strongly restrained
- Minimization 3: Identical residues frozen, protein backbone weakly restrained
- Minimization 4: No residues frozen, identical residues strongly restrained
- Minimization 5: No residues frozen, identical residues weakly restrained
- Minimization 6: All non-hydrogen atoms strongly restrained
- Minimization 7: Completely unrestrained proteins

The resulting minimized structures were the basis for our MD simulations using the GROMACS force field. We began the MD simulations at 0 K, and slowly warmed up to 310 K, using a linear annealing function over the first 25 ps of simulation time. The protein (and ligand, when present) was held under strong restraints during the warm-up sequence and over the next 125 ps the restraints were relaxed. The system began to equilibrate (energies leveled out) after the first 1 ns of run time.

4.2.5 Computational Studies of the Mouse Muscle nAChR Binding Site

The mouse muscle homology model was used to evaluate several intrasubunit chemical interactions that form the agonist binding site. Previous mutagenesis studies demonstrated that interactions between muscle receptor D89 and loop B residues (Figure 4.17) influence the binding of ACh and epibatidine differently than Nic (58, 59). Incorporation of several unnatural amino acids at D89, Nha and Akp, and at loop B residues W149 and T150 (alpha hydroxy acids tryptophan alpha hydroxy acid (Wah) and

threonine alpha hydroxy acid (Tah), respectively) resulted in different EC₅₀ shifts for ACh, Epi, and Nic (59, 60).

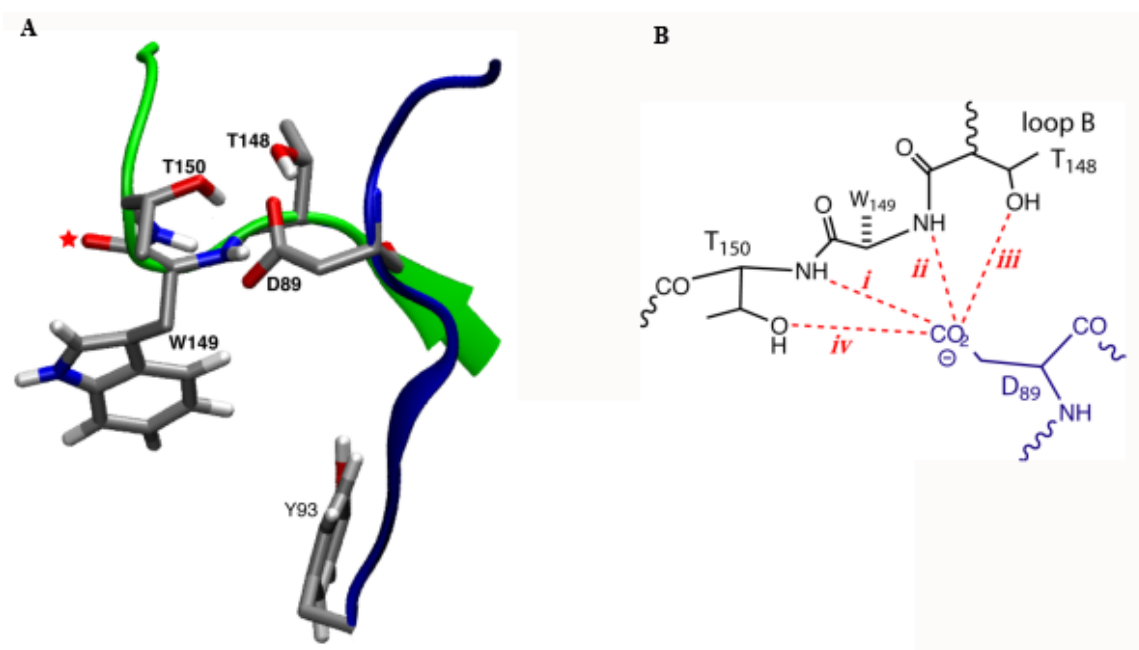


Figure 4.17 A) Image of the agonist binding site including the positioning of D89 and Loop B residues, T150 and T148. B) Schematic of potential hydrogen bonds (*i-iv*, red) between D89 (loop A, blue) and Loop B residues.

This hydrogen bonding network (Figure 4.17B) was perturbed most significantly by the D89N mutation, which eliminated the negative charge, eliminated a hydrogen bond, and introduced a possible dipole-dipole clash $\text{N}^{\delta-}-\text{H}^{\delta+}\cdots\text{H}^{\delta+}-\text{N}^{\delta-}$. This mutation increased EC₅₀ for both ACh and epibatidine, suggesting that hydrogen bonds *i* and *ii* were most influential during binding (Figure 4.17B). Additionally, double mutations between D89N/T150Tah and D89N/W149Wah were performed. The D89N/W149Wah mutation recovered wild type receptor activity, but D89N/T150Tah did not. These indicate that the hydrogen bonding network is asymmetric in its contributions to the agonist binding site (59, 60).

To further investigate this hydrogen bonding network the homology model of the mouse muscle extracellular domain was utilized to study these interactions. The mm_nachr models with CCh and without were used to monitor hydrogen bonds *i* through

iv analyzing both carboxylate oxygens (named OD1 and OD2) shown in Figure 18, resulting in a total of 8 possible hydrogen bonds. Two additional “control” hydrogen bonds within a well defined α helix were also monitored.

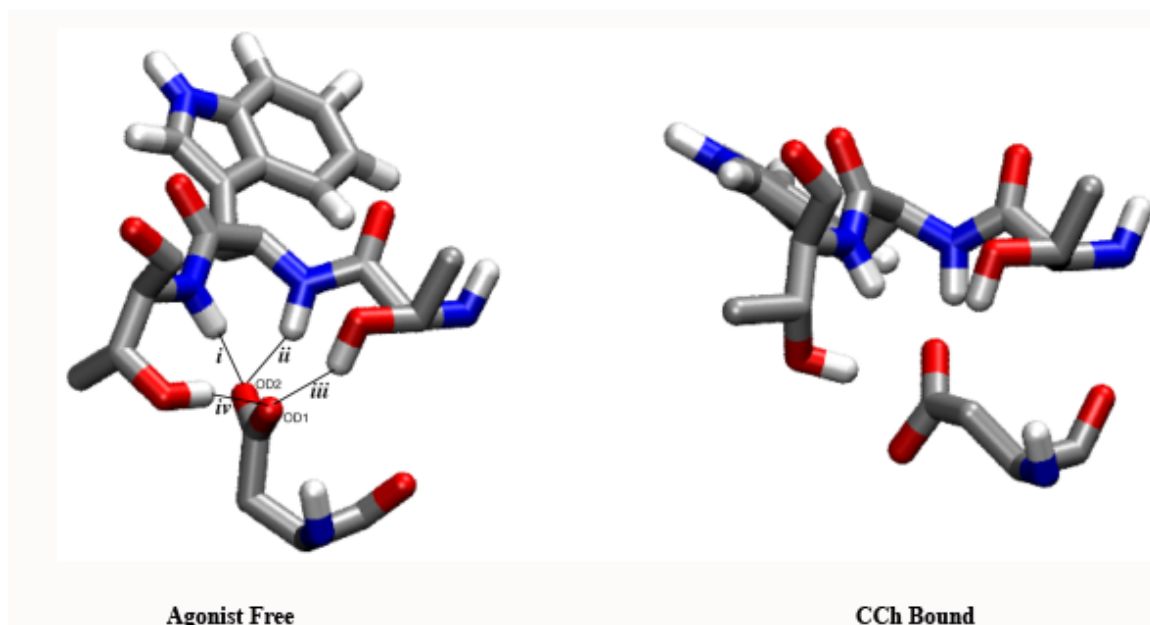


Figure 4.18. Agonist free and CCh bound structures of the mouse muscle agonist binding site from the homology model (mm_nachr). The structures were generated using the GROMACS g_cluster program taken from the final 500 ps of the 5ns mm_nachr MD simulations.

In the agonist free structure one of the carboxylate oxygens, OD2, makes hydrogen bonds with the backbone NH groups, *i* and *ii*. The other carboxylate, OD1, makes hydrogen bonds with the side chain hydroxyls, *iii* and *iv* (Figure 4.18). These are strong hydrogen bonds that frequently appear in the MD simulations, meaning they do not fluctuate (relative to the control hydrogen bonds). In contrast, when CCh is bound these hydrogen bonds begin to fluctuate significantly, being present only 34% of the time versus 94% in the agonist free structure. Overall, this difference is mostly observed between hydrogen bonds *i* and *ii* while *iii* and *iv* remain present (Figure 4.19). Additionally, the distance between D89 and W149 increases when agonist is bound. The MD simulations indicate that D89 is rotated into a less symmetrical position with respect to loop B upon agonist incorporation.

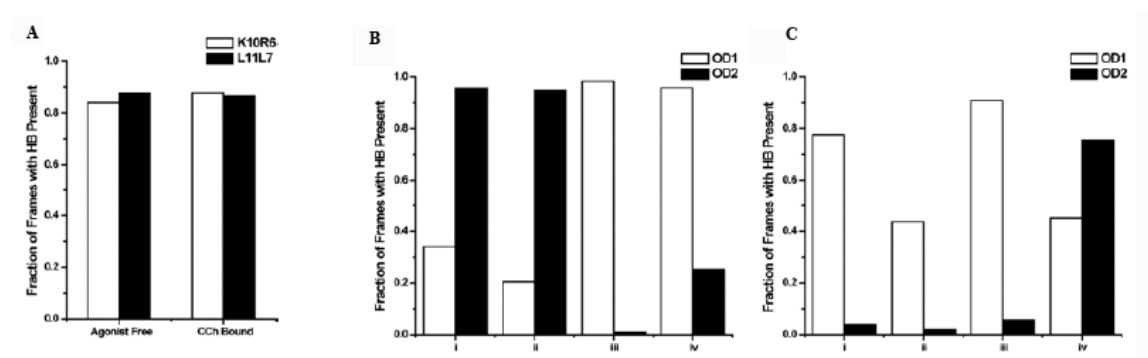


Figure 4.19 A) The “control” hydrogen bonds monitored between backbone amine of K10 and the backbone carbonyl of R6 (white bar) and backbone amide of L11 and backbone carbonyl of L7 (black bar). The hydrogen bonds (8) analyzed for the agonist free (B) structure and the CCh bound structure (C) are shown between OD1 (white) and OD2 (black) carboxylate oxygens. All of the data were acquired during the equilibrated final 500 ps of the 5 ns MD simulations. Data are expressed as the numbers of frames out of 1000 observed frames where the given hydrogen bond is present.

The mutagenesis studies performed by Sine and coworkers (58) established that the D89N mutation affects the kinetics of the association between the agonist and the unbound receptor. Therefore, we used our homology model to generate a new mm_nachr structure containing the D89N mutation, which we used for analysis of the hydrogen bonding network. We only constructed a model in the agonist free state since the mutation is implicated in the kinetics prior to agonist binding. Due to the orientation of the D89N mutation, we considered two different models labeled D89N1 and D89N2, which correspond to the positioning of the amide nitrogen relative to OD1 or OD2, respectively. Introduction of the D89N mutation disrupted the interactions between loop B and the side chain. In the agonist bound structure there are an average of 4.7 hydrogen bonds between the side chain and loop B, while in the D89N mutant there are ~1.5 hydrogen bonds (many are different than the original *i-iv*) (Table 4.4). These results indicate the importance of this hydrogen bonding network during agonist binding and establish important chemical-scale interactions between D89 and loop B.

Table 4.4 Molecular dynamics simulations of the D89/Loop B hydrogen bonds.

Structure	D89/Loop B Distance (Å) ^a	Mean # of D89/Loop B Hydrogen Bonds ^b	Loop B RMSD (wt vs. mutant) ^c
wt agonist free	4.3 ± 0.2	4.7 ± 0.8	-
wt CCh bound	5.2 ± 0.3	3.4 ± 0.8	-
D89N1	5.3 ± 0.3	1.6 ± 0.6	2.5 ± 0.1
D89N2	8.1 ± 0.5	1.5 ± 0.9	3.8 ± 0.3

All data were acquired over the last 500 ps of each simulation and are reported as the mean ± standard deviation. ^aDistance measured between D/N89 (γ carbon) to the W149 α carbon. ^bAll hydrogen bonds *i-iv* including both OD1 and OD2. ^cRMSD is calculated compared to the averaged last 500 ps from the agonist free wild type mm_nachr simulation. The average structure was determined using the program g_cluster.

4.3 Discussion and Conclusions

The muscle and neuronal nAChRs have many similarities, particularly with respect to the conservation of the aromatic box amino acids. However, there are many more subtle structural differences that contribute to agonist specificity, particularly nicotine, between these receptors that are a challenge to uncover. Conventional mutagenesis studies were performed to make nicotine a more potent agonist for the muscle nAChR. The introduction of a charged residue at αT196 provided the greatest increase in potency of the muscle nAChR for nicotine. Although this mutation does not equalize the muscle and neuronal nAChR potency for nicotine and ACh, this mutation provides enough of a shift so that analysis on the muscle receptor can be performed without using doses of nicotine that block the receptor. However, all of the mutations that increased the potency of nicotine increased that of ACh as well.

In the unnatural amino acid studies, it is surprising that altering the hydrogen bonding properties of several of the conserved residues in the extracellular domain of the nAChR did not alter agonist potency. This suggests that many of the conserved amino acids outside of the “box” are not as structurally important as the conserved residues that compose the agonist binding site. A more accurate description is that these outer box residues are important for shaping the agonist binding site, however individually they contribute less than the aromatic box residues to agonist binding.

After these initial studies, further mutagenesis was performed on several of these residues. One study evaluating the importance of backbone hydrogen bonds near the aromatic box discovered that the backbone N-H of S191 (one of the outer box mutations discussed above) makes an inter subunit hydrogen bond with the complementary face residues γ D174/ δ D180 after agonist binding (61). This residue is important for transferring crosstalk between the subunits that contribute to the agonist binding site.

Additionally, as discussed above, a series of mutagenesis studies was performed analyzing the hydrogen bonding network surrounding the aromatic box. These studies were performed on the loop A residue, D89, which is part of the highly conserved WxPD motif in loop A of the α subunit. These studies demonstrated that no single hydrogen bond was crucial for maintaining the structure of the agonist box, yet they all contribute to forming contacts between loops A and B. Additionally, it was determined that the charge on D89 did not interact with the cationic agonist, but instead contributed to a hydrogen bonding network with the backbone amides of α W149 and α T150. Differences were also observed between the more potent agonists ACh and epibatidine as compared with the less potent agonist nicotine. Nicotine only makes one contact with loop B (33), and perturbations between the D89 and loop B network do not shift EC₅₀ values of nicotine as much as they do for both ACh and epibatidine. Therefore, ACh and epibatidine are more sensitive to these perturbations and the outlying structure of the protein surrounding the binding site than nicotine.

The molecular dynamics simulations correlate well with the experimental data from our lab and others. Interestingly, the MD simulations suggest that D89 is positioned to interact with loop B in the agonist free structure and establishing more optimal interactions than in the carbamylcholine bound structure. Agonist binding (at least with CCh) does not dramatically shift the positioning of loop B, suggesting the agonist does not contribute to the structural orientation of the loop after binding. On the other hand, introduction of the D89N mutations into the simulation also reduces the number of interactions between loops A and B. When Asn is incorporated into the structure, loop B alters its conformation to accommodate the new side chain, however this changes its structural organization around the aromatic box. Our conclusion from these studies is

that the hydrogen bonding network between D89 and loop B originates to “preorganize” the aromatic box in anticipation of ligand binding (62).

Further advances and familiarity with unnatural amino acid mutagenesis have allowed for our exploration of structure/function studies with neuronal nicotinic receptors. These studies demonstrate that the cation- π interaction is conserved in the $\alpha 4\beta 2$ receptor where it contributes to the high affinity for both ACh and nicotine (43). The aromatic box is conserved in all receptors, and a cation- π interaction is present for both ACh and nicotine in the neuronal $\alpha 4\beta 2$ receptor, which has a high affinity for both agonists. Yet the muscle receptor does not utilize a cation- π interaction to bind the low affinity nicotine even though the same aromatic residues contribute to the binding site. These studies only reiterate the subtleties that contribute to the differences between nicotinic receptor subtypes.

In conclusion, all of the above studies indicate that the structural aspects of the acetylcholine receptor important for agonist specificity between muscle and neuronal types lie in the immediate vicinity outside of the “aromatic box”. These amino acids ultimately shape the box to accommodate the proper orientation of agonists important for necessary receptor function. It is likely that these residues also contribute to maintaining a preferred “preorganized” structure, optimal for ligand binding. Overall, many questions remain about the interactions involved in nicotine binding to the muscle and neuronal nAChRs, and continued studies probing receptor structure and function on the chemical-scale will enable our understanding of these important neuroreceptors.

4.4 Materials and Methods

4.4.1 Mutagenesis and Unnatural Amino Acid Suppression

The mouse muscle nAChR subunits, α , β , δ , and γ were all transcribed into mRNA from the pAMV vector as previously described (63) by *in vitro* runoff transcription using the Ambion (Austin, TX) T7 mMessage mMachine kit. Wild type mouse muscle nAChR subunits were injected in a 2:1:1:1 ratio; nonsense suppression experiments used a 10:1:1:1 ratio of α : β : δ : γ . Unnatural amino acids and aminoacyl-tRNA were prepared using previously reported methods and conjugated to the dCA dinucleotide as described (64). Aminoacyl tRNA was photolyzed (5 minutes) for deprotection prior to co-injection

with the mRNA (65). In several of the experiments noted above, the Leu9'Ser mutation in the β subunit ($\beta 9'$) was used to lower all EC_{50} values by approximately 40-fold (26, 66). Stage V-VI *Xenopus laevis* oocytes were injected with 50nL of mRNA/tRNA mixtures per injection. All oocytes used to study the nAChR were recorded in a Ca^{2+} -free ND96 solution (96 mM NaCl, 5 mM HEPES, 2 mM KCl, 1 mM $MgCl_2$).

4.4.2 Electrophysiology

All of the electrophysiological recordings were performed on the Axon Instruments, OpusXpress™. Stage V-VI *Xenopus laevis* oocytes were employed in all of the studies. Eight oocytes were simultaneously voltage clamped at -60 mV and dose-response relationships were obtained by delivery of various concentrations of ACh, nicotine, or Mg^{2+} in 1 mL aliquots. Oocytes were superfused with Ca^{2+} free ND96 solution at a flow rate of 1mL/min before application, 4mL/min during drug application, and washed at 3mL/min. Drug application was 15 s. Data were sampled at 125 Hz and filtered at 50 Hz. Acetylcholine and nicotine were purchased from Sigma/RBI/Aldrich. Epibatidine was purchased from Tocris as (\pm) epibatidine dihydrochloride. All the drugs were dissolved in sterile ddi water and diluted in Ca^{2+} free ND96. The data were analyzed using the Clampfit 9.0 software. The Hill equation was used to fit data where $I/I_{max} = 1/(1+(EC_{50}/[A])^{n_H})$, I is current peak at drug concentration (A), EC_{50} is the concentration of drug that activates 50% of the maximal response, and n_H is the hill coefficient.

4.4.3 Mouse Muscle Homology Model of D89N Mutant Structures

The D89N mutation was introduced into the mouse muscle homology model by mutating $\alpha 89$ to Asn in the PDB file of both α subunits in SwissPDB viewer. The two structures differed in the positioning of the NH_2 group of the side chain, D89N1 placed the NH_2 group in the same position as the OD1 group of the wild type mm_nachr structure, and D89N2 placed the NH_2 group in position with OD2. The D89N mm_nachr models were placed in a hexagonal periodic box, solvated, and treated using the same protocol developed for the wild type model.

All five of the mm_nachr structures (agonist free wt, CCh wt, nicotine wt, D89N agonist free, and D89 CCh) were treated similarly. The MD simulations were started at 0

K and warmed to 310 K over the first 25 ps of the run. Large restraints were used at first for both the protein and drug (if applicable) and slowly released over the next 100 ps. Then the protein was run unrestrained for an additional 5000 ps (wt) or 7500 ps (D89N structures). The D89N structures were generated with Michael M. Torrice and the analysis of the bonding network from g_cluster was performed by M.M.T (60, 67). The $\alpha 7$ homology model and molecular dynamics simulations were performed by E. James Petersson (51).

All of the molecular dynamics simulations were analyzed over the final 500 ps of trajectories to ensure equilibration of the system energies. Each of the trajectory files analyzed contained data for every 0.5 ps, producing 1000 frames/simulation. The programs g_dist and g_hbond within GROMACS were used to analyze distances and hydrogen bonds. The default cutoffs for determining hydrogen bonds were a distance of 3.5 Å with an acceptor-donor angle of 30°. RMSD values were calculated using g_rms and compared to the final 500 ps of data from the wild type, agonist free mm_nachr structure using g_cluster.

4.5 Cited References

1. Sine, S. M., and Engel, A. G. (2006) Recent advances in Cys-loop receptor structure and function, *Nature* 440, 448-455.
2. Changeux, J. P. (1983) Concluding remarks: on the "singularity" of nerve cells and its ontogenesis, *Prog Brain Res* 58, 465-478.
3. Changeux, J. P., Bon, F., Cartaud, J., Devillers-Thiery, A., Giraudat, J., Heidmann, T., Holton, B., Nghiem, H. O., Popot, J. L., Van Rapenbusch, R., and et al. (1983) Allosteric properties of the acetylcholine receptor protein from *Torpedo marmorata*, *Cold Spring Harb Symp Quant Biol* 48 Pt 1, 35-52.
4. Corringer, P. J., Le Novère, N., and Changeux, J. P. (2000) Nicotinic receptors at the amino acid level, *Annu Rev Pharmacol Toxicol* 40, 431-458.
5. Cassels, B. K., Bermudez, I., Dajas, F., Abin-Carriquiry, J. A., and Wonnacott, S. (2005) From ligand design to therapeutic efficacy: the challenge for nicotinic receptor research, *Drug Discov Today* 10, 1657-1665.
6. Ballivet, M., Patrick, J., Lee, J., and Heinemann, S. (1982) Molecular cloning of cDNA coding for the gamma subunit of *Torpedo* acetylcholine receptor, *Proc Natl Acad Sci U S A* 79, 4466-4470.
7. Giraudat, J., Devillers-Thiery, A., Auffray, C., Rougeon, F., and Changeux, J. P. (1982) Identification of a cDNA clone coding for the acetylcholine binding subunit of *Torpedo marmorata* acetylcholine receptor, *EMBO J* 1, 713-717.
8. Noda, M., Furutani, Y., Takahashi, H., Toyosato, M., Hirose, T., Inayama, S., Nakanishi, S., and Numa, S. (1982) Cloning and sequence analysis of cDNA for bovine adrenal preproenkephalin, *Nature* 295, 202-206.
9. Toyoshima, C., and Unwin, N. (1988) Ion channel of acetylcholine receptor reconstructed from images of postsynaptic membranes, *Nature* 336, 247-250.
10. Unwin, N., Toyoshima, C., and Kubalek, E. (1988) Arrangement of the acetylcholine receptor subunits in the resting and desensitized states, determined by cryoelectron microscopy of crystallized *Torpedo* postsynaptic membranes, *J Cell Biol* 107, 1123-1138.
11. Smit, A. B., Syed, N. I., Schaap, D., van Minnen, J., Klumperman, J., Kits, K. S., Lodder, H., van der Schors, R. C., van Elk, R., Sorgedrager, B., Brejc, K., Sixma, T. K., and Geraerts, W. P. (2001) A glia-derived acetylcholine-binding protein that modulates synaptic transmission, *Nature* 411, 261-268.
12. Unwin, N. (2005) Refined structure of the nicotinic acetylcholine receptor at 4Å resolution, *J Mol Biol* 346, 967-989.
13. Grutter, T., and Changeux, J. P. (2001) Nicotinic receptors in wonderland, *Trends Biochem Sci* 26, 459-463.
14. Karlin, A. (2002) Emerging structure of the nicotinic acetylcholine receptors, *Nat Rev Neurosci* 3, 102-114.
15. Damle, V. N., and Karlin, A. (1980) Effects of agonists and antagonists on the reactivity of the binding site disulfide in acetylcholine receptor from *Torpedo californica*, *Biochemistry* 19, 3924-3932.
16. Czajkowski, C., Kaufmann, C., and Karlin, A. (1993) Negatively charged amino acid residues in the nicotinic receptor delta subunit that contribute to the binding of acetylcholine, *Proc Natl Acad Sci U S A* 90, 6285-6289.

17. Arias, H. R. (1997) Topology of ligand binding sites on the nicotinic acetylcholine receptor, *Brain Res Brain Res Rev* 25, 133-191.
18. Galzi, J. L., Bertrand, D., Devillers-Thiery, A., Revah, F., Bertrand, S., and Changeux, J. P. (1991) Functional significance of aromatic amino acids from three peptide loops of the alpha 7 neuronal nicotinic receptor site investigated by site-directed mutagenesis, *FEBS Lett* 294, 198-202.
19. Galzi, J. L., Revah, F., Bouet, F., Menez, A., Goeldner, M., Hirth, C., and Changeux, J. P. (1991) Allosteric transitions of the acetylcholine receptor probed at the amino acid level with a photolabile cholinergic ligand, *Proc Natl Acad Sci U S A* 88, 5051-5055.
20. Ma, J. C., and Dougherty, D. A. (1997) The Cation-minus sign-pi Interaction, *Chem Rev* 97, 1303-1324.
21. Zhong, W., Gallivan, J. P., Zhang, Y., Li, L., Lester, H. A., and Dougherty, D. A. (1998) From ab initio quantum mechanics to molecular neurobiology: a cation-pi binding site in the nicotinic receptor, *Proc Natl Acad Sci U S A* 95, 12088-12093.
22. Brejc, K., van Dijk, W. J., Klaassen, R. V., Schuurmans, M., van Der Oost, J., Smit, A. B., and Sixma, T. K. (2001) Crystal structure of an ACh-binding protein reveals the ligand-binding domain of nicotinic receptors, *Nature* 411, 269-276.
23. Smit, A. B., Brejc, K., Syed, N., and Sixma, T. K. (2003) Structure and function of AChBP, homologue of the ligand-binding domain of the nicotinic acetylcholine receptor, *Ann N Y Acad Sci* 998, 81-92.
24. Dougherty, D. A., and Lester, H. A. (2001) Neurobiology. Snails, synapses and smokers, *Nature* 411, 252-253, 255.
25. Sullivan, D. A., and Cohen, J. B. (2000) Mapping the agonist binding site of the nicotinic acetylcholine receptor. Orientation requirements for activation by covalent agonist, *J Biol Chem* 275, 12651-12660.
26. Beene, D. L., Brandt, G. S., Zhong, W., Zacharias, N. M., Lester, H. A., and Dougherty, D. A. (2002) Cation-pi interactions in ligand recognition by serotonergic (5-HT_{3A}) and nicotinic acetylcholine receptors: the anomalous binding properties of nicotine, *Biochemistry* 41, 10262-10269.
27. Le Novère, N., Grutter, T., and Changeux, J. P. (2002) Models of the extracellular domain of the nicotinic receptors and of agonist- and Ca²⁺-binding sites, *Proc Natl Acad Sci U S A* 99, 3210-3215.
28. Schapira, M., Abagyan, R., and Totrov, M. (2002) Structural model of nicotinic acetylcholine receptor isotypes bound to acetylcholine and nicotine, *BMC Struct Biol* 2, 1.
29. Celie, P. H., van Rossum-Fikkert, S. E., van Dijk, W. J., Brejc, K., Smit, A. B., and Sixma, T. K. (2004) Nicotine and carbamylcholine binding to nicotinic acetylcholine receptors as studied in AChBP crystal structures, *Neuron* 41, 907-914.
30. Gerzanich, V., Peng, X., Wang, F., Wells, G., Anand, R., Fletcher, S., and Lindstrom, J. (1995) Comparative pharmacology of epibatidine: a potent agonist for neuronal nicotinic acetylcholine receptors, *Mol Pharmacol* 48, 774-782.
31. Lindstrom, J., Anand, R., Peng, X., Gerzanich, V., Wang, F., and Li, Y. (1995) Neuronal nicotinic receptor subtypes, *Ann N Y Acad Sci* 757, 100-116.

32. Akk, G., and Auerbach, A. (1999) Activation of muscle nicotinic acetylcholine receptor channels by nicotinic and muscarinic agonists, *Br J Pharmacol* 128, 1467-1476.
33. Cashin, A. L., Petersson, E. J., Lester, H. A., and Dougherty, D. A. (2005) Using physical chemistry to differentiate nicotinic from cholinergic agonists at the nicotinic acetylcholine receptor, *J Am Chem Soc* 127, 350-356.
34. Mayo, S. L., Olafcon, B. D., and Goddard, W. A., III. (1990) *J. Phys. Chem.* 94, 8897-8909.
35. Springer-Verlag Lindahl, E. H., B.; van der Spoel, D. (2001) *J. Mol. Modeling* 7, 306-317.
36. Chipot, C. M., B.; Pearlman, D. A.; Kollman, P. A. (1996) *J. Am. Chem. Soc.* 118, 2998-3005.
37. Caldwell, J. W., Kollman, P. A. (1995) *J. Am. Chem. Soc.* 117, 4177-4178.
38. Changeux, J. P. (2009) Nicotinic receptors and nicotine addiction, *C R Biol* 332, 421-425.
39. Hogg, R. C., Raggenbass, M., and Bertrand, D. (2003) Nicotinic acetylcholine receptors: from structure to brain function, *Rev Physiol Biochem Pharmacol* 147, 1-46.
40. Millar, N. S., and Gotti, C. (2009) Diversity of vertebrate nicotinic acetylcholine receptors, *Neuropharmacology* 56, 237-246.
41. Rush, R., Kuryatov, A., Nelson, M. E., and Lindstrom, J. (2002) First and second transmembrane segments of alpha3, alpha4, beta2, and beta4 nicotinic acetylcholine receptor subunits influence the efficacy and potency of nicotine, *Mol Pharmacol* 61, 1416-1422.
42. Chavez-Noriega, L. E., Gillespie, A., Stauderman, K. A., Crona, J. H., Claeps, B. O., Elliott, K. J., Reid, R. T., Rao, T. S., Velicelebi, G., Harpold, M. M., Johnson, E. C., and Corey-Naeve, J. (2000) Characterization of the recombinant human neuronal nicotinic acetylcholine receptors alpha3beta2 and alpha4beta2 stably expressed in HEK293 cells, *Neuropharmacology* 39, 2543-2560.
43. Xiu, X., Puskar, N. L., Shanata, J. A., Lester, H. A., and Dougherty, D. A. (2009) Nicotine binding to brain receptors requires a strong cation-pi interaction, *Nature* 458, 534-537.
44. Filatov, G. N., and White, M. M. (1995) The role of conserved leucines in the M2 domain of the acetylcholine receptor in channel gating, *Mol Pharmacol* 48, 379-384.
45. Labarca, C., Nowak, M. W., Zhang, H., Tang, L., Deshpande, P., and Lester, H. A. (1995) Channel gating governed symmetrically by conserved leucine residues in the M2 domain of nicotinic receptors, *Nature* 376, 514-516.
46. Revah, F., Bertrand, D., Galzi, J. L., Devillers-Thiery, A., Mulle, C., Hussy, N., Bertrand, S., Ballivet, M., and Changeux, J. P. (1991) Mutations in the channel domain alter desensitization of a neuronal nicotinic receptor, *Nature* 353, 846-849.
47. Prince, R. J., and Sine, S. M. (1996) Molecular dissection of subunit interfaces in the acetylcholine receptor. Identification of residues that determine agonist selectivity, *J Biol Chem* 271, 25770-25777.

48. Gao, F., Bren, N., Burghardt, T. P., Hansen, S., Henchman, R. H., Taylor, P., McCammon, J. A., and Sine, S. M. (2005) Agonist-mediated conformational changes in acetylcholine-binding protein revealed by simulation and intrinsic tryptophan fluorescence, *J Biol Chem* 280, 8443-8451.
49. Henchman, R. H., Wang, H. L., Sine, S. M., Taylor, P., and McCammon, J. A. (2003) Asymmetric structural motions of the homomeric alpha7 nicotinic receptor ligand binding domain revealed by molecular dynamics simulation, *Biophys J* 85, 3007-3018.
50. Henchman, R. H., Wang, H. L., Sine, S. M., Taylor, P., and McCammon, J. A. (2005) Ligand-induced conformational change in the alpha7 nicotinic receptor ligand binding domain, *Biophys J* 88, 2564-2576.
51. Petersson, E. J. (2005) Investigations of ion channel structure and function. I. Studies of nicotine binding to the acetylcholine receptor. II. Development of tools for studying learning and memory with unnatural amino acids., in *Chemistry and Chemical Engineering*, Caltech, Pasadena.
52. Notredame, C., Higgins, D. G., and Heringa, J. (2000) T-Coffee: A novel method for fast and accurate multiple sequence alignment, *J Mol Biol* 302, 205-217.
53. Schrodinger, I. Prime, Portland, OR.
54. Guex, N., and Peitsch, M. C. (1997) SWISS-MODEL and the Swiss-PdbViewer: an environment for comparative protein modeling, *Electrophoresis* 18, 2714-2723.
55. van der Spoel, D., Lindahl, E., Hess, B., van Buuren, A.R., Apol, E., Meulenhoff, P.J., Tieleman, D.P., Sijbers, A.L.T.M., Feenstra, K.A., R., v. D., and Berendsen, H.J.C. (2004) Gromacs User Manual Version 3.2.
56. Schuettelkopf, A. W., and F., v. A. D. M., . (2004) *Acta Crystal D60*, 1355-1363.
57. Breneman, C. M. a. W., K.B. (1990) Determining atom-centered monopoles from molecular electrostatic potentials. The need for high sampling density in formamide conformational analysis., *J. Comp. Chem.* 11, 361-373.
58. Lee, W. Y., and Sine, S. M. (2004) Invariant aspartic Acid in muscle nicotinic receptor contributes selectively to the kinetics of agonist binding, *J Gen Physiol* 124, 555-567.
59. Cashin, A. L. (2006) Chemical scale investigations of drug-receptor interactions at the nicotinic acetylcholine receptor., in *Chemistry and Chemical Engineering*, California Institute of Technology, Pasadena, CA.
60. Torrice, M. M. (2008) Chemical-scale studies of the nicotinic and muscarinic acetylcholine receptors, in *Chemistry and Chemical Engineering*, California Institute of Technology, Pasadena, CA.
61. Gleitsman, K. R., Kedrowski, S. M., Lester, H. A., and Dougherty, D. A. (2008) An intersubunit hydrogen bond in the nicotinic acetylcholine receptor that contributes to channel gating, *J Biol Chem* 283, 35638-35643.
62. Cram, D. J. (1986) Preorganization-From Solvents to Spherands, *Angewandte Chemie-International Edition in English* 25, 1039-1057.
63. Nowak, M. W., Gallivan, J. P., Silverman, S. K., Labarca, C. G., Dougherty, D. A., and Lester, H. A. (1998) In vivo incorporation of unnatural amino acids into ion channels in *Xenopus* oocyte expression system, *Methods Enzymol* 293, 504-529.

64. England, P. M., Lester, H.A., and Dougherty, D.A. (1999) Incorporation of esters into proteins: improved synthesis of the hydroxyacyl tRNAs., *Tetrahedron Letters* 40, 6189-6192.
65. Saks, M. E., Sampson, J. R., Nowak, M. W., Kearney, P. C., Du, F., Abelson, J. N., Lester, H. A., and Dougherty, D. A. (1996) An engineered *Tetrahymena* tRNA^{Gln} for in vivo incorporation of unnatural amino acids into proteins by nonsense suppression, *J Biol Chem* 271, 23169-23175.
66. Kearney, P. C., Nowak, M. W., Zhong, W., Silverman, S. K., Lester, H. A., and Dougherty, D. A. (1996) Dose-response relations for unnatural amino acids at the agonist binding site of the nicotinic acetylcholine receptor: tests with novel side chains and with several agonists, *Mol Pharmacol* 50, 1401-1412.
67. Cashin, A. L., Torrice, M. M., McMenimen, K. A., Lester, H. A., and Dougherty, D. A. (2007) Chemical-scale studies on the role of a conserved aspartate in preorganizing the agonist binding site of the nicotinic acetylcholine receptor, *Biochemistry* 46, 630-639.

Appendix A:

Studies of Ionotropic Glutamate Receptors in Mammalian Cells

A.1 Introduction

The use of nonsense suppression to incorporate unnatural amino acids into ion channels has greatly enhanced our ability to probe structure/function relationships in many different ion channels, from Cys-loop ligand-gated ion channels (LGICs) to ionotropic glutamate receptors and GPCRs (1-5). One large hurdle for nonsense suppression has been the expansion of this technique into mammalian cells. There are clear benefits to performing structure/function studies in mammalian cells not limited to the opportunity to use a more relevant biological system and the ability to study complex signaling networks. Generally, the *Xenopus laevis* oocyte is the primary heterologous expression system utilized for these studies, primarily due to ease of experimental procedure. Injection of DNA, mRNA, and aminoacyl tRNA into an oocyte (1 mm diameter) is much easier than transferring these material into very small, thin, and transparent mammalian cells. Early studies were able to incorporate small amounts of DNA, mRNA, and aminoacyl tRNA into mammalian cells using an electroporation protocol (6).

These protocols were difficult to perform, particularly in a high throughput manner. Additionally, electrophysiological assays performed on a single mammalian cell are not adapted for high-throughput structure/function analysis. Another complication arises due to the availability of the “limiting reagent,” aminoacyl tRNA. In order to electroporate mammalian cells, a small dish of adherent cells are used, but within that dish are approximately 5,000 cells. Electroporation results in only several hundred viable cells, an inefficient use of materials. In order to develop the mammalian cell method, we attempted to use new techniques to increase efficiency of transfection and assay analysis. The techniques we utilized in this study were the gene gun (for DNA transfection) and the Flexstation® as a high throughput assay of dose-response relationships.

The gene gun was initially developed as a biolistic particle delivery system for use in transformations performed on plants (7, 8). It is a mechanical method for transfecting cells that involves high-speed propulsion of subcellular particles coated with DNA/RNA/tRNA into cells. One feature of biolistic transfection is that the biochemical

nature of the material does not influence the transfection (i.e. being a lipid, etc.), which is a great advantage to the system. Additionally, more than one type of DNA (or additional biological molecule) may be introduced during the transfection. One of the most relevant advantages to this method is its efficiency, which has been demonstrated to be 160-fold more effective than lipofection, 189-fold more than electroporation, and 450-fold more effective than calcium phosphate precipitation, when analyzed by a luciferase activity assay (9). Recently, methods using the gene gun have been developed for transfections in mammalian cells and tissue slices, expanding this efficient transfection method to many different cell types (10-12). Three basic steps are required to use the gene gun; 1) coating the microcarriers with DNA or other biological material, 2) transferring the microcarriers to a cartridge used to make a “bullet,” and 3) firing the microcarriers into a mammalian cell using a pulse of helium gas (12).

Using a gene gun requires a hand held gun, such as the Bio-Rad Helios gene gun (used in the studies below). Several metal particles are often used for the microcarriers, such as gold and tungsten. We utilized gold particles due to their uniformity of size and shape and the increased stability of DNA on gold. The microcarriers are turned into a cartridge by attaching them to the inside of a piece of tubing. The cartridges are loaded into the gun and using an inert, diffusible, and low-density gas propellant (typically helium), the microcarriers are stripped from the cartridge and delivered into the cells.

Increasing transfection efficiency is one issue we wanted to address during our experiments with incorporating unnatural amino acids into mammalian cells. The other issue, developing a high-throughput assay, was the second. A new high-throughput system developed for studying mammalian cells was the Flexstation®, produced by Molecular Devices (Sunnyvale, CA). It is a fluorometric plate reader with a fluid transfer system. When used with reagents, such as the Membrane Potential Assay Kit® (Molecular Devices), devised for FLIPR (fluorometric imaging plate reader) and Flexstation®, a change in membrane potential (membrane potential dyes) can be observed and recorded. One advantage to these dyes is their sensitivity and fast response times, enabling accurate detection of changes in membrane potential due to ion channel activation. This membrane potential assay has been utilized in place of traditional patch clamping data (13-15).

Project Goals

The structure/function studies we envisioned for our mammalian cell experiments paralleled our previous studies of glutamate receptors in *Xenopus* oocytes (Chapter 2). Our goal was to generate NMDA receptors containing the homotyrosine mutation in the ligand-binding domain, and observe results re-confirming the previously determined relationship between clamshell closure and ligand efficacy. Ultimately, we wanted to use wild type NR1a/NR2B and NR1a/NR2BY705TAG THG73-hTyr NMDA receptors, expressed in human embryonic kidney (HEK293) cells. For our initial experiments, we tested the wild type NR1a/NR2B and NR1a/NR2BY705F mutant NMDA receptors. Although we wanted to perform experiments with the NMDA receptors, we also tested Cys-loop receptors (glycine and 5-HT₃) to gain more experience using the fluorescence assays and the Flexstation®.

A.2 Results and Discussion

Previous studies by K.L. Price and S.C.R. Lummis (University of Cambridge) demonstrated that the Cys-loop LGIC, 5-HT₃, could be studied using both Ca²⁺ and membrane potential-sensitive dyes on the Flexstation® (16). We utilized these methods for our examination of the NMDA receptor. The NMDAR experiments did not require the use of aminoacyl tRNA, therefore standard cell electroporation was utilized for transfection of wild type and mutant (NR1a/NR2BY705F) DNA into HEK293 cells. All of the NMDARs were transfected as cDNA and were in the pcDNA3.1 vector optimized for mammalian cell expression. To optimize the transfection efficiency we used the Nucleofector® System from AMAXA Biosystems (Lonza Walkersville Inc., Walkersville, MD). This system allows for direct transfection into the nucleus using electroporation.

Gene Gun Transfection

The gene gun was utilized to co-transfect the LGIC, 5-HT₃AS183TAG cDNA and THG-73-Lah (leucine alpha hydroxy acid) into HEK293 cells. These experiments were performed with John O'Brien and S.C.R. Lummis at the University of Cambridge, Laboratory of Molecular Biology. Using the protocol developed by O'Brien and Lummis (11, 12) we generated functional 5-HT₃ mutant receptors that responded to 5-HT (5-hydroxytryptamine) also known as serotonin.

Flexstation Analysis of Ligand Gated Ion Channels

We analyzed both wild type NMDA and 5-HT₃ receptors using the Flexstation. All of the cells were plated in 96-well plates designed for the fluorescence plate reader. Two different assay kits, the Membrane Potential Assay Kit and the Calcium Assay Kit (both from Molecular Devices), were used to analyze the response of the LGICs to varying drug applications. All cells were treated with the Flexstation buffer (see methods) optimized for use on the Flexstation. The buffer is used to wash the cells plated in 96-well plates (3X) prior to incubation with the fluorescent dyes. The dyes are also mixed with the Flexstation buffer (Methods) for dilution. The dyes are diluted as indicated by the protocols provided and incubated for 45 minutes (total) after addition to the cells in 96-well plates. The first 35 minutes the plates are stored in the dark at 37°C, followed by a 10-minute incubation at room temperature (~25°C).

The agonist solutions used for NMDA receptor activation were either glutamate and glycine or a NMDA/glycine combination. The agonists were always co-applied at 3X the desired final concentration. For example, to apply a 300 μ M glutamate dose, a 900 μ M sample was prepared. The concentrations of agonist are added at [3X] and added in 25 μ L aliquots to the wells, which already contain 125 μ L of solution prior to agonist (drug) application. The same protocol was used for serotonin applications.

Flexstation Acquired Data

Transformation of NMDA receptors expressed in HEK293 cells always resulted in unhealthy cell cultures. The cells would lose adhesion to the plates and become misshapen and often died. When these cells were put in the Flexstation and glutamate

and glycine were applied, often no change in membrane potential was observed. The FLIPR membrane potential assay kit measures a change in the potential across the cell membrane. Hyperpolarization results in less dye inside the cells and leads to a decrease in the signal. Membrane depolarization results in more dye inside the cells and leads to an increase in fluorescence signal. The signal is measured in relative fluorescent units (RFU). Previous experiments with 5-HT₃ receptors produced RFUs of ~5000 to 10,000. The studies with NMDA receptors did not result in consistent results and often the largest concentrations of agonist that were applied (glutamate and glycine) resulted in the largest decrease in fluorescence, indicating cell death (Figure A.1). The responses were inconsistent and further work will be required to increase cell viability after NMDA receptor transfections.

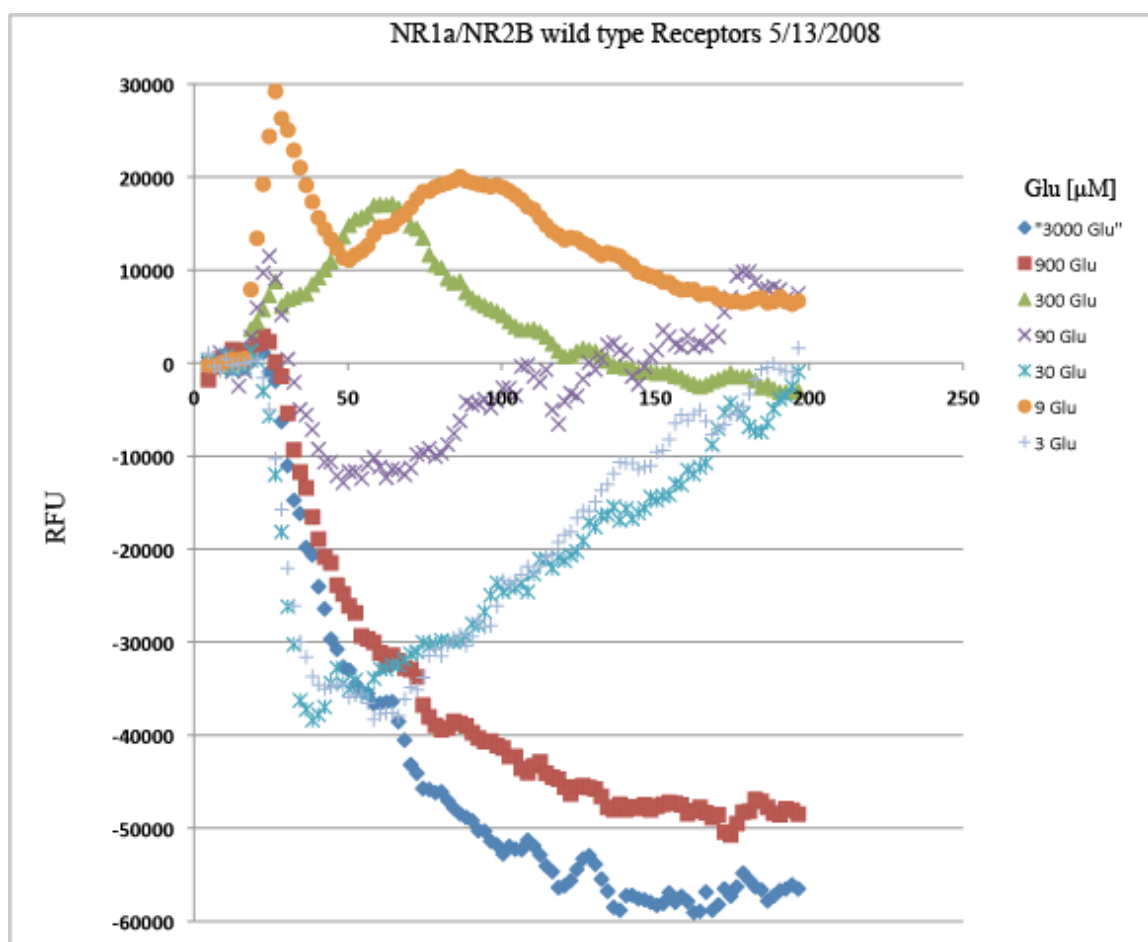


Figure A.1 Wild type NR1a/NR2B receptors response in cells on the Flexstation. The concentrations of glutamate are provided and always given in the presence of 30 μ M glycine.

Although we continued to study the NMDA receptors, in order to gain more experience with the fluorescence assays and the Flexstation, we studied wild type 5-HT₃ receptors and the mutation, 5-HT₃A S183TAG Lah-THG73, which were transfected using the gene gun. The wild type 5-HT₃ receptors responded to concentrations of serotonin as expected (Figure A.2). The RFU signal increases as the concentration of applied 5-HT increases.

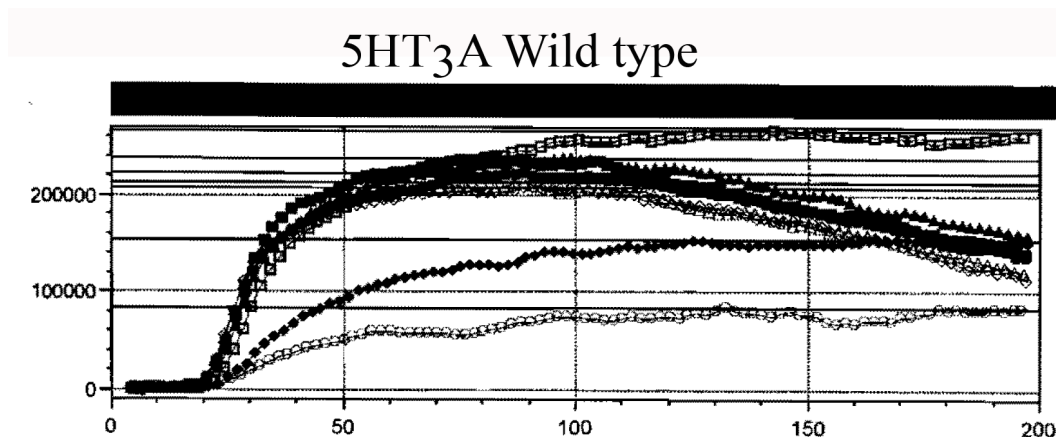


Figure A.2 Wild type 5-HT₃A receptors responding to increasing concentrations of serotonin. All fluorescence measurements are well above 0 RFU (the bottom axis). The largest signals appear over 20,000 RFU, (RFU = y-axis).

Similar results were observed for the 5-HT₃A S183Lah mutation. We only had enough of the aminoacyl Lah-THG73 tRNA to perform one injection with the gene gun, so our goal was to determine if this was a viable method of transfection. We did observe suitable receptor expression. We observed increasing RFU values as the concentration of applied 5-HT increased, similar to wild type 5-HT₃A receptors (Figure A.3).

Control experiments were performed to ensure that untransfected cells (Figure A.4) and cells transfected with only aminoacyl tRNA (Figure A.5) did not produce signals on the Flexstation. These results demonstrated no response in relative fluorescence units in response to varying doses of 5-HT. A very small amount of RFU was detected for one 5-HT application on the tRNA only cells (Figure A.5), which is an anomaly and likely undetectable when compared to cells expressing viable receptors.

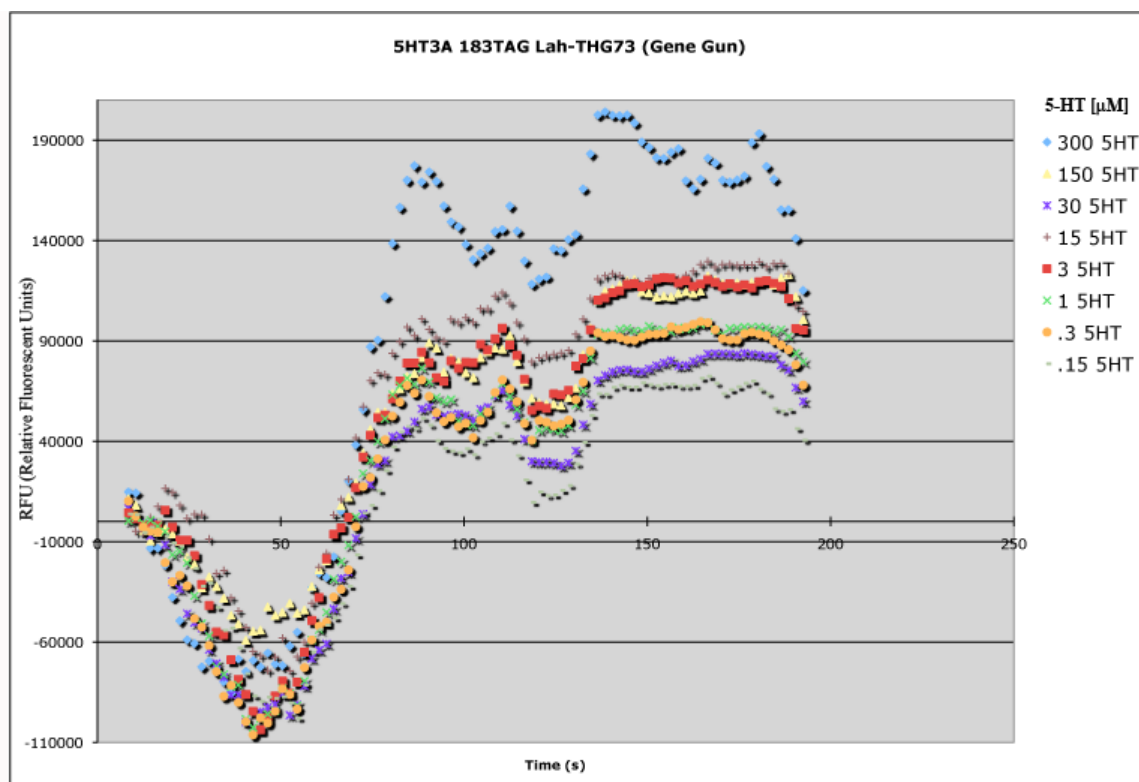


Figure A.3 Fluorescent responses from 5HT₃A S183TAG Lah-THG-73 mutant receptors to varying concentrations of serotonin. Both the cDNA and aminoacyl tRNA were transfected using the gene gun.

These results establish that we can generate viable cells via transfection with the gene gun, and that the Flexstation is a useful tool for high-throughput analysis of mammalian cells expressing ion channels via nonsense suppression. These studies should enable future experimentation of effective methods for transfecting aminoacyl tRNA and other biological compounds into mammalian cells. Additionally, our results suggest that using the Flexstation for analysis of ion channels expressed in mammalian cell lines is an effective, high-throughput strategy to parallel our other studies using the OpusXpress and oocytes. Further method development should optimize these procedures for use of mammalian cells to study a variety of LGICs.

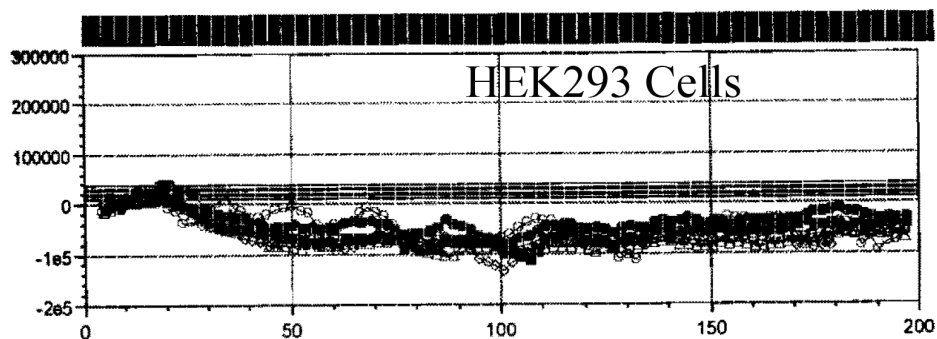


Figure A.4 Flexstation measurements of untransfected HEK293 cells to varying concentrations of 5-HT. No fluorescence was observed, as all above measurements are below zero.

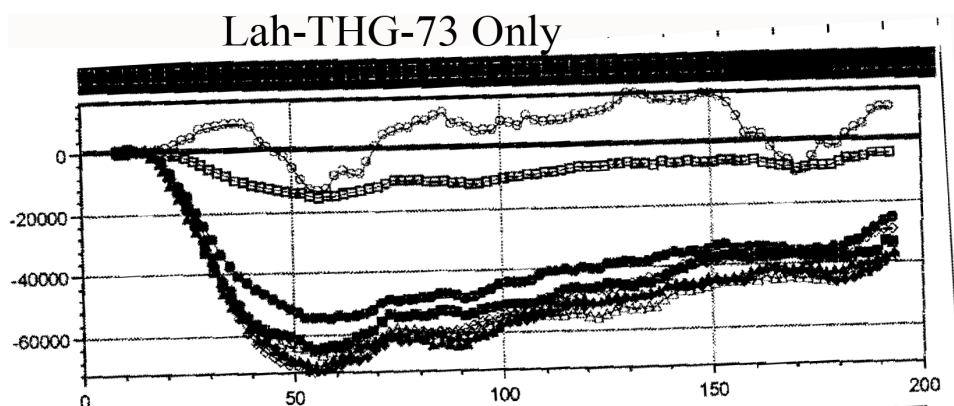


Figure A.5 Flexstation measurements of HEK293 cells transfected with Lah-THG73 tRNA only. No relative fluorescence was observed except for with the first concentration of 5-HT applied.

A.3 Methods

Protocol for NMDAR Transfections:

The following protocol was used:

- 1) Trypsin Digest 35 mm dish of HEK293 cells
 - a) add 1-2 mL EDTA, rinse and remove media
 - b) Mix trypsin w/ EDTA and add 1mL/35 mm plate, let sit for 5 minutes
- 2) Rinse cells with 5 mL media and resuspend 1 mL of cells in 15 mL media in a separate culture tube
- 3) Spin at 1000 rpm for 5 min.
- 4) Remove media (pellet should remain at the bottom of the tube)

5)*For use with AMAXA electroporator. Add 100 uL of Solution V to pellet of HEK293 cells and mix

a) Add DNA to solution with cells (1.0 µg/mL and add total of 5 µL cDNA, 2.5 µL of NR1a and 2.5 µL NR2B)

6) Put cells + Solution V + cDNA (~120 µL) into AMAXA cuvette

7) Electroporate with AMAXA

8) Remove cells with 1 mL warm media and resuspend in 15 mL culture tube

9) Plate into 96-well Flexstation® plate. 1.8 mL of cells/media get used per 3 rows of wells. 1 drop/plate well, using 5 mL pipette.

Gene Gun Protocol

The protocols outlined in O'Brien and Lummis (11, 12) were adapted for our experiments with aminoacyl tRNA. Microcarriers constructed from gold particles were used. cDNA was plated on a 1.0 µM diameter particle (Bio-Rad) by placing all material in a 1.5 mL microfuge tube and adding 50 µL spermidine with 25 µL cDNA (1 mg/mL) for transfection and 25 µL Lah-THG73 (1 µg/µL). The tube is vortexed and then 50 µL of 1 M CaCl₂ is added dropwise. This solution is incubated at room temperature for 5 min. then centrifuged for 3 sec. at 3000 rpm. Bullets were prepared as described in O'Brien and Lummis (11, 12).

Flexstation Buffer:

	Concentration (mM)	Volume mL (total of 100 mL)
Na ⁺	115	11.5
Ca ²⁺	1	1
K ⁺	1	1
Mg ²⁺	1	1
HEPES	10	10
Glucose	0.9	0.9
H ₂ O	-	74.6

*All of the cations are in solution with Cl⁻ counter ions.

Flexstation Data Workup

All data acquired on the Flexstation was analyzed in Excel (Microsoft).

A.4 Cited References

1. Beene, D. L., Brandt, G. S., Zhong, W., Zacharias, N. M., Lester, H. A., and Dougherty, D. A. (2002) Cation- π interactions in ligand recognition by serotonergic (5-HT_{3A}) and nicotinic acetylcholine receptors: the anomalous binding properties of nicotine, *Biochemistry* 41, 10262-10269.
2. Lummis, S. C., Beene, D. L., Lee, L. W., Lester, H. A., Broadhurst, R. W., and Dougherty, D. A. (2005) Cis-trans isomerization at a proline opens the pore of a neurotransmitter-gated ion channel, *Nature* 438, 248-252.
3. McMenimen, K. A., Dougherty, D. A., Lester, H. A., and Petersson, E. J. (2006) Probing the Mg²⁺ blockade site of an N-methyl-D-aspartate (NMDA) receptor with unnatural amino acid mutagenesis, *ACS Chem Biol* 1, 227-234.
4. Rodriguez, E. A., Lester, H. A., and Dougherty, D. A. (2007) Improved amber and opal suppressor tRNAs for incorporation of unnatural amino acids in vivo. Part 2: evaluating suppression efficiency, *RNA* 13, 1715-1722.
5. Torrice, M. M., Bower, K. S., Lester, H. A., and Dougherty, D. A. (2009) Probing the role of the cation- π interaction in the binding sites of GPCRs using unnatural amino acids, *Proc Natl Acad Sci U S A* 106, 11919-11924.
6. Monahan, S. L., Lester, H. A., and Dougherty, D. A. (2003) Site-specific incorporation of unnatural amino acids into receptors expressed in Mammalian cells, *Chem Biol* 10, 573-580.
7. Christou, P., McCabe, D. E., and Swain, W. F. (1988) Stable Transformation of Soybean Callus by DNA-Coated Gold Particles, *Plant Physiol* 87, 671-674.
8. Klein, T. M., Wolf, E.D., Wu, R., and Sanford, J.C. (1987) High-velocity microprojectiles for delivering nucleic acids into living cells., *Nature* 327, 70-73.
9. Wirth, M. J., and Wahle, P. (2003) Biolistic transfection of organotypic cultures of rat visual cortex using a handheld device, *J Neurosci Methods* 125, 45-54.
10. Joshi, P., and Dunaevsky, A. (2006) Gene-gun transfection of hippocampal neurons, *J Vis Exp*, 121.
11. O'Brien, J. A., and Lummis, S. C. (2006) Diolistic labeling of neuronal cultures and intact tissue using a hand-held gene gun, *Nat Protoc* 1, 1517-1521.
12. O'Brien, J. A., and Lummis, S. C. (2006) Biolistic transfection of neuronal cultures using a hand-held gene gun, *Nat Protoc* 1, 977-981.
13. Emkey, R., and Rankl, N. B. (2009) Screening G protein-coupled receptors: measurement of intracellular calcium using the fluorometric imaging plate reader, *Methods Mol Biol* 565, 145-158.
14. Sidach, S. S., Fedorov, N. B., Lippiello, P. M., and Bencherif, M. (2009) Development and optimization of a high-throughput electrophysiology assay for neuronal $\alpha 4\beta 2$ nicotinic receptors, *J Neurosci Methods* 182, 17-24.
15. Vasilyev, D. V., Shan, Q. J., Lee, Y. T., Soloveva, V., Nawoschik, S. P., Kaftan, E. J., Dunlop, J., Mayer, S. C., and Bowlby, M. R. (2009) A Novel High-Throughput Screening Assay for HCN Channel Blocker Using Membrane Potential-Sensitive Dye and FLIPR, *J Biomol Screen*.
16. Price, K. L., and Lummis, S. C. (2005) FlexStation examination of 5-HT₃ receptor function using Ca²⁺ - and membrane potential-sensitive dyes: advantages and potential problems, *J Neurosci Methods* 149, 172-177.

